

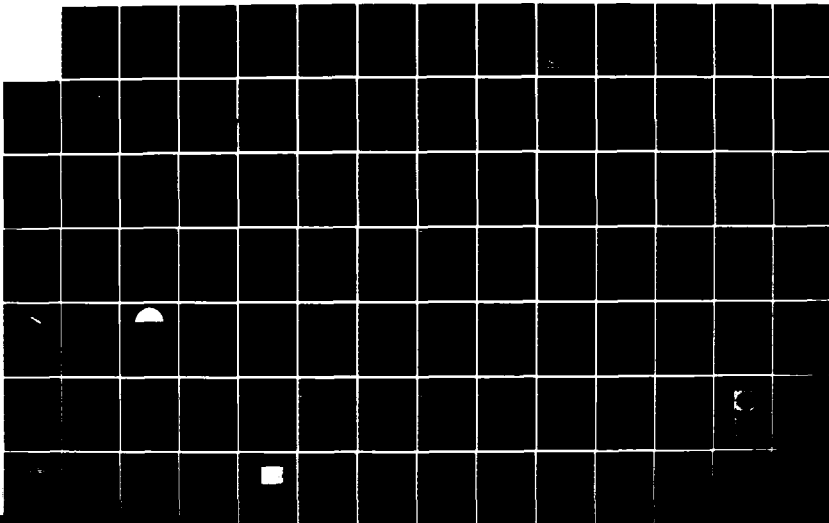
AD-A150 355

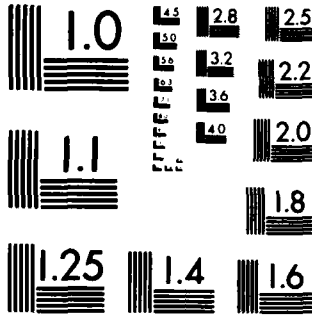
SIZE AND VELOCITY DISTRIBUTIONS OF PARTICLES AND  
DROPLETS IN SPRAY COMBUS. (U) ARIZONA STATE UNIV TEMPE  
DEPT OF MECHANICAL AND AEROSPACE ENG. E D HIRLEMAN  
01 NOV 84 N00014-79-C-0363 F/G 21/2

1/2

UNCLASSIFIED

NL





MICROCOPY RESOLUTION TEST CHART  
NATIONAL BUREAU OF STANDARDS-1963-A

①

NR-094 404

1132

AD-A150 355

Final Report

1 November 1984

Submitted to

Office of Naval Research

under

Contract No. N00014-79-C-0363

entitled

SIZE AND VELOCITY DISTRIBUTIONS OF PARTICLES AND DROPLETS  
IN SPRAY COMBUSTION SYSTEMS

1 March 1980 to 15 August 1984

by

E. Dan Hirlman, Principal Investigator  
Associate Professor  
Department of Mechanical and Aerospace Engineering  
Arizona State University  
Tempe, AZ 85287

DTIC FILE COPY

DTIC  
ELECTE  
FEB 13 1985  
S D  
B

DISTRIBUTION STATEMENT A  
Approved for public release  
Distribution Unlimited

SUMMARY

This research project was concerned with laser/optical techniques for size and velocity measurements of particles and droplets in spray combustion systems. The initial efforts were directed toward a novel method for simultaneous size and velocity measurements of individual particles. A prototype instrument was designed, constructed, calibrated, and successfully applied. Our efforts to verify the performance and accuracy of this diagnostic led to a parallel research effort on the laser diffraction droplet sizing technique. Significant contributions to the calibration and scattering inversion aspects of this technique were made. Discussed below are the contributions to the problem of aerosol characterization made as a

direct result of this research. *See also: Among the papers included in this final report are: Internal Transition for Particles in a Binary Near-forward Light Scattering; Non-invasive Laser-based Particle Velocity and Particle Sizing; DISCUSSION OF RESEARCH CONTRIBUTIONS (LSV) optical measurement techniques.*

1. Laser Particle-sizing Velocimeter H. J.

The clear need for simultaneous particle size and velocity measurements has prompted considerable research on the topic. We investigated a particular light scattering method for simultaneously measuring two-velocity components and the size of individual particles in the range 0.3 um - 20um. The LSV technique, originally proposed by Hirleman (1978), uses a novel non-Doppler technique for velocity determination. The method relies on a single beam transit-time velocity measurement termed the LIV as discussed by Hirleman (1980a), Hirleman (1981). One contribution of the work was a new optical system design which is applicable to conventional laser two-focus (L2F) velocimeters in addition to the LSV as discussed by Hirleman (1982c) and Hirleman and Yue (1983). Other researchers have adopted the velocimeter concepts developed under this project.

**PER LETTER**



By _____	
Distribution/ _____	
Availability Codes	
Dist	Avail and/or Special
<b>A1</b>	

A major consideration for a particle sizing system is that of calibration. The calibration problem is particularly challenging for the LSV which requires particles of known and controlled velocity, trajectory, and size. Conventional methods cannot satisfy these criteria and it was necessary to develop a new calibration technique by modifying a commercial TSI Model 3050 Vibrating Orifice Particle Generator. The standard generator produces a stream of monodisperse droplets which, unfortunately, are spaced about 4 diameters apart. This close spacing places 2 particles in the LSV probe volume at once which is unacceptable. We developed a programmable charge deflection system which takes 1 out of  $2^n$  droplets out of the stream using selective electrical charging and a pair of high voltage deflection plates. The system is described briefly in Yue et al. (1984) and a follow-up publication with more detail should be published by Anderson and Hirleman (1984).

Once an adequate calibration system was available we then initiated a detailed study of the performance of the LSV. Theoretical and experimental analyses of the instrument agreed well and indicated the ability of the LSV to measure two velocity components and size of individual droplets using an optical system comparable to that of a single component laser Doppler Velocimeter (LSV). We achieved size broadening of about 20% with non-Doppler velocity measurements accurate to about 1%. A unique feature of the LSV is an inherent capability of characterizing on-line the physical extent of the optical sample volume through the particle trajectory determination. The results of the LSV study are presented in detail by Yue et al. (1984), with some discussion by Hirleman (1984a). An updated version of Yue et al. (1984) will be submitted soon to an archival publication.

Laser diffraction methods for particle sizing are line-of-sight methods which analyze the scattering properties of an ensemble of particles. The electro-optical system required is considerably less complex than that used in single particle counting instruments and for that reason the system is more robust. We developed an in-house version of a laser diffraction instrument to use in aerosol analysis for comparison with the LSV. In the process of researching the laser diffraction technology we observed some serious deficiencies. In particular there were problems with calibration, operation in evaporating or combusting sprays, and inefficient scattering inversion algorithms. During the tenure of this project we made some original research contributions in these areas.

The problem of calibration of particle sizing instruments is always difficult. There are, however, some nice features of the laser diffraction technique which we exploited in developing a new calibration procedure. Laser diffraction methods are limited to particles larger than the wavelength and in that scattering regime the diffractively scattered light (described by Fraunhofer diffraction theory) dominates over refracted and reflected light in near-forward detector configurations. For that reason the forward scattering signature of a spherical particle is accurately approximated by the diffraction from either an opaque circular disc or a circular aperture of the same diameter. Our approach was to fabricate 2-D arrays of chrome discs using photomask technology from the integrated circuit industry. The particles were deposited on a glass substrate with a specified and accurately known size distribution. The concept was originally proposed by Hirleman (1982a, 1983a). This calibration device has since become a defacto standard for commercial laser diffraction instruments and is used by over 30 laboratories worldwide. The calibration method was

and is used by over 30 laboratories worldwide. The calibration method was further used with the support of this grant to make a careful characterization of laser diffraction instrument performance by Hirleman et al. (1984b).

A major weakness of laser diffraction instruments in general is a susceptibility to errors induced by beam steering caused by refractive index (thermal) gradients along the beam. This problem has been observed by ourselves during some laser diffraction experiments performed on a burning spray. However the line-of-sight nature of laser diffraction and the requisite extended sample volume make it possible to verify instrument performance and calibration on-line using the calibration devices discussed above. The known diffraction signature from a calibration source is modulated and superimposed on the actual diffraction pattern from the spray. Phase-sensitive detection allows one to verify that the calibration size distribution is reconstructed correctly to verify proper instrument operations. This idea and some proof-of-concept experiments are reported by Hirleman (1983a).

Another consideration with laser diffraction instruments is the scattering inversion software. The need for kHz temporal resolution for turbulence studies requires an improvement of about 3 orders of magnitude in processing speed over that available commercially today. For that reason we studied detection strategies in conjunction with inverse scattering algorithms to impact this problem. Our results are reported by Ruscelio and Hirleman (1981), Hirleman (1984a) and Koo and Hirleman (1984). We have studied an integral transform approach which potentially can provide the speed necessary. Our publications report on some detector configurations which can be used to implement this fast reconstruction algorithm.

## REFERENCES

The following publications referenced above were supported primarily by this Office of Naval Research research.

M. A. Anderson and E. D. Hirtleman, 1984. "Droplet Deflection System for the Vibrating Orifice Droplet Generator," to be submitted for publication in Review of Scientific Instruments.

J. H. Koo and E. D. Hirtleman, 1984. "Scattering Inversion Algorithms for Laser Diffraction Particle Sizing," presented at the Western States Section/Combustion Institute Spring Meeting, Boulder, CO, April 1984.

E. D. Hirtleman, 1978. "Laser Technique for Simultaneous Particle Size and Velocity Measurements," Optics Letters, Vol. 3, p. 19 (1978).

E. D. Hirtleman, 1980. "Recent Developments in Non-Doppler Laser Velocimeters," AIAA Paper 80-0350, presented at 18th AIAA Aerospace Sciences Meeting, Pasadena, California, January 14-16, 1980.

E. D. Hirtleman, 1982a. "Aperture Arrays for the Calibration of Droplet Sizing Instruments," CLEOS Conference Digest, Optical Society of America, Presented at the IEEE/OSA Conference on Laser and Electro-Optical systems, Phoenix, Arizona, April 16, 1982.

E. D. Hirtleman, 1982b. "Non-Doppler Laser Velocimetry: Single Beam Transit-time L1V," AIAA Journal, Vol. 20, p. 86 (1982).

E. D. Hirtleman, 1982c. "Optical System for Time-of-flight Laser Velocimeter," U.S. Patent Application 06/417150, filed September 13, 1982.

E. D. Hirtleman, 1983a. "On-Line Calibration Technique for Laser Diffraction Droplet Sizing Instruments," ASME paper 83-GT-232, American Society of Mechanical Engineers, New York, 1983, presented at the International Gas Turbine Conference, March, 1983, Phoenix, AZ.

E. D. Hirtleman, 1984a. "Particle Sizing by Optical, Nonimaging Techniques," Liquid Particle Size Measurement Techniques, ASTM publications STP848, ed. by J. M. Tishkoff, R. D. Ingebo, and, J. B. Kennedy, pp. 35-60, 1984.

E. D. Hirtleman, V. Oechsle, and N. A. Chigier, 1984b. "Response Characteristics of Laser Diffraction Particle Sizing Systems: Optical Sample Volume and Lens Effects," Optical Engineering, V. 23, pp. 610-619 (1984).

E. D. Hirtleman, 1984c. "Nonintrusive Laser Particle Sizing Techniques," Invited review paper, AIAA-83-1514, presented at the AIAA 18th Thermophysics Conference, June 1-3, 1983, Montreal, Canada, published in Combustion Diagnostics by Nonintrusive Methods, eds. T. D. McCay and J. A. Roux, Progress in Astronautics and Aeronautics, V. 92, pp. 177-207, AIAA, 1984.

E. D. Hirtleman and Y. Yue, 1983. "The Laser-two-focus Velocimeter," Proceedings of the Second Asian Congress on Fluid Mechanics, Science Press, Beijing, PRC, p. 112, 1983. Presented at the Congress, October 25, 1983, Beijing, PRC.

E. D. Hirtleman, Y. Yue, N. S. Berman, and D. X. Guan, 1984d. "Single-beam Transit-time Laser Velocimetry (LIV) in Turbulent Flow," Proceedings of the Conference on Laser Velocimetry, Lisbon, Portugal, 1984.

L. V. Ruscello and E. D. Hirtleman, 1981. "Determining Droplet Size Distributions in Sprays with a Photodiode Array," presented at the Western States Section/Combustion Institute Meeting, Tempe, Arizona, October 19-20, 1981.

Y. Yue, E. D. Hirtleman, and M. A. Anderson, 1984. "Simultaneous Particle Size and Velocity Measurements," presented at the Western States Section/Combustion Institute Spring Meeting, Boulder, CO, April 1984.

#### PERSONNEL

The following persons contributed to the research effort:

E. Dan Hirtleman, Principal Investigator, Associate Professor, Mechanical and Aerospace Engineering.

Joesph Koo, Ph.D. Student, Research Associate, Mechanical and Aerospace Engineering.

Philip Murtaugh, MS Student, Research Assistant, Mechanical and Aerospace Engineering.

Steve Walters, MS Student, Research Assistant, Electrical and Computer Engineering

L. Vincent Ruscello, MS Student, Research Assistant, Chemical and Bio Engineering.

Yao Yue, Visiting Research Associate, Mechanical and Aerospace Engineering.

mechanical and aerospace engineering

mechanical engineering, aerospace engineering, energy systems engineering, engineering science, materials science

**INTEGRAL TRANSFORM FOR PARTICLE SIZING  
BY NEAR-FORWARD LIGHT SCATTERING**

by

**J. H. Koo  
and  
E.D. Hirleman**

**Laser Diagnostics Laboratory  
Mechanical and Aerospace Engineering Department  
Arizona State University  
Tempe, Arizona 85287**

**Paper No. WSCI-84-33**

**1984 Spring Meeting  
Western States Section  
The Combustion Institute  
April 2-3, 1984  
University of Colorado  
Boulder, Colorado**



**College of Engineering & Applied Sciences  
Arizona State University  
Tempe, Arizona 85287**



CR-

### Abstract

The problem of droplet sizing in fuel sprays has been the subject of much research in recent years. The size distribution of particles and droplets are of crucial importance to the combustion processes in gas-turbine engines, combustion of coal slurries, liquid-fueled ramjets, and solid propellant rocket motors. The objective of this paper is to study the merits of the integral transform approach for measuring particle size distribution. Detailed parametric studies were made on both ideal and noisy data. Factors affecting the reconstruction of particle distribution were examined.

## I. Introduction

The problem of droplet sizing in fuel sprays has been the subject of much research in recent years.<sup>1-4</sup> The size distribution of particles and droplets are of crucial importance to the combustion processes in gas-turbine engines, combustion of coal slurries, liquid-fueled ramjets, and solid propellant rocket motors. Several books have been written covering general aspects of particle size measurement and analysis<sup>5-7</sup> and problems specific to fuel spray combustion systems.<sup>7-10</sup> The overall aim of detailed spray analysis in combustion systems is to increase combustion efficiency and to reduce emission of pollutants.

A number of different imaging methods have been used for droplet sizing in sprays, such as photographic and holographic methods. A disadvantage of these methods is the very tedious post-processing of data although some progress on quasi-real-time digital image processing<sup>11-12</sup> has been made. Single particle size/velocity analyzers based on light scattering have been developed over a number of years for clean room monitoring, pollution research and other studies.<sup>13,14</sup> Ensemble (multi-particle) methods using light scattering or extinction generally involve relatively simple electro-optical systems. As a result, these techniques are better suited for applications requiring autonomous operation. The trade-off here is the loss of information as the data is generally averaged over a line-of-sight and droplet velocity can not be obtained. The large number of potential applications and the wide-spread acceptance of the Malvern<sup>15</sup> laser diffraction particle sizing instruments by both the combustion research and industrial communities warrant further research on the method.

The objective of this paper is to study the merits of the integral transform approach for measuring particle size distribution. Detailed

parametric studies were made on both ideal and noisy data. Factors affecting the reconstruction of particle distribution were examined.

## II. Particle Sizing by Laser Diffraction

For measurement of size distribution of clouds of particles in fuel spray, the Fraunhofer diffraction method has proven to be one of the most convenient and reliable techniques. The classical Fraunhofer diffraction theory is only rigorously valid for particle sizes large compared with the wavelength (i.e.  $\frac{d}{\lambda} \geq 10$ ). It has been demonstrated that for near-forward scattering (small  $\theta$ ) can actually be approximated<sup>14</sup> by Fraunhofer diffraction even for particles with  $\frac{d}{\lambda} \approx 1$ . This phenomenon is the basis for a number of small particle sizing instruments based on light scattering. 14,16

### A. Theoretical Aspects

Dobbins et al<sup>1</sup> have shown that for particle distributions defined by an Upper Limit Distribution Function (no particles larger than  $D_u$ ), the scattered intensity vs the parameter  $\frac{\pi D_{32} \theta}{\lambda}$  was independent of most probable diameter  $\bar{D}$  where  $D_{32}$  is the Sauter Mean Diameter. For this reason,  $D_{32}$  can be obtained from the laser diffraction measurement independent of the form of size distribution. The author<sup>1</sup> estimated  $D_{32}$  by measuring the radial distance at which the scattered intensity falls to 10% of its on-axis value  $I_0$ .

Roberts and Webb<sup>2</sup> carried out a study to determine the sensitivity of Dobbins' method to different forms of size distribution. They concluded that the method was applicable to essentially any non-monodisperse particle distribution. Lefebvre et al have proven the practical usefulness of the method by an extensive series of measurements on fuel atomizers using Dobbins'

method.3,17,18 One drawback of Dobbins' technique is the fact that only the  $D_{32}$  rather than the complete distribution is measured.

Swithenbank et al.17,18 have proposed a modified version of Dobbins' method based on the measurement of the scattered "energy distribution" rather than the intensity distribution. Light is collected in an entire annular ring at a given angle in the focal plane rather than by a small detector. The general result is that one can determine the entire size distribution rather than only  $D_{32}$ .

The near-forward scattering intensity  $I_{\theta} = I(\theta)/I(0)$  from a general polydisperse aerosol is given by:

$$I_{\theta} = C_1 \int_0^{\infty} J_1^2(x\theta) x^2 n(x) dx \quad (1)$$

where:  $x$  is the particle size parameter given by  $\frac{\pi d}{\lambda}$ ,

$n(x)$  is the particle size distribution function,

$\theta$  is the scattering angle (approximation  $\sin\theta \sim \theta$  has been made),

$J_1$  is a Bessel function of the first kind and of order unity,

$C_1$  is a constant.

Equation (1) assumes that multiple scattering is insignificant and Fraunhofer diffraction applies.

The essence of the general laser diffraction particle sizing problem is to invert equation (1) to determine  $n(x)$  from the measured values of  $I_{\theta}$ .

Equation (1) can be rewritten in a discretized form

$$I_{\theta} = C_1 \sum_{i=1}^{n_s} J_1^2(x_i\theta) n(x_i) x_i^2 \Delta x \quad (2)$$

where  $n_s$  is the number of discrete particle sizes. Now let  $N_i = n(x_i)\Delta x$ , be the number of particles in the  $i$ th size interval and define  $A_i = N_i x_i^2$  which is proportional to the projected particle area in the  $i$ th size interval. Then equation (2) can be rearranged as follows:

$$I_\theta = C_1 \sum_{i=1}^{n_s} A_i J_1^2(x_i \theta) \quad (3)$$

For a series of measurements at  $n_d$  separate scattering angles, Equation (3) can be represented as a system of  $n_d$  equations in  $n_s$  unknowns:

$$I = CA \quad (4)$$

where:  $I$  is the scattering intensity measurement vector of length  $n_d$ ,

$C$  is an  $n_d$  by  $n_s$  scattering influence coefficient matrix;

and  $A$  is the unknown area distribution solution vector of length  $n_s$ .

Real detectors do not measure intensity but radiant flux, or intensity integrated over the finite area of the detector. Thus, the measured scattering pattern will not be just proportional to  $I_\theta$ , but will require integration of equations (2) or (3) over the finite  $\Delta\theta$  window for each detector.

#### B. Experimental Apparatus

The basic concept of the laser diffraction particle sizing method is illustrated in Figure 1. A collimated monochromatic laser beam is passed through the particle field. A Fourier transform lens is used to direct the light pattern onto a photodetector. When particles of different sizes are present in the light beam, a series of dark and light

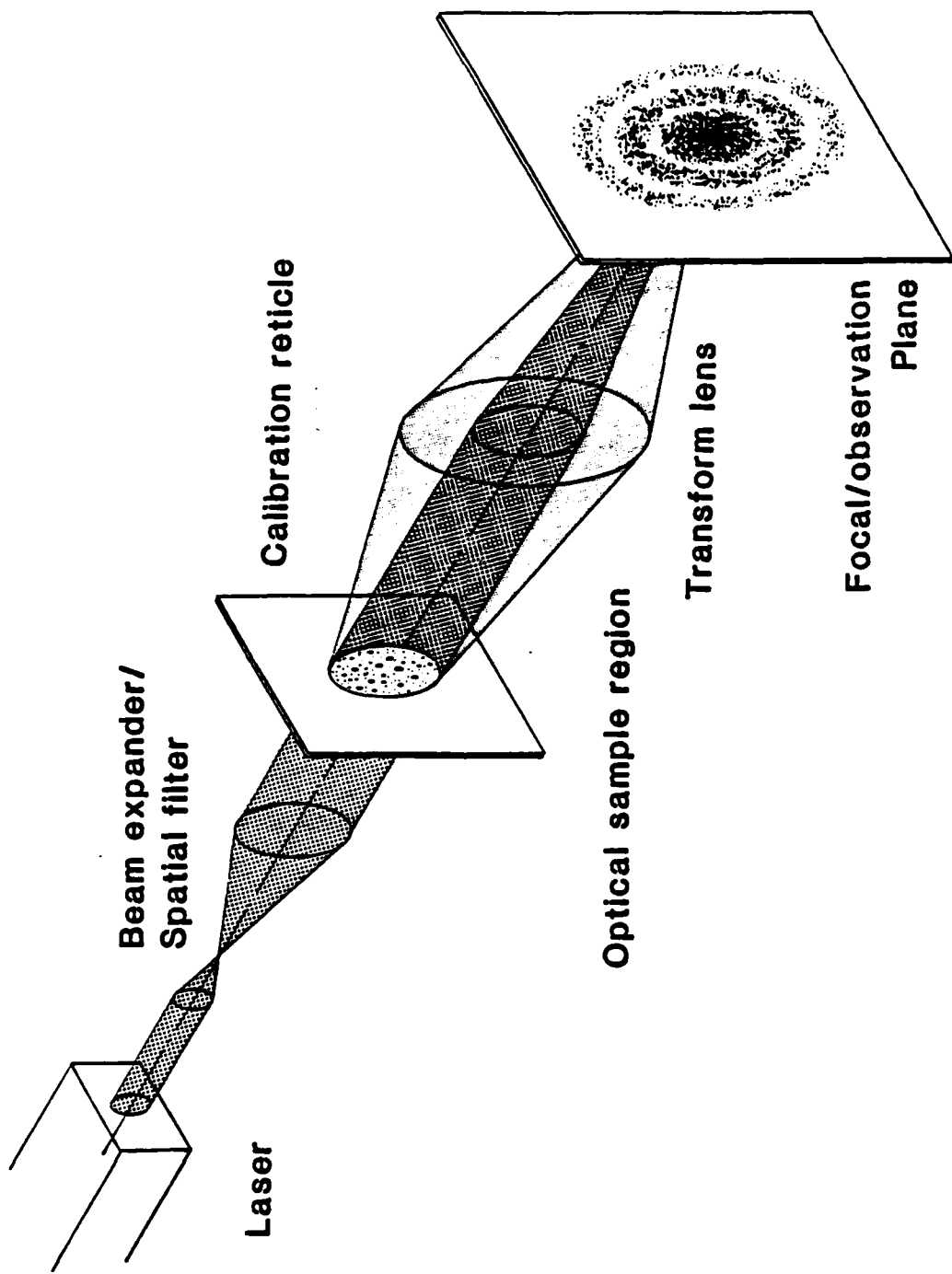


Figure 1. Schematic of laser diffraction apparatus for droplet sizing.

rings are generated at various radii, each light ring being a function of particle size. The analysis of the measured light intensity distribution into particle size distribution is done by using appropriate numerical inversion techniques.

### C. Numerical Scheme

The diffraction pattern is the sum of Bessel-squared terms, each with a different weighting coefficient given by the particle number or surface area distribution.

There are two basic approaches in solving the equations for  $n(x)$ , either an integral (or series) Bessel transform on Equation (2) or a matrix inversion process on Equation (3). The two approaches are discussed below:

#### a. Bessel Transform Inversion

Chin et al<sup>19</sup> (1955) were the first group of workers that attempted to perform an integral transform on Equation (2) for droplet sizing. Equation (2) is a classical Fredholm equation of the first kind.<sup>20</sup> An inversion relation due to Titchmarsh<sup>21</sup> gives the distribution function<sup>19</sup>:

$$n(x)x^2 = C_2 \int_0^{\infty} J_1(x\theta)Y_1(x\theta)x\theta \frac{d}{d\theta}(\theta^3 I_\theta) d\theta \quad (5)$$

where  $Y_1$  is the first order Bessel function of the second kind,

$C_2$  is a proportionality constant.

For practical purposes, intensity measurements can only be made over a finite range of scattering angles  $\theta$ . In the case of minimum angle  $\theta_{\min}$ , it is limited by the overwhelming intensity of undiffracted light near the axis at  $\theta = 0$ . For upper boundary,  $\theta_{\max}$  will be controlled by decreasing scattering

intensity at larger angles, i.e. signal/noise detection considerations. Based on the above, the Bessel transform integral of Equation (2) is approximated as:

$$n(x)x^2 = K \int_{\theta_{\min}}^{\theta_{\max}} \frac{d}{d\theta} (\theta^3 I(\theta)) J_1(x\theta) Y_1(x\theta) x \theta d\theta \quad (6)$$

Chin<sup>19</sup> et al, Abiss<sup>22</sup>, Fymat<sup>23</sup> and Ruscello and Hirleman<sup>24</sup> studied the scattering problem and found that this integral transform method is feasible.

The accuracy of reconstructing size distribution of different types of particle size distribution will be discussed in the last sections. Potential parameters of importances are  $\theta_{\min}$ ,  $\theta_{\max}$ ,  $\Delta\theta$  and the experimental errors in  $I_{\theta}$ . Results of some computer experiments in the solution of Equation (5) are shown in the following section. The results in the following section indicate that droplet size distributions can be accurately reconstructed with this technique.

#### b. Matrix Inversion Methods

The second approach to the problem is to solve a discretized version of Equation (2) by inverting the influence coefficient matrix C. Unfortunately C is ill-conditioned and near singular, making it impractical to invert directly. Due to the above nature, this becomes an ill-condition inverse problem. For this reason, least squares or minimization of error solutions are generally attempted. A set of values for  $n_1(x)$  are found which minimize the sum square error between the experimental measurement vector I and the matrix product CA in Eq. (2). Numerous workers have studied this approach, including Felton<sup>25</sup>, Alger<sup>26</sup>, Caroon and Borman<sup>27</sup>, Ruscello and Hirleman<sup>24</sup> and many others. The accuracy of the method of previous workers shows satisfactory results.

### III. Particle Size Distribution Functions for Sprays

A number of mathematical expressions<sup>28,29</sup> have been developed to model the droplet size distributions of sprays. Generally measured size distributions are discretized. Four typical size distributions are shown in the following;

a. Arithmetic normal distribution<sup>29</sup> by number

$$\frac{dN}{dd} = \frac{1}{\sigma\sqrt{2\pi}} \exp - \frac{(d-\bar{d})^2}{2\sigma^2} \quad (7)$$

where  $\bar{d}$  is the mean size,  $\sigma$  is the standard deviation

b. Log-normal distribution

This equation has resulted from the application of a statistical analysis of the breakup of liquids. The size distribution is based on an expression such as the following:<sup>29</sup>

$$\frac{dN}{dd} = \frac{6}{\pi\sqrt{2\pi} \sigma \bar{d}^4} \exp\left(-\frac{1}{2\sigma^2} \left(\ln \frac{d^2}{\bar{d}^2}\right)^2\right) \quad (8)$$

where  $\bar{d}$  is the median for the log-normal distribution and  $\sigma$  is the standard deviation.

c. Rosin-Rammler distribution

This equation was originally developed to express the size distribution of pulverized fuel and is usually expressed in the form,<sup>31</sup>

$$R = \exp\left(-\left(\frac{d}{\bar{d}}\right)^N\right) \quad (9)$$

where  $R$  is the volume fraction of particles with diameters greater than  $d$ ,  $\bar{d}$  is the Rosin-Rammler mean diameter, and  $N$  is a parameter related to the width of the distribution.

Differentiating equation (9) gives<sup>29</sup>:

$$\frac{dV}{dd} = \frac{Nd^{N-1}}{\bar{d}^N} \exp(-(d/\bar{d})^N) \quad (10)$$

d. Nukijama-Tanasawa distribution

This equation has the following form,<sup>29</sup>

$$\frac{dN}{dd} = ax^2 \exp(-bd^\beta) \quad (11)$$

where  $a$  is a constant and  $\beta$  varies little from unity.

The above form types of size distribution were used in the computer experiments and results will be discussed in Section IV.

#### IV. Factors Affecting Reconstruction of Particle Size Distribution

Some examples for the reconstructing of the size distribution will now be discussed.

In general, only three major factors will be affecting the inverting of the scattering data. They are (a) Maximum allowable angle ( $\theta_{max}$ ), (b) Angular Resolution ( $\Delta\theta$ ), and (c) Noise.

In actual experiments, the ideal behavior of scattered light intensity  $I(\theta)$  would be degraded by optical, electronic or mechanical noise. Different workers have proposed various methods in modelling noise in their analyses.

In practice, the measured light intensity  $I(\theta)$  is equal to the theoretical intensity  $I_t(\theta)$  with added noise in the following manner,

$$I_{exp}(\theta) = I_t(\theta) + \epsilon(\theta) \quad (12)$$

The  $\epsilon(\theta)$  term can be simulated to include three contributions:

- (a) a normally distributed random error with a standard deviation proportional to the magnitude of  $I_t(\theta)$ .<sup>25, 30, 32</sup>
- (b) a normally distributed random error with a constant standard deviation independent of the local value of  $I(\theta)$ .<sup>22</sup>. The standard deviation can be normalized by the on-axis scattering intensity  $I(0)$  or by the  $I(\theta_{max})$  at the maximum scattering angle.
- (c) a normally distributed random error with standard deviation  $(\theta)$  which is a function of this scattering angle as in  $\epsilon(\theta) = C_\epsilon(\theta)\theta^m$ .

The above contributions can be represented with an error expression in the following form,

$$\epsilon(\theta) = a + b\theta^m + cI_t(\theta) \quad (13)$$

where  $a$ ,  $b$ ,  $c$ , and  $m$  are arbitrary constants.

In all the computer experiments, the initial conditions for the random number generator were made the same, so that identical sequences of random numbers were produced and the effects of errors arising from the background and intensity-dependent noise sources can be separately investigated.

A log normal particle size distribution with a geometric mean size equals  $45 \mu\text{m}$  and a geometric standard deviation of 1.1 (denoted by LN-45, 1.1) was used for the parametric studies throughout this paper.

### Maximum Allowable Angle

Figure 2 shows a typical noiseless plot of intensity,  $I(\theta)/I(0)$  with scattering angle,  $\theta$  for  $\theta_{\max} = 3^\circ$  and  $\lambda = 0.6328 \mu\text{m}$ . The  $\frac{d(\theta^3 I(\theta))}{d\theta}$  term in equation (6) was plotted against  $(\theta)$  in figure 3 to serve as a criterion in determining the  $\theta_{\max}$  value for experimental and numerical purposes.

Figures 4-6 clearly shows that when  $\theta_{\max}$  departs from its optimal value, the quality of reconstruction of particle size distribution degrades. The values of  $\theta_{\max}$  were set at  $1^\circ$ ,  $3^\circ$  and  $10^\circ$ . In the present case  $\theta_{\max} = 3^\circ$  seems to be an optimal value for reconstruction of the particle size distribution. Smaller values underpredicted the assumed size distribution. Higher values do not provide a sufficient improvement in accuracy to justify the increase in computational time.

### Angular Resolution

After determining the optimal forward cone value we investigated the effect of the angular resolution,  $\Delta\theta$ . The results are illustrated in Figures 7-9 which show that independent of  $\Delta\theta$ , the mode radius seems to be accurately located in position but not in magnitude. This indicates that with a proper choice of  $\theta_{\max}$ , even a rough experiment with a small amount of data collected would yield the mode radius. For finer resolution (smaller  $\Delta\theta$  values) the results improve considerably across the whole distribution, and tend asymptotically to the assumed distribution. However, beyond a certain  $\Delta\theta$ , there does not seem to be any substantial improvement in the retrieval. Numerically,  $\Delta\theta$  is restricted by the need to compute  $\frac{d(\theta^3 I(\theta))}{d\theta}$  accurately in equation (5).

# LOG NORMAL (LN-45.,1.1)

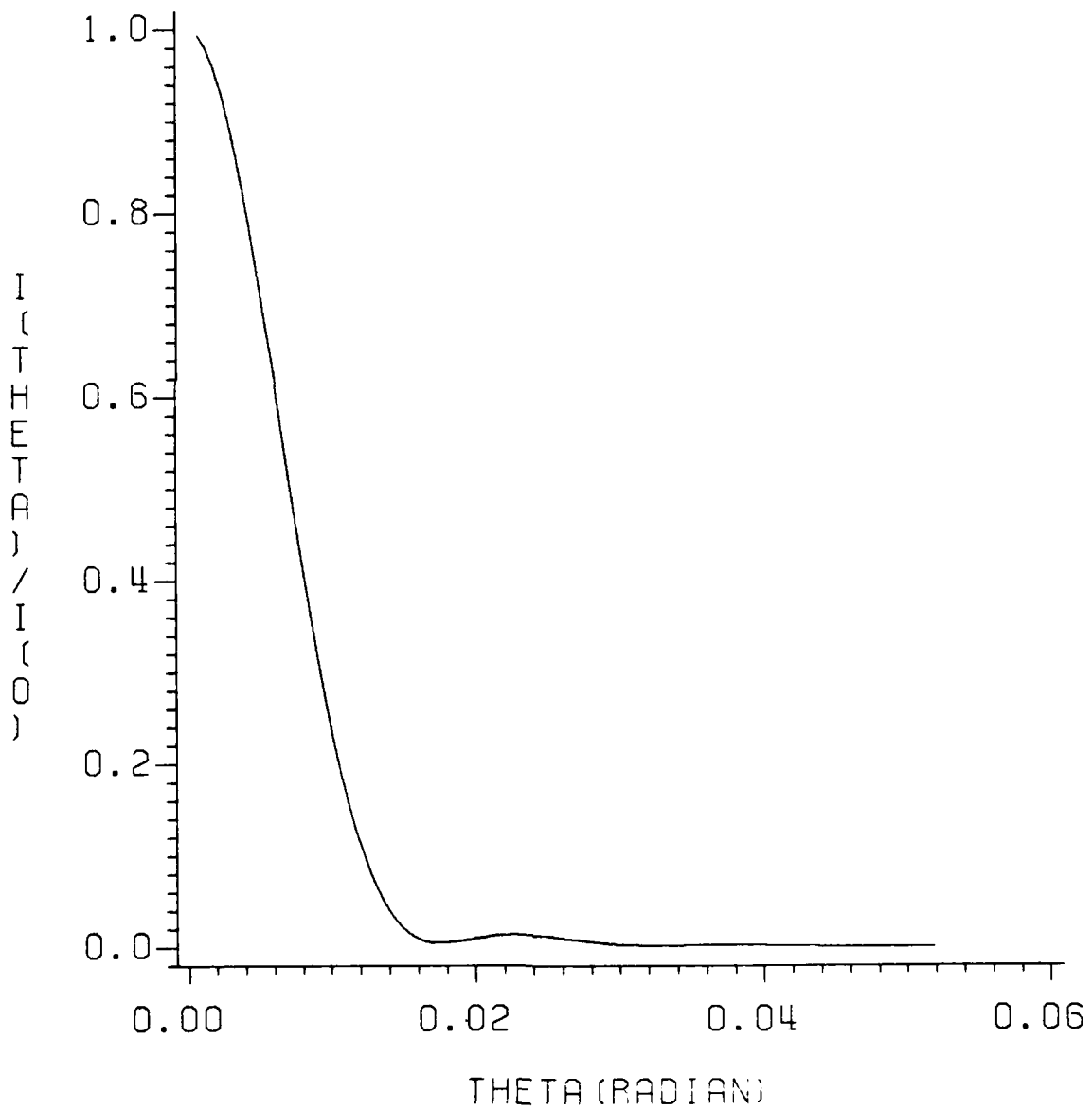


Figure 2. Typical plot of noiseless intensity  $I(\theta)/I(0)$  vs scattering angle,  $\theta$ .

# LOG NORMAL (LN-45.,1.1)

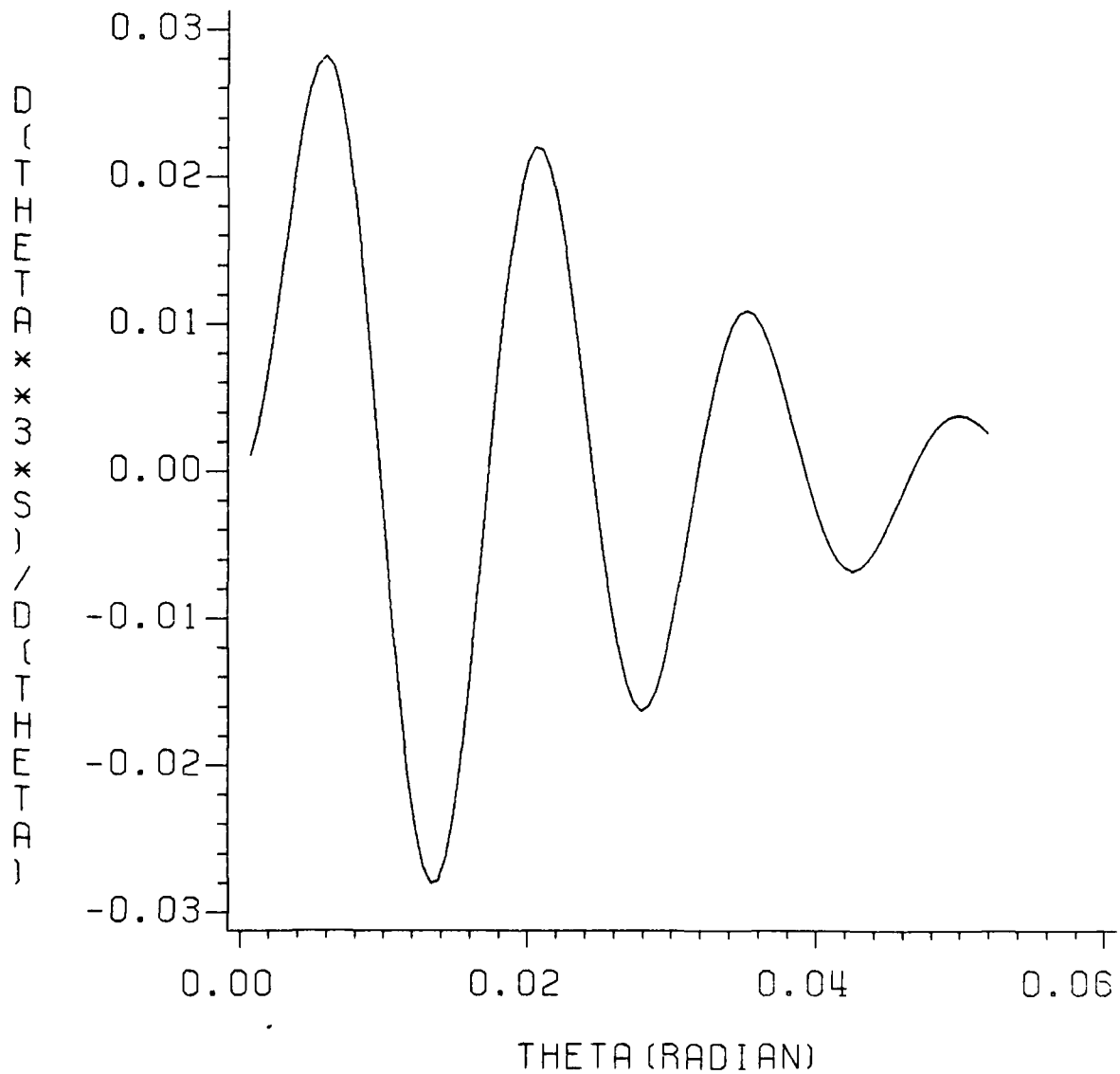


Figure 3. Plot of  $\frac{d(\theta^3 I(\theta))}{d\theta}$  vs.  $\theta$

LOG NORMAL DISTRIBUTION (LN-50.,1.1) ERR= 0,0.

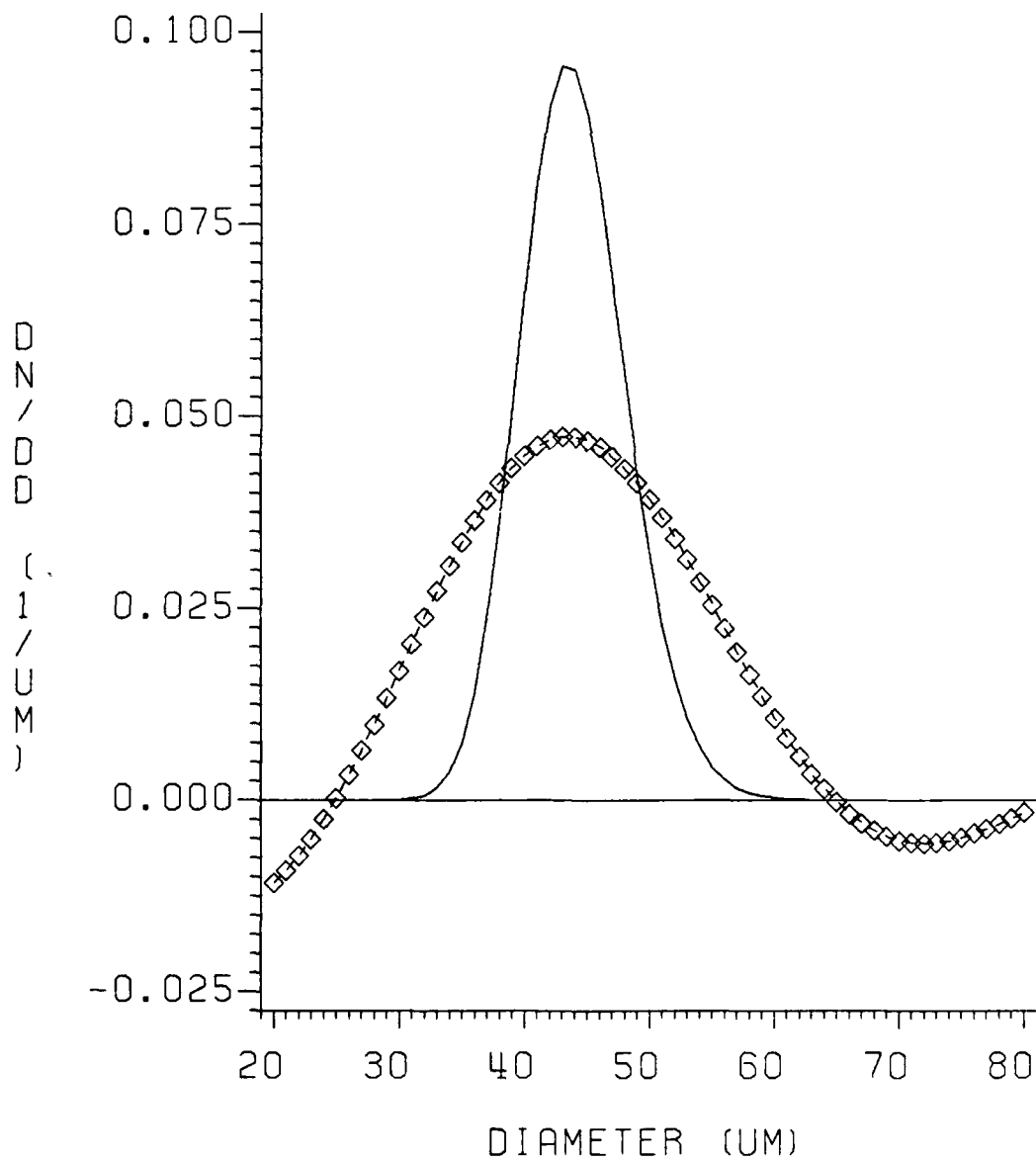


Figure 4. Effect of maximum scattering angle ( $\theta_{max}$ ) on the reconstruction of particle size distribution at  $\theta_{max} = 1^\circ$ .

LOG NORMAL DISTRIBUTION (LN-50.,1.1) ERR= 0,0.

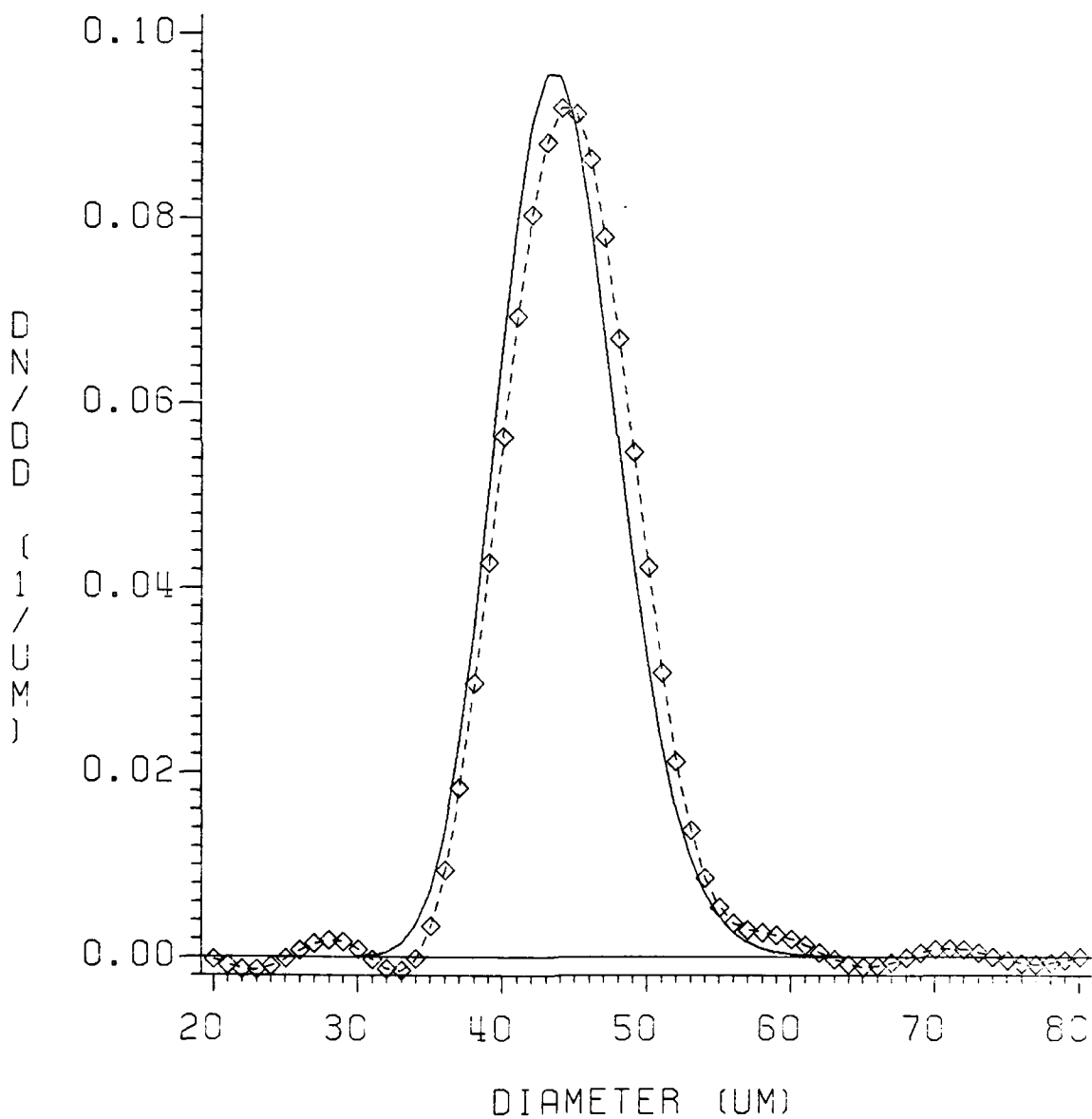


Figure 5. Effect of maximum scattering angle ( $\theta_{\text{max}}$ ) on the reconstruction of particle size distribution at  $\theta_{\text{max}} = 3^\circ$ .

LOG NORMAL DISTRIBUTION (LN-50.,1.1) ERR= 0,0.

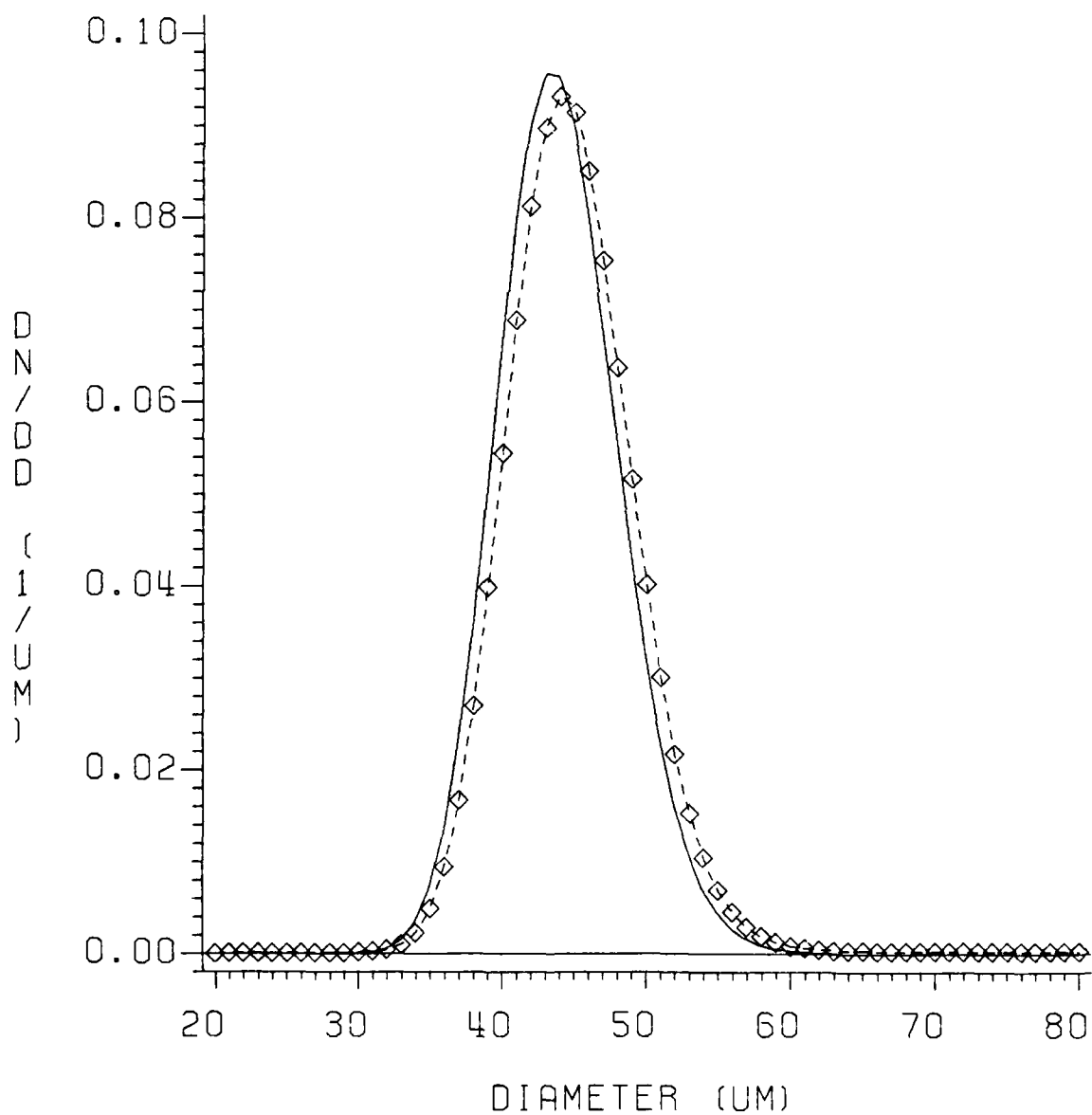


Figure 6. Effect of maximum scattering angle ( $\theta_{max}$ ) on the reconstruction of particle size distribution at  $\theta_{max} = 10^\circ$ .

LOG NORMAL DISTRIBUTION (LN-50.,1.1) ERR= 0,0.

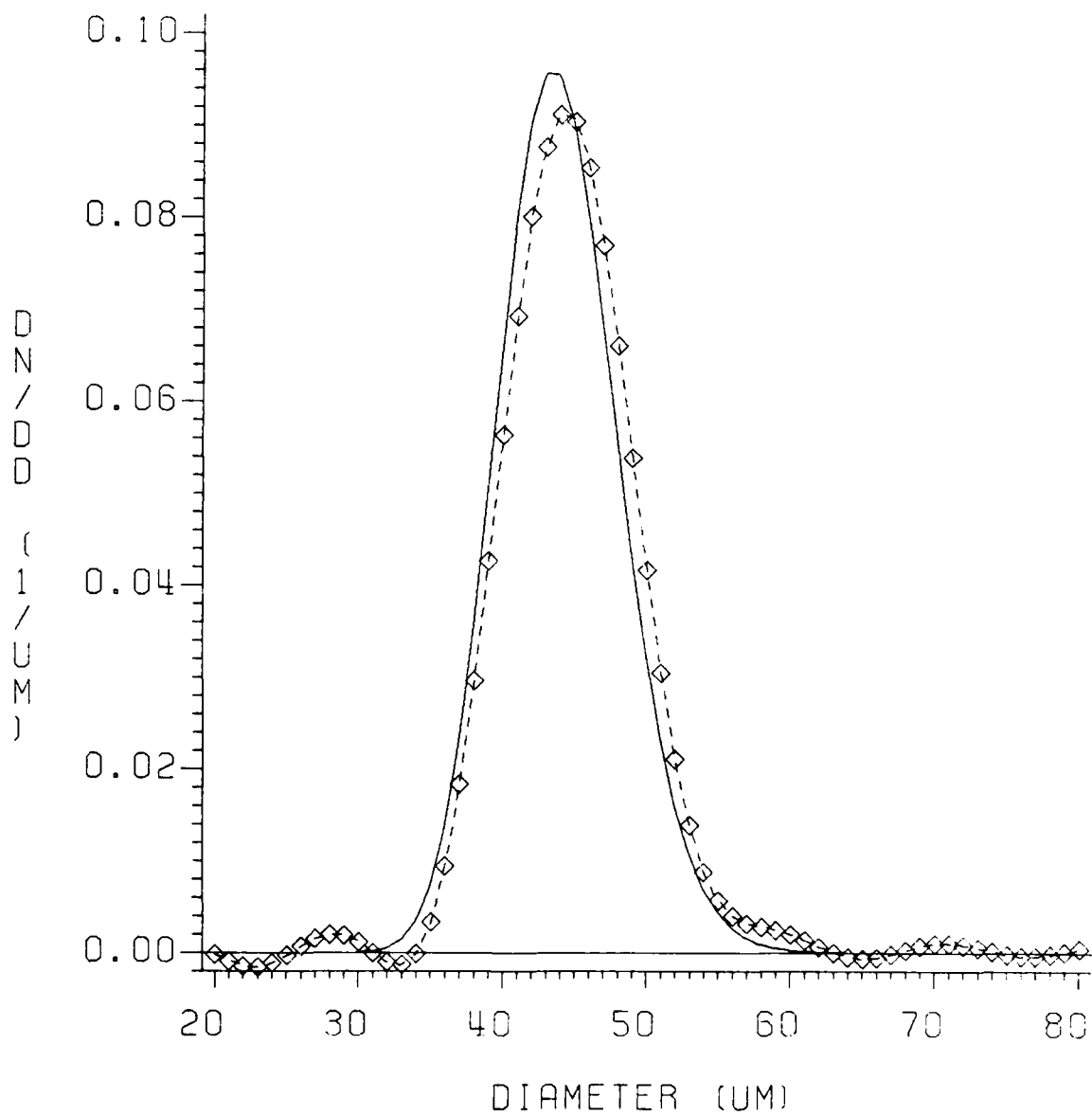


Figure 7. Effect of angular resolution on the reconstruction of particle distribution at  $\Delta\theta = .0996^\circ$

LOG NORMAL DISTRIBUTION (LN-50.,1.1) ERR= 0,0.

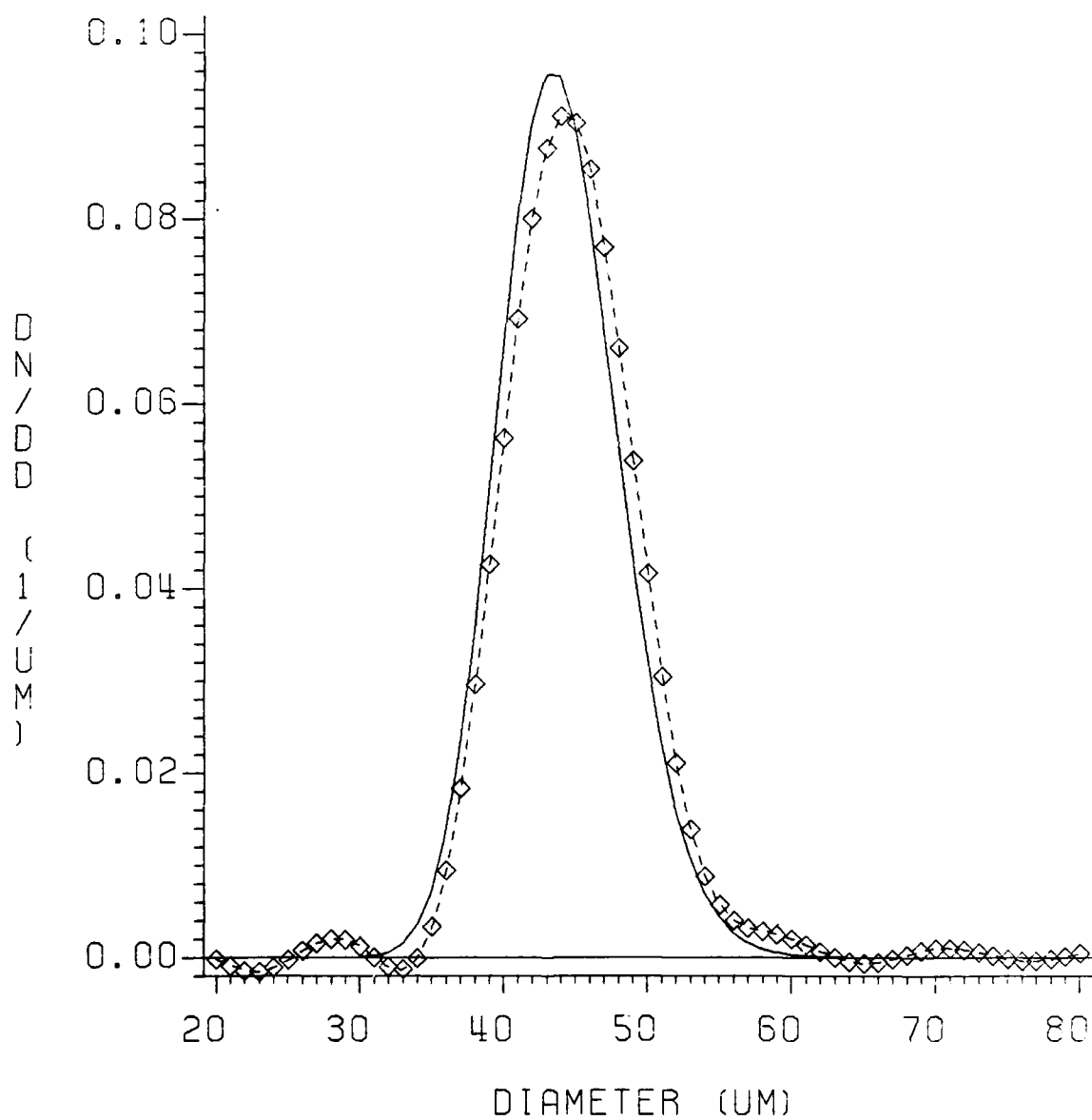


Figure 8. Effect of angular resolution on the reconstruction of particle distribution at  $\Delta\theta = .0299^\circ$

LOG NORMAL DISTRIBUTION (LN-50.,1.1) ERR= 0,0.

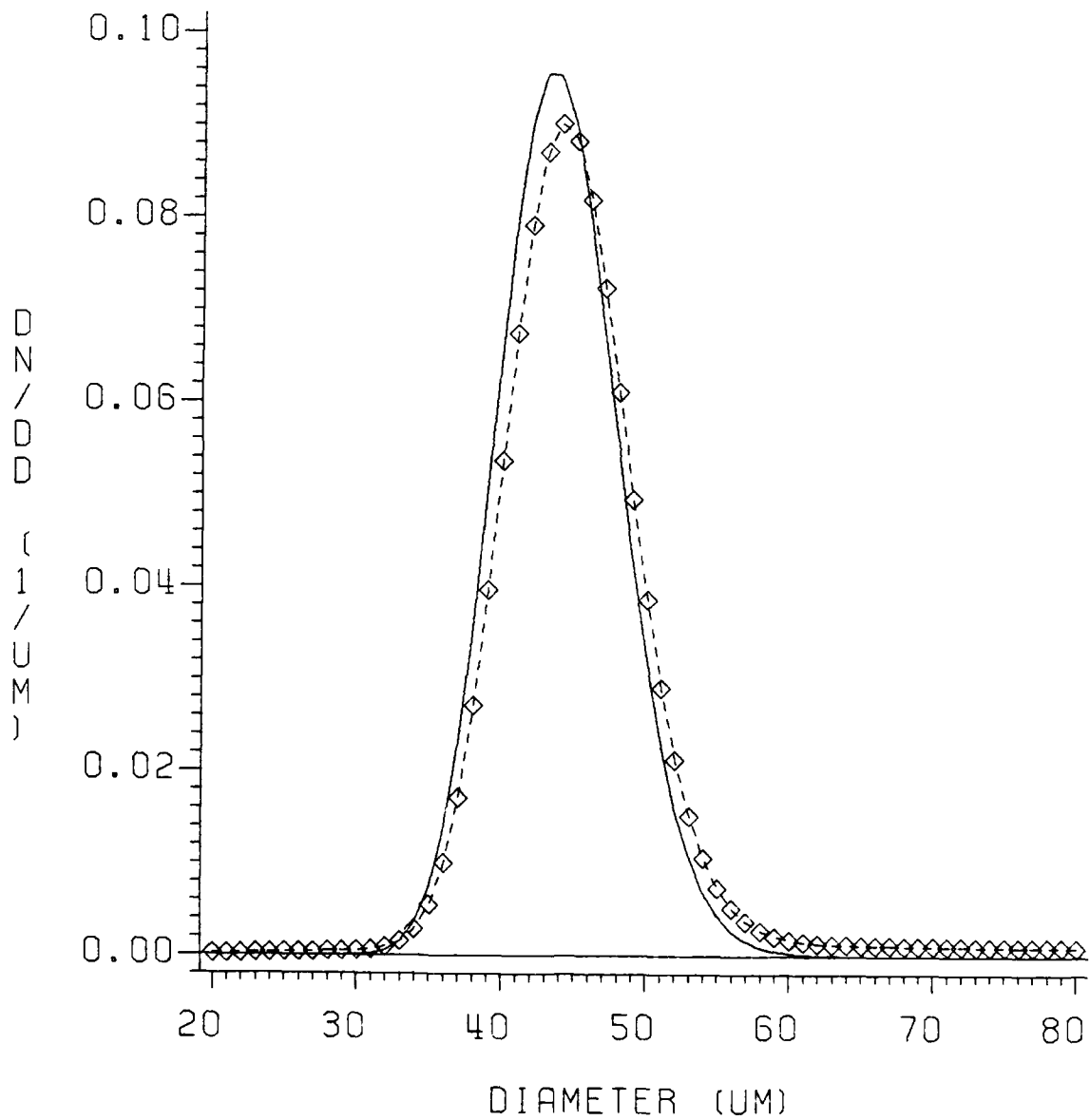


Figure 9. Effect of angular resolution on the reconstruction of particle distribution at  $\Delta\theta = 0.96 \times 10^{-3}$ .

### Noisy Data

Size distributions were also reconstructed from the inversion of noisy data generated by the methods discussed in the previous sections. For this study,  $\theta_{\max}$  was set at  $3^\circ$  and,  $\Delta\theta$  at  $\approx 0.0299^\circ$ .

Figures 10 and 11 show the plot of intensity vs. scattering angle and  $\frac{d(d\theta^3 I(\theta))}{d\theta}$  term vs.  $\theta$  with random noise added.

Normally distributed random noise was added as a constant percentage of the local value of  $I(\theta)$ . 5, 10 and 20% of the local values of  $I(\theta)$  were used. Figures 12-14 show the reconstitution of particle size using 5, 10 and 20% of the randomly generated noise. The results clearly show that it is possible to reconstruct the particle size distribution with up to 20% localized noise.

Figures 15-18 show the reconstruction of particle size distribution using normally distributed random errors with a constant standard deviation based on the peak intensity,  $I(0)$ . The noise levels simulated detector dynamic ranges of  $10^2$ ,  $10^3$ ,  $10^4$  and  $10^5$ . Adequate reconstruction of the size distribution can be obtained at a dynamic range of  $10^4$ . By way of reference, note that specifications of dynamic range for typical linear photodiode arrays (e.g. Reticon) with equal area detector elements are of the order 100:1. The corresponding results in Fig. 15 suggest that a standard diode array will not be an acceptable detection system for size distribution measurements by this method.

### VI. Conclusions

This study has led to the following conclusions:

1. The size distribution of spherical particles can be retrieved from the diffraction of light. The integral transform approach provides a good solution for low noise levels.

LOG NORMAL (LN-45.,1,1) ERR=.20,.0

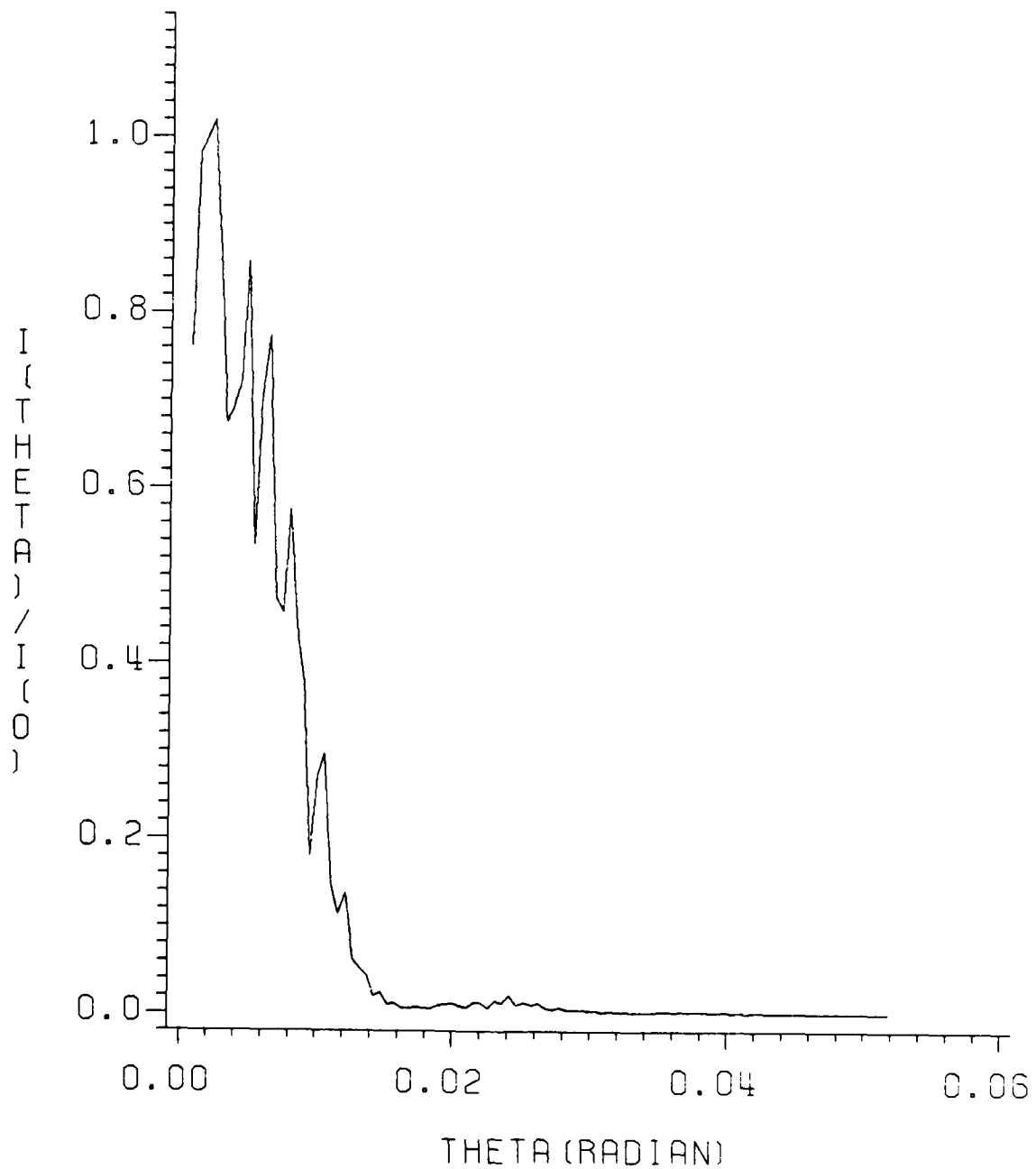


Figure 10. Plot of intensity  $I(\theta)/I(0)$  vs. scattering angle,  $\theta$  simulated with noise.

LOG NORMAL (LN-45.,1,1) ERR=.20,.0

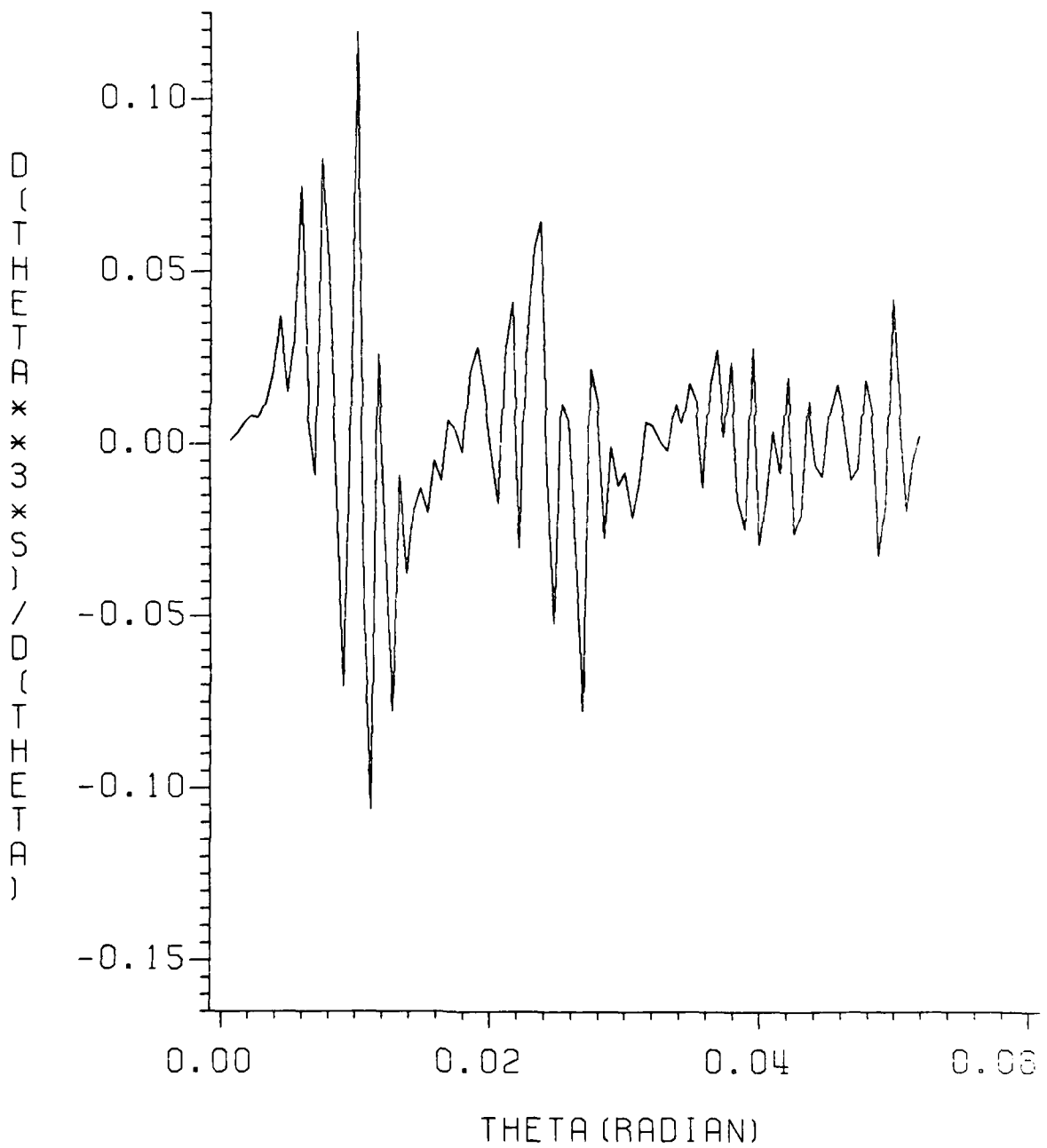


Figure 11. Plot of  $\frac{d^3 I(\theta)}{d\theta^3}$  vs.  $\theta$  with noise.

LOG NORMAL DISTRIBUTION (LN-50.,1.1) ERR=.05,0.

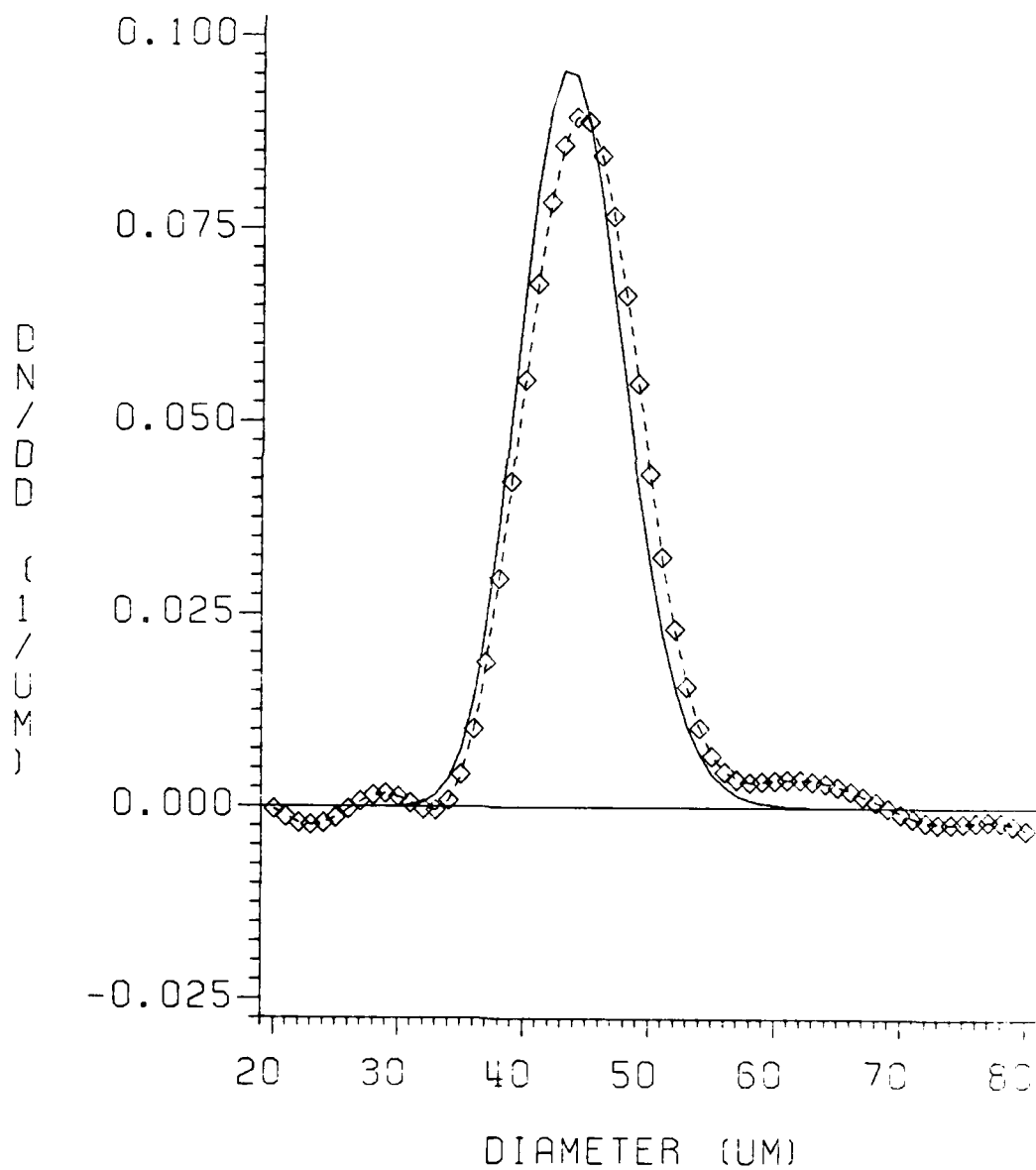


Figure 12. Effect of noise on the reconstruction of particle size distribution using local random errors with 5%.

LOG NORMAL DISTRIBUTION (LN-50.,1.1) ERR=.1,0.

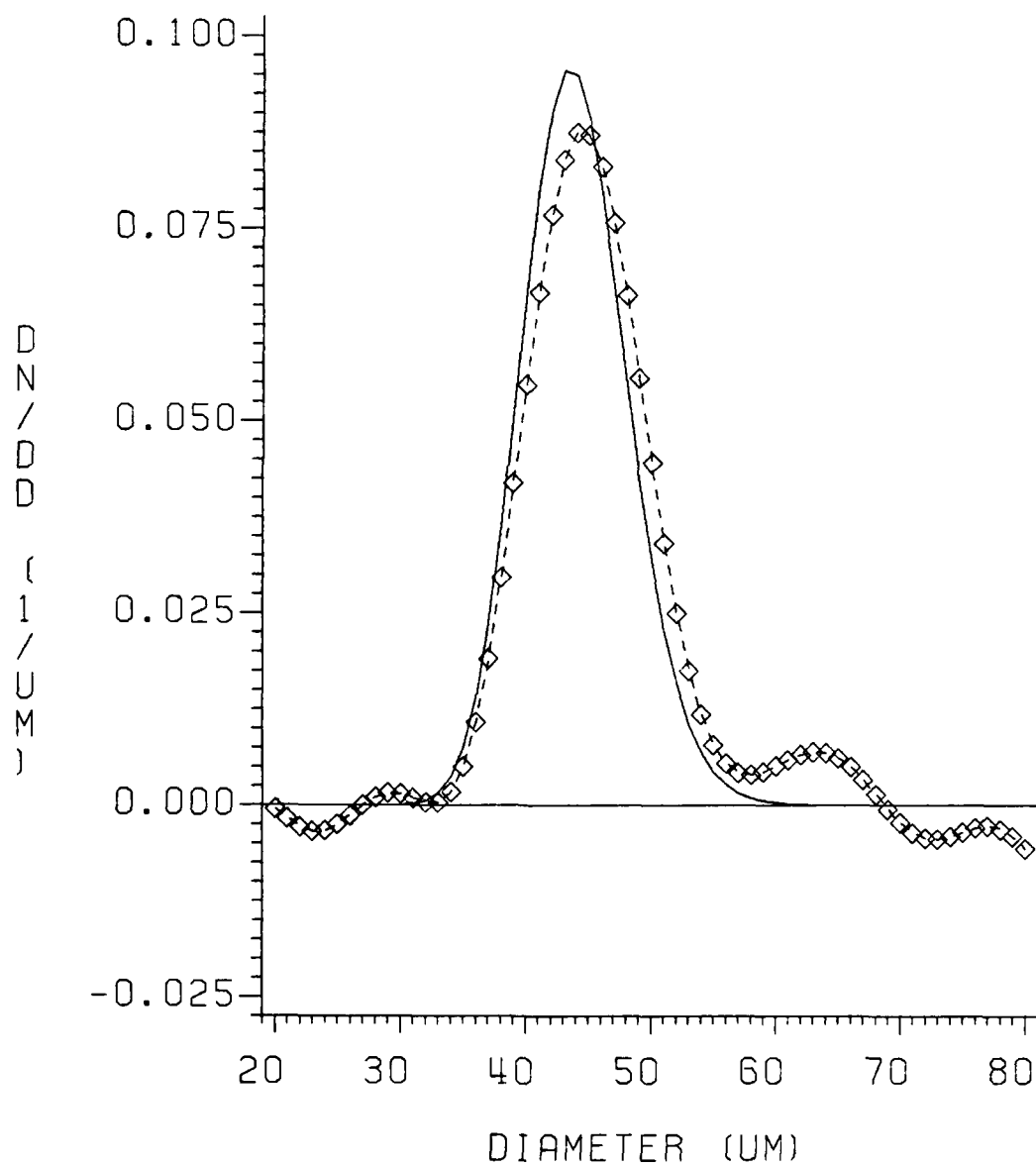


Figure 13. Effect of noise on the reconstruction of particle size distribution using local random errors with 10%.

LOG NORMAL DISTRIBUTION (LN-50.,1.1) ERR=.20,0.

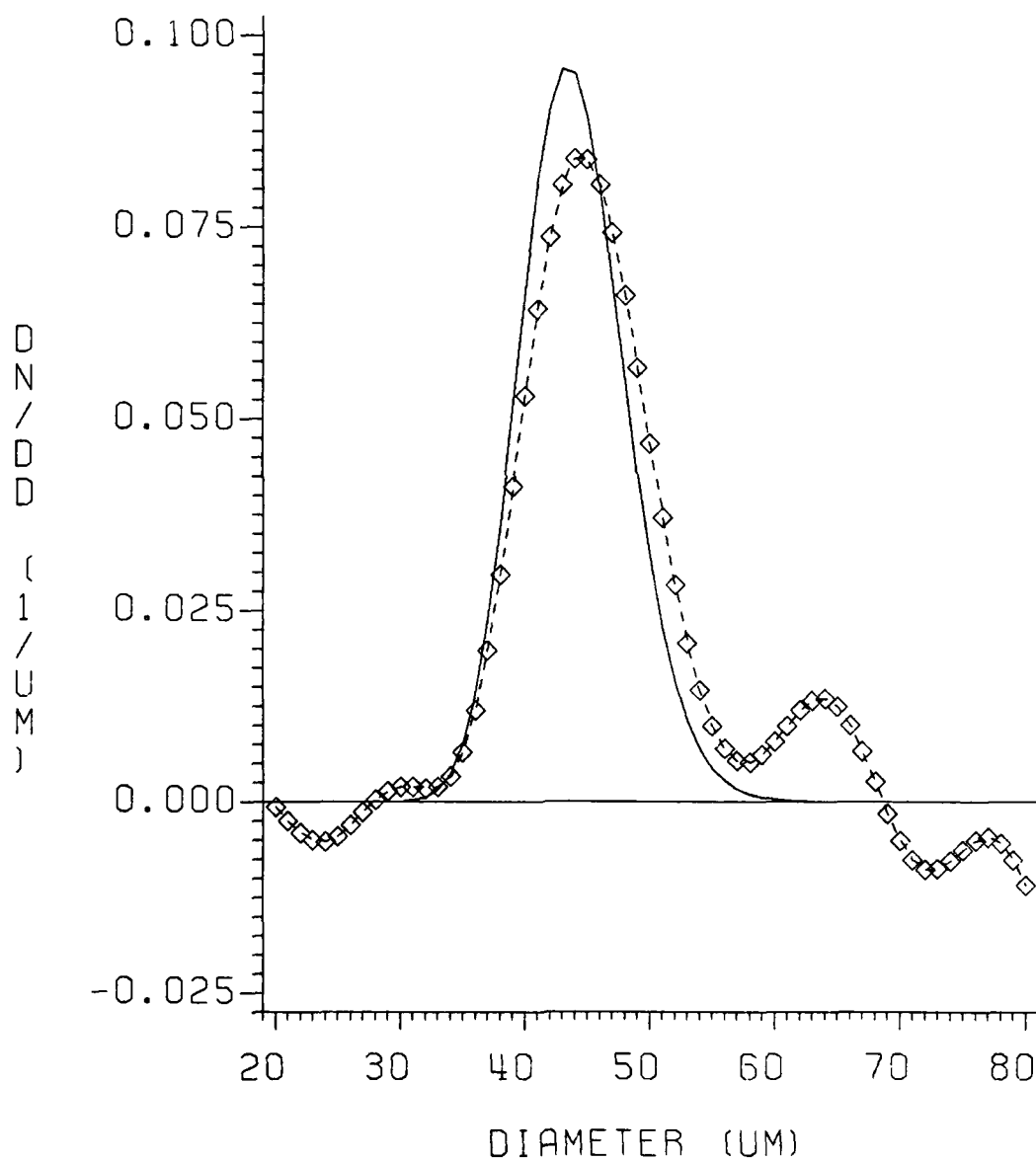


Figure 14. Effect of noise on the reconstruction of particle size distribution using local random errors with 20%.

LOG NORMAL DISTRIBUTION (LN-50.,1.1) ERR=0.,.01

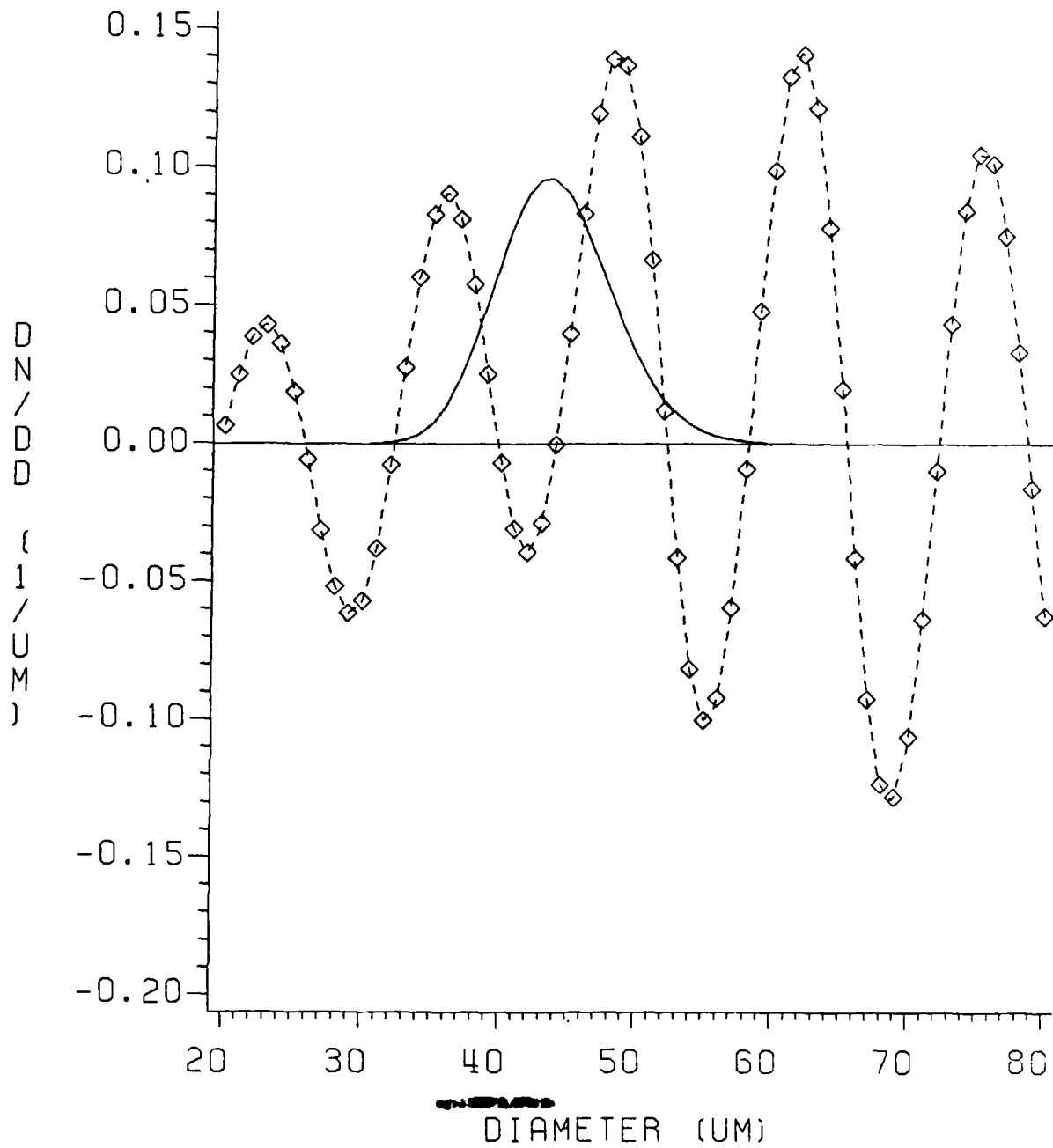


Figure 15. Effect of noise on the reconstruction of particle size distribution using ~~peak values~~ peak values of intensity with a dynamic range of 102. -26-

LOG NORMAL DISTRIBUTION (LN-50.,1.1) ERR=0.,.001

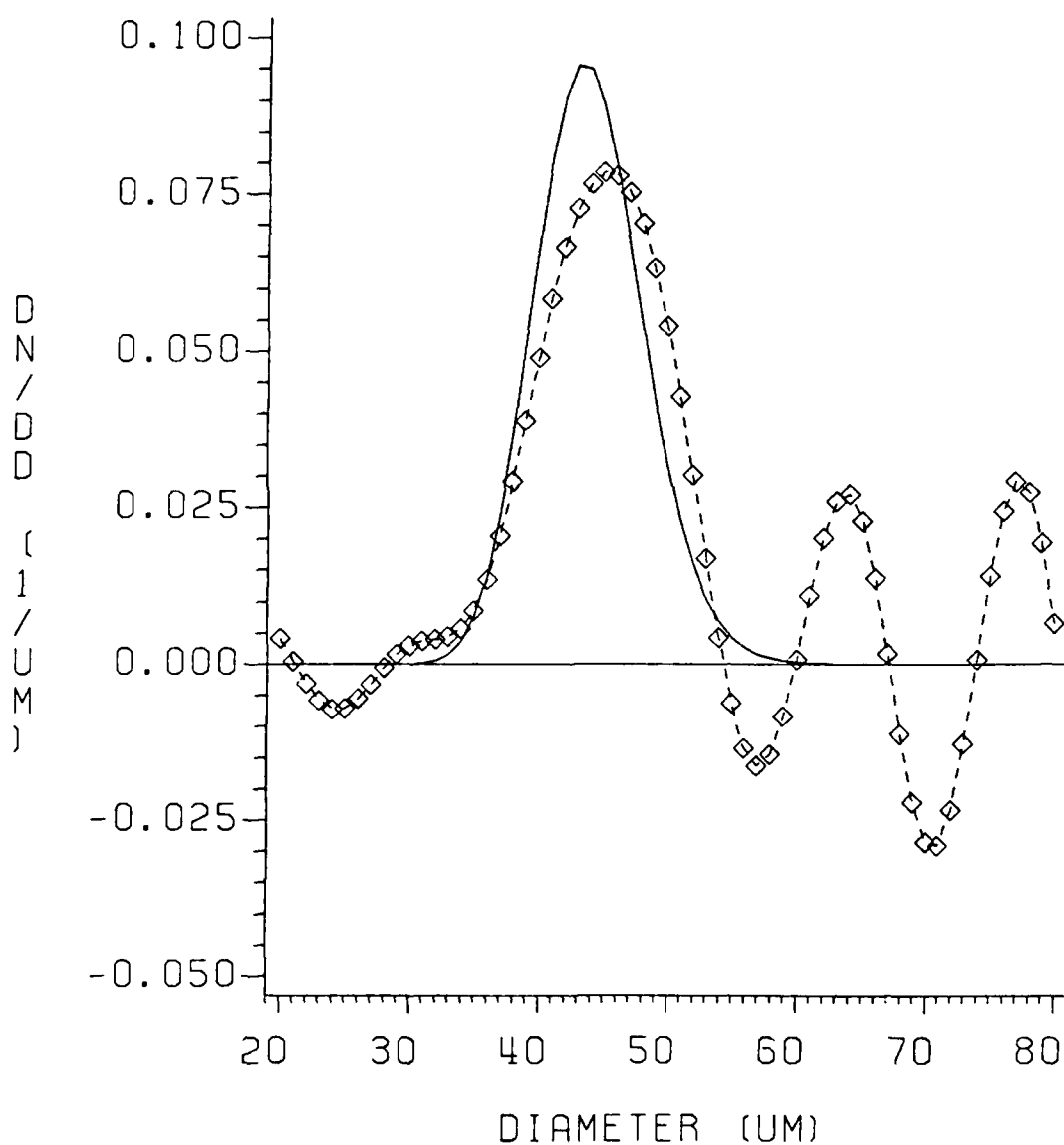


Figure 16. Effect of noise on the reconstruction of particle size distribution using ~~measured~~ peak values of intensity with a dynamic range of  $10^3$ .

~~measured~~

LOG NORMAL DISTRIBUTION (LN-50.,1.1) ERR=0.,.0001

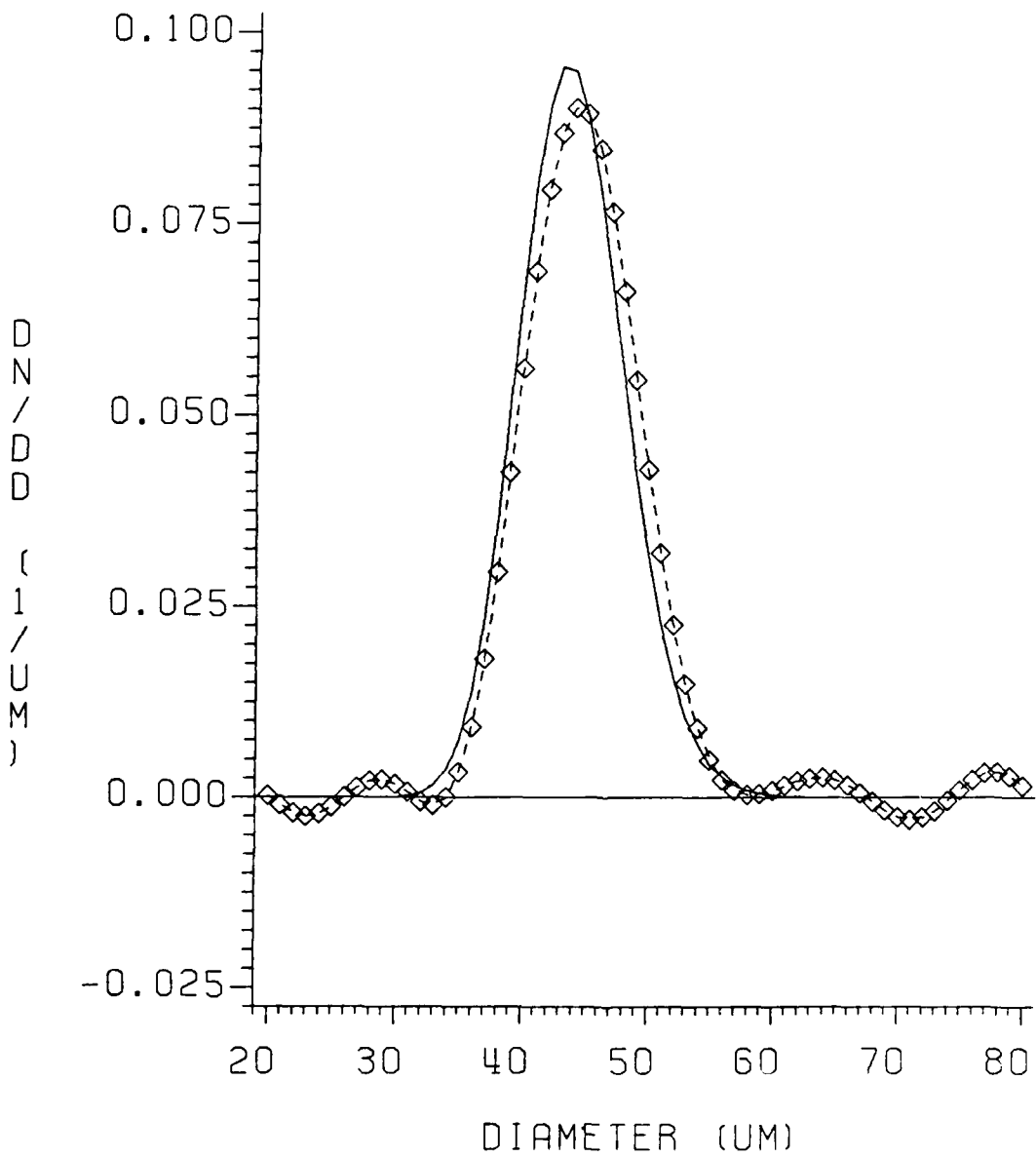


Figure 17. Effect of noise on the reconstruction of particle size distribution using ~~peak values~~ peak values of intensity with a dynamic range of  $10^4$

LOG NORMAL DISTRIBUTION (LN-50.,1.1) ERR=0.,.00001

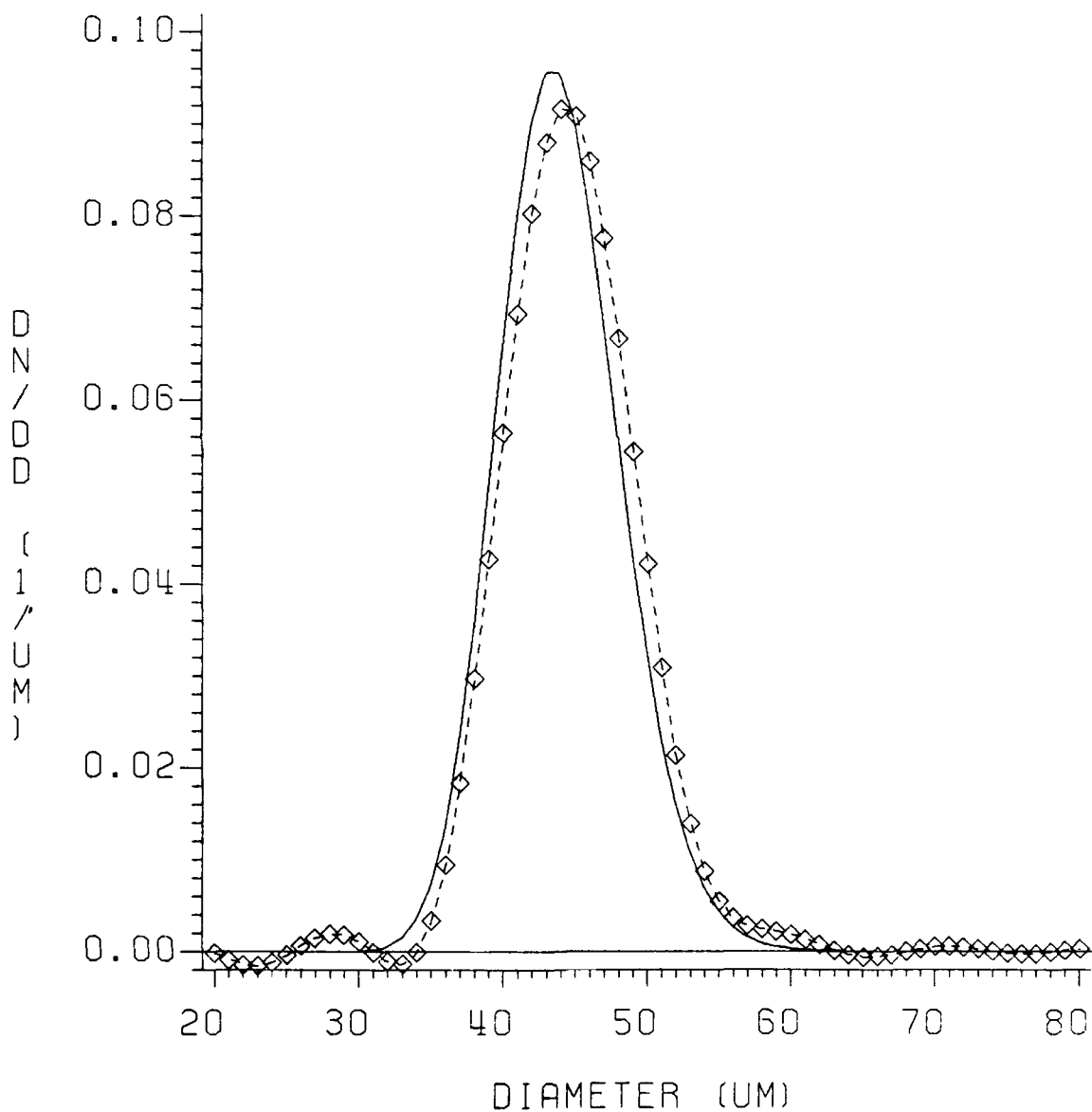


Figure 18. Effect of noise on the reconstruction of particle size distribution using ~~peak value~~ peak values of intensity with a dynamic range of  $10^3$ .

2. With proper forward cone angle ( $\theta_{\max}$ ) and angular resolution ( $\Delta\theta$ ), the solution is not seriously affected by random and systematic noise.
3. Examination of the integrand of the inversion formula can give insight in determining the  $\theta_{\max}$  to adequately reconstruct size distribution.

#### Acknowledgements

The authors gratefully acknowledge the support of the Office of Naval Research, Propulsion and Energetics Group, Dr. R.S. Miller, Director, and Garrett Turbine Engine Corporation Research Trust Fund at Arizona State University

#### VII. References

1. Dobbins, R.A., Crocco, L. and Glassman, I., "Measurement of Mean Particle Sizes of Sprays from Diffractively Scattered Light," AIAA Journal, Vol. 1, No. 8, pp. 1882-1886 (1963).
2. Dieck, R.H. and Roberts, R.L., "The Determination of the Sauter Mean Droplet Diameter in Fuel Spray Nozzles," Applied Optics, Vol. 9, No. 9, pp. 2007-2014 (1970).
3. Rizkalla, A.A. and Lefebvre, A.H., "The Influence of Air and Liquid Properties on Air Blast Atomization," Trans ASME Journal of Fluids Engineering, Vol. 97, pp. 316-320 (1975).
4. Tishkoff, J.M., Hammond, D.C., Jr., and Chraplyoy, A.R., "Diagnostic Measurements of Fuel Spray Dispersion," ASME, 80-WA/HT-35 (1980).
5. Allen, T., Particle Size Measurement, 3rd ed., Chapman S. Hall (1981).
6. Stockham, J.D. and Fuchtman, E.G., (eds.), Particle Size Analysis, Ann Arbor Science, Michigan (1979).
7. Cadle, R.D., Particle Size - Theory and Industrial Applications, Reinhold Publishing Corp. (1965).
8. Goulard, R. (Ed.), Combustion Measurements - Modern Techniques and Instrumentation, Hemisphere (1976).
9. Zinn, B.T. (Ed.), Experimental Diagnostics in Gas Phase Combustion Systems, American Institute of Aeronautics and Astronautics (1977).
10. Thompson, H.D. and Stevenson, W.H. (Ed.), Laser Velocimetry and Particle Sizing, Hemisphere (1979).

11. Simmons, H.C. and Lapera, D.J., "A High-Speed Spray Analyzer for Gas Turbine Fuel Nozzles," Parker Hannifin Corp., Cleveland, Ohio, ASME Gas Turbine Conference (1969).
12. Chigier, N.A., "Drop Size and Velocity Instrumentation," Progress in Engineering and Combustion Sciences, Vol. 9, pp. 155-177 (1983).
14. Hirleman, E.D., "Laser-based Single Particle Counters for in situ Particulate Diagnostics," Optical Engineering, Vol. 19, No. 6, pp. 854-860 (1980).
15. Malvern Instruments Ltd., Malvern, England.
16. Kerker, M., The Scattering of Light and Other Electromagnetic Radiation, Academic Press (1969).
17. Swithenbank, J., Beer, J., Taylor, D., Abbott, D., and McCreath, G., "A Laser Diagnostic Technique for the Measurement of Droplet and Particle Size Distribution," in Experimental Diagnostics in Gas Phase Combustion Engines, Progress in Aeronautics and Astronautics Series, B.T. Zina (Ed.), Vol. 53, pp. 421- (1977).
18. Swithenbank, J. and Taylor, D.S., "Size Distribution Measurement for Near Mono-disperse Particles and Sprays," Department of Chemical Engineering and Fuel Technology, University of Sheffield, Report HIC 315 (1979).
19. Chin, J.H., Shepceovich, C.M., and Tribis, M., "Determination of Particle Size Distribution in Polydisperse Systems by means of measurements of angular variation of intensity of forward scattered light at very small angles," J. Phys. Chem., Ithaca, Vol. 5, pp. 841-844 (1955).
20. Delves, L.M. and Welsh, J. Numerical Solution of Integral Equations, Clarendon Press, pp. 175-188 (1974).
21. Titchmarsh, E.C., "Extensions of Fourier's Integral Formula to Formula involving Bessel Functions," Proc. London Math. Soc., Vol. 23, XXIII (1925).
22. Abbiss, J.B., "Theoretical Aspects of the Determination of Particle-size Distributions from Measurements of Scattered Light Intensity," Royal Aircraft Establishment Technical Report 70151, Farnborough, England (1970).
23. Fymat, A.L. and Mease, K.D., "Reconstructing the Size Distribution of Spherical Particles from Angular Forward Scattering Data," in Remote Sensing of the Atmosphere: Inversion Methods and Applications, A.L. Fymat and V.E. Zuer (Ed.), Elsevier, Amsterdam (1980).
24. Ruscello, L.V. and Hirleman, E.D., "Measurement of Droplet Size Distributions Using a Photodiode Array," Paper 81-49, 1981 Fall Meeting, Western States Section Combustion Institute, Oct. 19-20, 1981, Arizona State University, Tempe, AZ.

25. Felton, P.G., "Measurement of Particle/Droplet Size Distributions by a Laser Diffraction Technique," presented at the 2nd European Symposium on Particle Characterization, Nuremberg, W. Germany, Sept. 24-26 (1979).
26. Alger, T.W., "Polydisperse - particle Size Distribution Function Determined from Intensity Profile of Angularly Scattered Light," Applied Optics, Vol. 18, pp. 3494 (1979).
27. Caroon, T.A. and Borman, G.L., "Comments on Utilizing the Fraunhofer Diffraction Method for Droplet Size Distribution Measurement," Combustion Science Technology, Vol. 19, pp. 255 (1979).
28. Mugele, R.A. and Evans, H.D., "Droplet Size Distribution in Sprays," Industrial and Engineering Chemistry, Vol. 43, No. 6, pp. 1317-1374 (1951).
29. Williams, A., Combustion of Sprays of Liquid Fuels, Paul Elek (Scientific Books) Ltd. (1976).
30. Santer, R. and Herman, M., "Particle Size Distributions from Forward Scattered Light using the Chahine Inversion Scheme," Applied Optics, Vol. 22, No. 15, pp. 2294-2301 (1983).
31. Rosin, P., Rammler, E., J. Inst. Fuel, Vol. 7, pp 29 (1933)
32. Chow, L.C. and Tien, C.L., "Inversion Techniques for Determining the Droplet Size Distribution in Clouds: Numerical Examination," Applied Optics, Vol. 15, No. 2, pp. 378-383 (1976).

## **Nonintrusive Laser-Based Particle Diagnostics-Invited Review**

E.D. Hirleman

*Reprinted from Combustion Diagnostics by Nonintrusive Methods, edited by Jeffrey A. Roux and T. Dwayne McCay, Vol. 92 of Progress in Astronautics and Aeronautics, 1984.*

# Nonintrusive Laser-Based Particle Diagnostics

E. Dan Hirleman\*

Arizona State University, Tempe, Arizona

## Abstract

The evolution of nonintrusive optical techniques for particle size analysis has provided an array of powerful diagnostics. The techniques either probe the light scattering/attenuation properties of the aerosol particles or form photographic or holographic images. This paper discusses the theoretical basis for in situ particle sizing techniques and reviews some practical applications as well. A number of subtle considerations which affect the reliability and interpretation of data from optical particle sizing instruments are discussed.

## Nomenclature

$C_{sc}$	= partial light scattering cross section
$d$	= particle diameter
$D_{32}$	= volume-to-surface area mean diameter
$F$	= differential light scattering cross section
$i_1, i_2$	= scattering intensity functions
$I$	= intensity or time-averaged radiant energy per unit area normal to the propagation direction
$I_{sc}$	= scattered intensity
$I_{inc}$	= intensity incident upon a particle
$J_1$	= spherical Bessel function of first kind and first order
$k$	= proportionality constant in Eq. (7)
$n$	= complex refractive index
$n(\alpha)$	= particle number distribution function
$N$	= exponent parameter for Rosin-Rammler particle size distribution

---

Presented as Paper 83-1514 at the AIAA 18th Thermophysics Conference, Montreal, Canada, June 1-3, 1983. Copyright American Institute of Aeronautics and Astronautics, Inc., 1983. All rights reserved.

\*Associate Professor, Mechanical and Aerospace Engineering.

- $P_{sc}$  = scattered optical power  
 $r$  = distance from origin to observation point in particle centered light scattering coordinate system  
 $S$  = light scattering signal amplitude  
 $x$  = mean diameter in Rosin-Rammler particle size distribution  
 $\alpha$  = particle size parameter  $\pi d/\lambda$   
 $\delta$  = fringe spacing  
 $\lambda$  = wavelength  
 $\theta$  = scattering angle measured from the incident beam propagation vector  
 $\varphi$  = azimuthal scattering angle

### Introduction

There are many instances when conventional batch sampling methods for particle size analysis are either impractical or impossible to implement. Further, it is often the case that the intrusive nature of sampling methods introduce unacceptable levels of interference into the aerosol flow of interest. For these reasons the development of nonintrusive optical diagnostics for particle size and concentration measurements has been the objective of a significant amount of research and development. Successful applications of this technology are being reported with increasing frequency.

Optical techniques for particle measurements can be divided into three broad areas. First, photographic and holographic methods analyze simultaneously recorded images of a number of individual particles to build a discrete particle size histogram. Secondly, ensemble or multi-particle analyzing methods utilize aggregate light scattering or extinction properties of a large number of particles to determine parameters of the particle size distribution. Finally, single particle counters (SPC) size and count individual particles traversing a relatively small optical sample volume, and a sequence of particles are sampled in order to build up a discrete size distribution. The three approaches are complementary in the sense that they are optimized for different types of applications.

Single particle counters are the optimum choice for analyzing particles greater than about  $0.3 \mu\text{m}$  in applications demanding high specificity and the potential for simultaneous velocity measurements. The existing commercial technology of imaging techniques is generally limited to particles larger than a few micrometers with time response longer than a few seconds. Imaging techniques can provide information on particle morphology not retrievable with light scattering methods. Ensemble methods generally

require less sophisticated optical systems for implementation but inherently provide less information as the optical characteristics of the individual particles are superimposed and can never be totally recovered.

This paper first presents a brief discussion of the fundamental principles of light scattering which underlie laser-based particle sizing technology. Then details of some of the techniques for nonintrusive particle diagnostics are reviewed. For the purposes of this paper an instrument is considered to be nonintrusive if no sampling probes are involved and the working space between optical elements and the optical measurement volume is on the order of 10 cm or greater.

### Light Scattering by Particles

An infinite, planar electromagnetic wave can propagate through a homogeneous, nonabsorbing medium undisturbed. This propagation is rigorously described by Maxwell's equations.<sup>1</sup> However it is also useful to consider Huygens' principle<sup>2</sup> which states that each point on a wavefront (surface of constant phase in the electromagnetic wave field) serves as the source of spherical secondary wavelets such that the wavefront at some later time is determined by the envelope of these wavelets. The secondary wavelets propagate with the same frequency and speed as the primary wave would at each point in space. The fact that an infinite planar wavefront in a homogeneous medium propagates as a plane wave is readily visualized with Huygens' construction.<sup>2</sup>

If we consider the homogeneous medium to be a gas, then the secondary wavelets derive from electrons in the molecules comprising the gas which are harmonically accelerated by the time-varying E-field in the electromagnetic wave. This occurs because each accelerating electron, by virtue of Ampere's and Faraday's Laws,<sup>2</sup> produces its own secondary electromagnetic wave (i.e. a scattered wavelet) which propagates spherically outward. The superposition of these scattered wavelets with the unscattered incident wave define the entire electromagnetic field. From a quantum point of view, the gas molecule absorbs a photon which causes an electron to be excited into a virtual (unstable or disallowed) state for a very short ( $< \text{psec}$ ) time. In elastic scattering events of interest here the electron then drops back to its original state emitting a second photon of the same frequency as the incident photon. This emission or scattering process is random in the sense that the photon can propagate with equal probability in any direction (at least in the plane normal to the polarization vector of the

incident E-field). The memory of the molecule retains only the phase and polarization of the incident photon and not the direction of incidence.

It is also possible for the energy coupled into the electron from the incident photon to be dissipated by collisions of the excited electron with other nuclei or electrons. In that situation the photon energy would have been absorbed and converted into thermal (internal kinetic) energy. Both the scattering and absorption processes are included in rigorous light scattering theory.

### Individual Spherical Particles

The parameters controlling the scattering of planar electromagnetic radiation by isolated spherical particles are the size parameter  $\alpha$ , the complex refractive index  $n$  of the particle relative to the surroundings, and the polarization state of the incident radiation. The three scattering regimes of importance can be delineated as Rayleigh scattering for  $\alpha \ll 1$ , geometric optics for  $\alpha \gg 1$ , and Lorenz-Mie scattering for  $\alpha \sim 1$ . For visible radiation Rayleigh scattering approximations are valid for particle diameters  $d < 0.05 \mu\text{m}$ , and geometric optics approximations for roughly  $d > 5 \mu\text{m}$ . In the Rayleigh regime all of the electrons (or charge dipoles) in a particle are subjected to the same E-field by virtue of their close proximity (relative to the wavelength) and therefore oscillate in phase. The properties of the scattered radiation are then given in a very simple form applicable to the harmonic oscillation of a charge dipole. In the geometric optics limit, the wavelength is much smaller than the particle dimensions and the incident radiation can be considered to be a bundle of rays. The scattered field at any point distant from the particle (far field) can be calculated by coherent superposition of the refracted and reflected rays with the diffracted field.

In contrast with the Rayleigh scattering and geometric optics regimes, no approximations are possible for particle sizes on the order of the wavelength and the complete set of Maxwell's equations must be solved for the particle and the surroundings. The theoretical difficulties here arise from the fact that the E-fields experienced by the various electrons or charge dipoles distributed throughout the particle depend on position, and therefore these electrons emit secondary wavelets which are out of phase. The formulation for this intermediate case, known as Lorenz-Mie theory, is the general solution for all particle sizes. Exhaustive treatises of light scattering are given by van de Hulst<sup>3</sup> and Kerker.<sup>4</sup> Computer codes for calculating the

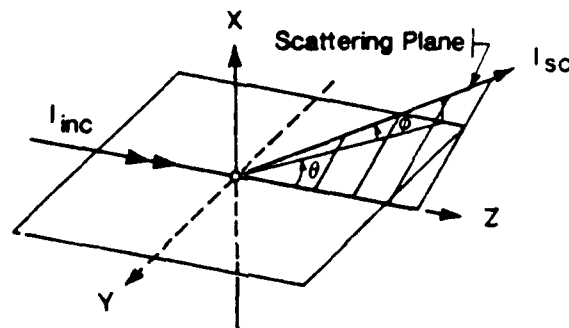


Fig. 1 Light scattering coordinate system. The functions  $i_1$  and  $i_2$  are for scattered light polarized perpendicular and parallel to the scattering plane respectively.

scattering characteristics of spherical particles of arbitrary size are readily available.

Consider the scattering geometry in Fig. 1 with a particle at the origin illuminated by linearly polarized electromagnetic radiation propagating in the +z direction with incident intensity  $I_{inc}$ . The scattered intensity  $I_{sc}$  at some point a distance  $r$  from the origin is given by

$$I_{sc} = \frac{I_{inc}\lambda^2}{4\pi^2r^2} [i_1(\alpha, n, \theta)\sin^2\phi + i_2(\alpha, n, \theta)\cos^2\phi] \quad (1)$$

where  $i_1$  and  $i_2$  are dimensionless intensity functions for scattered light polarized perpendicular and parallel to the scattering plane, respectively. The functions  $i_1$  and  $i_2$  are composed of spherical Bessel and associated Legendre functions and their first derivatives, and are integral parts of Lorenz-Mie theory.<sup>3,4</sup> It is convenient to normalize Eq. (1) by the incident intensity and other constants and define the differential scattering cross section  $F$ :

$$F \equiv i_1(\alpha, n, \theta)\sin^2\phi + i_2(\alpha, n, \theta)\cos^2\phi \quad (2)$$

Some computations of  $F$  are shown<sup>5</sup> in Figs. 2-4. Figure 2 indicates the angular dependence of the scattered light for particle diameters of 0.1, 0.5, and 1.0  $\mu\text{m}$ , and Fig. 3 for 5.0 and 10.0  $\mu\text{m}$  particles as well. Note the lobe structure which becomes a dominant factor as particle size increases. Figure 4 indicates the dependence of  $F$  on particle size. In the Rayleigh regime  $F$  increases as diameter to the sixth power, and then gradually changes to a diameter-squared dependence in the geometric optics regime. The oscillations present for  $\theta = 45$  and 90 deg in Fig. 4 are typical for off-axis scattering of nonabsorbing (no imaginary component of the refractive index) particles. Forward scattering (small

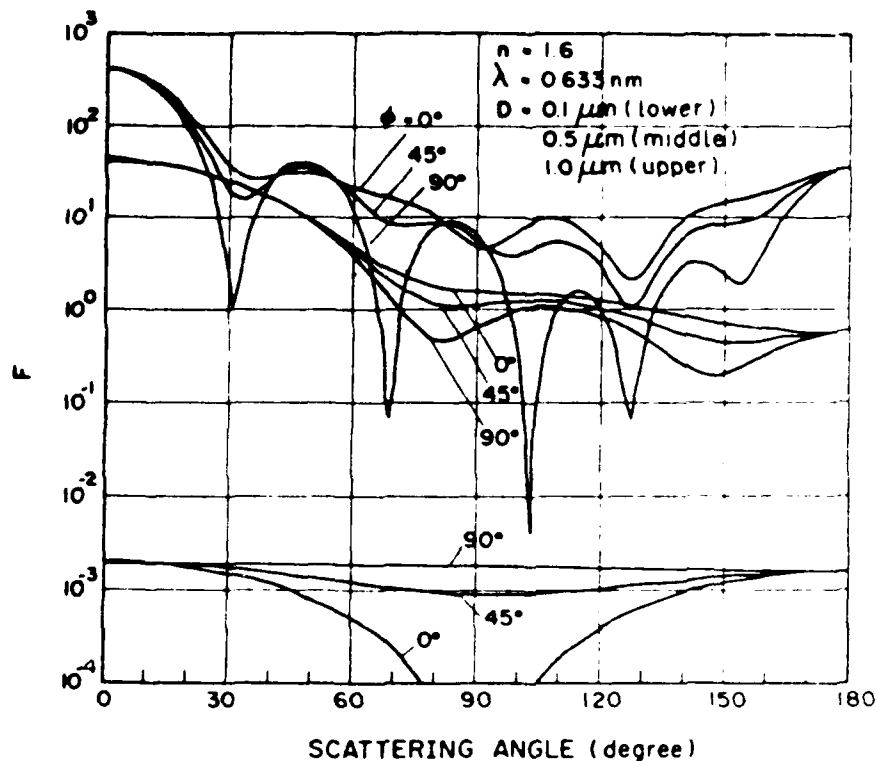


Fig. 2 Lorenz-Mie theory calculations of differential scattering cross-section  $F$  as a function of scattering angle  $\theta$  for various particle diameters after Handa et al.<sup>5</sup>

$\theta$ ) properties generally display much less structure as is also evident in Fig. 4.

The radiant power  $P_{SC}$  scattered into a detector with a finite collection aperture is obtained by integrating the scattered intensity over the solid angle subtended by the detector

$$P_{SC} = \frac{I_{inc}\lambda^2}{4\pi^2} \iint F(\alpha, n, \theta, \phi) \sin\theta \, d\theta \, d\phi \quad (3)$$

The partial scattering cross section for a particular detector is defined as the scattered power divided by the incident intensity

$$C_{SC} = \frac{\lambda^2}{4\pi^2} \iint F(\alpha, n, \theta, \phi) \sin\theta \, d\theta \, d\phi \quad (4)$$

Note that Eqs. (3) and (4) apply in a practical measuring system only if the scattered light wave experiences negligible distortion due to secondary scattering off of other particles in the field before reaching the detector. In other words Eqs. (3) and (4) are applicable in single

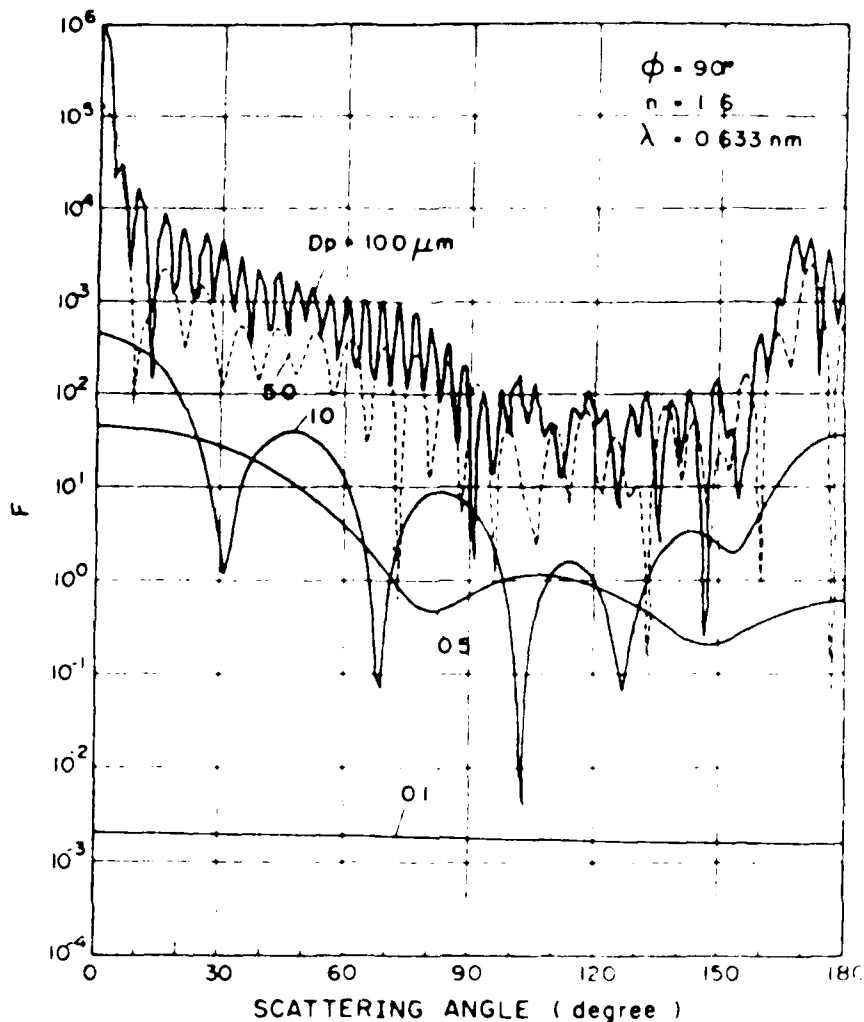


Fig. 3 Lorenz-Mie theory calculations of differential scattering cross-section  $F$  as a function of scattering angle  $\theta$  for various particle diameters after Handa et al.<sup>5</sup>

scattering aerosols and must be altered when multiple scattering (secondary scattering events) is significant.

#### Individual Nonspherical Particles

It is not possible at present to calculate the scattering and absorption characteristics of particles of arbitrary shape and refractive index. There has, however, been some progress on theoretical models and calculations for certain nonspherical shapes such as ellipsoids,<sup>4</sup> spheroids,<sup>6,7</sup> clusters of spheres,<sup>8</sup> and cylinders.<sup>9</sup> The calculations are often valid for only limited values of refractive index.

Some experimental work on the scattering characteristics of nonspherical particles has been performed. The

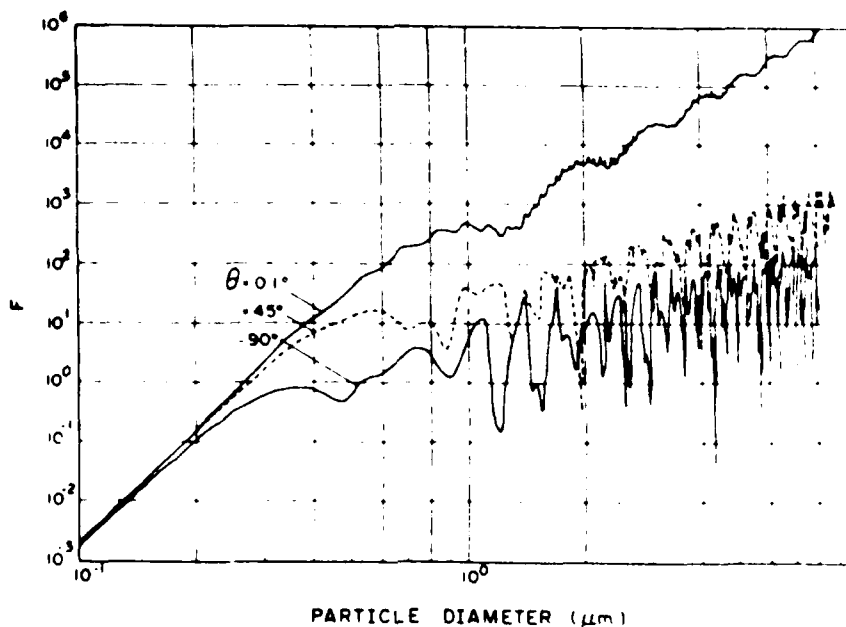


Fig. 4 Lorenz-Mie theory calculations of differential scattering cross-section  $F$  as a function of particle diameter for various  $\theta$  after Handa et al.<sup>5</sup>

use of microwave radiation with wavelengths on the order of 1 cm permits the study of scattering by arbitrary shapes.<sup>10,11</sup> Forward scattering by agglomerates of spherical particles has also been observed experimentally.<sup>12</sup>

The results of these studies indicate that -- near-forward scattering characteristics of nonspherical particles are predicted reasonably well by calculations for spherical particles of equal cross-sectional area. The off-axis scattering characteristics however are strongly dependent on the detailed particle shape. Concerning extinction (scattering plus absorption) spheres of equal volume or surface area have been used to approximate these optical properties of nonspherical particles.<sup>13</sup>

#### Scattering by an Ensemble of Particles

Often in particle diagnostics experiments it is either undesirable or impossible to define an optical sample volume small enough to ensure that less than one particle on average is in the volume. In that case the aggregate scattering properties of a number of particles are measured. Interpretation of the resulting ensemble or multiparticle scattering measurements (not to be confused with multiple scattering) is straightforward if the detected light has undergone only one scattering event. That is, if single scattering is predominant then the presence of other particles in the aerosol cloud has a negligible effect. In

that situation light scattering in the far field is just the superposition of isolated single scattering contributions from each particle in the scattering volume. If there are a very large number of randomly positioned particles in the optical sample volume then superposition of the scattered intensity contributions (incoherent scatter) describes ensemble scattering properties. Conversely, if there are either relatively few particles or the particles are positioned in regular or quasi-ordered fashion then interference phenomena become important and the superposition must use scattered E-fields (coherent scatter) rather than intensities.

There are practical situations where single scattering approximations are not valid. For example two particles spaced closer than a few diameters apart will scatter as a single entity and Lorenz-Mie theory would not apply. Fortunately this situation occurs rather infrequently. Of more practical concern is the case where the particles on average are well separated but particles adjacent to the sample volume distort the scattered wave before it reaches the detector.

### Multiple Scattering

As the physical size of an aerosol cloud increases, the probability that a scattered photon or ray will encounter another particle and be scattered again before leaving the aerosol increases as well. This phenomenon, termed multiple scattering, will clearly alter the characteristics of the scattered light which finally reaches the detector of a diagnostic instrument. Therefore the presence of multiple scattering significantly complicates the interpretation of light scattering measurements. The level of multiple scattering can be ascertained from the level of attenuation of the incident beam. For an axisymmetric aerosol with a centered optical sample volume the fraction of detected scattered light which has undergone only one scattering event is approximately equal to the square root of the fraction transmission of the incident beam. Some degree of multiple scattering is inherent in all measurements and the significance of this effect depends on the application. In particular, the anisotropy of the single scattering signature of the aerosol of interest plays a significant role in determining the sensitivity of measurements to multiple scattering. For example, Felton<sup>14</sup> performed a series of laser diffraction particle size measurements on 45  $\mu\text{m}$  polystyrene latex spheres in a water flow cell. The ensemble scattering method assumed that the particle size distribution was Rosin-Rammler and determined the mean diameter

and a width parameter. Measurements were taken for a series of latex particle concentrations which gave transmission fractions from 0.92 to 0.03. With increasing concentrations (decreasing optical transmission) the mean diameter decreased as expected since the secondary scattering events further diffused the forward scattered light giving the appearance of smaller particles. At 50% transmission Felton<sup>14</sup> observed approximately a 5% decrease in apparent mean diameter relative to the high transmission (single scattering) limit.

### Ensemble (Multiparticle) Sizing Techniques

Optical techniques which analyze the light scattering and extinction properties of an ensemble of particles are invaluable in some applications. For measurements of particles smaller than about  $0.1 \mu\text{m}$ , ensemble methods are the only viable options since SPC and imaging techniques generally cannot distinguish these particles. The lower size limit of a typical SPC is determined by one of two factors. First, scattering signals from individual small particles become rapidly indistinguishable from detector shot noise since the scattering cross sections decrease as  $d^6$  in the Rayleigh regime. Second, typical particle number densities increase as  $d^{-4}$  (Junge distribution) making it eventually impossible to maintain the presence of only one particle in the optical sample volume. Imaging techniques are useless for particles smaller than several wavelengths, and since visible or in some cases near ultraviolet radiation is generally used imaging methods are limited to particles several  $\mu\text{m}$  and above.

Ensemble measurements inherently contain less information than SPC and imaging data as the scattering or extinction is averaged over all particle sizes in the aerosol. In some situations it is possible to mathematically invert the set of ensemble measurements and reconstruct or estimate the size distribution. The maximum resolution possible for the reconstructed size distribution is determined by the number of optical property measurements (e.g. the number of scattering angles), but practical considerations often limit here. It is often advantageous to estimate average parameters of the aerosol such as a mean diameter rather than perform the complete inversion. Similarly the form of the size distribution can be assumed and the measurements used to estimate the best fit parameters for the assumed size distribution.

Several ensemble-averaged optical properties of aerosols can be used in size analysis. These include spectral extinction, the angular dependence of scattered

light, and finally for very small particles the spectral properties of the scattered light as Doppler-shifted by the Brownian motions of the particles. The following paragraphs discuss in further detail these ensemble methods.

### Extinction Methods

The amount of light removed from a beam passing through an aerosol directly indicates the extinction cross sections of the particles along the beam path. If the refractive index and the volume concentration of the particles are known, then the volume-to-surface area mean diameter  $D_{32}$  (or Sauter Mean Diameter, SMD) can be determined from a single transmission measurement.<sup>15</sup> Further, the authors<sup>15</sup> studied the ratio of the transmittance at two probe wavelengths and found that it exhibited monotonic behavior when plotted as a function of  $D_{32}$  for nonabsorbing particles in the range  $\lambda_1/3 < D_{32} < \lambda_2$ . Ariessohn et al.<sup>16</sup> also studied this two-wavelength approach and found that the specific form of the particle size distribution, if it was not very narrow, had little influence on the measurement. The authors<sup>16</sup> considered measurements on coal ash particles which are weakly absorbing and found a compressed but useful sizing range of roughly  $\lambda_2/10 < D_{32} < 1.3\lambda_2$  for  $\lambda_1 = 0.325 \mu\text{m}$  and  $\lambda_2 = 3.39 \mu\text{m}$ . Lester and Wittig<sup>17</sup> and Bro<sup>18</sup> utilized a similar method in shock tube studies of soot formation. Powell et al.<sup>19</sup> used spectral transmission data coupled with scattering measurements to study smoke particle sizes. Although in the works referenced above only mean diameters are determined, there have also been a number of studies on the use of spectral transmission measurements to determine the size distribution as well.<sup>20</sup> For optimum sensitivity the wavelengths used must roughly bracket the particle sizes of interest, so these techniques are in general useful for intermediate particle sizes near practical wavelengths.

### Multiangle Scattering Measurements

It is clear from Figs. 2-4 that the angular scattering characteristics of an ensemble of particles will contain information on the particle size distribution. For small particles, say several  $\mu\text{m}$  and below, it is necessary to measure scattering characteristics over a large range of scattering angles. This can be accomplished for  $\theta$  from 2 deg to 178 deg using a polar nephelometer as discussed by Hansen and Evans.<sup>21</sup> Hansen then used this technique<sup>22</sup> to estimate size distributions and refractive indices of an atmospheric aerosol. In some situations it is impractical to traverse a detector around the aerosol to measure angular

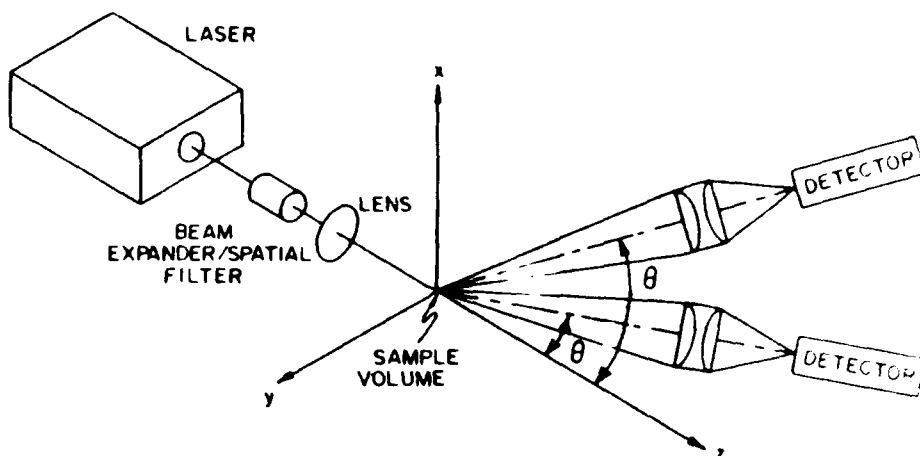


Fig. 5 Generalized schematic of a laser-based single particle counter.

scattering characteristics, and a few detectors at selected scattering angles are used.

Multiangle ensemble scattering techniques are utilized in some situations where SPC and imaging methods are not applicable. Measurements in solid-propellant rocket exhausts where the particle velocities are very high and the run times very short have been made by McCay et al.<sup>23</sup> using multiangle scattering and extinction. Measurements of soot particle sizes in flames require ensemble methods because of the small sizes (<100 nm). Recent studies on soot by Santoro and Semerjian<sup>24</sup> and Chang and Penner<sup>25</sup> have been completed although the presence of nonspherical agglomerates complicate interpretation of the data. The authors<sup>23-25</sup> used an optical system similar to that in Fig. 5 but with some detectors oriented in the backscatter direction because of the small particle sizes. Measurement of the polarization state of the scattered radiation is also useful in particle size analysis by ensemble multiangle scattering.

One problem for all multiwavelength or multiangle diagnostics for particle sizes of several micrometers and below is that the scattering characteristics can be strongly influenced by the refractive index which is in general not known. By increasing the number of measurements and assuming that the size distribution is monodisperse or of some particular form it is possible in theory to determine the refractive index along with the size distribution.<sup>22,24,26</sup>

As particle size increases it can be seen from Fig. 3 that the energy is scattered predominantly into the near-forward directions. Further, for particles greater than several  $\mu\text{m}$  the dominant contributor to the forward lobe is diffractive scatter as opposed to refraction or reflection.

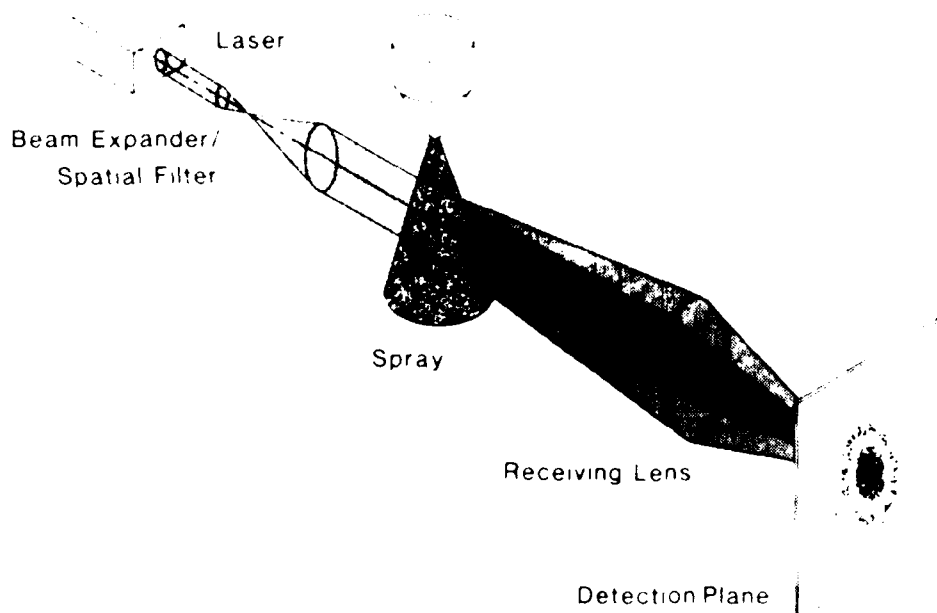


Fig. 6 Schematic of laser diffraction particle sizing instrument.

Analysis of the forward diffraction lobe has become a common diagnostic for particles and droplets larger than several micrometers in diameter.

The generalized schematic of a laser diffraction particle sizing apparatus is shown in Fig. 6. The beam from a laser, typically a several mW He-Ne model, is spatially filtered, expanded, and collimated to several mm diameter at the  $1/e^2$  intensity points. This collimated probe beam is directed through the aerosol of interest and the transmitted (unscattered) portion is focused on-axis to a spot at the back focal plane of the receiving lens. Light scattered by particles in the probe beam which passes through the aperture of the receiving lens is directed to off-axis points on the observation or detection plane. A monodisperse ensemble of spherical particles large compared to the wavelength would produce the characteristic Airy diffraction pattern shown in Fig. 6 as described by Fraunhofer diffraction theory

$$I(\theta) = I_{inc} \frac{\alpha^4 \lambda^2}{16\pi^2} \left( \frac{2J_1(\alpha\theta)}{\alpha\theta} \right)^2 \quad (5)$$

where  $J_1$  is the first-order Bessel function of first kind. The obliquity correction  $(1 + \cos^2\theta)/2$  has been neglected in Eq. (5) and the small angle approximation of  $\sin \theta = \theta$  has been made.

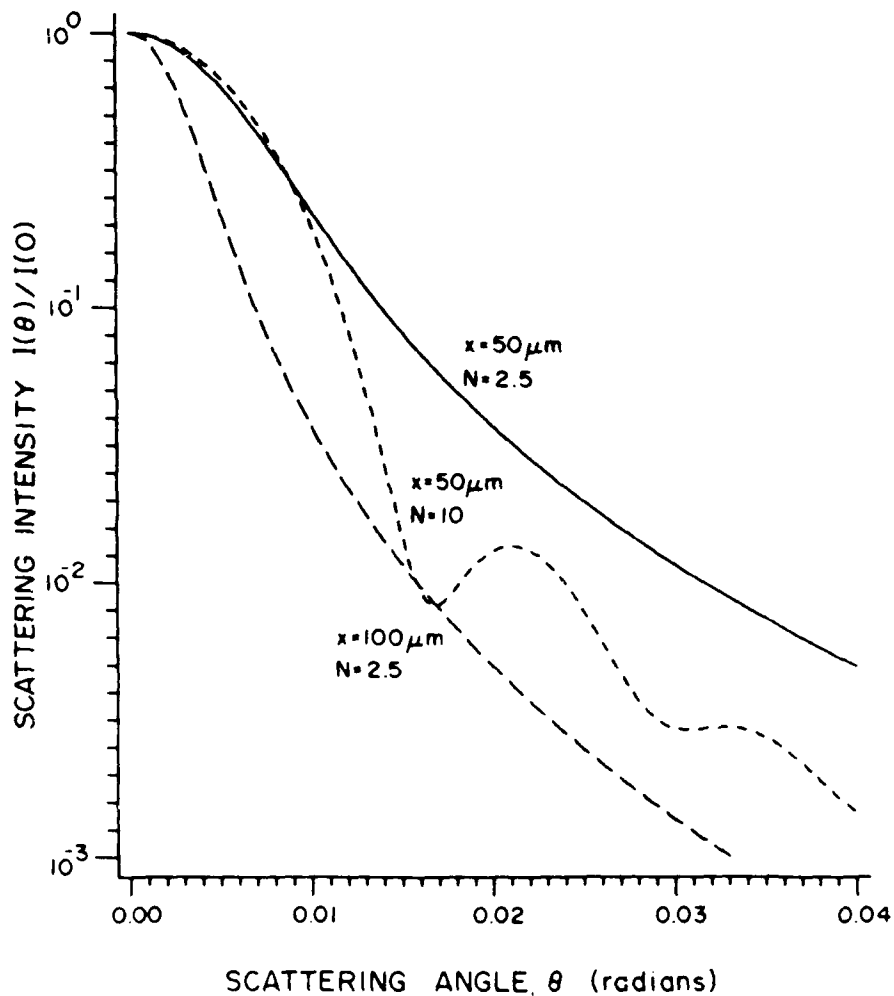


Fig. 7 Forward scattering signatures calculated using Fraunhofer diffraction theory for Rosin-Rammler particle size distributions.  $\lambda = 0.6328 \mu\text{m}$ .

In practical systems a distribution of particle sizes or a polydispersion is generally encountered. The composite scattered intensity profile is a linear combination of the characteristic profile of each droplet size with a weighting coefficient equal to the number of particles of that size in the sample volume. The diffraction signature of a polydisperse spray is given by

$$I(\theta) = I_{inc} \int_0^{\infty} \frac{\alpha^4 \lambda^2}{16\pi^2} \left( \frac{2J_1(\alpha\theta)}{\alpha\theta} \right)^2 n(\alpha) d\alpha \quad (6)$$

where  $n(\alpha)d\alpha$  is the number of particles in the laser beam with sizes between  $\alpha$  and  $\alpha + d\alpha$  and truncation of light diffracted at large angles by the receiving lens has been neglected.<sup>27</sup> A primary effect of broadened size distribu-

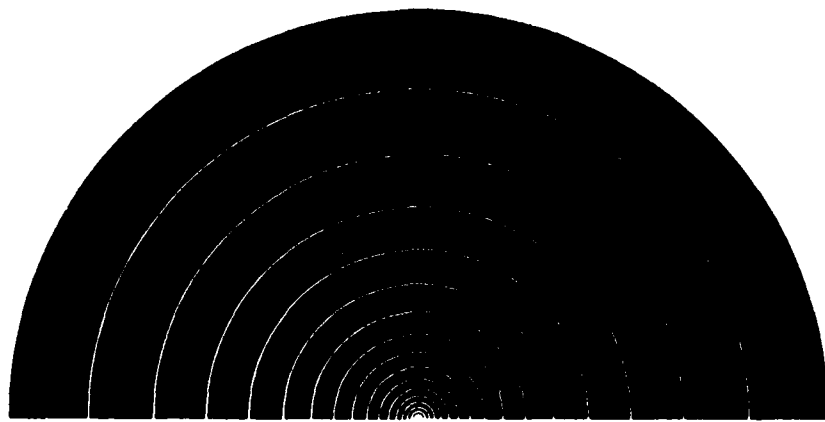


Fig. 8 Reproduction of the photosensitive elements of a monolithic P on N photodiode array detector after Hirleman.<sup>27</sup>

tions is elimination of the contrast in the diffraction pattern as shown in the diffraction signatures calculated for several Rosin-Rammler particle size distributions in Fig. 7. The two parameters in a Rosin-Rammler distribution are the mean diameter  $x$  and the exponent  $N$ . The width of the distribution increases with decreasing  $N$ , and as  $N$  approaches infinity the distribution becomes monodisperse.

The basic task in laser diffraction particle sizing is to detect and analyze the diffraction signature  $I(\theta)$ , and then mathematically invert Eq. (6) to determine parameters of the particle size distribution. Chin et al. in 1955<sup>28</sup> proposed several detection techniques, one of which was to traverse a pinhole/photodetector assembly across the diffraction pattern. Due to the mechanical traverse this detection approach requires a significant amount of time to cover the entire diffraction pattern. Further, the large dynamic range of the diffraction signature given by Eqs. (5) and (6) is another difficulty for such systems.

The advantages of real time analysis of the entire diffraction signature as opposed to traversing a detector across either the diffraction pattern itself or a photographic image thereof are obvious. Developments in monolithic solid state multielement detector arrays in the 1970's improved the situation by allowing the entire diffraction signature to be analyzed instantaneously. A monolithic detector designed for forward scattering measurements is shown in Fig. 8. Note the increasing thickness of the annular detector elements which, when coupled with increasing length (circumference), result in a significant increase in detector area as radius increases. This effect compresses the dynamic range of the scattering measurements. A detector similar to that in Fig. 8 designed for parts recognition applications<sup>29</sup> is utilized in a commercial laser

diffraction particle sizing instrument<sup>30</sup> based on the work of Swithenbank et al.<sup>31</sup>

A number of data processing methods have been used to extract particle size information from measured diffraction patterns. Chin et al.<sup>28</sup> utilized the integral transform derivation of Titchmarsh<sup>32</sup> to analytically invert Eq. (6) to obtain  $n(\alpha)$ . Dobbins et al.<sup>33</sup> somewhat paradoxically observed that the diffraction signatures were relatively independent of the form of the droplet size distribution and depended primarily on  $D_{32}$ . The authors<sup>33</sup> utilized a single parameter of the diffraction pattern, the angle at which the scattered light intensity is down to 10% of the on-axis value, to determine  $D_{32}$ . Others<sup>34,35</sup> have since modified slightly this approach and it is still in use today.

Swithenbank et al.<sup>31</sup> analyzed the diffraction pattern with the annular ring detector discussed above and subsequently did a numerical inversion (as opposed to integral transform) of a discretized form of Eq. (6) to obtain the volume distribution in 7 discrete size bins. The inversion problem is ill-conditioned and as a second approach the authors<sup>31</sup> assumed that the size distribution was of the Rosin-Rammler form with two independent parameters. Recent data processing developments do not require an assumption of the form of the size distribution.<sup>30,36</sup>

#### Diffusion Broadening Spectroscopy

One problem with spectral extinction and multiangle scattering measurements of small particles is the dependence on refractive index which is generally unknown and might even vary between particles. One diagnostic which for certain applications does not require knowledge of the refractive index is diffusion broadening spectroscopy. Light scattered by molecules or particles is Doppler shifted due to Brownian motion. The magnitude of the frequency shift depends on the velocity of the particle and the angle at which the scattered radiation is collected. Light scattered from a large number of particles undergoing Brownian motion in a medium with a mass mean velocity of zero contains a distribution of frequencies centered around the incident laser frequency. If the light scattered by these particles is collected and mixed on a single detector (homodyne detection) then the frequency differences between waves scattered from the various particles will be present in the detector output with a resulting spectrum centered around zero frequency. The theoretical analysis for predicting the power spectrum and autocorrelation function of the homodyne scattered light signal for particles suspended in a stagnant or laminar flow is well known.<sup>37</sup>

The predictions depend on the scattering angle, the particle diameter, and the diffusion coefficient which in turn depends on temperature and viscosity. By measuring the half-width of the power spectra<sup>38</sup> after Penner et al. or the correlation time<sup>39</sup> from photon correlation after King et al. the diffusion coefficient of the particles can be determined. Introduction of some assumptions concerning the diffusion coefficient then allows the particle size of a monodisperse aerosol to be determined.

The optical system required for diffusion broadening spectroscopy is rather simple as shown in Fig. 5. The laser focus diameter is selected to minimize broadening effects due to finite particle residence time.<sup>39</sup> The output from the detector would then go to a spectrum analyzer or a digital photon correlator.

Diffusion broadening spectroscopy has been used successfully in flames<sup>37-39</sup> and other particle systems. It is only useful for particle diameters less than about 100 nm because the frequency shifts become very small as the Brownian diffusion velocities decrease for larger particles. Further, this technique is only independent of refractive index for monodisperse aerosols, and successful application in polydisperse systems seems unlikely.

#### Laser/Optical Single Particle Counters (SPC)

A generalized schematic of an optical SPC is presented in Fig. 5. The output beam from a laser or other source of radiation is directed (and typically focused) into the optical sample volume. This sample or probe volume can be thought of as that region of space where a single particle can generate a sufficient detector signal to be discriminated or "seen" over the background noise. As individual particles pass through the sample volume they interact with the incident radiation beam (i.e., scatter, absorb, and/or fluoresce light) and are observed by detection optics oriented at some angle(s)  $\theta$  with respect to the beam propagation direction. The single particle signals obtained at the photodetector(s) are processed to provide information on the size and possibly the velocity of each particle. The various SPC approaches to particle sizing are discussed below.

#### Light Scattering Cross-section Measuring Techniques

The most common approach to particle sizing involves the principle that the amount of the light scattered by a particle is a nominally monotonic increasing function of

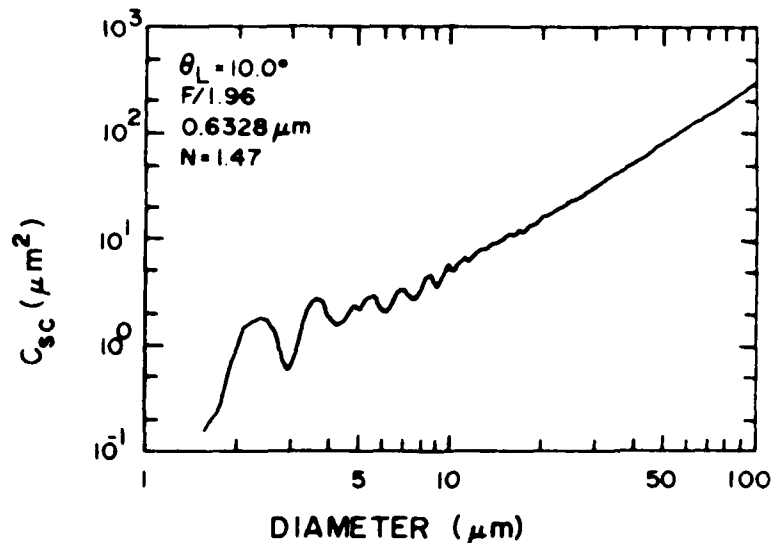


Fig. 9 Partial light scattering cross sections for spherical particles with refractive index  $n=1.47$  for  $f/1.96$  receiving optics oriented for  $10$  deg off-axis collection in the plane normal to the direction of polarization of the incident beam. The Lorenz-Mie theory calculations used  $\lambda = 0.6328 \mu\text{m}$ .

particle size. It follows that measurement of a scattering or extinction cross section can be used to infer particle size. The SPC scattering signal response  $S$  to a particle in an incident radiation field (uniform over the particle) of intensity  $I_{inc}$  is given by

$$S = k I_{inc} C_{sc} \quad (7)$$

where  $k$  is the system gain in transducing radiant energy to voltage using a photodetector and  $C_{sc}$  is the partial light scattering cross section as determined from Eq. (4). The partial cross sections, as opposed to total cross sections, depend on the specific finite aperture detector configuration in use. A response function  $S(d)$  relating measured signal levels to the diameters of spherical particles of known refractive index passing through a SPC sample volume of known incident intensity  $I_{inc}$  can be determined from theoretical calculations of  $C_{sc}(d)$ . Here the factor  $k$  must be determined by calibration.

A plot of partial light scattering cross section for spherical particles illuminated by a coherent uniphase wave calculated using a Lorenz-Mie theory computer code<sup>3</sup> is given in Fig. 9. The calculations are for an off-axis  $f/1.96$  collection lens centered at  $\theta = 10$  deg from the incident radiation propagation direction (forward scattering). The oscillatory behavior is due to resonance interactions in the scattering process and results in ambiguities in particle

size determination from SPC scattering measurements. Another problem inherent in using the laser as a SPC radiation source is the nonuniform intensity profile across the beam.<sup>12,40</sup> An ambiguity in signal levels arises for in situ SPC since the particles are free to traverse the sample volume at any position. Thus, particles will experience different peak incident intensities  $I_{inc}$  depending on the trajectory and even a monodisperse (uniform size) aerosol will generate a broad distribution of signal amplitudes  $S$ .

A number of methods have been devised to eliminate the unknown incident intensity effect in cross-section measuring techniques. The basic approaches include: 1) analysis of only those particles which pass through a selected portion of the beam of known and constant intensity, 2) analysis of all particles and later correction for the known distribution of particle trajectories and corresponding incident intensities, 3) use of the ratio of scattering signals at two or more angles to cancel the incident intensity effect.

For in situ measurements various optical methods of discriminating those particles which pass through a control portion of the beam have been used, including coincidence detectors at 90 deg by Ungut et al.<sup>41</sup> and in the forward direction by Knollenberg.<sup>42</sup> It has also been suggested that a pointer laser beam tightly focussed within a larger probe beam be used to discriminate those particles which pass through the center of the probe beam.<sup>43</sup> This latter approach does not eliminate the ambiguity, but rather shifts the problem to the pointer beam where the effect is less significant. It is also possible to change the intensity profile across the laser beam from Gaussian to something approximating a tophat using specially designed filters. However any beam degradation due to windows or refractive index fluctuations would spread the profile and reintroduce the intensity ambiguity. It appears that no definitive studies on the use of tophat profiles have been reported.

Another somewhat similar technique proposed by Hirleman<sup>44</sup> involves the use of signals generated by particles traversing two adjacent laser beams. The dual peak signature is used to determine two velocity components and the trajectory of each particle. Given known laser beam properties the incident intensity history for a particle is then completely determined which permits a real time correction for the intensity ambiguity. After  $I_{inc}$  in Eq. (7) is determined a calibrated response function prediction such as Fig. 9 would be used to relate signal amplitudes to particle size. This technique<sup>44</sup> has been proposed for light scattering, extinction, and fluorescence cross-section measurements although experiments to date have used only light scattering.

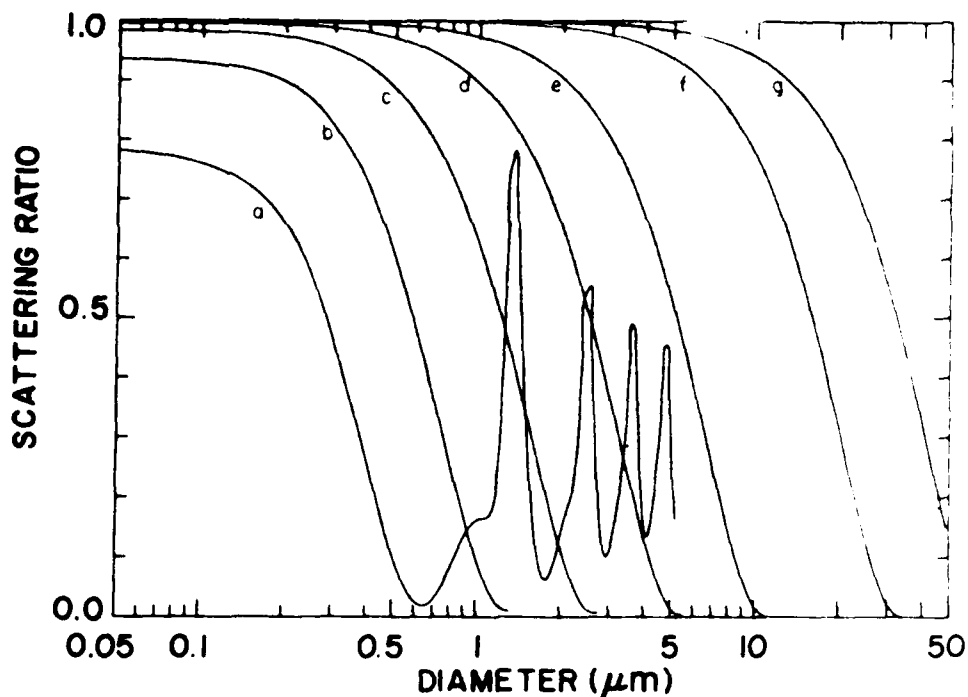


Fig. 10 Response functions for ratio-type SPC. The data apply to spherical particles with  $n=1.56-0.471$  (soot) and  $\lambda = 0.6328 \mu\text{m}$ . The scattering angle pairs are a)48/24 deg, b)24/12 deg, c)12/6 deg, d)6/3 deg, e)3/1.5 deg, f)1/0.5 deg, g)0.5/0.25 deg. All but the 48/24 deg curve were truncated after the first minimum.

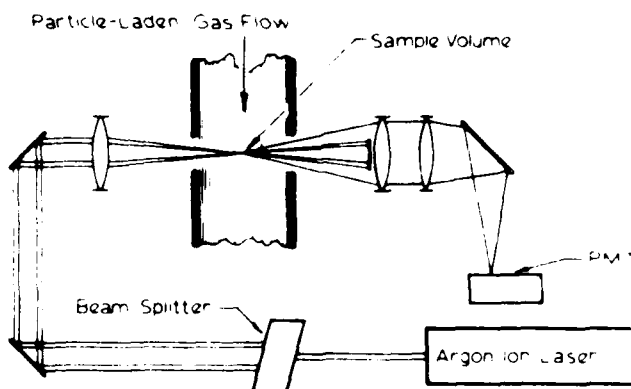


Fig. 11 Schematic of optical system for particle sizing interferometer after Houser.<sup>51</sup>

A second general approach to the ambiguous incident intensity problem is to correct after the fact. One implementation of this approach proposed by Holve and Self<sup>45</sup> is to first consider the distribution of scattering signal pulse heights generated by particles of one size passing with equal probability through all portions of the laser beam focus region. The optical system required again is like Fig. 5 using a single near-forward off-axis detector. The signal height distribution from a polydispersion is then

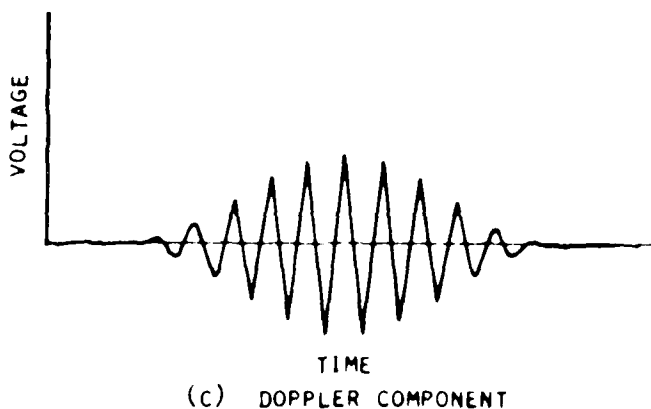
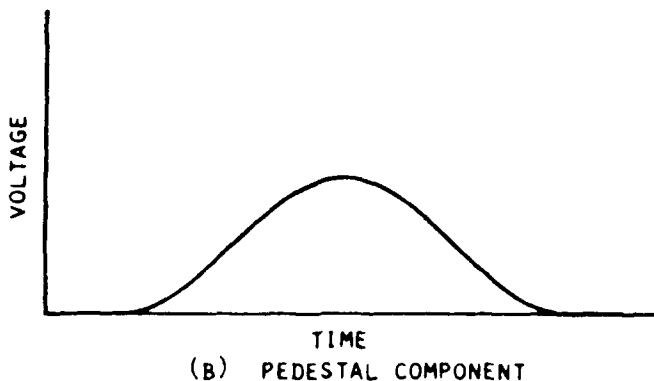
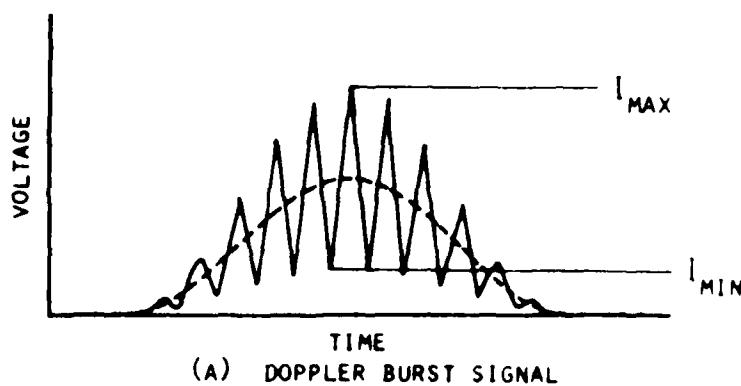


Fig. 12 Signals from particle sizing interferometer after Bachalo.<sup>58</sup>

a linear combination of the monodisperse particle response distributions. A numerical scheme was developed<sup>45</sup> to invert the resulting system of equations and solve for the linear coefficients which are proportional to concentrations in the discretized particle size intervals. This approach<sup>45</sup> has been successfully used for sizing burning droplets and particulates emitted from a coal combustor.

#### Scattering Intensity Ratio Techniques

The final method to eliminate the incident intensity ambiguity in SPC is to utilize the ratio of scattered light

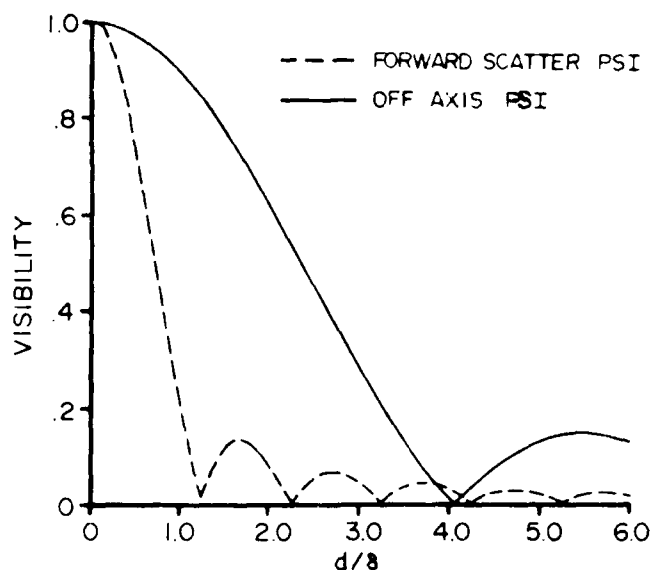


Fig. 13 Calculations for the fringe visibility  $V$  as a function of particle diam to fringe spacing ratio  $d/\delta$  for particle sizing interferometers (PSI). The data apply to a PSI collecting all of the forward scattered light and to an off-axis PSI with an  $f/2$  collection lens oriented at  $\theta = 20$  deg.

signals from two or more scattering angles to determine particle size. This approach is often used in ensemble multiangle scattering measurements where the relative scattering profile rather than the absolute scattering at some angle is used. Hodkinson<sup>46</sup> suggested and Gravatt<sup>47</sup> implemented an SPC based on the ratio technique which used scattering ratios from near-forward scattering angles where the sensitivity to particle shape and refractive index is minimized. The optical configuration of ratio counters can be similar to that in Fig. 5, although annular detection schemes are often used.<sup>12,48</sup> A set of response functions for a ratio SPC is plotted in Fig. 10. One problem evident from Fig. 10 is the multivalued response function plotted for the largest angle pair. Outsize particles, or those larger than the first minimum in the ratio response functions in Fig. 10, will be incorrectly sized by ratio instruments which utilize only a single pair of scattering angles. The multiple ratio concept (MRSPC) developed by Hirleman and coworkers<sup>12,48</sup> was designed to eliminate this ambiguity problem.

Ratio counters still have an optical sample volume which depends on particle size and corrections for this effect must be considered.<sup>12</sup> Also, since forward scattering is generally used, ratio counters are relatively insensitive to particle shape and refractive index.<sup>12</sup>

A possible advance for ratio schemes may be to integrate photodiode array detectors to allow more scattering

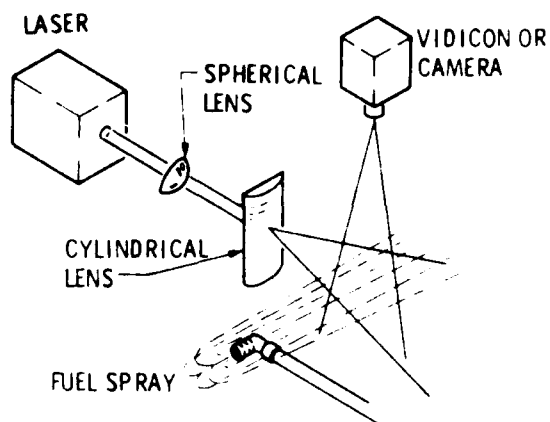


Fig. 14 Schematic of imaging particle sizing system after Fleeter et al.<sup>60</sup>

data to be collected without simply adding photomultiplier tubes. Bartholdi et al.<sup>49</sup> used a linear photodiode array in an SPC application and we are studying the use of intensified versions of the detector in Fig. 8.

Ratio SPC are applicable in the nominal size range of 0.3 - 10.0  $\mu\text{m}$  for practical laser sources. They have been successfully applied in engine exhausts,<sup>48</sup> flame studies,<sup>5</sup> fluidized bed off-gas,<sup>51</sup> and in several other applications.

### Particle Sizing Interferometry

Another approach which can provide particle size information independent of incident intensity is particle sizing interferometry (PSI). A schematic is shown in Fig. 11. As a single particle passes through the intersection region of two nonparallel laser beams, Doppler-shifted scattered light waves from each beam emanate from the particle. Heterodyning the two contributions of scattered light at a detector will produce the Doppler-difference frequency which is directly related to the particle velocity and the angle between the laser beam propagation vectors. This principle underlies the laser Doppler velocimeter (LDV). A particle crossing the LDV beam intersection region will produce an approximately Gaussian signal (pedestal) with the modulated Doppler-difference component written on the pedestal<sup>52</sup> as shown in Fig. 12. The ratio of the modulated signal amplitude to the pedestal amplitude, which is termed the visibility, provides a measure of particle size as shown by Farmer<sup>52</sup> and others<sup>53,54</sup> who used a scalar description of the process. For large apertures which collect all of the forward scattered (diffracted) light the visibility  $V$  as a function of particle diameter  $d$  and fringe

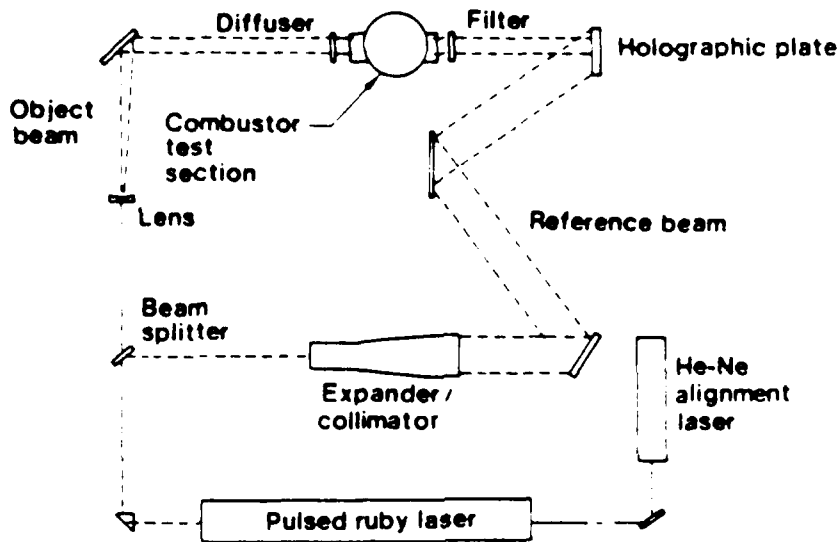


Fig. 15 Schematic of holographic particle sizing system after Chigier.<sup>62</sup>

spacing  $\delta$  was shown by Robinson and Chu<sup>54</sup> to be

$$V = \frac{2J_1(\pi d/\delta)}{\pi d/\delta} \quad (8)$$

where  $J_1$  is a first-order Bessel function of first kind. A plot of  $V$  is given in Fig. 13.

Calculations considering the complete problem of scattering by a sphere simultaneously in two coherent, collimated laser beams<sup>55</sup> predicted a strong dependence of the visibility on particle refractive index, the detector aperture, and detector position relative to the beams. A number of experimental studies have confirmed the importance of careful receiving optics design<sup>55,56</sup> although conflicting observations have also been made.<sup>57</sup>

Another related approach is the off-axis PSI proposed by Bachalo<sup>58</sup> which utilizes the interference of refracted or reflected light scattering contributions rather than the diffractive scatter of a conventional PSI.<sup>52</sup> This method is applicable to particles significantly larger than the wavelength and is based on the difference in optical path length traveled by refracted rays from the two crossed beams which pass through the particle and arrive coincidentally at the detector. The visibility response function for a typical off-axis PSI collection angle<sup>57</sup> of 20 deg is also shown in Fig. 13, and the expanded  $d/\delta$  sizing range for this concept is apparent.

Although the visibility is a relative measurement, absolute light scattering cross sections and incident laser beam intensity distributions still control the PSI. Only those particles which scatter enough light to be detected

above the background noise level will be sized. Thus a PSI will "size" the particles using a relative measurement but the frequency at which particles are "seen" or counted is biased toward large particles.

To correct some serious problems in sizing particles traversing the edge of off-axis PSI probe volumes, it has been suggested that the amplitude of the Doppler bursts from PSI instruments be used to size particles. The incident intensity ambiguity is reintroduced and a correction must be made. Those particles traversing the center of the intersection region can be discriminated using coincidence detection with small aperture detectors or using an additional, tightly focused pointer beam. Unfortunately the latter approach merely shifts the trajectory ambiguity problem from the PSI beams to the Gaussian pointer beam.

### Photographic and Holographic Methods

Several different imaging methods have been used for particle and droplet sizing. These rely on a short light pulse to "freeze" the particle images so that direct measurements of size may be made. In the case of double flash photography two closely spaced light pulses are used to obtain double images of each droplet so that velocity can also be determined. Single and double pulse holography have been used as well, with the advantage that a volume of the aerosol can be captured rather than the limited depth of field afforded by photographic methods. The problem with both photographic and holographic methods is the tedious and expensive post processing needed to extract the data. Also, quantitative measurements of particle size distributions with imaging techniques are realistic only for particle sizes greater than 5  $\mu\text{m}$  at best.

Automated data processing for particle photography has been reported by Simmons and Lapera<sup>59</sup> and Fleeter et al.<sup>60</sup> In the first system<sup>59</sup> a strobe light was used to form the image on a vidicon tube. The image is scanned to obtain drop size information and the cycle repeated roughly 10 times per second. Mean diameters and size distributions, were obtained at each point in the spray.<sup>59</sup> Fleeter et al.<sup>60</sup> utilize a pulsed ruby laser as shown in Fig. 14 to illuminate the particles which are imaged onto a 512x512 diode array camera. The image is then digitized<sup>60</sup> and transferred to a computer memory for processing. Knollenberg<sup>42</sup> analyzes individual particles by projecting images onto a linear photodiode array.

One correction factor required in the data analysis of incoherent imaging techniques is the effective depth of field vs droplet size. (Large particles are visible over a

larger axial distance from the exact object plane than small particles.) This correction is analagous to sample volume corrections required with SPC and is mandatory before useful data can be obtained.

Photographic image analysis is a very convenient method of particle and droplet sizing under cold flow conditions. One limitation is the typical resolution limit of about five micrometers. In hot flows one would expect substantially poorer results due to image distortion by refractive index fluctuations in the flow. Performance also suffers in applications where windows must be located between the spray and the camera, particularly when the optical aperture is limited. In a recent study of optical methods for Diesel engine research, the threshold of size detection was  $35 \mu\text{m}$  for high-speed photography and  $8 \mu\text{m}$  for holography.<sup>61</sup>

Pulsed holography eliminates the sample volume correction required for photographic methods since the holograms, which contain three-dimensional information, can be observed in two dimensions while the third is scanned. A schematic diagram of a holographic system is shown in Fig. 15. Holographic methods for particle and droplet size analysis have apparently been used to observe particles down to about  $5 \mu\text{m}$ .<sup>63,64</sup> Note however that the resolution of a holographic system is typically several micrometers so that the accuracy in sizing such small particles is very poor. Another problem encountered in particle holography is performance degradation when the laser beam transmission drops below about 10%.<sup>65</sup>

### Conclusions

Laser-based techniques for nonintrusive diagnostics of particle size and concentration distributions have been reviewed. The most common diagnostics are imaging and light scattering techniques, and each instrument has its own unique set of limitations and range of applicability. It is imperative that the subtle factors which control the accuracy and reliability of data obtained with laser/optical instruments be understood by the user.

### Acknowledgments

The author's research in optical particle diagnostics has been generously supported over the past five years by the National Science Foundation, Particulate and Multiphase Processes Group, Dr. Morris Ojalvo, Program Director, and by the Office of Naval Research, Propulsion Group, Dr. Albert D. Wood, Project Director.

## References

- 1Born, M. and Wolf, E., Principles of Optics, Sixth edition, Pergamon Press, New York, 1980.
- 2Hecht, E. and Zajac, A., Optics, Addison-Wesley, New York, 1974.
- 3van de Hulst, H. C., Light Scattering by Small Particles, John Wiley and Sons, New York, 1957.
- 4Kerker, M., The Scattering of Light and Other Electromagnetic Radiation, Academic Press, New York, 1969.
- 5Handa, T., Suda, K., Nagashima, T., Kaneko, K., Yamamura, T., Takahashi, Y., and Suzuki, H., "Size Determination of Submicron Particulates by Optical Counter," Fire Research, Vol. 1, 1978, pp. 255-263.
- 6Asano, S., "Light Scattering Properties of Spheroidal Particles," Applied Optics, Vol. 18, 1979, pp. 712-723.
- 7Latimer, P. and Wamble, F., "Light Scattering by Aggregates of Large Colloidal Particles," Applied Optics, Vol. 21, 1982, pp. 2447-2455.
- 8Borghese, F., Denti, P., Toscano, G., and Sinden, C. I., "Electromagnetic Scattering by a Cluster of Spheres," Applied Optics, Vol. 18, 1979, pp. 116-120.
- 9Albini, F. A. and Nagelberg, E. R., "Scattering of a Plane wave by an Infinite Inhomogeneous, Dielectric Cylinder - An application of the Bern Approximation," Journal of Applied Physics, Vol. 33, 1962, pp. 1706-1713.
- 10Schuerman, D. W., Wang, R. T., Gustafson, B. A. S., and Schaefer, R. W., "Systematic Studies of Light Scattering. 1. Particle Shape," Applied Optics, Vol. 20, 1981, pp. 4039-4050.
- 11Zerull, R. H. and Giese, R. H., in Planets, Stars and Nebulae Studied with Photopolarimetry, T. Gehrels, ed., University of Arizona Press, Tucson, Ariz., 1974, p. 901.
- 12Hirleman, E. D. and Moon, H. K., "Response Characteristics of the Multiple Ratio Single Particle Counter," Journal of Colloid and Interface Science, Vol. 87, 1982, pp. 124-139.
- 13Chylek, P. and Ramaswamy, V., "Lower and Upper Bounds on Extinction Cross Sections of Arbitrarily Shaped Strongly Absorbing or Strongly Reflecting Nonspherical Particles," Applied Optics, Vol. 21, 1982, pp. 4339-4344.
- 14Felton, P.G., "Measurement of Particle/Droplet Size Distributions by a Laser Diffraction Technique," 2nd European Symposium on Particle Characterization PARTEC, Nurnberg, West Germany, September 24, 1979, Report HIC 326 Dept. of Chem. Engr., Univ. of Sheffield, Sheffield, England.

- 15Dobbins, R. A. and Jizmagian, G. S., "Particle Size Measurements Based on Use of Mean Scattering Cross Sections," Journal of the Optical Society of America, Vol. 56, 1966, pp. 1351-1354.
- 16Ariessohn, P. C., Self, S. A., and Eustis, R. H., "Two-wavelength Laser Transmissometer for Measurements of Mean Size and Concentration of Coal Ash Droplets in Combustion Flows," Applied Optics, Vol. 19, 1981, pp. 3775-3781.
- 17Lester, T. W., and Wittig, S. L. K., "Particle Growth and Concentration Measurements in Sooting Homogeneous Hydrocarbon Combustion Systems," in Proceedings of the Tenth International Shock Tube Symposium, G. Kamimoto, ed., The Shock Tube Research Society, Kyoto, Japan, 1975.
- 18Bro, K., "The Optical Dispersion Quotient Method for Sizing of Soot in Shock-induced Combustion," Ph.D. Thesis, Purdue University, Lafayette, Ind., 1978.
- 19Powell, E. A., Cassonova, R. A., Bankston, C. P., and Zinn, B. T., "Combustion-Generated Smoke Diagnostics by Means of Optical Measurement Techniques," Experimental Diagnostics in Gas Phase Combustion: AIAA Progress in Aeronautics and Astronautics, Vol. 53, B. T. Zinn, ed., AIAA, New York, 1977, pp. 449-463.
- 20Fymat, A. L., "Analytical Inversions in Remote Sensing of Particle Size Distributions: Multispectral Extinctions in the Anomalous Diffraction Approximation," Applied Optics, Vol. 17, 1978, pp. 1675-1676.
- 21Hansen, M. A. and Evans, W. H., "Polar Nephelometer for Atmospheric Particulate Studies," Applied Optics, Vol. 19, 1980, pp. 3389-3395.
- 22Hansen, M. Z., "Atmospheric Particulate Analysis Using Angular Light Scattering," Applied Optics, Vol. 19, 1980, pp. 3441-3448.
- 23McCay, T.D., Mundy, W.C., Mann, D.M., and Meserve, G.S., "Laser Mie Scattering Measurements of Particle Size in Solid Rocket Motor Exhaust," JANNAF 12th Plume Technology Meeting, CPIA Publication #332, Dec. 1980, p. 145.
- 24Santoro, R. J. and Semerjian, H. G., "Interpretation of Optical Measurements of Soot in Flames," AIAA Paper 83-1516, 18th Thermophysics Conference, Montreal, Canada, June 1983.
- 25Chang, P. H. P. and Penner, S. S., "Particle Size Measurements in Flames using Light Scattering: Comparison with Diffusion Broadening Spectroscopy," Journal of Quantum Spectroscopy and Radiation Transfer, Vol. 25, 1981, pp. 97-110.
- 26Powell, E. A. and Zinn, B. T. "In-situ Measurements of Complex Refractive Index of Combustion Generated Particulates," AIAA Paper 83-1518, 18th Thermophysics Conference, Montreal, Canada, June 1983.

- 27Hirleman, E. D., "On-line Calibration Technique for Laser Diffraction Droplet Sizing Instruments," ASME Paper 83-GT-232, 20th International Gas Turbine Conference, Phoenix, Ariz., March 1983.
- 28Chin, J. H., Slepceovich, C. M., and Tribus, M., "Determination of Particle Size Distributions in Polydisperse Systems by Means of Measurements of Angular Variation of Intensity of Forward Scattered Light at Very Small Angles," Journal of Physical Chemistry Ithaca, Vol. 5, 1955, p. 841.
- 29Recognition Systems Inc., Van Nuys, Calif.
- 30Malvern Instruments Ltd., Malvern, Worcestershire, England.
- 31Swithenbank, J., Beer, J., Taylor, D. S., Abbot, D., and McCreath, C. G., "A Laser Diagnostic Technique for the Measurement of Droplet and Particle Size Distribution," Experimental Diagnostics in Gas-Phase Combustion Systems: AIAA Progress in Astronautics and Aeronautics, Vol. 53, B. T. Zinn, ed., AIAA, New York, 1977, pp. 421-447.
- 32Titchmarsh, E. C., "Extensions of Fourier's Integral Formula to Formulae involving Bessel Functions," Proceedings London Mathematical Society, Vol. 23, 1924, p. xxii.
- 33Dobbins, R. A., Crocco, L., and Glassmann, I., "Measurement of Mean Particle Sizes of Sprays from Diffractively Scattered Light," AIAA Journal, Vol. 1, 1963, pp. 1882-1806.
- 34Roberts, J. H. and Webb, M. J., "Measurement of Droplet Size for Wide Range Particle Distributions," AIAA Journal, Vol. 2, 1964, pp. 583-585.
- 35Dieck, R. H. and Roberts, R. L., "The Determination of the Sauter Mean Droplet Diameter in Fuel Spray Nozzles," Applied Optics, Vol. 9, 1970, pp. 2007-2014.
- 36Alger, T. W. "Polydisperse-particle Size Distribution Function Determined from Intensity Profile of Angularly Scattered Light," Applied Optics Vol. 18, 1979, p. 3494.
- 37Benedek, G. B., Polarization, Matter, and Radiation, Presses Universitaires de France, Paris, 1969.
- 38Penner, S. S., Bernard, J. M., and Jerskey, T., "Laser Scattering from Moving Polydisperse Particles in a Flame: Preliminary Experiments," Acta Astronautica, Vol. 3, 1976, p. 93.
- 39King, G. B., Sorenson, C. M., Lester, T. W., and Merklin, J. F., "Photon Correlation Spectroscopy used as a Particle Size Diagnostic in Sooting Flames," Applied Optics, Vol. 21, 1982, pp. 976-978.
- 40Hirleman, E. D., "Laser-based Single Particle Counters for in-situ Particulate Diagnostics," Optical Engineering, Vol. 19, 1980, pp. 854-860.

41Ungut, A., Yule, A. J., Taylor, D. S., and Chigler, N. A., "Simultaneous Velocity and Particle Size Measurements in Two Phase Flows by Laser Anemometry," AIAA Paper 78-74, 16th Aerospace Sciences Meeting, Huntsville, Ala., Jan. 1978.

42Knollenberg, R. G., "The Use of Low Power Lasers in Particle Size Spectroscopy," Practical Applications of Low Power Lasers, SPIE, Vol. 92, 1977, pp. 137-152.

43Hess, C., Spectron Development Laboratories, Private Communication, May 1983.

44Hirleman, E. D., "Laser Technique for Simultaneous Particle Size and Velocity Measurements," Optics Letters, Vol. 3, 1978, pp. 19-21.

45Holve, D. and Self, S. A., "Optical Particle Sizing for in situ Measurements, Parts I and II," Applied Optics, Vol. 18, 1979, pp. 1632-1652.

46Hodkinson, J. R., "Particle Sizing by Means for the Forward Scattering Lobe," Applied Optics, Vol. 5, 1966, p. 839.

47Gravatt, C. C., "Real Time Measurement of the Size Distribution of Particulate Matter by a Light Scattering Method," APCA Journal, Vol. 23, 1973, p. 1035.

48Hirleman, E. D., "Optical Technique for Particulate Characterization in Combustion Environments: The Multiple Ratio Single Particle Counter," Ph.D. Thesis, Purdue University, West Lafayette, Ind., 1977.

49Bartholdi, M., Salzman, G. C., Hiebert, R. D., and Seger, G., "Single Particle Light Scattering Measurements with a Photodiode Array," Optics Letters, Vol. 1, 1977, pp. 223-225.

50Samuelson, G. S., Hack, R. L., Poon, C. C., and Bachalo, W. D., "Study of Soot Formation in Premixed and Nonpremixed Flows with Complex Aerodynamics," Paper WSSCI-80-10, presented at the Western States Section Combustion Institute Meeting, Irvine, Calif., April 22, 1980.

51Houser, M. J. "Particle Field Diagnostics: Applications of Intensity Ratioing, Interferometry, and Holography," Optical Engineering, Vol. 19, 1980, pp. 873-877.

52Farmer, W. M., "Measurement of Particle Size, Number Density, and Velocity Using a Laser Interferometer," Applied Optics, Vol. 11, 1972, p. 2603.

53Fristrom, R. M., Jones, A. R., Schwar, M. S. R., and Weinberg, F. S., "Particle Sizing by Interference Fringes and Signal Coherence in Doppler Velocimetry," Faraday Symposia of the Chemical Society, Vol. 1, 1973, p. 183.

54Robinson, D. M. and Chu, W. P. "Diffraction Analysis of Doppler Signal Characteristics for a Cross-beam Laser Doppler Anemometer," Applied Optics, Vol. 14, 1975, p. 2177.

55Chu, W. P. and Robinson, D. M., "Scattering from a Moving Spherical Particle by Two Crossed Coherent Plane Waves," Applied Optics, Vol. 16, 1977, p. 619.

56Yule, A. J. Chigier, N. A., Atakan, S., and Ungut, A., "Particle Size and Velocity Measurement by Laser Anemometry," AIAA Paper 77-214, 15th Aerospace Sciences Meeting, Los Angeles, Calif., January 1977.

57Farmer, W. M., "Measurement of Particle Size and Concentrations Using LDV Techniques," Proceedings of The Dynamic Flow Conference, Dynamic Flow Conference, DK 2740, Skovlunde, Denmark, 1978.

58Bachalo, W. D., "Method for Measuring the Size and Velocity of Spheres by Dual-Beam Light-Scatter Interferometry," Applied Optics, Vol. 19, 1980, pp. 363-370.

59Simmons, H. C. "The Correlation of Drop-size Distributions in Fuel Nozzle Sprays," Journal of Engineering for Power, Vol. 99, 1977, pp. 309-314.

60Fleeter, R., Toaz, R., and Sarohia, V., "Application of Digital Image Analysis Techniques to Antimisting Fuel Spray Characterization," ASME Paper 82-WA/HT-23, American Society of Mechanical Engineers, New York, 1982.

61Lennert, A. E., SOWLS, R. E., Belz, R. A., Goethert, W. H., and Bentley, H. T., "Electro-optical Techniques for Diesel Engine Research," Experimental Diagnostics in Gas Phase Combustion: AIAA Progress in Astronautics and Aeronautics, Vol. 53, B. T. Zinn, ed., AIAA, New York, 1977, pp. 629-656.

62Chigier, N., "Spray Combustion Processes: A Review," ASME Paper 82-WA/HT-86, American Society of Mechanical Engineers, New York, 1982.

63Trolinger, J. D. "Particle Field Diagnostics by Holography," Paper 80-0018, 18th Aerospace Sciences Meeting, Pasadena, Calif., January, 1980, American Institute of Aeronautics and Astronautics, New York, 1980.

64Thompson, B. J., "Holographic Particle Sizing Techniques," Journal of Physics E, Vol. 7, 1974, pp. 781-788.

65Jones, A. R., "Error Contour Charts Relevant to Particle Sizing by Forward-Scattered Lobe Methods," Journal of Physics D, Vol. 10, 1977, pp. L163-L165.

A150 355

## Response Characteristics of the Multiple-Ratio Single-Particle Counter

E. D. HIRLEMAN AND H. K. MOON

*Mechanical Engineering Department, Arizona State University, Tempe, Arizona 85281*

Received March 30, 1981; accepted June 12, 1981

The importance of aerosols and aerosol processes has prompted considerable research into techniques for particulate characterization. As batch sampling probe techniques often introduce unacceptable perturbations into the flow and can have serious uncertainties associated with possible alterations of the aerosol in the sample line, *in situ* optical methods have received much interest. This paper is concerned with a laser light-scattering technique for *in situ* analysis of individual particles, the multiple-ratio single-particle counter (MRSPC). In particular a thorough study of the response characteristics of the MRSPC was completed, including both experimental and theoretical analyses of nonideal effects associated with particle size distribution measurements. The effects of unknown refractive index, nonspherical particle shape, size-selective sampling bias, and instrument resolution were considered. Theoretical predictions of MRSPC performance for these nonideal conditions were found to agree quite well with experiments performed here. The overall analysis indicates that the MRSPC can make *in situ* measurements of volume-equivalent size distributions of moderately nonspherical particles of unknown refractive index with uncertainties on the order of 50%.

### 1. INTRODUCTION

Aerosol concentrations and size distributions are of fundamental importance to the study of particulate emissions and fuel spray combustion. The environmental impact of particulate emissions has been a serious problem since large-scale use of combustion began. This problem will become even more acute as alternate fuels such as coal, synthetics, and heavy residual fuels furnish increasing portions of the expanding U. S. energy requirements. Particulates represent a large fraction of the primary pollutants emitted from coal combustion, and evaluation of improved particulate control devices will require continued development of advanced particulate analysis techniques. The implications of particulate emissions are also severe for advanced open-cycle gas turbine power plants, as combustion exhaust particles can drastically reduce the life of turbine blades.

The numerous methods for particulate characterization have been reviewed elsewhere (1). Briefly, most of the conventional particle analyzers such as cascade impactors, commercial optical particle counters, and electrical mobility analyzers require batch sample extraction and thus suffer from the common problems of flow interference and alteration of aerosol properties in the sampling probe lines. *In situ* optical techniques are clearly superior for combustion applications where performance criteria like minimal flow interference, real time analysis, and high-temperature operation are imperative. The three classes of *in situ* optical methods include imaging or holographic techniques; ensemble analyzing methods; and single-particle analyzers. In general, these optical techniques eliminate the disadvantages of conventional sampling methods, but unfortunately also introduce their own set of limitations and uncertainties. For example, optical techniques can be quite sen-

sitive to particle shape and composition or refractive index (2, 3, 4). This is important, for example, in combustion applications where particle characteristics are generally unknown and variable.

In order for the data from an optical particle analyzer to be reliably interpreted, several performance characteristics of the instrument must be well understood. These include:

1. Response to a very polydisperse aerosol, i.e., one with particle sizes outside the nominal sizing range of the instrument.
2. Response to particles of unknown and variable refractive index and composition.
3. Response to nonspherical particles.
4. Properties of the optical sample volume, including possible dependence on particle size and the corresponding probe volume correction.
5. Resolution, or the instrument response to a monodisperse aerosol allowed to flow through all portions of the sample volume.

A discussion of the performance of a number of single-particle counters with regard to these factors has been presented recently by Whitby and Willeke (2) and Hirleman (3). In the present paper, response characteristics of a particular laser light-scattering single-particle counter, the multiple-ratio single-particle counter (MRSPC), were investigated both theoretically and experimentally.

## 2. MULTIPLE-RATIO SINGLE-PARTICLE COUNTER (MRSPC)

That subset of laser/optical instruments for aerosol characterization known as single-particle counters (SPC) in general analyze light scattered by particles passing individually through focused light beams to determine particle size. Ratio-type SPC in particular derive size from a ratio of the amount of laser light scattered by single particles into two separate viewing or detection angles. The use of two near-forward scattering

angles for ratio measurements as suggested by Hodkinson (5) and initially implemented by Gravatt (6) has some advantages. First, the ratios are relatively weak functions of particle shape and refractive index, which is important in the analysis of generally nonspherical combustion particulates of unknown and varying composition. Second, the ratio approach eliminates some of the problems associated with particle-to-particle variation in incident illumination intensity introduced either by the nonuniform intensity profile across laser beams or by beam energy fluctuations.

A typical response function prediction for the ratio-type SPC is shown in Fig. 1. The data in Fig. 1 assume annular detectors axisymmetric with respect to the laser beam collecting equal solid angle conical sheets of scattered light of constant scattering angle  $\theta$  (measured from the laser beam propagation vector). The curves corresponding to refractive indices of  $n = 1.40$  (typical of liquid hydrocarbon) and  $n = 1.56-0.4$  (soot) (7) were computed using Lorenz-Mie theory for the scattering of plane electromagnetic waves by spherical particles (8, 10). Oscillations in the response function for the nonabsorbing (real index) hydrocarbon particles are typical of those encountered in all scattering SPC which utilize monochromatic light (2, 11, 12, 13). In contrast, for absorbing soot particles the oscillations are clearly damped out. Also plotted in Fig. 1 is the  $12^\circ/6^\circ$  ratio as calculated from the theory for Fraunhofer diffraction of plane waves by circular disks (5).

The good agreement between diffractive calculations and Lorenz-Mie predictions for soot is not necessarily expected as diffraction theory is valid only when  $d \gg \lambda$ , a condition which is clearly not satisfied for the particle size range of Fig. 1. However, if the scattering process is considered to consist of the superposition of reflection, refraction, and diffraction contributions (admittedly non-rigorous for  $d \sim \lambda$ ) then small angle forward scattering by absorbing spheres should be

predominately the diffraction contribution. Note also that Fig. 1 indicates only that the *shape* of the forward scattering lobe (i.e., ratios) is predicted reasonably well by diffraction theory; absolute forward scattering cross sections will not, in general, be adequately modeled by diffraction theory.

For very small particles in the Rayleigh scattering regime,  $d \ll \lambda$ , the scattering at small forward angles is nominally isotropic, and the scattering ratios approach 1.0. As particle size increases the scattered energy shifts toward the forward direction resulting in the familiar Mie lobe structure (2, 16) and lower ratios. Finally, as the first minimum in the scattering pattern moves in to  $12^\circ$  at  $\alpha \cong 18$ , the ratio for  $12^\circ/6^\circ$  becomes very small. Unfortunately as particle size increases past the first minimum in the response curve, the ratio continues to oscillate at nonzero values as shown in Fig. 2. Thus a measured  $48^\circ/24^\circ$  ratio of say 0.5 corresponds to many possible particle sizes (multivalued response), and a  $48^\circ/24^\circ$  single ratio SPC with a nominal size range of 0.06 to  $0.6 \mu\text{m}$  will incorrectly size particles larger than  $0.6 \mu\text{m}$ . It was this problem that provided impetus for the multiple-ratio SPC (4, 13), where additional ratios are used as on-line consistency checks to detect this non-unique response problem. In MRSPC prac-

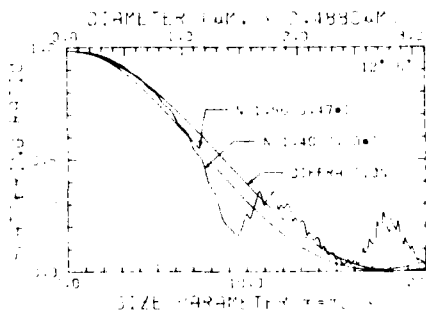


FIG. 1. Scattering ratio response curves for  $12^\circ/6^\circ$ . The curves for  $n = 1.40$  and  $n = 1.56-0.47i$  were calculated for spherical particles using Lorenz-Mie theory. The third curve was calculated using Fraunhofer diffraction theory with the obliquity correction.

*Journal of Colloid and Interface Science*, Vol. 87, No. 1, May 1982

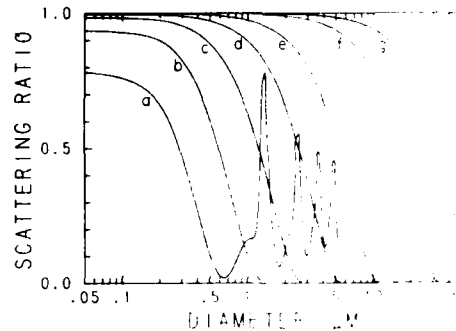


FIG. 2. Response function for a ratio-type light scattering SPC. The data were calculated for spherical particles with  $n = 1.56-0.47i$  (soot) and  $\lambda = 0.488 \mu\text{m}$ . The scattering angle pairs are (a)  $48^\circ/24^\circ$ , (b)  $24^\circ/12^\circ$ , (c)  $12^\circ/6^\circ$ , (d)  $6^\circ/3^\circ$ , (e)  $3^\circ/1.5^\circ$ , (f)  $1^\circ/0.5^\circ$ , and (g)  $0.5^\circ/0.25^\circ$ . The latter curves were truncated at the first minimum although all of the response curves have oscillations after the first minimum similar to the data for  $48^\circ/24^\circ$ .

tice, a particle is sized using the scattering ratio measured with the largest angle pair which indicates a size consistent with that determined by all smaller angle pairs. This procedure eliminates multivalued response errors and ensures that a particle is sized using the most sensitive possible response curve. A dynamic range of 10 is typical for adequate sensitivity using one particular angle pair, and with the use of several angles the MRSPC can potentially cover sizes from about 0.1 to  $10 \mu\text{m}$  (3).

A schematic of a typical MRSPC configuration is shown in Fig. 3. The incident laser beam is focused by a lens of typically 10- to 40-cm focal length to a focus spot of 10- to  $200\text{-}\mu\text{m}$  radius at the  $1/e^2$  intensity points. The receiving system collects light scattered by particles passing near the focus spot, separates it into the various scattering angles, and directs it to photodetectors. Signals from the various photodetectors are then processed to determine the scattering ratios of interest. MRSPC working spaces of 20-60 cm are typical allowing for true *in situ* operation.

The simplest optical receiving system for a ratio-type SPC would consist of several

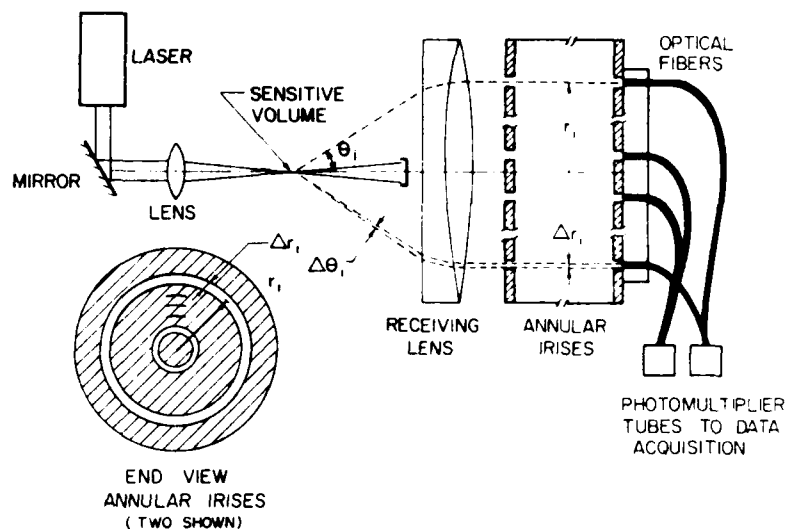


FIG. 3. Schematic of MRSPC with a lens/annular iris plate receiving system.

off-axis lens/pinhole/photodetector combinations. However, it is advantageous to use coaxial annular detection as in Fig. 3 because some of the orientation effects present with nonspherical particles are averaged out. There are a number of effectively equivalent optical techniques for separating scattered light into portions of constant scattering angle  $\theta$ . Gravatt (6) used a set of conical irises to mask the scattered light. Another general approach which decreases the physical dimensions of the receiving optics is to place a lens one focal length behind the laser beam focus and refract the angularly scattered light to be nominally parallel to the laser beam axis. This method has been used in a large number of investigations (4, 14, 15, 16). The scattering angles can then be separated using a series of lenses with increasing diameters (15) or by using series of plates with concentric annular irises to separate the scattered light into annular rings (4, 16). A fiber optic receiving head as originally proposed by McSweeney and Rivers (18) and adopted by others (4, 6, 16) can then direct the concentric rings of scattered light to separate detectors. Unfortunately spherical ab-

errations in the receiving lens can cause axial misalignment of the fields of view of the various detectors resulting in decreased resolution. This problem was solved recently (17) by designing and photoetching annular irises which inherently correct for the lens aberrations and eliminate the misalignment problem.

Several signal processing methods for ratio-type SPC are possible. Gravatt (6) performed an analog integration of the scattering signals produced by particles traversing a Gaussian ( $TEM_{00}$ ) laser beam before performing the ratio operation. This has some advantages over simple peak height detection which would be more sensitive to high-frequency noise on the signals. In the present study digital signal processing techniques with high-speed (20-MHz) analog-to-digital conversion coupled with digital peak height estimation techniques were used (19). The microcomputer controlled system then calculates the various ratios, makes the logical decision about which ratio to use for sizing, determines the size from the appropriate response calibration curve, and finally builds the size distribution histogram.

### 3. RESPONSE CHARACTERISTICS

It is imperative to fully understand the response characteristics of any optical particle analyzers designed for *in situ* operation. This is true because in general there is no opportunity for redundant analyses; the particles can only be studied for the short time they are resident in the light beam. The following discusses some of the most critical nonideal effects which must be considered when interpreting *in situ* particle counter data. In particular theoretical and experimental investigations of MRSPC response characteristics are presented.

#### 3.1 Refractive Index Effects

It is an unfortunate characteristic of light scattering by small particles and hence of most optical aerosol analyzers that the particle refractive index (or composition) is an important parameter. Generally, an SPC is calibrated with spherical particles of some particular index of refraction, but in practical application different refractive indices may be encountered. Sizing errors due to variations in refractive index depend on the SPC configuration, a worst case is probably the 90° (right-angle) scattering SPC where errors on the order of 300% are possible (4) if absorbing particles are analyzed using a calibration curve for nonabsorbing particles. Ratio-type SPC configurations are relatively insensitive to refractive index variations since forward scattering is used. Figure 1 demonstrates the refractive index effects for the 12°/6° scattering ratio which are quite indicative of those for other scattering angle pairs. Response curves for nonabsorbing and weakly absorbing particles typically oscillate about the corresponding predictions for strongly absorbing particles and diffraction. As the complex portion of the refractive index increases the ratio response curves collapse onto the monotonous decreasing function for soot to within a few percent regardless of the specific values of the real

and imaginary parts of  $n$ . When using the MRSPC to analyze aerosols of unknown refractive index it is advantageous to use the  $n = 1.56 - 0.47i$  data (or something similar) as the assumed response curve in order to distribute sizing errors both plus and minus (4). An envelope of response curves for a broad range of practical refractive indices will typically fall within  $\pm 25\%$  of the soot curve. Boron and Waldie (20) studied the problems introduced by assuming the diffraction theory curve for the response model and found sizing errors up to 40% for polystyrene latex spheres in air ( $n = 1.605$ ). However, it is clear from Fig. 1 that the diffraction prediction distributes sizing errors unevenly toward large sizes.

Quantitative results for sizing errors due to variations in refractive index are shown in Table I. To calculate the data in Table I a Lorenz-Mie theory computer code was used to determine the actual scattering ratio for a particular refractive index and particle size. This actual ratio was then used in conjunction with the assumed ratio response curve for  $n = 1.56 - 0.47i$  to determine the corresponding "measured" particle size. The (normalized) sizing error was then defined as the difference between the "measured" size and the actual size divided by the actual size assumed for the calculation. The calculations were carried out at  $\alpha$  intervals of 0.25 over one decade in particle size up to the first minimum in the diffraction pattern for each respective angle pair. Decreasing the step size was found to have little effect on the data of Table I.

The data in Table I indicate the largest or worst case errors to be about 35%, encountered for nonabsorbing aerosols as expected. However, for absorbing particles such as other estimates for soot ( $n = 1.57 - 0.56i$ ,  $n = 1.74 - 0.74i$ ) and graphite ( $n = 2.51 - 1.36i$ ) the errors are maximum about 10% but with root mean square errors of only a few percent. It is clear that the MRSPC does provide a reasonable measurement of

TABLE I

MRSPC Particle Sizing Errors for Spherical Particles of Various Refractive Indices with  $n = 1.56-0.47i$ , as Assumed Response Curve

Index of refraction	6°/3°		12°/6°		24°/12°	
	Max % error	rms % error	Max % error	rms % error	Max % error	rms % error
1.56-0.47i	0.0	0.0	0.0	0.0	0.0	0.0
1.57-0.56i	0.8	0.1	1.6	0.5	1.6	0.7
1.74-0.74i	3.1	0.7	4.9	1.6	4.8	2.3
2.51-1.36i	4.5	1.0	10.7	2.7	10.4	4.8
1.57-0.0i	28.4	8.3	30.1	12.1	35.0	16.1
1.40-0.0i	25.3	9.2	28.5	13.6	30.1	11.9
1.40-0.05i	11.1	4.0	12.5	7.1	11.7	7.6
1.40-0.1i	8.7	2.4	10.0	5.0	9.9	6.7
1.40-0.25i	5.7	1.3	5.8	2.6	5.8	3.8
1.33-0.0i	24.1	10.1	32.2	14.8	18.9	10.0

particle size even for unknown refractive index.

### 3.2 Nonspherical Particle Effects

Laser-based SPC measure an optical equivalent particle diameter, i.e., the diameter of a sphere of refractive index corresponding to the assumed response function which has the same light-scattering properties as the particle being analyzed. This optical dimension is important for radiation and visibility considerations but often the aerodynamic equivalent diameter is of more interest. To reliably interpret SPC data, the equivalent particle size actually determined by a particular instrument must be understood. Inference of an equivalent diameter other than that explicitly measured is then a justifiable possibility.

Practical aerosols deviate significantly from the ideal case of spherical particles. Soot and diesel smoke particles are chained agglomerates of tens or a few hundred primary soot nuclei (21). The primary soot particles are nominally spherical with diameters 0.01-0.05  $\mu\text{m}$  and agglomerate to dimensions up to several micrometers. Other possible particle shapes can range from needle-like asbestos fibers to hollow fly-ash

cynospheres. To actually predict the response of a particular instrument would require a general solution to the problem of light scattering by irregular particles which is presently not possible except for select special cases. Fortunately, the forward scatter configuration makes it possible to theoretically approximate MRSPC response to nonspherical particles.

As previously mentioned light scattering by particles can be viewed (to first order) as the superposition of three contributions: reflection of radiation from the particle surface; refraction (and absorption) of radiation passing through the particle; and finally, diffraction of the light passing around the particle. Scattering patterns for spherical particles considerably larger than the wavelength have in fact been quantitatively calculated by summing contributions from these three effects (22) and found to be in relatively good agreement with the rigorous Lorenz-Mie theory. In the case of near-forward scattering (small  $\theta$ ) utilized in the MRSPC, the diffraction contribution is dominant. Unfortunately, classical Fraunhofer diffraction theory is not rigorously valid for particle sizes on the order of the wavelength, and absolute scattering intensity calculations from scalar diffraction theory for small par-

ticles can be in considerable error. However, the shape of the forward scattering lobe, as indicated by scattering ratios, can be predicted quite well for spherical particles (5) using diffraction theory as indicated by Fig. 1. The good agreement between diffraction and Lorenz-Mie calculations for highly absorbing refractive indices is not surprising since most of the radiation incident on the spherical particle cross section would be absorbed, leaving a very small refraction contribution to the energy scattered in the forward direction. Since very little surface reflection will occur in the forward direction, only the diffraction contribution from a "disk" remains. When the complex portion of the refractive index goes to zero (negligible absorption), the transmitted or refracted energy becomes significant and results in a fringe structure of constructive and destructive interference due to coherent mixing of the refracted and diffracted waves. This phenomenon is indicated by the oscillations in the ratio responses shown in Figs. 1 and 2. Similar behavior is observed for all other angle pairs of Fig. 2 with nonabsorbing particles.

On the basis of applicability of diffraction theory to forward scattering calculations for spherical particles with diameters on the order of the wavelength, it is reasonable to postulate that forward lobe scattering ratios as measured by the MRSPC for individual nonspherical particles can also be approximated using diffraction theory. Hodkinson (22), Zerull *et al.* (23), and Pinnick *et al.* (24) have obtained some experimental results for forward scattering from a cloud of nonspherical particles which support this postulate. Unfortunately there is no exact theory for light scattering by irregular particles to check the diffraction approximation as is possible for spherical particles using Lorenz-Mie theory.

Some further indication of the validity of this postulate was obtained by observing the scattering characteristics of clusters of spherical polystyrene particles deposited on

microscope slides. Figure 4 shows the "images" of 2.02- $\mu\text{m}$  polystyrene spheres (note that 2.02  $\mu\text{m}$  is approximately the imaging resolution limit) projected onto a ground glass plate using a microscope objective. By traversing the microscope objective along the laser beam axis, images of far-field scattering patterns from the particles of Fig. 4 could be observed as shown in Fig. 5. In Fig. 5 contributions from the single particles are quite difficult to resolve and the far-field scattering patterns from the multiplet particles approach a nominally symmetric form indicative of a sphere of diameter larger than that of the individual particles. Note the progression of diameters of the first dark ring (or first minimum) in scattering patterns of the singlet on the left, the doublet in the top center, and the triplets in Fig. 5. The decreasing ring sizes and corresponding angles of the first scattering minima demonstrate increasing equivalent particle sizes as expected. Further experiments with 1.011- $\mu\text{m}$  spheres and other multiplet particle formations (4) also supported the postulate that the dominant properties of forward scattering by nonspherical particles with dimensions on the order of the wavelength can be estimated with reasonable certainty using diffraction theory. The MRSPC collects scattering in concentric annular rings centered in the nonspherical particle scattering patterns such as Fig. 5 and "sees" an equivalent spherical particle.

After establishing the validity of a diffraction approximation, it was important to make some predictions of MRSPC response to specific nonspherical particle geometries. Predictions of the scattering ratios from several two-dimensional particle shape projections of practical interest in combustion applications are presented in Table II. The last two agglomerates in Table II are projections of actual particle shapes observed in electron micrographs of diesel exhaust particles by Vuk and Johnson (27). The calculations summed the Fraunhofer (far-field) scattered light amplitude contributions from each con-



FIG. 4. Photograph of 2.02- $\mu\text{m}$  polystyrene spheres on a microscope slide, with the particles in best focus and illuminated with an argon-ion laser beam.



FIG. 5. Far-field scattering patterns from particles shown in Fig. 6. The imaged plane here was further from the particles than that in Fig. 4.

*Journal of Colloid and Interface Science*, Vol. 87, No. 1, 1982

TABLE II  
MRSPC Response to the Nonspherical Particle Shapes Indicated

Particle shape	$\bar{\alpha} = 3$		$\bar{\alpha} = 6$		$\bar{\alpha} = 9$		$\bar{\alpha} = 12$	
	12°/6°	6°/3°	12°/6°	6°/3°	12°/6°	6°/3°	12°/6°	6°/3°
	1.15	1.17	1.07	1.10	1.02	1.08	0.92	1.10
	1.05	1.06	0.98	0.99	0.98	0.99	0.96	1.01
	1.32	1.33	1.18	1.29	1.05	1.20	0.76	0.76
	1.05	1.06	0.98	0.99	0.97	0.99	0.95	1.00
	1.48	1.50	1.28	1.43	0.96	1.18	0.77	0.59
	1.00	1.00	0.93	0.93	0.93	0.94	0.94	0.95
	1.16	1.17	1.09	1.12	1.07	1.11	0.99	1.12
	1.29	1.25	1.15	1.21	1.07	1.17	0.96	1.17

Note. The quantity  $\alpha_{\text{predicted}}/\bar{\alpha}$  is tabulated as calculated using diffraction theory.

cular subparticle (4). The results apply to plane electromagnetic waves incident on particles with indicated cross sections normal to the radiation and for axially symmetric annular detectors. This symmetric detection geometry utilized in the MRSPC is advantageous in reducing the effects of nonspherical particle orientation on the measured size, as the results in Table II are independent of particle rotation about an axis normal to the plane of the paper. Note, however, that three-dimensional nonspherical particles will have different projections and hence different responses if rotated about an axis in the plane of the paper.

The size of the particles in Table II are presented on an area-equivalent diameter basis, such that

$$\bar{\alpha} = \frac{\pi d}{\lambda} = \frac{\pi}{\lambda} \left( \frac{4A}{\pi} \right)^{1/2}$$

where  $A$  is the total cross-sectional area of

the cluster projected normal to the light beam, and  $\bar{\alpha}$  and  $\bar{d}$  are the area-equivalent size parameter and diameter, respectively. For the  $\bar{\alpha} = 3$  doublet, each individual sphere would be of size parameter  $\alpha = 3/(2)^{1/2}$  to give the appropriate total area. Also, a value for  $\alpha_{\text{predicted}}/\bar{\alpha}$  of 1.0 would indicate that the MRSPC would "measure" a particle diameter corresponding exactly to the cross-sectional area of the irregular particle. Table II indicates that the MRSPC does quite well in indicating cross-sectional area for nearly spherical shapes with increasing discrepancies as the aspect ratio increases. Note also that the sizes as seen by 12°/6° and 6°/3° ratios are equal to typically within about 10%.

A set of experiments were also performed to provide further understanding of the MRSPC response to nonspherical aerosols. Nonspherical particles of a known and constant shape would have been best for these



FIG. 6. Scanning Electron micrograph of 1.15- $\mu\text{m}$  (volume-equivalent diameter)  $(\text{NH}_4)_2\text{SO}_4$  particles on a Nucleopore filter at 10,000 $\times$  magnification.

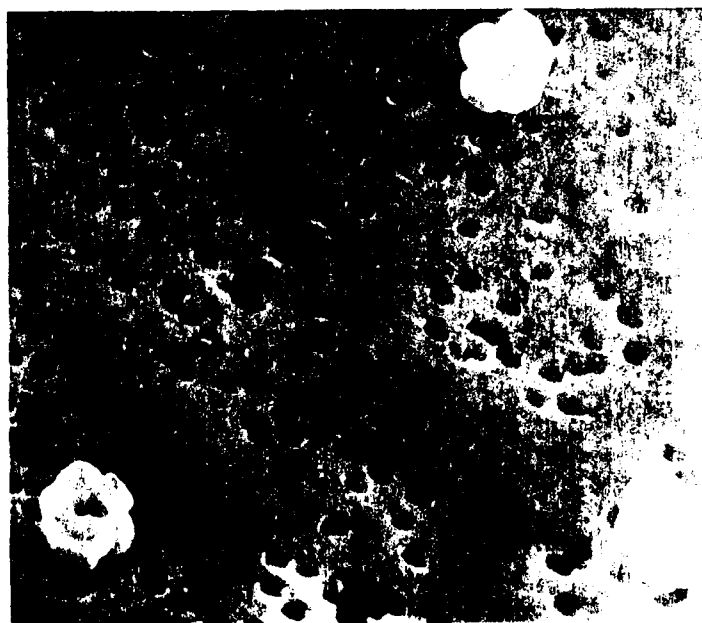


FIG. 7. Scanning Electron micrograph of 2.6- $\mu\text{m}$  (volume-equivalent diameter) NaCl particles on Nucleopore filter at 5200 $\times$  magnification.

calibrations but unfortunately such particles are very difficult to produce. We utilized constant-volume particles of NaCl and  $(\text{NH}_4)_2\text{SO}_4$  produced from isopropanol solutions with a Thermo-Systems Inc. Model 3050 vibrating orifice droplet generator. Scanning electron micrographs of the nonspherical crystals used in these experiments are shown in Figs. 6 and 7.

The MRSPC response to these particles was measured for  $12^\circ/6^\circ$  and  $6^\circ/3^\circ$  scattering ratios and the results are plotted at corresponding volume equivalent diameters in Figs. 8 and 9. Also plotted for reference are Lorenz-Mie theory calculations for spherical particles of the bulk refractive index of NaCl or  $(\text{NH}_4)_2\text{SO}_4$ . Each symbol represents the mean value of measurements of at least 450 particles, and the 95% confidence interval is also indicated by the symbol dimensions. The larger standard deviations for  $6^\circ/3^\circ$  were due to less off-axis overlap of the sample volumes at the smaller scattering angles.

As expected, the data differ from the theoretical predictions for spherical particles, although surprisingly the experimental results seem to follow to some extent the larger scale oscillations in the Lorenz-Mie curves.

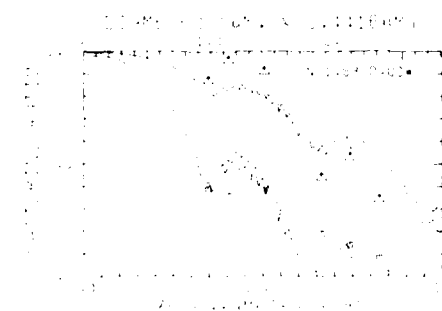


FIG. 8. Scattering ratios for  $6^\circ/3^\circ$  (upper curve) and  $12^\circ/6^\circ$  (lower curve). The solid curves are Lorenz-Mie theory predictions for spherical  $(\text{NH}_4)_2\text{SO}_4$  particles. The indicated data points for particles as shown in Fig. 8 are plotted as volume-equivalent diameters. The standard deviations of the data, averaged over all measurements for each of the two angle pairs are indicated by the two symbol sizes.

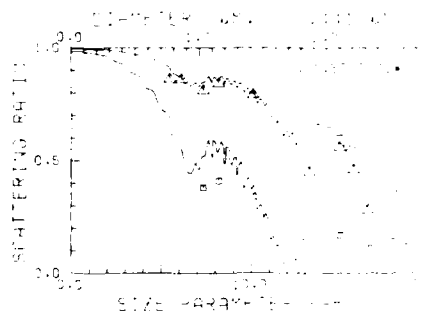


FIG. 9. Scattering ratios for  $6^\circ/3^\circ$  (upper curve) and  $12^\circ/6^\circ$  (lower curve). The solid curves are Lorenz-Mie theory predictions for spherical NaCl particles. The indicated data points for particles as shown in Fig. 9 are plotted as volume-equivalent diameters. The standard deviations of the data averaged over all measurements for each of the two angle pairs are indicated by the two symbol sizes.

Also of interest is the fact that the NaCl data seem to agree with predictions as well as for  $(\text{NH}_4)_2\text{SO}_4$  despite a greater degree of nonsphericity for sodium chloride crystals as shown in Figs. 6 and 7. The standard deviation of the NaCl data was somewhat greater indicating a greater sensitivity to varying particle orientations in the sample volume for the more irregular geometry.

These experimental and theoretical results confirm that MRSPC response is indeed relatively insensitive to particle shape. We conclude that light-absorbing particles with aspect ratios up to 4:1 and nonabsorbing particles with deviations from spherical as much as NaCl in Fig. 7 will be sized by the MRSPC to within about 40% of the cross-sectional area equivalent diameter. The sizing uncertainty for cases of nonspherical particles with aspect ratios close to one will be much better, on the order of 10–20%. In practice the shape contribution to MRSPC response uncertainties is quite comparable in magnitude to unknown refractive index effects.

### 3.3 Sample Volume Correction

In order to resolve scattering from individual submicron particles with an SPC it

is generally necessary to use a focused laser beam as the incident light source. The most common laser mode is the fundamental  $TEM_{00}$ , which possesses a Gaussian radial intensity distribution across the beam. In that case the optical sample volume of an SPC designed for *in situ* operation becomes somewhat poorly defined. Here the optical sample volume can be considered as that region in space where particles are "seen" by the SPC. For example, very small particles will generate sufficient signals to be detected above the background or threshold noise level only when passing near the focus center of highest intensity. Conversely, particles of larger scattering cross sections can be detected even when passing through off-center portions of the laser beam with lower incident intensity. Thus uncorrected laser particle counter data are heavily weighted toward large particles and this size-selective sampling bias must be considered for accurate determination of particle size distributions.

To adequately model this size-selective sampling effect the following aspects of an SPC must be considered.

1. Intensity distribution near the laser focus.
2. Light-scattering characteristics of spherical particles based on Lorenz-Mie theory and irregular particles using the diffraction approximations.
3. The geometry and optical properties of the receiving optics including finite field of view effects.
4. Data acquisition electronics.

In practice the optical sample volume of *in situ* SPC is generally defined by the receiving optics field of view along the laser beam axis and in the radial direction by the laser focus intensity distribution. This is true because equal intensity contours near a Gaussian laser beam focus are very elongated in the axial direction (25). Typical sample volume dimensions are 20-100  $\mu\text{m}$

radially (at the  $1/e^2$  intensity points) and several millimeters axially.

A theoretical discussion of  $TEM_{00}$  laser beams and intensity distribution properties near a focus with emphasis on *in situ* SPC applications has been presented elsewhere by Hirleman and Stevenson (25). Techniques for experimentally measuring laser focus properties include traversing a small wire or pinhole across the beam or by magnifying the beam onto a photodiode array. Theory and experiment have been found to agree quite well here (3, 4, 17, 19). In order to theoretically predict the sample volume a one-dimensional, uniform particle flow was initially assumed. A plane containing the laser beam axis was divided into a two-dimensional grid. The light scattered by a particle situated at the center of each grid cell, proportional to the laser intensity at that cell, was integrated over the viewing aperture of each detector. It was then necessary to assume a threshold or minimum recognizable signal level for each detector. Particles at grid cells which generated sufficient scattered energy signals at each detector would then be "seen" by the MRSPC. The summation of the area of all grid cells which generated detectable signals for a given particle size then represents the sensitive area  $A_s$  or in other words the projection of the optical sample volume into a plane normal to the particle flow. This area is then a function of particle scattering characteristics since better scatterers generate detectable signals even when passing through the shoulders of the Gaussian intensity distribution. Theoretical predictions of the sample volume sensitive area for a particular MRSPC (17) are shown in Fig. 10. Again the response for nonabsorbing polystyrene spheres ( $n = 1.605$ ) shows much more oscillatory behavior than does the prediction for spherical soot particles. The threshold scattering cross section ( $A_s = 0$ ) for the polystyrene in Fig. 10 corresponded to a diameter of 0.422  $\mu\text{m}$  for a He-Cd laser with  $\lambda = 0.4416 \mu\text{m}$ . As ex-

pected this corresponds to a larger soot particle size due to the absorption.

In order to experimentally verify the model used to predict Fig. 10 it is necessary to generate a calibration aerosol of known and preferably constant concentration. In the experiments reported here appropriately diluted isopropanol solutions of polystyrene spheres were atomized and dried using standard techniques (4) to produce a calibration aerosol. Since the processes of deposition and agglomeration in the nonideal calibration aerosol system are effectively impossible to model, it was decided to independently measure the aerosol concentration at the MRSPC sample volume. This was done using a conventional 90°, white-light SPC similar to that of Borho (26). A 100-W mercury lamp with a 0.25-mm<sup>2</sup> arc size was used to illuminate the particles. A 0.6-mm slit imaged at 1:1 served as the receiving aperture in front of a photomultiplier tube oriented at right angles to the incident light beam from the arc lamp. The optics defined a sensitive area of dimensions 1.27 × 0.6 mm as projected normal to the plane of the incident and scattered beams for this 90° SPC. The incoherent light source was advantageous here in order to define a sample volume with approximately a "tophat" intensity distribution. This then eliminated the size-selective sampling bias problems associated with Gaussian laser beam intensity profiles. An indication of the intensity profile across the white-light SPC sample volume is shown in Fig. 11. Here a 1024-element linear photodiode array (25- $\mu$ m centers) was placed at the sample volume, and a signal proportional to the intensity incident on each diode is displayed by a digital oscilloscope in Fig. 11. The intensity profile in the sample volume is nearly flat with edge effects contributing approximately a 15% uncertainty.

The sample volumes of the MRSPC and the 90° white-light SPC were overlapped for the experiments. Polystyrene spheres of 1.011, 2.02, and 3.0  $\mu$ m flowing in air exited

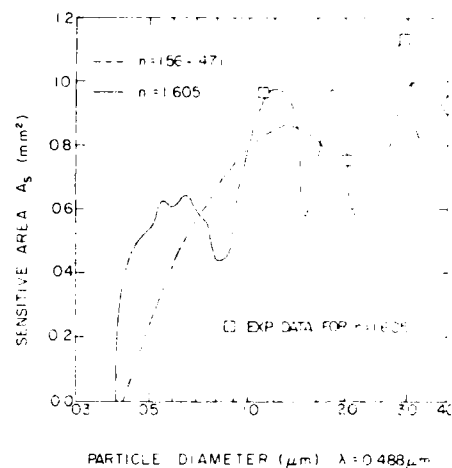


FIG. 10. Plot of sensitive area  $A_s$  vs particle size for 12°/6° ratio pair. Plotted with the theoretical predictions are experimental data for polystyrene calibration spheres ( $n = 1.605$ ) taken at  $\lambda = 0.4416 \mu\text{m}$ . One undetermined calibration factor for the experimental data (the same factor for all 3 data points) was fixed by optimizing the fit between theory and experiment.

a 5-cm tube and passed through the SPC sample volumes. This calibration aerosol jet was several times larger than the largest dimension of the optical sample volume. The absolute concentration of the calibration aerosol was measured in real time with the 90° SPC. The sensitive area of the MRSPC was then easily determined from the known aerosol velocity and the results plotted in Fig. 10.

The agreement between theory and experiment in Fig. 10 is quite good for the limited number of data points. Unfortunately, particles smaller than 1.0  $\mu$ m were very difficult to detect with the 90° SPC and it was not practical to atomize particles larger than 3.0  $\mu$ m. However, the predictions, although tedious, are reasonably straightforward and without highly speculative assumptions. We therefore conclude that the model is quite adequate for use in predicting probe volume corrections for an MRSPC.

In practice it is necessary to assume some type of mean or averaged curve for the probe

## SINGLE-PARTICLE COUNTER

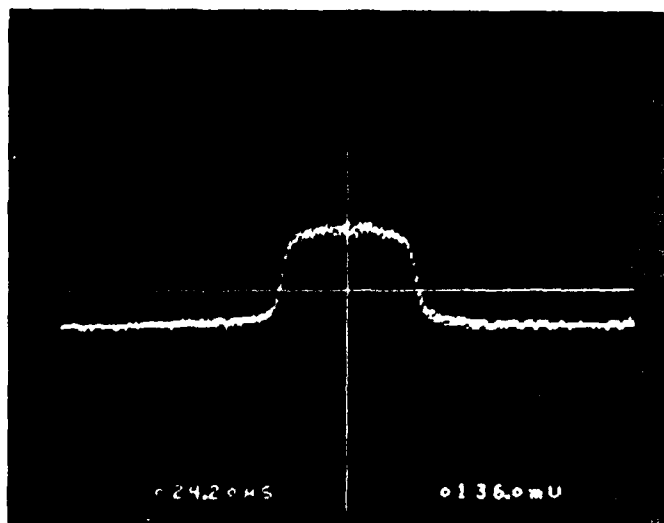


FIG. 11. Scan of output from 1024-element linear photodiode array facing the incident beam at the sample volume of the 90° white-light SPC. The diodes are on 25- $\mu\text{m}$  centers and the incident beam width shown is about 1.27 mm.

volume correction as again it depends on the unknown particle refractive index. Predictions such as in Fig. 10 indicate that a mean correction curve (e.g., of soot) for unknown particle compositions will introduce an uncertainty of about 30% in size distribution with an MRSPC.

### 3.4 Resolution

The resolution of a SPC is defined in terms of response to a monodisperse (uniform size) aerosol. A number of factors including electronics and data acquisition system errors, multivalued response functions, illumination intensity fluctuations, finite receiving aperture, and finite sample volume effects combine to produce a broadened SPC particle size distribution output response even for a monodisperse aerosol of spherical particles. This broadening is important in determining the ability of an SPC to resolve detailed structure of narrow and/or bimodal particle size distributions.

Resolution can be quantified in terms of  $\Delta d/d$ , where  $\Delta d$  is a statistical measure of

the uncertainty (or response broadening) in determining the size of a particle of diameter  $d$ . Since SPC response functions and sensitivity are functions of diameter the resolution  $\Delta d/d$  is dependent on  $d$  as well. Note that the resolution  $\Delta d/d$  is also related to the discrete size bin increments of a particular instrument, since it is clearly useful to divide the size range into intervals much smaller than the broadening errors  $\Delta d$ . Often the size bin increments are fixed coarse enough to ensure that most particles in a monodisperse aerosol are classified into one size bin. A priori information about the refractive index and the amount of deviation from spherical particle shapes should also influence the size increments in reported size distribution.

In order to study MRSPC resolution the computer simulation discussed in the previous section on sample volume effects was utilized. A map of ratio response as a function of position in the sample volume was made assuming one-dimensional particle trajectories normal to the laser beam (4). This was again accomplished by tracing

scattered light rays through the annular iris receiving system accounting for variations in both  $\theta$  and  $\phi$  (azimuthal) scattering angles.

A typical MRSPC response distribution predicted for a monodisperse aerosol is shown in Fig. 12. Broadening due to different dependencies of collection aperture on particle position for the 12 and 6° detectors is clear in Fig. 12. This prediction is typical of that expected for the range of angles and annular receiving-system designs of *in situ* MRSPC.

Experimental measurements of resolution have been made by the first author at two previous laboratories in addition to data taken in the present work. The measurements of  $\Delta d/d$  at 12°/6° for nominally 1- $\mu\text{m}$  polystyrene spheres were 0.41 (4), 0.40 (4), and 0.29 here (17). The latter two measurements were for similar but not identical lens/annular iris plate receiving-system designs. The prediction of resolution for the 0.40 data point was 0.28. Although detailed predictions of resolution for the latest design are not presently available, recent design improvements (17) should improve the predicted resolution to somewhat better than the 0.28 value. We feel that experimental errors account for the small difference between predicted and measured resolution and that the computer simulation is quite adequate. In practical applications of *in situ* MRSPC a  $\Delta d/d$  of approximately 0.30 is expected (3).

#### SUMMARY AND CONCLUSIONS

The development of accurate *in situ* techniques for measuring concentrations and size distributions of aerosols in combustion environments constitutes a broad and fundamentally important task. Laser techniques have great potential for this application but a number of real effects must be considered to ensure reliable measurements. A detailed analysis of several important potential problems with emphasis on the multiple-ratio counter (MRSPC) was completed.

*Journal of Colloid and Interface Science*, Vol. 87, No. 1, May 1982

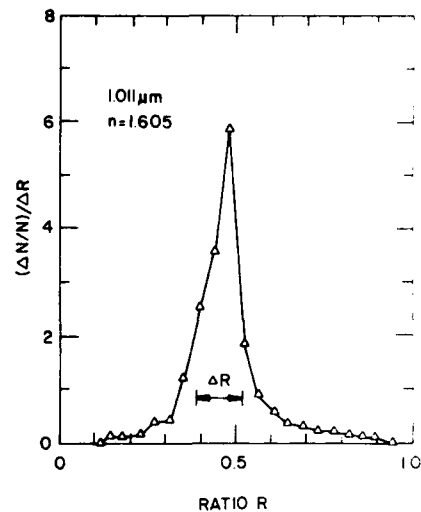


FIG. 12. Response probability distribution function of a 12°/6° MRSPC to 1.011- $\mu\text{m}$  polystyrene spheres in air. Here  $N$  is the number of counts at a particular ratio value.

First, an analysis of the effects of unknown particle refractive index was completed and indicated the relative advantages of forward scattering instruments. Second, a model was postulated to allow prediction of the response of ratio counters to nonspherical particles. Some experimental measurements supported the theory and a subsequent analytical study on a range of particle geometries expected in combustion environments confirmed that forward scattering ratio instruments are relatively insensitive to particle shape and surface characteristics. Next, a comprehensive computer simulation was developed to allow complete theoretical analysis of the laser MRSPC system. Detailed predictions of the dependence of sample volume on particle size and resolution were made and experimental work confirmed the validity of the model. The overall analysis indicated that the MRSPC can make *in situ* measurements of the size distribution of moderately nonspherical particles of unknown refractive index with a total uncertainty on the order of 50%.

## ACKNOWLEDGMENTS

Long-term support of the National Science Foundation during work on the topic of this paper is gratefully acknowledged. NSF support included a Graduate Fellowship for Ph.D. Studies, (E.D.H.) a Research Initiation Grant NSF No. 78-06210, and a Specialized Research Equipment Grant NSF No. 78-11462. This funding was through the Solid and Particulate Processes Program, Dr. Morris Ojalvo, Director.

## REFERENCES

1. Lundgren, D. A., *et al.*, Eds., "Aerosol Measurements." Univ. of Florida Press, Gainesville, Fla. 1976.
2. Whitby, K. T., and Willeke, K., in "Aerosol Measurements" (D. A. Lundgren *et al.*, Eds.). Univ. of Florida Press, Gainesville, Fla., 1976.
3. Hirleman, E. D., *Opt. Eng.* **19**, 854 (1980).
4. Hirleman, E. D., "Optical Technique for Particulate Characterization in Combustion Environments: The Multiple Ratio Single Particle Counter." Ph.D. dissertation, Purdue University, W. Lafayette, Indiana, August 1977.
5. Hodkinson, J. R., *Appl. Opt.* **5**, 839 (1966).
6. Gravatt, C. C., *J. Air Pollut. Control Assoc.* **23**, 1035 (1973).
7. Dalzell, W. H., and Sarofim, A. F., *J. Heat Transfer* **91**, 100 (1969).
8. Kerker, M., "The Scattering of Light and Other Electromagnetic Radiation," Academic Press, New York, 1969.
9. Dave, J. V., "Subroutines for Computing the Parameters of the Electromagnetic Radiation Scattered by a Sphere," IBM Report 320-3237, IBM Palo Alto Scientific Center, Palo Alto, Calif., May 1968, unpublished.
10. van de Hulst, H., "Light Scattering by Small Particles." Wiley, New York, 1957.
11. Oeschburg, F., *J. Aerosol Sci.* **3**, 307 (1972).
12. Holve, D., and Self, S. A., *Appl. Opt.* **18**, 1632 (1979).
13. Hirleman, E. D., and Wittig, S. L. K., in "Sixteenth Symposium (International) on Combustion," p. 245. The Combustion Institute, Pittsburg, Penn., 1977.
14. Kreikebaum, G., and Shofner, F. M., "Design Considerations and Field Performance for a Ratio-type Laser Light Scattering Instrument," presented at International Conference of Environmental Sensing and Assessment, Las Vegas, Nevada, Sept. 14, 1975, unpublished.
15. Ho, C. W., Tveten, A. B., Chan, P. W., and She, C. Y., *Appl. Opt.* **17**, 631 (1978).
16. Wittig, S. L. K., Hirleman, E. D., and Christiansen, J. V., in "Evaporation-Combustion of Fuels" (J. T. Zung, Ed.), p. 198. Amer. Chem. Soc., Wash. D. C., 1978.
17. Moon, N. K., "Response Characteristics of the Multiple Ratio Single Particle Counter," M. S. thesis, Arizona State University, Mechanical Engineering Dept., June 1980.
18. McSweeney, A., and Rivers, W., *Appl. Opt.* **11**, 2101 (1972).
19. Hirleman, E. D., Non-Doppler laser velocimetry: Single-beam transit-time LIV, *AIAA J.* **20**, 86 (1982).
20. Boron, S., and Waldie, B., *Appl. Opt.* **17**, 1644 (1978).
21. Vuk, C. T., Jones, M. A., and Johnson, J. H., "The Measurement and Analysis of the Physical Characteristics of Diesel Particulate Emissions," SAE Paper 760131, February 1976, unpublished.
22. Hodkinson, J. R., in "Electromagnetic Scattering" (M. Kerker, Ed.). MacMillan Co., New York, 1963.
23. Zerull, R. H., Giese, R. H., and Weiss, K., *Appl. Opt.* **5**, 839 (1966).
24. Pinnick, R. G., Carroll, D. E., and Hofmann, D. J., *Appl. Opt.* **15**, 384 (1976).
25. Hirleman, E. D., and Stevenson, W. H., *Appl. Opt.* **17**, 3496 (1978).
26. Borho, D. I. K., *Staub Reinhalt. Luft* **30**, 479 (1970).

# Response characteristics of laser diffraction particle size analyzers: optical sample volume extent and lens effects

**E. Dan Hirlleman**

Arizona State University  
Mechanical and Aerospace Engineering  
Department  
Tempe, Arizona 85287

**V. Oechsle  
N. A. Chigier**

Carnegie-Mellon University  
Mechanical Engineering Department  
Pittsburgh, Pennsylvania 15213

**Abstract.** The response characteristics of laser diffraction particle sizing instruments were studied theoretically and experimentally. In particular, the extent of optical sample volume and the effects of receiving lens properties were investigated in detail. The experimental work was performed with a Malvern Instruments Ltd. Model 2200 particle size analyzer using a calibration reticle containing a two-dimensional array of opaque circular disks on a glass substrate. The calibration slide simulated the forward-scattering characteristics of a Rosin-Rammler droplet size distribution. The reticle was analyzed with collection lenses of 63 mm, 100 mm, and 300 mm focal lengths using scattering inversion software that determined best-fit Rosin-Rammler size distribution parameters. The Malvern 2200 data differed from the predicted response for the reticle by about 10%. The discrepancies are attributed to nonideal effects in the detector elements and the lenses. A set of calibration factors for the detector elements was determined here that corrected for the nonideal response of the instrument. The response of the instrument was also measured as a function of reticle position, and the results confirmed a theoretical optical sample volume model presented here.

**Keywords:** particle sizing and spray analysis; laser diffraction particle sizing; instrumentation; instrument for particle sizing in sprays.

**Optic / Engineering 23(5), 610-619 (September/October 1984).**

## CONTENTS

1. Introduction
2. Theory
  - 2.1. Diffraction by spherical particles
  - 2.2. Inversion of scattering data
  - 2.3. Optical sample volume: influence of particle position
3. Experimental
  - 3.1. Calibration studies
  - 3.2. Effect of reticle rotation
  - 3.3. Effect of reticle position
4. Conclusions
5. Acknowledgments
6. References

## 1. INTRODUCTION

Light scattering by particles and droplets has been used as a sizing diagnostic for many years.<sup>1</sup> For particles significantly larger than the wavelength ( $D/\lambda > 10$ ), most of the light is scattered in the forward direction at small scattering angles as measured from the incident beam propagation direction. Under these conditions Fraunhofer diffraction theory adequately describes the scattering phenomena for most applications.<sup>2</sup> Analysis of forward-scattering signatures has been used to infer information about particle and droplet size distributions<sup>3,5</sup> for many years. Commercial in-

struments based on this general approach have been available for about 10 years.<sup>6-8,\*,†,‡</sup>

The schematic of a common laser diffraction apparatus is shown in Fig. 1. This technique has been rather extensively reviewed elsewhere,<sup>5,9</sup> and we summarize only some important aspects here. A laser beam is collimated to several millimeter diameter and passed through the particle stream or cloud. Some of the laser energy that is scattered by particles in the beam is collected by the receiving or transform lens and directed to the back focal plane for processing. The intensity distribution on this back focal or transform plane is directly related to the Fourier transform of the intensity distribution in the front focal plane of the lens.

Interrogation of the diffraction signature can be performed using detector(s) located in the transform plane or by using transmission masks of special design at the transform plane<sup>8,‡</sup> followed by a field lens and single detector. Early implementations of the former approach involved translation of a single detector across the transform plane, but more recently photodetector arrays have been used to simultaneously sample the entire diffraction pattern.

In this paper we consider the configuration proposed by Swithenbank et al.,<sup>6</sup> which is the basis for a series of commercial instruments manufactured by Malvern Instruments Ltd. Those researchers<sup>6</sup> utilized a monolithic photodiode array detector composed of 31 semicircular concentric annular detectors developed by Recognition Systems Inc. (Van Nuys, California). The scattering

Invited Paper PS 108 received March 31, 1984; revised manuscript received July 2, 1984; accepted for publication July 6, 1984; received by Managing Editor July 13, 1984.

© 1984 Society of Photo-Optical Instrumentation Engineers

\*Malvern Instruments Ltd., Malvern, Worcestershire, England  
†Compagnie Industrielle des Lasers (CILAS), Marcoussis, France  
‡Leeds and Northrup, Microtrac Division, Largo, Florida

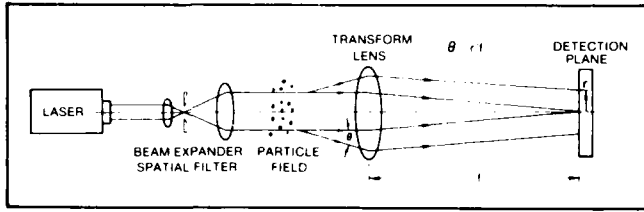


Fig. 1. Schematic of laser diffraction particle sizing instrument.

inversion techniques include those which assume the form of the distribution function (e.g., Rosin-Rammler or log-normal) and perform a least squares analysis of the scattering data to determine the best-fit size distribution parameters. Other inversion methods are available<sup>3,9,10,\*</sup> that do not invoke the assumption of a size distribution form. For the present study we consider the Rosin-Rammler size distribution software and present experimental results obtained using a calibration reticle designed to simulate a Rosin-Rammler size distribution. However, the results and models presented here are relevant to general laser diffraction particle sizing problems and are not limited to the Malvern instrument or a particular size distribution function.

## 2. THEORY

### 2.1. Diffraction by spherical particles

Consider particles illuminated by a collimated laser beam as in Fig. 1. A monodisperse ensemble of spherical particles that are large compared to the wavelength would produce the characteristic Airy diffraction pattern (neglecting anomalous diffraction), as described by Fraunhofer diffraction theory<sup>1,2</sup>:

$$I(\theta) = cI_{\text{inc}} \frac{\pi^2 D^4}{16\lambda^2} \left[ \frac{2J_1(\pi D\theta/\lambda)}{(\pi D\theta/\lambda)} \right]^2, \quad (1)$$

where  $I(\theta)$  is scattered intensity at the angle  $\theta$  measured from the laser beam axis,  $c$  is a proportionality constant,  $I_{\text{inc}}$  is the intensity of the incident beam,  $J_1$  is the first-order Bessel function of first kind,  $D$  is the particle diameter, and  $\lambda$  is the laser wavelength. The obliquity correction has been neglected in Eq. (1), and the small angle approximation of  $\sin\theta = \theta$  has been made. The coefficient of the bracketed squared term is the on-axis scattering intensity  $I(0)$ .

In practical systems a distribution of particle sizes, or a polydispersion, is generally encountered. The composite scattered intensity profile is a linear combination of the characteristic profiles of each droplet size with a weighting coefficient equal to the number of particles of that size in the sample volume. The diffraction signature of a polydisperse spray is given by

$$I(\theta) = cI_{\text{inc}} \int_0^{\infty} \frac{\pi^2 D^4}{16\lambda^2} \left[ \frac{2J_1(\pi D\theta/\lambda)}{(\pi D\theta/\lambda)} \right]^2 n(D)dD, \quad (2)$$

where  $n$  is a differential number distribution such that  $n(D)dD$  is the number of particles in the laser beam with sizes between  $D$  and  $D + dD$ . Note that Eq. (2) assumes a uniform intensity profile across the laser beam (constant  $I_{\text{inc}}$ ); also  $n(D)$  integrated over all particle sizes is the total number of particles in the beam.

The scattered light that is refracted by the receiving lens in Fig. 1 is directed onto the transform plane at radial positions given by (neglecting lens aberrations)

$$r = f\theta, \quad (3)$$

where  $f$ ,  $r$ , and  $\theta$  are defined in Fig. 1. Note that Eq. (3) is independent of scattering particle position. Consider an array of annular detector elements where  $r_{ij}$  and  $r_{oj}$  are the inner and outer radii, respectively, of the  $j^{\text{th}}$  ring detector. The  $j^{\text{th}}$  detector collects (neglecting vignetting by the receiving lens aperture) a hollow cone of scattered light defined by inner and outer scattering angles  $\theta_{ij}$  and  $\theta_{oj}$ , which are related to  $r$  through Eq. (3). The scattered light energy  $S_j$  collected by the  $j^{\text{th}}$  finite aperture annular ring detector is obtained by integrating  $I(\theta)$  from Eq. (2) over the aperture,<sup>6</sup> giving

$$S_j = cI_{\text{inc}} \int_0^{\infty} \frac{\pi D^4}{4} \left( J_{0ij}^2 + J_{1ij}^2 - J_{0oj}^2 - J_{1oj}^2 \right) n(D)dD, \quad (4)$$

where

$$J_{npj}^2 = J_n^2 \frac{\pi D r_p}{\lambda f}, \quad (5)$$

with  $n$  indicating the order of the Bessel function and  $p$  indicating inner  $i$  or outer  $o$  detector radius.

### 2.2. Inversion of scattering data

The inverse scattering problem, that is, to determine the particle size distribution  $n(D)$  from measured light-scattering signatures  $I(\theta)$  or  $S_j$ , has been studied for many years. Integral transform inversions of Eq. (2) are possible,<sup>3,9</sup> but are not commonly used at present. Generally the size distribution is divided into a finite number of discrete size classes, typically of the order  $2^3$  or  $2^4$ . In some cases the size distribution function is assumed to follow some common form with two degrees of freedom, such as Rosin-Rammler<sup>6,\*</sup> or log-normal. Other approaches<sup>10,\*</sup> do not constrain the results to a particular form and are termed model-independent inversion methods.

In this paper we will confine our attention to Rosin-Rammler size distribution models. The Rosin-Rammler distribution function is given by<sup>11</sup>

$$R = \exp \left[ - \left( \frac{D}{\bar{x}} \right)^N \right], \quad (6)$$

where  $R$  is the volume fraction of particles with a diameter greater than  $D$ ,  $N$  is a parameter related to the polydispersity of the distribution ( $N = \infty$  is monodisperse), and  $\bar{x}$  is a representative mean diameter such that 37.8% of the total particle volume is greater than  $\bar{x}$ .

The scattering inversion problem then becomes one of determining values of  $\bar{x}$  and  $N$  for which corresponding predictions for  $S_j$  from Eq. (4) match measured scattering data. The Malvern ST1800 and 2200 instruments divide the particle sizes into 15 discrete size intervals and sum the scattering from pairs of adjacent ring detector elements to give effectively 15 scattering measurements. The set of diameter limits  $D_{1k}$  and  $D_{1k}$  (Table I) are fixed by the detector geometry such that the so-called "energy distribution," or  $I(\theta)\theta$ , is in a sense optimized. The scattering function  $I(\theta)\theta$  reaches a maximum at the angle  $\theta_{\text{mx}}$  given by

$$\frac{\pi D \theta_{\text{mx}}}{\lambda} = 1.35^* \quad (7)$$

and at a radial position on the detector plane from Eq. (3) given by

\*Malvern Instruments Ltd., Malvern, Worcestershire, England

**TABLE I. Size Class Limits for Malvern 2200 Laser Diffraction Particle Sizing Instrument with 300 mm Focal Length Receiving Lens\***

Size class No.	Lower size limit $D_L$ ( $\mu\text{m}$ )	Upper size limit $D_U$ ( $\mu\text{m}$ )
1	261.6	564.0
2	160.4	261.6
3	112.8	160.4
4	84.3	112.8
5	64.6	84.3
6	50.2	64.6
7	39.0	50.2
8	30.3	39.0
9	23.7	30.3
10	18.5	23.7
11	14.5	18.5
12	11.4	14.5
13	9.1	11.4
14	7.2	9.1
15	5.8	7.2

\*Malvern Instruments Ltd., Malvern, Worcestershire, England

$$\frac{\pi D r_{\text{mx}}}{\lambda f} = 1.357. \quad (8)$$

Note that an incorrect value of 1.375 has appeared in the literature<sup>6,9</sup> as the right-hand side of Eqs. (7) and (8). A particular annular detector element with  $r_{ij}$  and  $r_{oj}$  specified is most responsive to particles in a finite size range with diameter limits determined by Eq. (8). For example, from Table II consider composite ring detector No. 14 comprised of elements 27 and 28 with  $r_{o14} = 11.501$  mm. For  $f = 300$  mm and  $\lambda = 0.6328 \mu\text{m}$ , the value  $D_{L14} = D_{U15} = 7.224 \mu\text{m}$  satisfies Eq. (8) with the incorrect constant 1.375.

Once the set of  $D_U$  and  $D_L$  is determined, it is useful to define a scattering influence coefficient matrix  $C$  such that a unit volume of particles in the size interval from  $D_{Lk}$  to  $D_{Uk}$  produces a scattering signal  $C_{kj}$  on the  $j^{\text{th}}$  detector element.  $C_{kj}$  is given to within a constant by

$$C_{kj} = \frac{\int_{D_{Lk}}^{D_{Uk}} \frac{\pi D^2}{4} \left( J_{0ij}^2 + J_{1ij}^2 - J_{0oj}^2 - J_{1oj}^2 \right) n(D) \frac{\pi D^3}{6} dD}{\int_{D_{Lk}}^{D_{Uk}} n(D) \frac{\pi D^3}{6} dD}, \quad (9)$$

where the denominator is just the total particle volume in the  $k^{\text{th}}$  size interval. Note that knowledge of the size distribution function is required to solve Eq. (9) as formulated. Since again  $n(D)$  is not known *a priori*, it is convenient to assume that the unit volume for the  $k^{\text{th}}$  size interval is divided into, say, 100 discrete subintervals of equal volume. Then  $n(D)$  is calculated for each subinterval, and Eq. (9) is evaluated numerically. The  $\bar{C}$  matrix generated here in this manner agrees with that used in the Malvern 2200 instruments to better than 1%. Definition of  $C$  on a volume basis is not optimal, but is convenient in this case because the Rosin-Rammler distribution in Eq. (6) is on a volume basis. The predicted scattering signature then becomes a matrix equation:

$$\bar{S} = \bar{C} \bar{V}, \quad (10)$$

where  $V_k$ , the  $k^{\text{th}}$  element of  $\bar{V}$ , is the volume fraction of particles with diameters between  $D_{Lk}$  and  $D_{Uk}$ . One problem with Rosin-

**TABLE II. Dimensions of the Annular Detector Elements of the Malvern 2200 Photodiode Array Detector\***

Detector ring No.	Inner radius (mm)	Outer radius (mm)
1	0.149 (0.124)	0.218
2	0.254	0.318
3	0.353	0.417
4	0.452	0.518
5	0.554	0.625
6	0.660	0.737
7	0.772	0.856
8	0.892	0.986
9	1.021	1.128
10	1.163	1.285
11	1.321	1.461
12	1.496	1.656
13	1.692	1.880
14	1.915	2.131
15	2.167	2.416
16	2.451	2.738
17	2.774	3.101
18	3.137	3.513
19	3.549	3.978
20	4.013	4.501
21	4.536	5.085
22	5.121	5.738
23	5.773	6.469
24	6.505	7.282
25	7.318	8.184
26	8.219	9.185
27	9.220	10.287
28	10.323	11.501
29	11.537	12.837
30	12.873	14.300

\*The only discrepancy is the inner radius of Ring No. 1 which was reported<sup>14</sup> as 0.124 mm. However, the corresponding elements of the scattering matrix used in the Malvern 2200 instrument (Malvern Instruments Ltd., Malvern, Worcestershire, England) are consistent with the value of 0.149 mm shown here.

Rammler distributions typical of liquid sprays is the presence of significant particle volume below the smallest  $D_L$ . In contrast, there is very seldom significant volume above the largest  $D_U$ . To account for this problem another column of the  $\bar{C}$  matrix can be generated, and another entry in the  $\bar{V}$  vector representing the particle volume below the smallest value of  $D_L$  can be used in the solution. The inverse scattering problem can then be posed: find the values of  $\bar{V}$  and  $N$  and the corresponding  $\bar{V}$  that minimize the magnitude or sum square of the residual error vector  $\bar{r}$  defined by

$$\bar{r} = \bar{S}_{\text{exp}} - \bar{C} \bar{V}, \quad (11)$$

where  $\bar{S}_{\text{exp}}$  is the measured scattering signature. The best-fit (in the least squares sense) Rosin-Rammler parameters were found using a modified Newton-Raphson scheme. The algorithm developed here gives results that are virtually identical to that of the Malvern instruments. In the simulations that follow we used our inversion algorithm, but the results are indicative of Malvern instrument performance.

**2.3. Optical sample volume: influence of particle position**

It is often pointed out that ideally the response of laser diffraction systems is not dependent on particle position relative to the receiving lens. This claim is true only when vignetting is not a factor, that is, when all scattering energy leaving the particle strikes within the clear aperture of the receiving lens. Laser diffraction instrument response does, therefore, depend on particle position, lens aperture, and particle size as it dictates the angular distribution of scattered energy. Consider Fig. 2 showing the important parameters of the problem, which include the receiving lens diameter  $d_l$  and focal length  $f$ ; the receiving lens  $F\# = f/d_l$ ; the inner and outer radii of

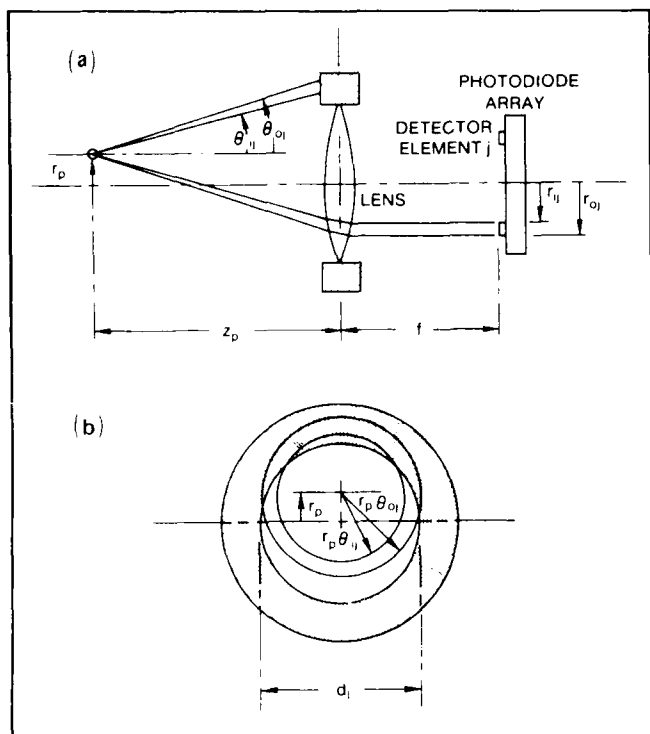


Fig. 2. Geometry of laser diffraction optical system and parameters of importance in characterizing vignetting and the optical sample volume. (a) side view, and (b) end view at principal plane of lens.

the  $j^{\text{th}}$  annular ring detector,  $r_{i_j}$  and  $r_{o_j}$ , respectively; and the particle position represented as a distance  $r_p$  from the optical axis and distance  $z_p$  from the lens. Ideally, the receiving lens converts angular scattering information to spatial information, as given by Eq. (3). Recall that each detector ring collects scattered energy over a finite conical shell limited by  $\theta_{i_j}$  and  $\theta_{o_j}$ , which are related to  $r_{i_j}$  and  $r_{o_j}$  through Eq. (3). We define first the angular collection efficiency  $\eta_\theta(r_p, z_p)$  as the fraction of energy that is scattered by a particle at  $(r_p, z_p)$  between scattering angles  $\theta$  and  $\theta + d\theta$  and that passes through the lens' clear aperture and reaches the detection plane. We neglect lens aberrations and azimuthal variations in the scattering for the purposes of this analysis. Under those assumptions  $\eta_\theta$  for any  $\theta$  is just the length of the arc that falls inside the receiving lens aperture divided by the circumference of the circle of radius  $z_p\theta$  in Fig. 2(b), where  $\tan\theta \approx \theta$  is assumed. The collection efficiency  $\eta_j$  for the  $j^{\text{th}}$  annular detector element is obtained by integrating over the limiting scattering angles for that ring:

$$\eta_j = \frac{\int_{\theta_{i_j}}^{\theta_{o_j}} \eta_\theta I(\theta) d\theta}{\int_{\theta_{i_j}}^{\theta_{o_j}} I(\theta) d\theta} \quad (12)$$

where both  $\eta_j$  and  $\eta_\theta$  are functions of  $r_p$  and  $z_p$ . Thus, to determine  $\eta_j$  for any detector requires integration of the scattering intensity  $I(\theta)$  over  $\theta$ , which in turn requires knowledge of the size distribution for use in Eq. (2). Since the size distribution is generally not known *a priori*, it is of interest to obtain approximate results for Eq. (12) that are of general applicability.

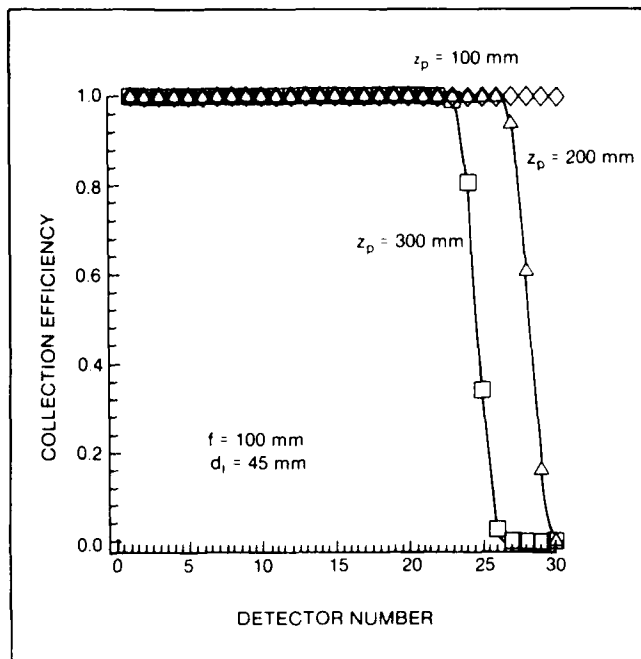


Fig. 3. Collection efficiency  $\eta$  averaged over radial positions in an 8 mm circle for the indicated positions  $z_p$ . Predictions assume  $f = 100$  mm and a Gaussian beam with  $1/e^2$  radius of 4.5 mm.

Two approaches can be used. First  $\eta_\theta$  can be assumed constant, assigned a representative value, and taken out of the integral in Eq. (12). This approach introduces significant errors for detector elements where  $\theta_{i_j}$  falls completely within the lens aperture and  $\theta_{o_j}$  is truncated. A second approach is to assume that  $I(\theta)$  is nearly constant over the  $\theta$  range of each detector element (i.e., thin ring detectors) and take it out of the integral in Eq. (12). We have chosen the latter approach and found that for typical size distributions found in sprays the errors are rather small, on the order of a few percent. For that assumption we obtain

$$\eta_j = \frac{1}{(\theta_{o_j} - \theta_{i_j})} \int_{\theta_{i_j}}^{\theta_{o_j}} \eta_\theta d\theta \quad (13)$$

where the dependence on  $r_p$  and  $z_p$  is again implied but not specified.

To model the response of a laser diffraction instrument to particles distributed over a plane normal to the optical axis at  $z_p$ , the collection efficiency  $\eta_j(r_p, z_p)$  must be integrated over all  $r_p$  as weighted by the local incident laser intensity. We denote the collection efficiency averaged over a plane in this manner as  $\eta_j(z_p)$ . For the calibration studies here particles on the calibration reflect were randomly distributed in an 8 mm diameter circle, and the laser beam is assumed to have a Gaussian intensity profile with 4.5 mm radius at the  $1/e^2$  intensity points. The results are insensitive to minor deviations from the assumed Gaussian profile. Figure 3 is a plot of plane-averaged  $\eta_j(z_p)$  for a 100 mm lens for several values of  $z_p$ . Note the expected dependence of collection efficiency, which is constant at 1.0 until the onset of the vignetting.

An indicator for the onset of vignetting at the  $j^{\text{th}}$  detector of a laser diffraction system is obtained from geometrical relations in Fig. 2, assuming small  $\theta^2$ :

$$d_l - 2r_p = \frac{r_{o_j}}{f} \quad (14)$$

For example, take  $r_p = 4.5$  mm, which is the nominal  $1/e^2$  radius of the Malvern 2200 beam. For the  $f = 100$  mm,  $d_l = 45$  mm lens used in Fig. 3 and the outermost ring detector in Table II, we obtain  $z_p = 125.9$  mm. When there is not significant scattered energy on the detector element of interest (e.g., due to the presence of only large particles), then the effect of vignetting would be negligible and Eq. (14) is a conservative indicator. Another criterion that includes this effect has also been derived<sup>13</sup>:

$$\frac{d_l - 2r_p}{2z_p} = \frac{3.83\lambda}{\pi D}, \tag{15}$$

which assumes that energy scattered by a particle  $D$  outside the first minimum in the diffraction pattern is not significant. For the previous example, the particle diameters of interest would have to be  $5.4 \mu\text{m}$  or smaller to predict significant vignetting at  $z_p = 125.9$  mm by the criterion of Eq. (15).

To predict the response of a laser diffraction instrument to a particle size distribution, the scattering contribution from each particle size on each ring must be adjusted by the collection efficiency. The scattered energy collected on the  $j^{\text{th}}$  detector would then be

$$S_j = cI_{\text{inc}} \sum_k \frac{\pi D_k^2}{4} \eta_j(z_p) \times \left( J_{0j}^2 + J_{1j}^2 - J_{00j}^2 - J_{10j}^2 \right) M(D_k), \tag{16}$$

where  $M$  is the effective number of particles of size class  $k$  on the calibration reticle ("effective" here means that each particle is weighted by the local incident intensity).

**3. EXPERIMENTAL**

In order to investigate the theoretical models presented above, a series of calibration experiments was performed on the Malvern 2200 particle size analyzer in the Mechanical Engineering Department at Carnegie-Mellon University. Since it is effectively impossible to design an actual spray with the definition, stability, and repeatability required for detailed calibration studies, another method was necessary. For this purpose we utilized an artificial "aerosol" composed of an array of chrome thin-film circles on a transparent glass substrate. The calibration reticle\* used 10,491 of these particles randomly positioned in an 8 mm circle to simulate a Rosin-Rammler distribution of spherical particles, following Eq. (6). Specifically, we used reticle model RR-50-3.0-0.08-102-CF Serial No. 111 with nominal parameters  $\bar{x} = 50 \mu\text{m}$ ,  $N = 3.0$ , and 0.08 as the area fraction obscured by the chrome particles. The continuous Rosin-Rammler size distribution is approximated on the reticle using 23 discrete particle sizes ranging from  $5.2 \mu\text{m}$  to  $92.7 \mu\text{m}$ . Data points for the cumulative and differential "volume" distributions for the reticle are shown in Figs. 4 and 5. Also plotted in Figs. 4 and 5 are the Rosin-Rammler curves that describe the best-fit parameters  $\bar{x}$  and  $N$  (in the least squares sense) to the actual reticle size distribution. The inherent assumption that the two-dimensional circles on the reticle simulate the forward-scattering characteristics of spherical particles of the same diameter is well-justified for the size range of interest here. The differences between best-fit and nominal Rosin-Rammler parameters are the result of nonideal effects in the reticle fabrication process coupled with the discrete nature of the size distribution.

Another estimate of the most representative parameters for the size distribution on the reticles was obtained by calculating a predicted scattering signature on the Malvern 2200 detectors using

\*Laser Electro-optics Ltd., Tempe, Arizona

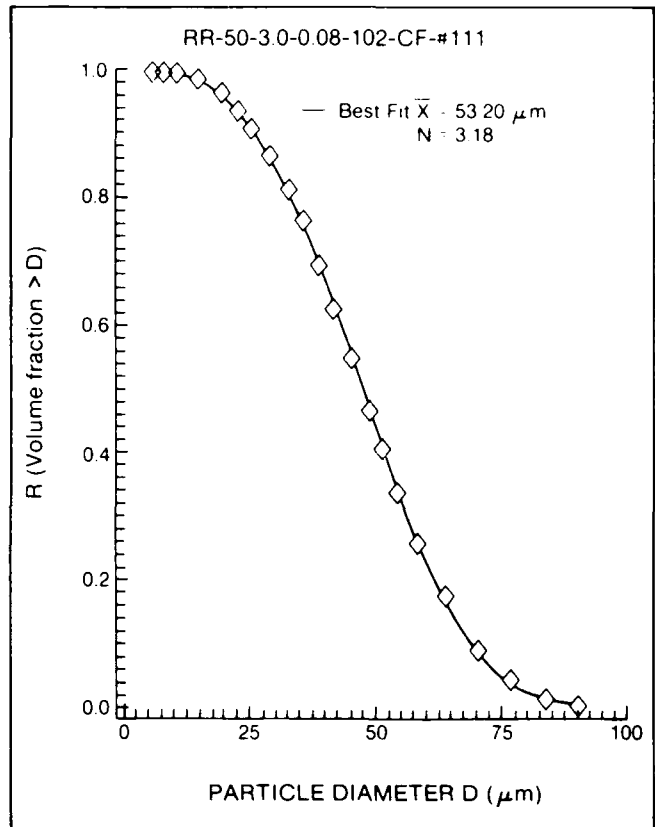


Fig. 4. Cumulative volume fraction  $R$  vs diameter  $D$  for calibration reticle RR-50-3.0-0.08-102-CF-#111. The 22 data points are plotted at the volume mean diameters corresponding to the intervals between the 23 particle sizes on the reticle. The solid curve is for the least squares fit Rosin-Rammler distribution with  $\bar{x} = 53.20$  and  $N = 3.18$ .

TABLE III. Representative Rosin-Rammler Parameter Values for Calibration Reticle RR-50-3.0-0.08-102-CF-#111

Least squares fit criterion	$\bar{x}$	$N$	$D_{32}$
Cumulative volume fraction $R$	53.20	3.18	40.27
$dV/dD$	52.81	3.18	39.98
Inversion of predicted diffraction signature, $f = 300$ mm	52.73	3.30	40.47
Actual $D_{32}$ based on number distribution	—	—	40.31
Average of above	52.91	3.22	40.26

Eq. (3) and the known number distribution on the reticle accounting for the intensity distribution and particle overlap. These predicted signal levels were then input to the inversion software as synthetic data, and the best-fit Rosin-Rammler parameters were calculated. The results are summarized in Table III.

All experiments reported here were performed by first taking a background signal through a clear region of the reticle substrate and then moving the reticle to roughly center ( $\pm 0.5$  mm) the sample area in the laser beam. The scattering data used by the instrument inversion software are the differences of these two measurements at each detector; therefore, to first order, the scattering contribution from random imperfections and impurities in the glass substrate are subtracted out. A new background signature

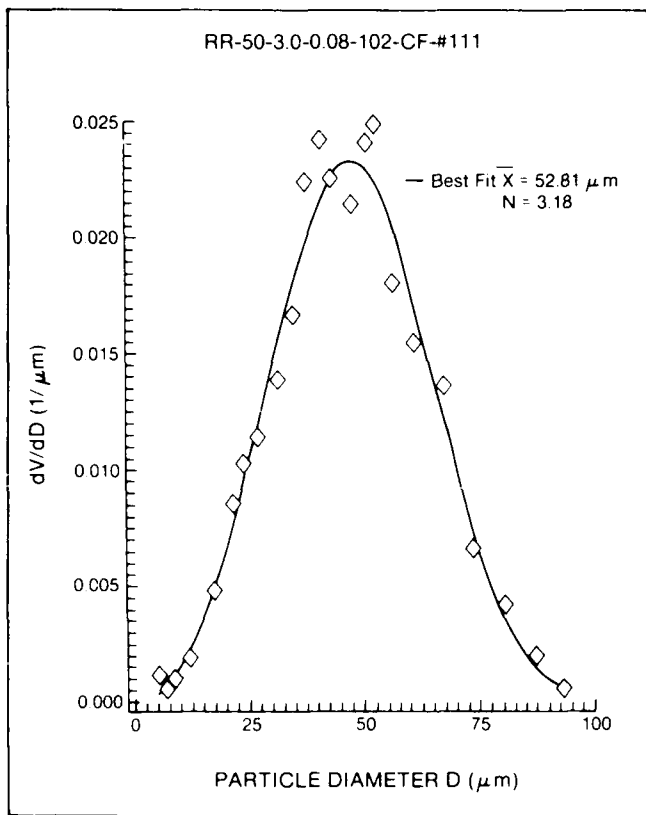


Fig. 5. Differential volume distribution  $dV/dD$  vs particle diameter  $D$  for calibration reticle RR-50-3.0-0.08-102-CF-#111. The data points correspond to the 23 discrete particle sizes on the reticle and the solid curve is for the least squares fit Rosin-Rammler distribution with  $\bar{x} = 52.81$  and  $N = 3.18$ .

was taken before each run, thereby making all experiments independent.

### 3.1. Calibration studies

We performed a series of experiments using three standard Malvern lenses of 63 mm, 100 mm, and 300 mm focal length. For each lens at least 14 independent runs were made with the reticle in a position  $z_p$  where vignetting effects are not present. The results of the experiments are summarized in Table IV, where  $\bar{x}$  and  $N$  are the best-fit parameters determined by the Malvern instrument and  $D_{32}$  is calculated from those. The predicted values were determined by calculating a scattering signature using Eq. (4) for the known size distribution on the reticle and then simulating the Malvern inversion process of Eq. (11). The Gaussian laser beam intensity distribution was considered, and lens aberrations were neglected.

We wish to focus on two different discrepancies elucidated by Table IV. First, the Malvern response to the same reticle varies, depending on the lens. This discrepancy is due in part to the discrete nature of the Malvern size classes and the reticle size

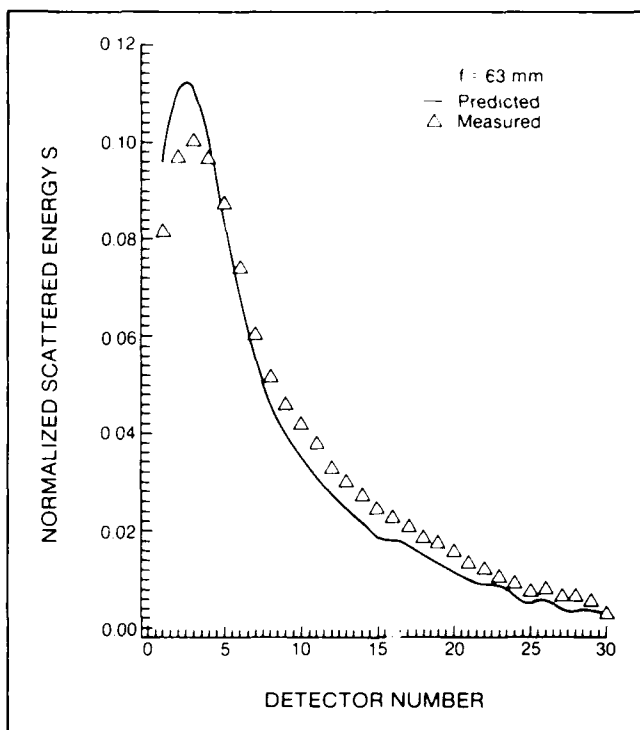


Fig. 6. Normalized scattered energy  $S$  vs detector number predicted for calibration reticle RR-50-3.0-0.08-102-CF-#111 on Malvern 2200 instrument with  $f = 63$  mm and  $z_p = 50$  mm. The solid line is a spline fit through the calculated values (neglecting lens aberrations), and the experimental data points are averages for each detector over 10 independent runs. Both signatures were normalized to 1.0, and the standard deviations were less than the symbol dimensions.

distribution, but detector calibration errors and nonideal lens effects are present as well. The predicted values in Table IV indicate much smaller changes. The second major discrepancy in Table IV is between the absolute values of the data and predictions. This difference is attributable to absolute calibration or sizing errors—either in the instrument or the reticle. We suspect the instrument because the reticle is extremely well defined and because of other reasons discussed below.

A better indication of the scattering physics is obtained from Figs. 6 to 8, where the predicted and measured scattering signatures are shown. The measured data are averaged separately for each detector after the integrated signal over all 30 detectors is normalized to 1.0. Discrepancies between experiment and predictions in Figs. 6 to 8 are statistically significant. The differences are also plotted as calibration factors in Figs. 9 to 11. Raw scattering data from the 30 Malvern detectors must be multiplied by the appropriate calibration factor to bring the instrument into agreement with the calculated scattering signature for the reticle.

An independent calibration of the detectors was obtained by illuminating the entire array (with no receiving lens installed) with an incoherent light beam of uniform intensity profile.<sup>12</sup> The uniform

TABLE IV. Predicted and Measured Response of Malvern 2200 to Calibration Reticle RR-50-3.0-0.08-102-CF-#111 at Positions Where Vignetting is Negligible (standard deviations of measurements also tabulated)

Focal length (mm)	No. of runs	Measured			Predicted			Adjusted measured		
		$\bar{x}$	$N$	$D_{32}$	$\bar{x}$	$N$	$D_{32}$	$\bar{x}$	$N$	$D_{32}$
63	14	47.30 ± 1.57	3.25 ± 0.15	36.06 ± 0.53	51.54	3.54	40.54	51.54	3.04	38.29
100	18	47.91 ± 1.04	3.63 ± 0.15	37.97 ± 0.35	52.03	3.46	40.62	52.15	3.22	39.66
300	28	55.19 ± 0.39	3.00 ± 0.06	40.76 ± 0.32	52.73	3.30	40.47	53.92	3.02	39.94

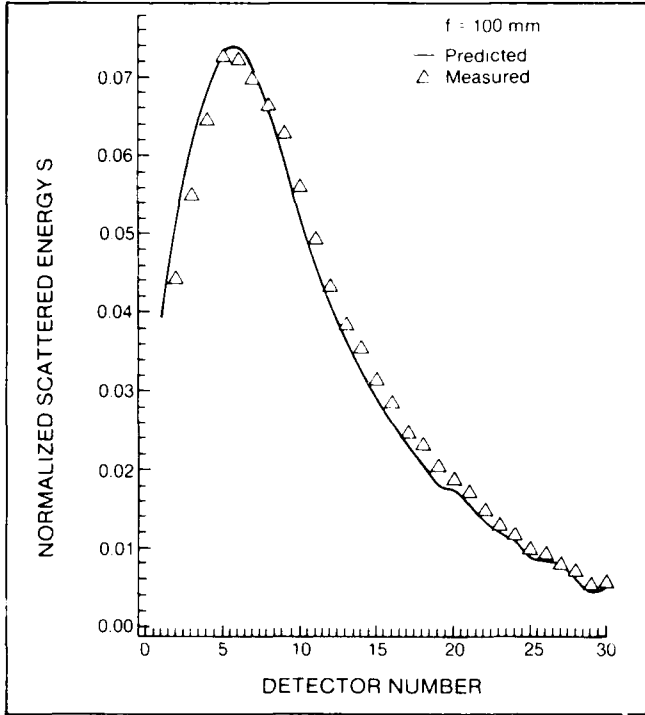


Fig. 7. Normalized scattered energy  $S$  vs detector number predicted for calibration reticle RR-50-3.0-0.08-102-CF-#111 on Malvern 2200 instrument with  $f = 100$  mm and  $z_p = 100$  mm. The solid line is a spline fit through the calculated values (neglecting lens aberrations), and the experimental data points are averages for each detector over 10 independent runs. Both signatures were normalized to 1.0, and the standard deviations were less than the symbol dimensions.

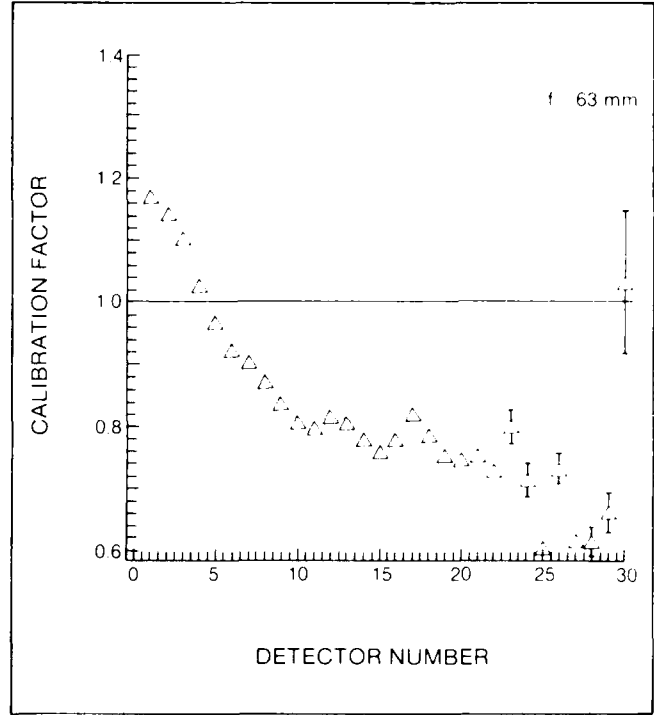


Fig. 9. Calibration factor vs detector number for the Malvern 2200 instrument at Carnegie-Mellon University for the  $f = 63$  mm lens. The calibration factors bring the mean values of the scattering data of Fig. 6 into agreement with predictions for reticle RR-50-3.0-0.08-102-CF-#111. The uncertainty bars are determined from the relative standard deviations for the data in Fig. 6.

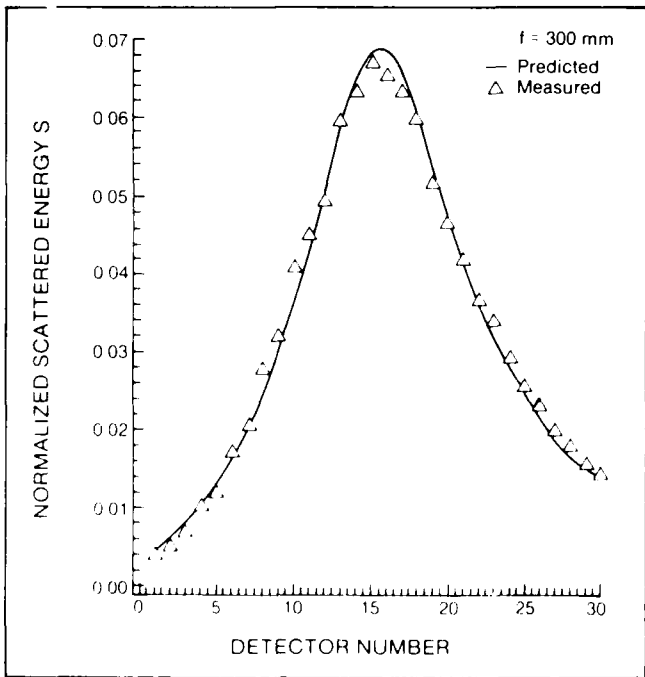


Fig. 8. Normalized scattered energy  $S$  vs detector number predicted for calibration reticle RR-50-3.0-0.08-102-CF-#111 and #115 on Malvern 2200 instrument with  $f = 300$  mm and  $z_p = 300$  mm. The solid line is a spline fit through the calculated values (neglecting lens aberrations), and the experimental data points are averages for each detector over 38 independent runs. Both signatures were normalized to 1.0, and the standard deviations were less than the symbol dimensions.

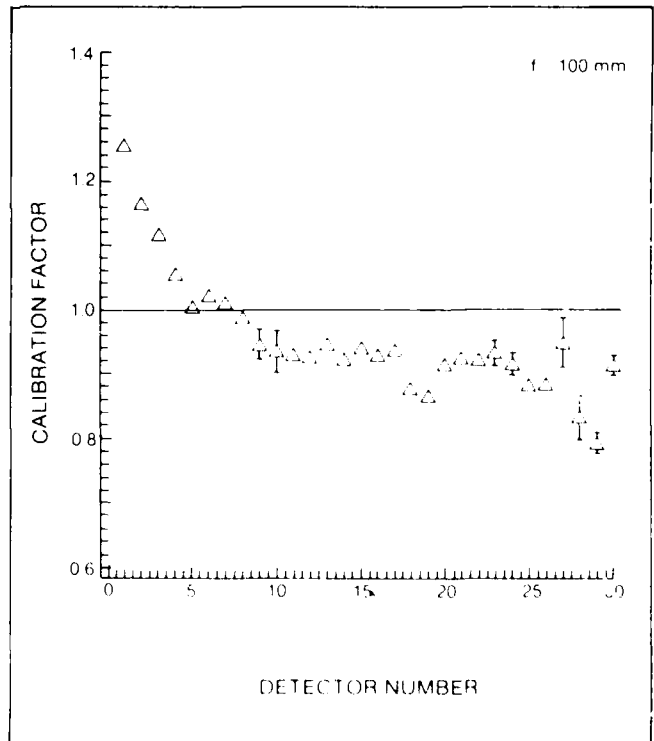
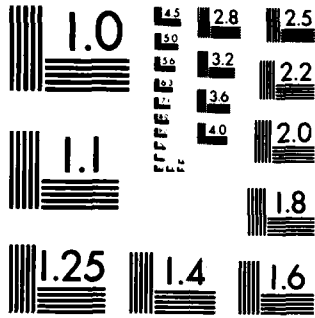


Fig. 10. Calibration factor vs detector number for the Malvern 2200 instrument at Carnegie Mellon University for the  $f = 100$  mm lens. The calibration factors bring the mean values of the scattering data of Fig. 7 into agreement with predictions for reticle RR-50-3.0-0.08-102-CF-#111. The uncertainty bars are determined from the relative standard deviations for the data in Fig. 7.





MICROCOPY RESOLUTION TEST CHART  
NATIONAL BUREAU OF STANDARDS-1963-A

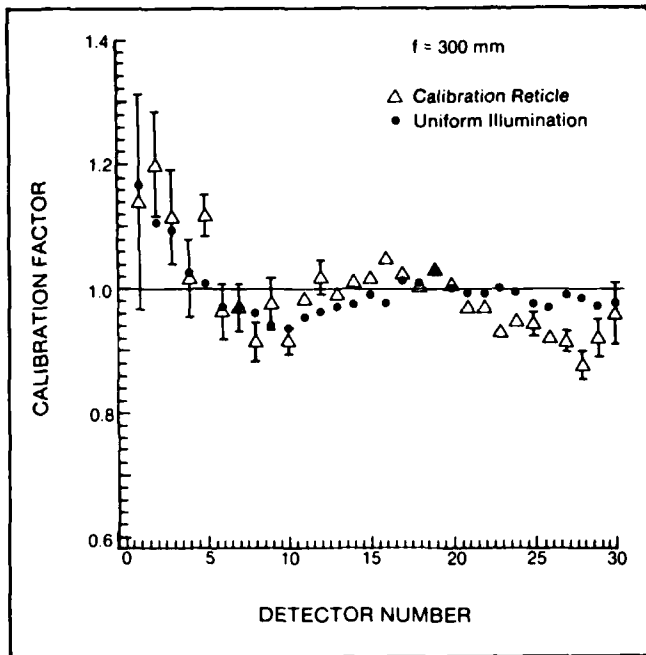


Fig. 11. Calibration factor vs detector number for the Malvern 2200 instrument at Carnegie-Mellon University for the  $f = 300$  mm lens. The calibration factors bring the mean values of the scattering data of Fig. 8 into agreement with predictions for reticle RR-50-3.0-0.08-102-CF-#111 and #115. The uncertainty bars are determined from the relative standard deviations for the data in Fig. 8.

illumination calibration data plotted in Fig. 11 were obtained using solar illumination. Runs at eight different incident intensity levels were combined using least squares fitting to obtain adequate signal-to-noise ratio over the large dynamic range of detector areas. We and others<sup>12</sup> have also used light sources such as dc lamps to obtain a similar calibration. Though this uniform intensity calibration did not simulate either the monochromatic properties of the laser, the variations in angle of incidence of light on the detector surface, or the lens aberrations that will be present in actual experiments, it does provide some useful data.

Deviation of the uniform illumination calibration factors in Fig. 11 from 1.0 is due to nonuniform responsivity of the detectors or errors in the geometrical parameters in Table II. Differences between the uniform illumination calibration factors in Fig. 11 and the reticle-derived factors in Figs. 9 to 11 should then be due to lens aberrations and/or variations in detector efficiency with angle of incidence. Note that the reticle calibrations were performed at only one laser power so that the signal-to-noise ratio varied across the detector as reflected by the larger uncertainties in the calibration factors for detector elements that had low signal levels in Figs. 6 to 8.

To further clarify the sources of error, a column for adjusted (using the calibration factors measured here) measured data is shown in Table IV. There the mean measured diffraction signatures were corrected using the uniform illumination calibration factors of Fig. 11, and the scattering inversion was performed on this adjusted data. The improvement in the adjusted measured values for the shorter focal length lenses is due to the large calibration factors for the inner detectors, where most of the diffraction information in Figs. 6 and 7 is concentrated. Conversely, most of the diffracted energy for the 300 mm lens is in the middle detector elements where the calibration factors in Fig. 11 are near unity. Though a substantial fraction of the calibration errors is due to detector nonidealities, it appears that the differences between the reticle-derived factors in Figs. 9 to 11 are significant. Our calculations suggest that lens aberrations rather than angle-of-incidence effects are probably responsible.

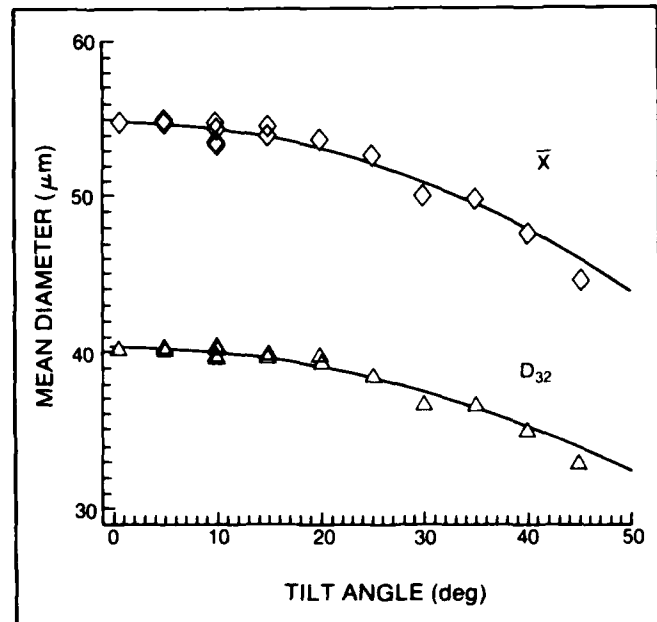


Fig. 12. Mean diameters  $\bar{x}$  and  $D_{32}$  vs reticle tilt angle  $\alpha$  (measured from normal incidence). The data were obtained on a Malvern 2200 instrument with calibration reticle RR-50-3.0-0.08-102-CF-#111. Four runs were made at each angle; the solid curve is a prediction from Eq. (19).

### 3.2. Effect of reticle rotation

One practical problem with glass calibration slides in laser diffraction instruments is that of reflections. It is helpful to tilt the slides a few degrees from perpendicular to the laser beam to direct multiple reflections away from the detector elements. To ensure that this approach does not significantly alter the scattering signature we made a theoretical analysis and performed a series of verification experiments.

Consider first that a circle tilted an angle  $\phi$  projects an ellipse when viewed from the original perpendicular direction. The area  $A_e$  of the projected ellipse is related to the lengths of the major and minor axes, which are  $D$  and  $D\cos\phi$ , respectively:

$$A_e = \frac{\pi D^2 \cos\phi}{4} \quad (17)$$

Now optical techniques based on forward scatter are to first order independent of particle composition and surface characteristics<sup>15,16</sup> and are responsive to projected area-equivalent size parameters. For that reason we calculate the area-equivalent diameter  $D_e$  for the projected ellipse such that the area of a circle of diameter  $D_e$  is equal to that of the ellipse:

$$\frac{\pi}{4} D_e^2 = \frac{\pi D^2}{4} \cos\phi \quad (18)$$

$$D_e = D (\cos\phi)^{1/2} \quad (19)$$

As a first-order prediction we then postulate that characteristic sizes measured by laser diffraction particle sizing instruments should vary as the square root of the cosine of the tilt angle. In Fig. 12 we have plotted experimental data for calibration runs with tilt angles up to 45°. The experimental data are the best-fit Rosin-Rammler size parameter  $\bar{x}$  and the volume-to-surface-area mean diameter  $D_{32}$ :

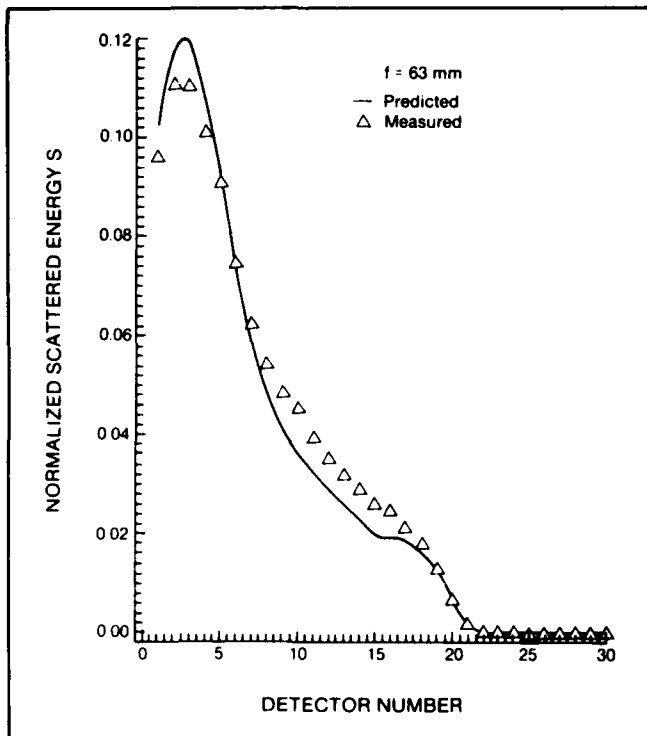


Fig. 13. Normalized scattered energy  $S$  vs detector number predicted for calibration reticle RR-50-3.0-0.08-102-CF-#111 on Malvern 2200 instrument with  $f = 63$  mm and  $z_p = 254$  mm. The solid line is a spline fit through the calculated values after correction by the calibration factor, and the experimental data points are averages for each detector over 10 independent runs. Both signatures were normalized to 1.0, and the standard deviations were less than the symbol dimensions.

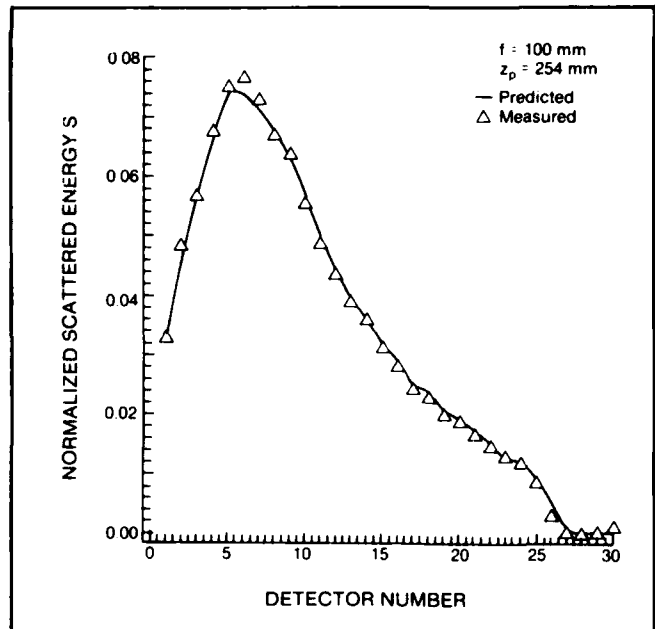


Fig. 14. Normalized scattered energy  $S$  vs detector number predicted for calibration reticle RR-50-3.0-0.08-102-CF-#111 on Malvern 2200 instrument with  $f = 100$  mm and  $z_p = 254$  mm. The solid line is a spline fit through the calculated values after correction by the calibration factor, and the experimental data points are averages for each detector over 28 independent runs. Both signatures were normalized to 1.0, and the standard deviations were less than the symbol dimensions.

$$D_{32} = \frac{\int_0^{\infty} D^3 n(D) dD}{\int_0^{\infty} D^2 n(D) dD} \quad (20)$$

The experimental values of  $D_{32}$  were calculated by numerically integrating Eq. (20) using the number distribution version of Eq. (6) with the best-fit values of  $\bar{x}$  and  $N$ . The prediction is Eq. (19) matched at  $\phi = 0$ . It is clear that the predictions and experiments agree very well. Figure 12 demonstrates that tilting the calibration reticles a few degrees to minimize reflections has no appreciable effect on the results.

### 3.3. Effect of reticle position

The analytical model derived in the section above was utilized to predict the response of the Malvern instrument as a function of reticle distance from the receiving lens. The results presented in Figs. 13 and 14 are for positions  $z_p$  far enough from the lens that vignetting is clearly present. The predicted curves in Figs. 13 and 14 were obtained by correcting the  $S_j$  predicted from Eq. (16) using the measured calibration factors in Figs. 9 to 11. Theory and experiment are in very good agreement.

Another indication of the effects of vignetting are shown in Fig. 15 and 16. The theoretical curves here were obtained by performing the best-fit Rosin-Rammler inversion on predicted scattering signatures such as those shown in Figs. 13 and 14. As the reticle is

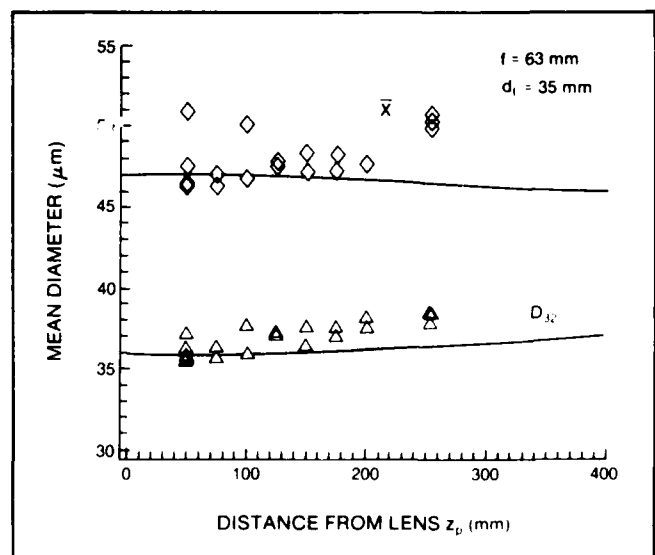


Fig. 15. Mean diameters  $\bar{x}$  and  $D_{32}$  vs  $z_p$  for the Malvern 2200 instrument with  $f = 63$  mm. The solid lines are predictions after accounting for the calibration factors, and each data point is an independent run.

moved away from the lens (increasing  $z_p$ ), light scattered at large angles is truncated by the lens aperture and does not reach the detector. Since small particles preferentially diffract light onto these outer detectors, a bias toward large particles is predicted. The experiments confirm this, although the major effect on the Rosin-Rammler parameters is to decrease  $N$  rather than increase  $\bar{x}$ . An increase in  $N$  narrows the distribution by cutting off volume at both large and small particle sizes. However, the small sizes lose more projected area that dominates the diffraction process; therefore increasing  $N$  at constant  $\bar{x}$  increases the mean diameter, as

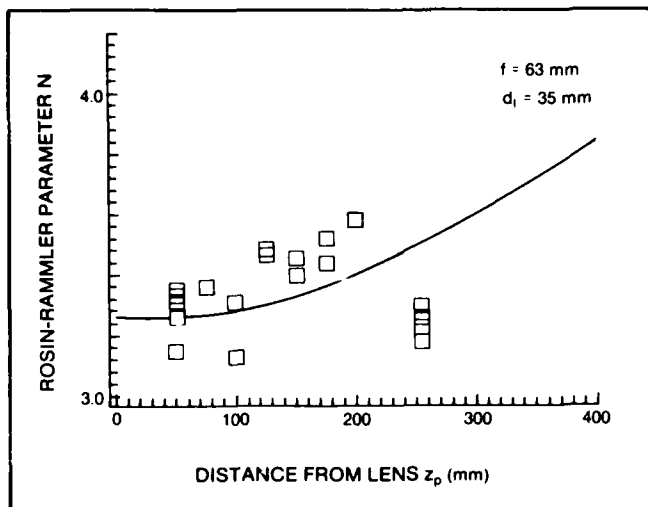


Fig. 16. Rosin-Rammler exponent  $N$  vs  $z_p$  for the Malvern 2200 instrument with  $f = 63$  mm. The solid line is the prediction after accounting for the calibration factors, and each data point is an independent run.

demonstrated by the  $D_{32}$  data in Figs. 15 and 16. The agreement between theory and experiment is good, considering that the predictions do not account for nonideal lens effects.

#### 4. CONCLUSIONS

Laser diffraction techniques are widely used for particle size distribution measurements. Under certain very ideal conditions the response of these instruments does not depend on the particle positions in the incident beam, and some instrument configurations do not, in theory, require calibration. Unfortunately the practical realities of finite aperture lenses, responsivity variations between elements in monolithic photodiode arrays, and lens aberrations need to be accounted for.

In this paper we report a detailed study of these nonideal effects using a commercial Malvern 2200 laser diffraction particle sizing instrument and a calibration reticle. We observed variations of about 15% in the instrument response with three standard receiving lenses

( $f = 63$  mm, 100 mm, and 300 mm). These variations were due to a combination of detector calibration errors and nonideal lens effects. A set of calibration factors for each of the 30 detectors and three lenses was developed.

A theoretical model predicting the dependence of instrument response on particle position was developed and verified experimentally. The model can be used to characterize the optical sample volume and the biasing involved when aerosols of large dimensions are analyzed. Finally, the practice of rotating calibration slides a few degrees from normal incidence to minimize reflection effects was shown theoretically and experimentally to have negligible effect on calibration measurements.

#### 5. ACKNOWLEDGMENTS

This research was supported by the Office of Naval Research, NASA Lewis Research Center, Parker-Hannifin Corporation, and Garrett Turbine Engine Company.

#### 6. REFERENCES

1. M. Kerker, *The Scattering of Light and Other Electromagnetic Radiation*, Academic Press, New York (1969).
2. H. C. van de Hulst, *Light Scattering by Small Particles*, John Wiley and Sons, New York (1957).
3. J. H. Chin, C. M. Sliepcevich, and M. Tribus, *J. Phys. Chem.* Ithaca 5, 841 (1955).
4. R. A. Dobbins, L. Crocco, and I. Glassmann, *AIAA J.* 1, 1882 (1963).
5. E. D. Hirtleman, "Particle Sizing by Optical Nonimaging Techniques," in *Liquid Particle Size Measurement Techniques*, J.M. Tishkoff, ed., ASTM STP-848 (1984).
6. J. Swithenbank, J. Beer, D. S. Taylor, D. Abbot, and C. G. McCreath, in *Experimental Diagnostics in Gas-Phase Combustion Systems: AIAA Progress in Astronautics and Aeronautics*, B. T. Zinn, ed., AIAA 53, 421 (1977).
7. J. Cornillault, *Appl. Opt.* 11(2), 265 (1972).
8. A. L. Wertheimer and W. L. Wilcock, *Appl. Opt.* 15(6), 1616 (1976).
9. L. Bayvel and A. R. Jones, *Electromagnetic Scattering and Applications*, Applied Science Publishers, London (1981).
10. T. W. Alger, *Appl. Opt.* 18, 3494 (1979).
11. R. A. Mugele and H. D. Evans, *Ind. Eng. Chem.* 43(6), 1317 (1951).
12. L. W. Dodge, *Appl. Opt.* 23, 2415 (1984).
13. E. D. Hirtleman, Paper 83-GT-232 presented at the 28th Int. Gas Turbine Conference, ASME, New York (1983).
14. J. Swithenbank and D. S. Taylor, Report HIC-315, Dept. of Chem. Eng., University of Sheffield, Sheffield, U.K. (1979).
15. J. R. Hodgkinson, *Appl. Opt.* 5(1), 839 (1966).
16. E. D. Hirtleman and H. K. Moon, *J. Colloid Int. Sci.* 87(1), 124 (1982).

SINGLE BEAM LASER VELOCIMETRY (LIV) IN TURBULENT FLOWS

E. Dan Hirsleman  
Y. Yue

Mechanical and Aerospace Engineering Department  
Arizona State University  
Tempe, Arizona 85287, U.S.A.

and

N. S. Berman  
D. X. Guan

Chemical and Bioengineering Department  
Arizona State University  
Tempe, Arizona 85287, U.S.A.

ABSTRACT

It is possible to determine velocity information on individual particles in a flow by measuring the time for each particle to traverse through a single TEM<sub>00</sub> laser beam. The advantages associated with the relatively simple optical system of this single beam velocimeter (LIV) are sufficient to warrant further study of its potential performance in turbulent flows. The LIV transit-time measurement must necessarily be made at a constant fraction of the peak scattering signal amplitude to obtain an unambiguous measure of the particle speed in the plane normal to the laser beam. Unfortunately the precision of individual LIV velocity measurements based on the pulse width or transit-time determination is significantly less than generally obtained for individual Doppler bursts with counter-type laser Doppler velocimeters. In this paper we consider measurement of turbulence intensity with LIV using particle arrival statistics. In particular we derive expressions for the probability density distribution of waiting-times between particle events in isotropic turbulent flow. The feasibility of obtaining turbulence information from waiting-time distributions is discussed.

INTRODUCTION

Since its inception in the 1960's the field of laser velocimetry (LV) for flow diagnostics has matured in a rather traditional way. Much of the emphasis today concerns the application of LV as an experimental tool in the study of complex fluid mechanics rather than further development. Indeed the laser Doppler velocimeter (LDV) is becoming a common but relatively sophisticated transducer in fluids engineering practice. There are, however, several facets of the basic science of laser velocimetry which are still active areas of scientific inquiry and research. For example the problem of velocity bias has been discussed for many years but is still the focus of recent contributions to the literature by Flack (1982), Stevenson et al (1982), and Edwards and Jensen (1982) among others. Considerable research has also been directed in recent years towards less conventional LV methodologies which do not utilize the Doppler effect. The laser two-focus velocimeter (L2V) has been studied by numerous investigators including Shodi (1978), Richards and Brown (1984), and Yue and Hirsleman (1982). The single-beam transit-time laser velocimeter (LIV) has been studied by Hirsleman (1981) and Holve (1982). Hirsleman (1978) and Yue and Hirsleman (1984) have developed a particle-sizing velocimeter (LSV) which measures two velocity components using the LIV concept applied to two adjacent beams.

A rather unique approach initiated by Erdmann and Gellert (1976) and Erdmann (1980) and uses the particle arrival rate statistics rather than individual velocity measurements to obtain turbulence information. Using a related technique Tan and Berman (1982) have made

turbulence measurements from the probability-after-effect for two separated LDV probe volumes.

In this paper we consider the LIV and its potential performance in diagnostics of turbulent flow. The LIV, which measures the seed particle residence time in a single laser beam, is interesting because of the relative simplicity of the optical system. The LIV, L2V and LDV operated in the conventional single particle counter processor mode are similar in the sense that they discretely sample the velocity of individual particles and then average over many particles to obtain velocity distribution statistics. One distinction is the relatively poor velocity measurement precision of the transit-time LIV. For typical conditions the intrinsic LIV velocity broadening might be 2% where that for L2V or LDV would be roughly an order of magnitude better. This level of LIV precision generally will produce a negligible error in mean velocity determination for typical numbers of velocity samples but could have a very significant impact on estimates of turbulence intensity and higher order moments. For that reason it is important to consider alternative methods to obtain accurate measurements of turbulence intensity using LIV.

As discussed above an additional form of information available from laser velocimeters is the time-history of particle arrivals at the optical sample volume. In this paper we present a theoretical analysis of the potential for using waiting-time distributions in conjunction with the transit-time LIV.

INDIVIDUAL VELOCITY REALIZATIONS WITH LIV

A schematic of a general LIV system is shown in Fig. 1. A single laser beam is conditioned and focused into the optical sample volume. Light scattered by particles passing through the beam is collected by a photodetector and the signals processed for velocity information. Axial discrimination of the probe volume is performed by the detector optics.

The symmetry inherent in the Gaussian intensity profile across TEM<sub>00</sub> laser beams permits a velocity measurement with the LIV. Signal processing requires measurement of the transit-time of particles crossing the laser beam as reflected by the pulse width of single particle scattering signals which are Gaussian in time. Here the transit-time is necessarily measured at a constant fraction of pulse height rather than with respect to an absolute threshold level. The intensity profile  $I$  across a TEM<sub>00</sub> laser beam is given by

$$I(x,y) = I(0,0) e^{-2(x^2 + y^2)/w^2} \quad (1)$$

where  $w$  is the beam radius at the  $1/e^2$  intensity points. Separating the Cartesian variables we obtain:

$$I(x,y) = I(0,0) e^{-2x^2/w^2} e^{-2y^2/w^2} \quad (2)$$

A particle traveling across the laser beam parallel to

the x-axis at a constant y will experience a Gaussian incident intensity history with a constant 1/e<sup>2</sup> width independent of the value of y. In that case only x is a function of time as given by:

$$x = v_L t \tag{3}$$

where v<sub>L</sub> is the particle speed in the x-y plane and we assume x=0 at t=0. Substituting Eq. (3) into Eq. (2) obtains:

$$I(t) = I(0,0) e^{-2 y^2/w^2} e^{-2 v_L^2 t^2/w^2} \tag{4}$$

The first exponential in Eq. (4) is just a constant and the LIV scattering signatures are Gaussian in time. Then measuring the relative pulse width or transit-time t<sub>t</sub> between the 1/e<sup>2</sup> points of a particle scattering signal determines the speed in a plane normal to the laser beam axis as given by:

$$v_L = w/t_t \tag{5}$$

Rudd (1974) considered an analog differentiation approach for measuring the transit-time t<sub>t</sub>. Hirleman (1978) and Holve (1982) have used analog constant-fraction discriminator modules to make the necessary pulse width measurement. Hirleman (1978, 1982) developed a digital signal processing algorithm which improves the precision of the measurement. The scattering signal is digitized and the parameters controlling the precision of the pulse width estimation are:

- (1) the number of samples n of the waveform between the 1/e<sup>2</sup> points,
- (2) the noise-to-signal ratio (N/S) assuming random Gaussian noise.

A plot of the relative error in estimating the 1/e<sup>2</sup> width of a Gaussian signal is shown in Fig. 2. Note that with 12 samples on a Gaussian waveform the 1/e<sup>2</sup> width can be estimated with a relative standard deviation roughly equal to the noise-to-signal ratio. Also plotted in Fig. 2 are data for LIV measurements on droplets in the primary stream from a vibrating orifice droplet generator after Yue et al (1984). The actual noise-to-signal ratio at the photodetector output for the measurements of Fig. 2 was about 5% and the measured LIV precision agrees reasonably well with prediction.

It is clear that an LIV transit-time measurement is less precise than that possible with a single Doppler burst from an LDV. With a sufficient number of particles the mean velocity can be estimated with adequate certainty using LIV but estimates of turbulence intensity and higher moments are more difficult for reasonable sample sizes. The broadening represented by the ordinate of Fig. 2 will appear as artificial turbulence in LIV measurements. For this reason we are investigating the use of particle arrival time statistics to facilitate LIV measurements of turbulence intensity.

#### PARTICLE ARRIVAL STATISTICS IN LASER VELOCIMETRY

Statistical properties of particle arrival times in individual realization laser velocimeters have received relatively little attention from LV researchers over the years. In LDV work the particle arrival process has generally been considered a nuisance as the discrete sampling of velocity only during the presence of a particle is the source of velocity bias. Recently some workers have considered the arrival process on its own merits with the intent of identifying and hopefully extracting useful information. Erdmann and coworkers (1976, 1980, 1981) have done extensive work on particle arrivals using statistical analysis of the number of particle events in a series of finite sampling times. Tan and Berman (1982) developed a probability-after-effect method in which the number of particle counts from two displaced LDV probe volumes were analyzed. These methods determine turbulence intensity and in the latter technique both Lagrangian and Eulerian time scales were measured. Yue and Hirleman (1982)

studied particle event rates in laser-two-focus velocimeters.

In this paper we consider the distribution of waiting-times between particle events at a single LV probe volume. The theoretical analysis is directly applicable to single beam laser light scattering instruments for particle size and velocity instruments such as LIV. However the development can also be applied to LDV systems under some conditions. The schematic in Fig. 3 demonstrates our conceptual model where an optical probe volume with projected cross-sectional areas s<sub>x</sub>, s<sub>y</sub>, and s<sub>z</sub> is shown. We assume that all particles which pass into the optical probe volume will be "seen" by the LV and registered as single particle events. This assumption implies that particle coincidence effects are negligible and that particle residence times in the sample volume are small compared to both the mean time between particle arrivals and to characteristic time scales of the flow. Although the specific geometry of the probe volume and the orthogonal sensitive areas will in general be complex functions of particle size and in some cases particle trajectory (LDV) we neglect those effects for the present. We assume that the LV seed particles are randomly distributed in space and are swept through a stationary probe volume by the fluid velocity. One might envision a conveyor belt with randomly distributed particles passing through the sample region with a direction and speed dictated by the local, instantaneous fluid velocity. The number of particles n sampled by an LV during a measurement time t is a stochastic variable. The probability P<sub>t</sub>(n) of sampling n particles during t is described by the Poisson distribution (Chandrasekhar, 1943):

$$P_t(n) = \frac{\langle \rho V \rangle^n e^{-\langle \rho V \rangle}}{n!} \tag{6}$$

where ρ is the particle number density, V is the volume of the fluid sampled (i.e. swept through s<sub>x</sub>, s<sub>y</sub>, s<sub>z</sub>) during the time t, and brackets < > indicate the expected value over time t. For a given fluid velocity constant over t the expected volume sampled is equal to the product of the sensitive area, the velocity, and the sampling time interval. Here the velocity-time product represents the length of the fluid filament which passed through the probe volume between time zero and time t. For the general case we can write:

$$\langle \rho V \rangle = \langle \rho \underline{s} \cdot \underline{v} t \rangle \tag{7}$$

where the tilda indicates vector quantities, v is the velocity, and s represents the orthogonal projected areas of the sample volume defined positive pointing into the sample volume. The absolute value in Eq. (7) is necessary because the probability of registering a particle event does not in general depend on the sense of the velocity components. It is convenient to think of taking the absolute value of each velocity component separately in Eq. (7).

Consider starting a timer at some random, arbitrary time when there is not necessarily a particle event. The probability F(τ>t) of waiting longer than a time t for the next particle is just the probability that there were zero particles during t:

$$F(\tau>t) = e^{-\langle \rho \underline{s} \cdot \underline{v} t \rangle} \tag{8}$$

Similarly, the probability of registering zero particle events before t + Δt is given by:

$$F(\tau < t + \Delta t) = e^{-\langle \rho \underline{s} \cdot \underline{v} (t + \Delta t) \rangle} \tag{9}$$

where here the expectation is over the time t + Δt. Now the probability of a particle event between t and t + Δt is the difference between Eqs. (7) and (6). The probability density distribution P(t) of waiting time t for the next event is then obtained in the limit:

$$P(t) = \lim_{\Delta t \rightarrow 0} \frac{F(\tau < t) - F(\tau < t + \Delta t)}{\Delta t} \tag{10}$$

Substituting Eqs. (8) and (9) we obtain:

$$P(t) = \frac{d}{dt} \langle \rho_2 \cdot |y|t \rangle e^{-\langle \rho_2 \cdot |y|t \rangle} \quad (11)$$

Phenomenologically Eq. (11) can be considered in two parts. The exponential term indicates the probability of no particles arriving between 0 and t and the differential coefficient represents the probability of a particle arriving during the next dt. The fact that the two probabilities are multiplied reflects the logical AND nature of waiting a time t for the next event; i.e. there must be no particle events between 0 and t and then an event in the next dt.

Equation (11) is valid for describing the waiting time for one particle event following a start time where the expectation can be evaluated. In turbulent flow the expectation term will depend on the velocity at time zero  $y(0)$  and the probability in Eq. (11) will therefore be conditional on  $y(0)$ . The expectation in Eq. (11) is a complex function of the velocity distribution function, correlation functions, and particle density-velocity correlations. We previously assumed that the particles are randomly distributed in space, i.e. that there is no correlation between particle density and velocity. Further we assume that the geometric characteristics of the optical probe volume are also independent of velocity (constant  $g$ ) which is a very good assumption for single beam laser light scattering instruments but less so for interferometric (LDV) systems. Under those assumptions we write:

$$\langle \rho_2 \cdot |y|t \rangle = \rho_{2x} \langle |v_x|t \rangle + \rho_{2y} \langle |v_y|t \rangle + \rho_{2z} \langle |v_z|t \rangle \quad (12)$$

For laminar flow in the +x direction the values in the expectation terms are constant and:

$$\langle \rho_2 \cdot |y|t \rangle = \rho_{2x} v_{x0} t \quad (13)$$

where  $v_{x0}$  is the mean flow velocity. Defining a particle event rate parameter  $\lambda$  which for this special case of laminar flow we subscript  $\lambda_0$ :

$$\lambda_0 = \rho_{2x} v_{x0} \quad (14)$$

For laminar flow Eq. (11) then simplifies to:

$$P(t) = \lambda_0 e^{-\lambda_0 t} \quad (15)$$

Now for turbulent flow with the assumption of constant  $\rho$  and  $g$  the result is not so simple as we must determine the expectations in Eq. (12). For isotropic turbulence we can express the expectation of the velocity at any time t conditional on the velocity  $y(0)$ :

$$\langle \underline{v}t | \underline{y}(0) \rangle = \underline{y}t + (\underline{y}(0) - \underline{y}_0) \int_0^t R(t) dt \quad (16)$$

where R is the velocity autocorrelation function,  $y_0$  is the mean velocity vector, and the backslash character \ is used to denote a conditional probability. The constraints on the correlation function include  $R=1$  as  $t \rightarrow 0$  and  $R \rightarrow 0$  as  $t \rightarrow \infty$ . Again the absolute values required in Eq. (12) complicate the use of Eq. (16).

An expression for the autocorrelation function R is needed and we adopt one of typical form:

$$R(t) = e^{-t/T_c} \quad (17)$$

where  $T_c$  is a flow correlation or persistence time.

At this point we can substitute Eq. (13) and its derivative into Eq. (11) to obtain the waiting time probability density  $P(t|y(0))$  conditional on  $y_0$ . To obtain  $P(t)$  for an ensemble of measurements in turbulent flow we must integrate over the probability distribution of velocities at time zero. For random starts of the timer this is just the actual velocity distribution function  $f(y)$ . We can write:

$$P(t) = \int P(t|y) f(y) dy \quad (18)$$

where  $y(0)$  has been replaced with  $y$ .

Limiting case  $t \ll T_c$

The introduction of the velocity autocorrelation function into the integrals through Eq. (12) multiplies the complexity of the mathematics several fold. A limiting case of interest is that of waiting times small compared to the flow persistence time  $T_c$ . Under those conditions the correlation function R is 1.0, i.e. during a relatively short waiting-time the velocity effectively does not change and Eq. (16) simplifies to  $\langle \underline{v}t | \underline{y}(0) \rangle = \underline{y}(0)t$ . Eq. (11) then becomes:

$$P(t|y) = \rho_2 \cdot |y| e^{-\rho_2 \cdot |y|t} \quad (19)$$

where again the notation  $y(0)$  for initial velocity has been dropped.

Consider now the rather typical cylindrical optical probe volume of Fig. 3 where  $s_z \ll s_x$  and  $s_x = s_y$ . If the mean flow is oriented in the +x direction then Eq. (19) becomes:

$$P(t|y) = (\rho_{2x} |v_x| + \rho_{2y} |v_y|) e^{-(\rho_{2x} |v_x| + \rho_{2y} |v_y|)t} \quad (20)$$

Since the  $v_z$  terms drop out then Eq. (18) becomes:

$$P(t) = \int \int P(t|y) f(v_x) f(v_y) dv_x dv_y \quad (21)$$

where  $P(t|y)$  can be obtained from Eq. (20). Assuming Gaussian, isotropic turbulence:

$$f(v_x) = \frac{1}{\sqrt{2\pi} v_0 \xi} \exp \left\{ -\frac{(v_x - v_0)^2}{2 v_0^2 \xi^2} \right\} \quad (22)$$

and:

$$f(v_y) = \frac{1}{\sqrt{2\pi} v_0 \xi} \exp \left\{ -\frac{(v_y)^2}{2 v_0^2 \xi^2} \right\} \quad (23)$$

where  $\xi$  is the turbulence intensity. Eq. (21) can then be integrated to obtain:

$$P(t) = \lambda_0 e^{-\lambda_0 t + \frac{1}{2} (\lambda_0 t \xi)^2} \left\{ \frac{1}{\sqrt{\pi}} \xi \left[ \frac{1}{2} \operatorname{erfc} \left( \frac{1}{\sqrt{2}} (\lambda_0 t \xi - \frac{1}{\xi}) \right) \right. \right. \\ \left. \left. + e^{-\frac{1}{2} (\lambda_0 t \xi)^2} \operatorname{erfc} \left( \frac{1}{\sqrt{2}} \lambda_0 t \xi \right) \right] + \frac{1}{2} e^{-\frac{1}{2} (\lambda_0 t \xi)^2} \right. \\ \left. \operatorname{erfc} \left( \frac{1}{\sqrt{2}} \lambda_0 t \xi \right) \operatorname{erfc} \left( \frac{1}{\sqrt{2}} (\lambda_0 t \xi - \frac{1}{\xi}) \right) (1 - 2\lambda_0 t \xi^2) \right\} \quad (24)$$

where erf indicates the error function and the complement  $\operatorname{erfc}(x) = 1 - \operatorname{erf}(x)$ . The absolute values in Eq. (20) were taken into account by breaking Eq. (21) into two integrals for positive and negative velocities. The only approximation in arriving at Eq. (24) is that  $\operatorname{erfc}((\lambda_0 t \xi - 1/\xi)/\sqrt{2}) = 1$  which for  $\xi = 0.4$  introduces a maximum of 0.4% error.

The limiting behavior of this expression is given by:

$$\lim_{t \rightarrow 0} P(t) = \lambda_0 \left( \sqrt{\frac{2}{\pi}} \xi + 1 \right) = \lambda' \quad (25)$$

and:

$$\lim_{t \rightarrow \infty} P(t) = 0 \quad (26)$$

Recall that these Eqs. (24-26) are valid for waiting times small compared to the flow correlation time ( $t \ll T_c$ ) with  $\rho$  and  $g$  constant. Note that Eq. (24) deviates from the Poisson distribution valid for laminar flow as given in Eq. (15) in both the coefficient and the exponent.

DISCUSSION

To gain some insight into the structure of the final expression for the probability density distribution of the waiting-time consider Fig. 4 where  $P(t)$  for laminar flow from Eq. (15) and the full expression Eq. (24) for  $\xi = 0.4$  have been plotted. The same curves are also shown on a log scale in Fig. 5 where a third curve described by the approximation  $P(t) = \lambda_0^{-1} e^{-\lambda_0 t}$  with  $\lambda_0$  as defined in Eq. (25) plotted as well. Deviation of Eq. (24) for turbulent flow from the Poisson form is rather small which is significant since  $\lambda_0$  is in general unknown. There is however a significant change in  $P(t)$  with turbulence intensity indicated by an increase in the mean particle arrival rate. Holding the mean velocity constant and increasing the turbulence intensity increases the particle event rate. Particle events are not conserved because the diffusive effect of turbulence increases the number of particles crossing a in both directions while maintaining the net particle flux constant. This is shown in Fig. 6 where the long-time-averaged expectation of the particle event rate  $\langle \lambda \rangle$  for turbulent flow was found by integrating Eq. (24) from zero to infinity. Note that  $\langle \lambda \rangle$  is the inverse of the mean waiting-time.

Recall that Figs. 4-6 apply to the case where  $t \ll T_0$ . For finite  $T_0$  there is no simple closed form expression for  $P(t)$ . In Fig. 7 the effect of  $T_0$  is indicated for one example with the flow correlation time  $T_0$  equal to the mean waiting-time. The data of Fig. 7 were obtained by numerically integrating Eq. (18) accounting for  $R(t)$  in Eqs. (16) and (17).

Given the overall objective of determining turbulence intensity from measured  $P(t)$  it is necessary to formulate a strategy for extracting  $\xi$  from experimental data in the form of Fig. 5 as described by Eq. (24) for  $t \ll T_0$ . Unfortunately  $\lambda_0$  given in Eq. (14) is an unknown in Eq. (24) in addition to the unknown turbulence intensity  $\xi$ . We envision three possible approaches to obtain  $\xi$  from measured  $P(t)$ . First the deviation of  $P(t)$  from the Poisson form  $\lambda \exp(-\lambda t)$  could be determined. This general technique which does not require knowledge of  $\lambda_0$  has been successfully demonstrated using another signal processing method which counts particle events in finite time intervals by Erdmann (1980) and Tan and Berman (1982). However the deviation of Eq. (24) from Poisson is small and experimental errors will be critical. We have made some numerical experiments by generating synthetic  $P(t)$  data using assumed values of  $\lambda_0$  and  $\xi$  accounting for typical sources of experimental errors and uncertainties. A least squares technique was used to determine best fit values of  $\lambda_0$  and  $\xi$ . The parameters in the simulation included the minimum time interval measured  $t_{min}$  (limited by instrument dead time and noise),  $t_{max}$ , and the number of discrete time intervals in the histogram. Our results confirm the feasibility of the approach.

Another method for data analysis would be to eliminate  $\lambda_0$  as an unknown by determining it independently. In that situation it might be possible to use Fig. 6 to determine  $\xi$ . Direct measurement of  $\lambda_0$  would require the turbulence intensity to be eliminated while maintaining  $p$ ,  $g$ , and  $v_0$  constant. It is probably more practical to measure  $p$  and  $g$  (which are necessary for particle size distribution measurements) and  $v_0$  to determine  $\lambda_0$  from Eq. (14).

CONCLUSIONS

The single-beam transit-time laser velocimeter (LIV) can make reliable measurements of mean velocity but is not very accurate in determining low to moderate levels of turbulence intensity. Consideration of the waiting-time distribution for particle events in LIV holds some promise for measurements under those conditions. Experimental investigation of the theoretical analysis presented here is warranted.

ACKNOWLEDGEMENTS

This work was supported in part by the Office of Naval Research under Contract N00014-79-C-0363, Dr. Dick Miller program manager, and by the National Science Foundation through Grant CPE-8022433.

REFERENCES

Chandrasekhar, S., 1943, "Stochastic Problems in Physics and Astronomy," *Rev. Modern Phys.*, 15, 1.

Edwards, R.V., and Jensen, A.S., 1983, "Particle Sampling Statistics in Laser Anemometers: Sample and Bold and Saturable Systems," *J. Fluid Mech.*, 133, 397-411.

Erdmann, J.C., and Gellert, R.I., 1976, "Particle Arrival Statistics in Laser Anemometry of Turbulent Flow," *Appl. Phys. Lett.*, 29, 408.

Erdmann, J. C., 1980, "Statistics of Random Flow Analyzed by Optical Techniques," *Optica Acta*, 27, 31.

Erdmann, J.C. and Tropes, C., 1981, "Turbulence-induced Statistical Bias in Laser Anemometry", Seventh Biennial Symposium on Turbulence, Univ. of Missouri, Rolla, September 21-23, 1981.

Flack, R.D., 1982, "Influence of Turbulence Scale and Structure on Individual Realization Laser Velocimeter Biases," *J. Phys. E, Sci. Inst.*, 15, 1038-1044.

Hirleman, E. D., 1978, "Laser Technique for Simultaneous Particle Size and Velocity Measurements," *Optics Letters*, 3, 19-21.

Hirleman, E.D., 1982, "Non-Doppler Laser Velocimetry: Single Beam Transit-time LIV," *AIAA Journal*, 20, 86, presented as Paper AIAA-80-0350, 18th AIAA Aerospace Sciences Meeting, Pasadena, CA.

Holve, D.J., 1982, "Transit-timing Velocimetry for Two-phase Reacting Flows," *Comb. Flame.*, 48, 105-108.

Richards, P.H. and Brown, R.G.W., 1982, "Measurements in Shear Layers in Transonic Flows with a Laser Transit Anemometer," *J. Phys. D, Appl. Phys.*, 15, 1891-1905.

Rudd, M. J., 1974, in Proceedings of the Second International Workshop on Laser Velocimetry, Eng. Exp. Station Bull. No. 144, Purdue Univ., Vol. II, 300.

Shohl, R., 1976, "The Laser-dual-focus Velocimeter," AGARD Conference Proceedings, No. 193, Paper 21.

Stevenson, W.H., Thompson, D., and Roesler, T., 1982, "Direct Measurement of Laser Velocimeter Bias Errors in a Turbulent Flow," *AIAA Journal*, 20, 1720-1723.

Tan, H., and Berman, N.S., 1982, "A Laser Method to Determine Turbulence Intensity using the Probability After Effect," *J. Phys. E, Sci. Inst.*, 15, 906.

Yue, Y. and Hirleman, E. D., 1982, "Advanced Laser-two-focus Velocimeter," *Keine Tengbao*, 21, 1296.

Yue, Y., Hirleman, E.D., and Anderson, M.F., 1984, "Simultaneous Measurements of Two Velocity Components and Size of Individual Droplets using Laser Light Scattering," Paper 84-34, Western States Section, Combustion Institute, April 2, 1984, University of Colorado, Boulder.

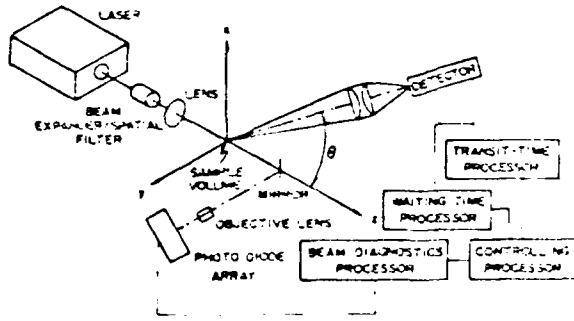


Fig. 1 Schematic of L1V system.

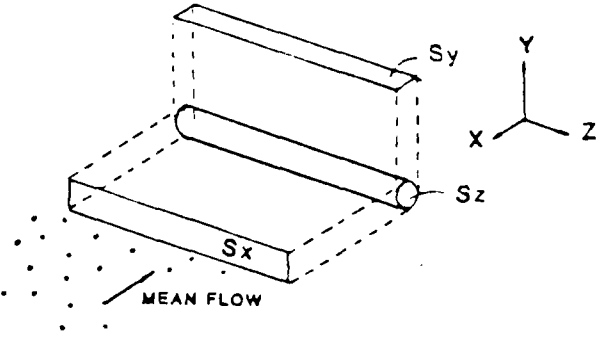


Fig. 3 Cylindrical optical probe volume typical of LV systems. Laser beam(s) propagate along +z axis and mean flow is shown in +x direction.

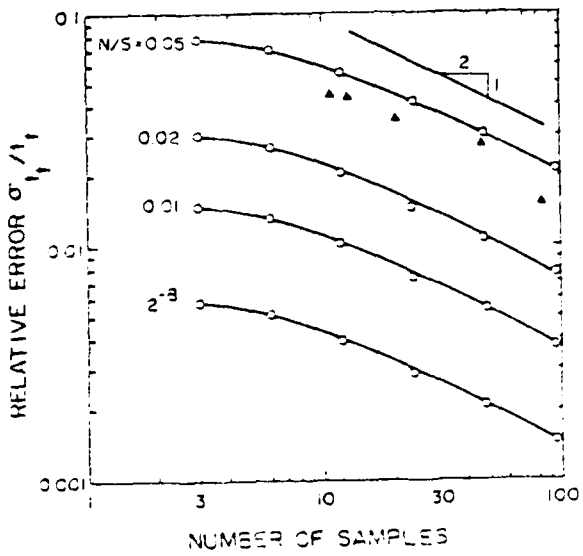


Fig. 2 Relative error for estimating the  $1/e^2$  transit time  $t_t$  from discrete samples of a Gaussian signal. The noise is assumed to be random and normally distributed. The noise-to-signal ratio N/S is based on the rms of the noise and the peak amplitude of the Gaussian signal. The solid lines are curves drawn through the open circles which were determined from a numerical simulation of least squares fits of noisy data to Gaussian curves. The triangles were L1V data for an actual N/S of about 0.5 after Yae et al (1984).

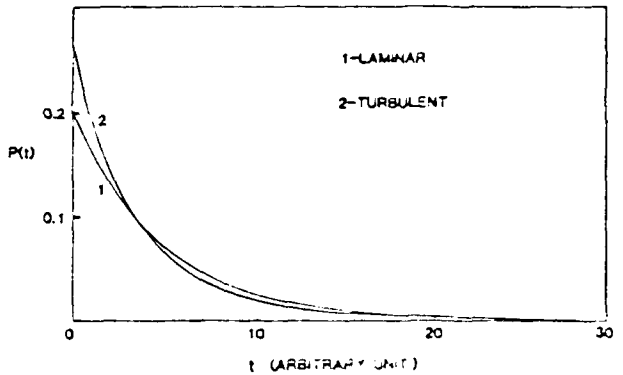


Fig. 4 Plot of waiting-time probability density  $P(t)$  for laminar flow from Eq. (15) and turbulent flow  $\xi = 0.4$  from Eq. (24). The particle event rate for laminar flow at the mean velocity is  $\lambda_0 = 0.2$  per unit time.

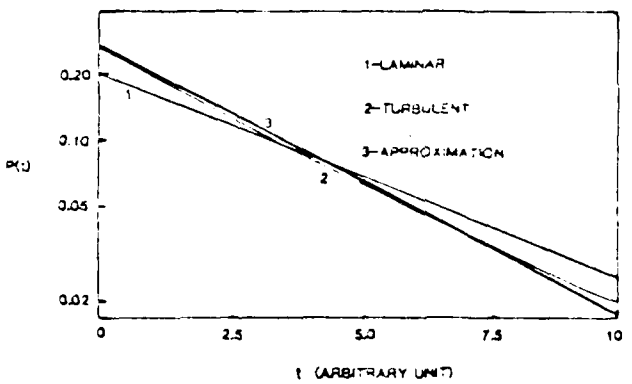


Fig. 5 Log plot of waiting-time probability density  $P(t)$  for laminar flow from Eq. (15) and turbulent flow  $\xi = 0.4$  from Eq. (24). Also plotted is an approximation to the turbulent case of the form  $P(t) = \lambda' e^{-\lambda' t}$  where  $\lambda'$  is given in Eq. (25).  $\lambda_0 = 0.2$  per unit time.

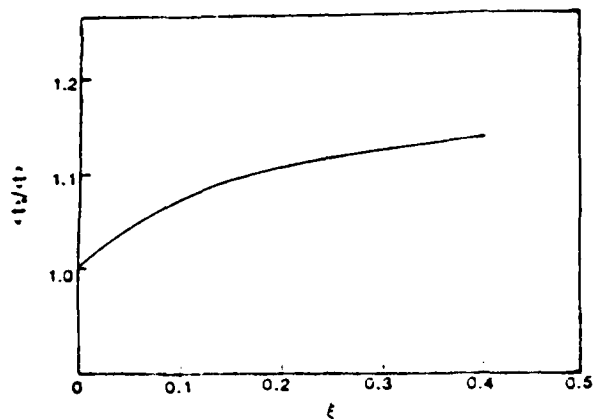


Fig. 6 Plot of the total particle arrival rate  $\lambda$  for turbulent flow normalized to that for laminar flow with the same mean velocity  $\lambda_0$  as a function of turbulence intensity  $\xi$ . Results obtained by integrating Eq. (24) are valid for the limit  $t \ll T_c$ .

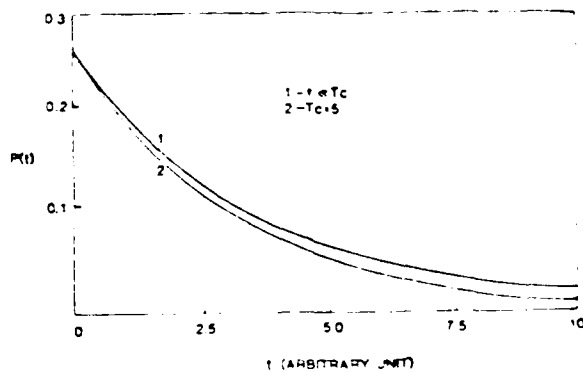


Fig. 7 Plot of waiting time probability density  $P(t)$  for turbulent flow  $\xi = 0.4$  and  $\lambda_0 = 0.2$  per unit time. The first curve corresponds to Eq. (24) which is valid in the limit  $t \ll T_c$ . The second curve was calculated by integrating Eq. (11) over the velocity distribution functions in Eqs. (22) and (32) assuming the autocorrelation function is of the form in Eq. (17) with  $T_c = 1/\lambda_0 = 5$  time units. In this case  $T_c$  is therefore equal to the mean waiting time between events.

# AIAA'83

**AIAA-83-1514**

**Non-Intrusive Laser Particle Diagnostics**

**(Invited Review)**

E.D. Hirleman, Arizona State Univ., Tempe,  
AZ

## **AIAA 18th Thermophysics Conference**

June 1-3, 1983  
Montreal, Canada

For permission to copy or republish, contact the American Institute of Aeronautics and Astronautics  
1290 Avenue of the Americas, New York, NY 10104

# NONINTRUSIVE LASER-BASED PARTICLE DIAGNOSTICS

E. Dan Hirleman

Laser Diagnostics Laboratory  
Arizona State University  
Tempe, Arizona

## Abstract

The evolution of nonintrusive optical techniques for particle size analysis has provided an array of powerful diagnostics. The techniques either probe the light scattering/attenuation properties of the aerosol particles or form photographic or holographic images. This paper discusses the theoretical basis for in-situ particle sizing techniques and reviews some practical applications as well. Further, a number of subtle considerations which affect the reliability and interpretation of data from optical particle sizing instruments are discussed.

## Nomenclature

$C_{sc}$	partial light scattering cross section ( $m^2$ )
$d$	particle diameter (m)
$D_{32}$	volume-to-surface area mean diameter (m)
$F$	differential light scattering cross section
$i_1, i_2$	scattering intensity functions
$I$	intensity or time averaged radiant energy per unit area normal to the propagation direction ( $W/m^2$ )
$I_{sc}$	scattered intensity ( $W/m^2$ )
$I_{inc}$	intensity incident upon a particle ( $W/m^2$ )
$J_1$	spherical Bessel function of first kind and first order
$k$	proportionality constant in Eq. (7)
$n$	complex refractive index
$n(a)$	particle number distribution function
$N$	exponent parameter for Rosin-Rammler particle size distribution
$P_{sc}$	scattered optical power (W)
$r$	distance from origin to observation point in particle centered light scattering coordinate system (m)
$S$	light scattering signal amplitude
$x$	mean diameter in Rosin-Rammler particle size distribution
$a$	particle size parameter $\pi d/\lambda$
$\delta$	fringe spacing (m)
$\lambda$	wavelength (m)
$\theta$	scattering angle measured from the incident beam propagation vector azimuthal scattering angle

## I. Introduction

There are many instances when conventional batch sampling methods for particle size analysis are either impractical or impossible to implement. Further, it is often the case that the intrusive nature of sampling methods introduce unacceptable levels of interference into the aerosol flow of interest. For these reasons the development of nonintrusive optical diagnostics for particle size and concentration measurements has been the objec-

\*Associate Professor, Mechanical and  
Aerospace Engineering  
Member AIAA

tive of a significant amount of research and development. Successful applications of this technology are being reported with increasing frequency.

Optical techniques for particle measurements can be divided into three broad areas. First, photographic and holographic methods analyze simultaneously recorded images of a number of individual particles to build a discrete particle size histogram. Secondly, ensemble or multiparticle analyzing methods utilize the light scattering or extinction integrated over the contributions from a large number of particles to determine parameters of the particle size distribution. Finally, single particle counters (SPC) size and count individual particles traversing a relatively small optical sample volume, and a sequence of particles are sampled in order to build up a discrete size distribution. The three approaches are complementary in the sense that they are optimized for different types of applications.

Single particle counters are the optimum choice for analyzing particles roughly 0.5 $\mu$ m and above in applications demanding high specificity and the potential for simultaneous velocity measurements. The existing commercial technology of imaging techniques is generally limited to particles larger than a few micrometers with time response longer than a few seconds. Imaging techniques can provide information on particle shape and other characteristics not retrievable with light scattering methods. Ensemble methods generally require less sophisticated optical systems for implementation but inherently provide less information as the optical characteristics of the individual particles are superimposed and can never be totally recovered.

This paper first presents a brief discussion of the fundamental principles of light scattering which underlie laser-based particle sizing technology. Then details of some of the techniques for nonintrusive particle diagnostics are reviewed. For the purposes of this paper an instrument is considered to be nonintrusive if no sampling probes are involved and the working space between optical elements and the optical measurement volume is on the order of 10 cm or greater.

## II. Light Scattering by Particles

An infinite, planar electromagnetic wave can propagate through a homogeneous, nonabsorbing medium undisturbed. This propagation is rigorously described by Maxwell's equations [1]. However it is also useful to consider Huygens' principle [2] which states that each point on a wavefront (surface of constant phase in the electromagnetic wave field) serves as the source of spherical secondary wavelets such that the wavefront at some later time is determined by the envelope of these wavelets. The secondary wavelets propagate with the same frequency and speed as the primary wave would at each point in space. That an infinite

planar wavefront in a homogeneous medium propagates as a plane wave is readily visualized with Huygens' construction [2].

If we consider the homogeneous medium to be a gas, then the secondary wavelets derive from electrons in the molecules comprising the gas which are harmonically accelerated by the time-varying E-field in the electromagnetic wave. This occurs because each accelerating electron, by virtue of Ampere's and Faraday's Laws [2], produces its own secondary electromagnetic wave (i. e. a scattered wavelet) which propagates spherically outward. The superposition of these scattered wavelets with the unscattered incident wave define the entire electromagnetic field. From a quantum point of view, the gas molecule absorbs a photon which causes an electron to be excited up into a virtual (unstable or disallowed) state for a very short ( $\ll$  psec) time. In elastic scattering events of interest here the electron then drops back to its original state emitting a second photon of the same frequency as the incident photon. This emission or scattering process is random in the sense that the photon can propagate with equal probability in any direction (at least in the plane normal to the polarization vector of the incident E-field). The memory of the molecule retains only the phase and polarization of the incident photon and not the direction of incidence.

It is also possible for the energy coupled into the electron from the incident photon to be dissipated by collisions of the excited electron with other nuclei or electrons. In that situation the photon energy would have been absorbed and converted into thermal (internal kinetic) energy. Both the scattering and absorption processes are included in rigorous light scattering theory.

#### Individual Spherical Particles

The parameters controlling the scattering of planar electromagnetic radiation by spherical particles are the size parameter  $\alpha$ , the complex refractive index  $n$  of the particle relative to the surroundings, and the polarization state of the incident radiation. The three scattering regimes of importance can be delineated as Rayleigh scattering for  $\alpha \ll 1$ , geometric optics for  $\alpha \gg 1$ , and Lorenz-Mie scattering for  $\alpha \sim 1$ . For visible radiation Rayleigh scattering approximations are valid for particle diameters  $d < 0.05 \mu\text{m}$ , and geometric optics approximations for roughly  $d > 5 \mu\text{m}$ . In the Rayleigh regime all of the electrons (or charge dipoles) in a particle are subjected to the same E-field by virtue of their close proximity (relative to the wavelength) and therefore oscillate in phase. The properties of the scattered radiation are then given in a very simple form applicable to the harmonic oscillation of a charge dipole. In the geometric optics limit, the wavelength is much smaller than the particle dimensions and the incident radiation can be considered to be a bundle of rays. The scattered field at any point separated from the particle can be calculated by superimposing refracted and reflected rays with the diffracted field.

In contrast with the Rayleigh scattering and geometric optics regimes, no approximations are possible for particle sizes on the order of the wavelength and the complete set of Maxwell's equations must be solved for the particle and the surroundings. The theoretical difficulties here arise from the fact that the E-fields experienced by the various electrons or charge dipoles distributed throughout the particle depend on

position, and therefore these electrons emit secondary wavelets which are out of phase. The formulation for this intermediate case, known as Lorenz-Mie theory, is the general solution for all particle sizes. Exhaustive treatises of light scattering are given by van de Hulst [3] and Kerker [4]. Computer codes for calculating the scattering characteristics of spherical particles of arbitrary size are readily available.

Consider the scattering geometry in Fig. 1 with the particle situated at the origin illuminated by electromagnetic radiation propagating in the +z direction with incident intensity  $I_{inc}$ . The scattered intensity  $I_{sc}$  at a distance  $r$  from the origin is given by:

$$I_{sc} = \frac{I_{inc} \lambda^2}{4\pi r^2} [i_1(\alpha, n, \theta) \sin^2 \phi + i_2(\alpha, n, \theta) \cos^2 \phi] \quad (1)$$

where  $i_1$  and  $i_2$  are dimensionless intensity functions for scattered light polarized perpendicular and parallel to the scattering plane respectively. The functions  $i_1$  and  $i_2$  are composed of spherical Bessel and associated Legendre functions and their first derivatives, and are integral parts of Lorenz-Mie theory [3,4]. It is convenient to normalize Eq. (1) by the incident intensity and other constants and define the differential scattering cross section  $F$ :

$$F = i_1(\alpha, n, \theta) \sin^2 \phi + i_2(\alpha, n, \theta) \cos^2 \phi \quad (2)$$

Some computations of  $F$  are shown in Figs. 2, 3 and 4. Figure 2 indicates the angular dependence of the scattered light for particle diameters of 0.1, 0.5, and 1.0  $\mu\text{m}$ , and Fig. 3 for 5.0 and 10.0  $\mu\text{m}$  particles as well. Note the lobe structure which becomes a dominant factor as particle size increases. Figure 4 indicates the dependence of  $F$  on particle size. In the Rayleigh regime  $F$  increases as diameter to the sixth power, and then gradually changes to a diameter-squared dependence in the geometric optics regime. The oscillations present for  $\theta = 45$  and 90 degrees in Fig. 4 are typical for off-axis scattering of nonabsorbing (no imaginary component of the refractive index) particles. Forward scattering (small  $\theta$ ) properties generally display much less structure as is also evident in Fig. 4.

The radiant power  $P_{sc}$  scattered into a detector with a finite collection aperture is obtained by integrating the scattered intensity over the solid angle subtended by the detector:

$$P_{sc} = \frac{I_{inc} \lambda^2}{4\pi} \iint F(\alpha, n, \theta, \phi) \sin \theta \, d\theta \, d\phi \quad (3)$$

The partial scattering cross section for a particular detector is defined as the scattered power divided by the incident intensity:

$$C_{sc} = \frac{\lambda^2}{4\pi} \iint F(\alpha, n, \theta, \phi) \sin \theta \, d\theta \, d\phi \quad (4)$$

#### Individual Nonspherical Particles

It is not possible at present to calculate the scattering and absorption characteristics of particles of arbitrary shape and refractive index. There has, however, been some progress on theoretical models and calculations for certain nonspherical shapes such as ellipsoids [4], spheroids [6,7], clusters of spheres [8], and

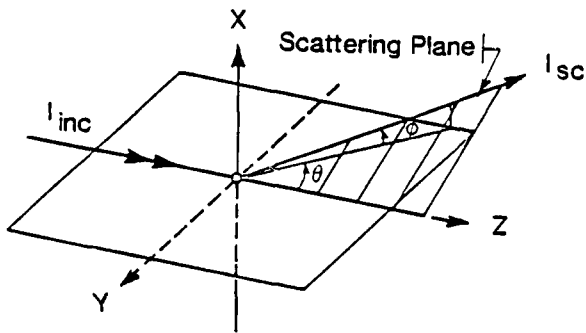


Fig. 1 Light scattering coordinate system. The functions  $i_1$  and  $i_2$  are for scattered light polarized perpendicular and parallel to the scattering plane respectively.

cylinders [9]. The calculations are often valid for only limited values of refractive index.

Some experimental work on the scattering characteristics of nonspherical particles has been performed. The use of microwave radiation with wavelengths on the order of 1 cm permits the study of scattering by arbitrary shapes [10,11]. Forward scattering by agglomerates of spherical particles has also been observed experimentally [12].

The results of these studies indicate that the near-forward scattering characteristics of nonspherical particles are predicted reasonably well by calculations for spherical particles of equal cross-sectional area. The off-axis scattering characteristics however are strongly dependent on the detailed particle shape. Concerning extinction, (scattering plus absorption), spheres of equal volume and surface area can be used to approximate these optical properties of nonspherical particles [13].

#### Scattering by an Ensemble of Particles

When electromagnetic radiation is incident on an ensemble of particles the results can sometimes be calculated by merely summing the contributions from individual particles. However the spacing and the positions of the particles in addition to the physical extent of the aerosol can be important. For example, if the particles are spaced less than about 3 diameters apart they scatter as a single entity. Further, if the particles are situated in a regular pattern, say in a lattice, the phases of the scattered waves emanating from each particle must be considered. In that case the ensemble-scattered intensity at some point away from the aerosol must be found by first summing the electrical field (considering phase) contribution from each particle and then squaring the sum to determine scattered intensity. Conversely, if there are many particles randomly positioned relative to each other then the phases are random as well and the scattering can be found by directly summing the intensity contributions from each particle. In the latter case we have incoherent scatter, and in the former coherent scatter.

#### Multiple Scattering

As the physical dimensions of an aerosol cloud increase the probability that a scattered photon or ray will encounter another particle and be scattered again before leaving the aerosol

increases as well. This phenomenon, termed multiple scattering, will clearly alter the characteristics of the scattered light which finally reaches the detector of a diagnostic instrument. The presence of multiple scattering complicates significantly the interpretation of light scattering measurements. The onset of multiple scattering can be ascertained from the level of attenuation of the incident beam. It has been suggested that less than 90% transmission indicates multiple scattering [4], although probabilistic considerations of an optical mean free path would suggest that multiple scattering becomes important at transmission levels less than about 60%.

#### III. Ensemble (multiparticulate) Sizing Techniques

Optical techniques which analyze the light scattering and extinction properties of an ensemble of particles are quite useful in several situations. First, for measurements of particles smaller than about  $0.1 \mu\text{m}$ , ensemble methods are the only viable options since SPC and imaging techniques generally cannot distinguish smaller particles. The lower size limit of a typical SPC is determined either by signal-to-noise considerations, since scattering cross sections decrease as  $d^6$  in the Rayleigh regime but the noise level is fixed by detector shot noise, or by the large particle number densities encountered at small particle sizes which make it impossible to maintain the presence of only one particle in the optical sample volume. Imaging techniques are useless for particles smaller than several wavelengths, and since visible or in some cases near ultraviolet radiation is generally used imaging methods are limited to particles several  $\mu\text{m}$  and above.

Ensemble measurements inherently contain less information than SPC and imaging data as the scattering or extinction is accumulated over all particle sizes in the aerosol. In some situations it is possible to mathematically invert the set of ensemble measurements and reconstruct or estimate the size distribution. The resolution possible for

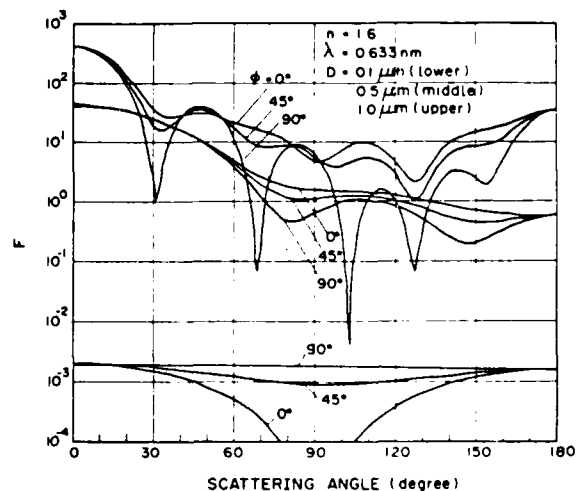


Fig. 2 Lorenz-Mie theory calculations of differential scattering cross-section  $F$  as a function of scattering angle  $\theta$  for various particle diameters after Handa et al. [5].

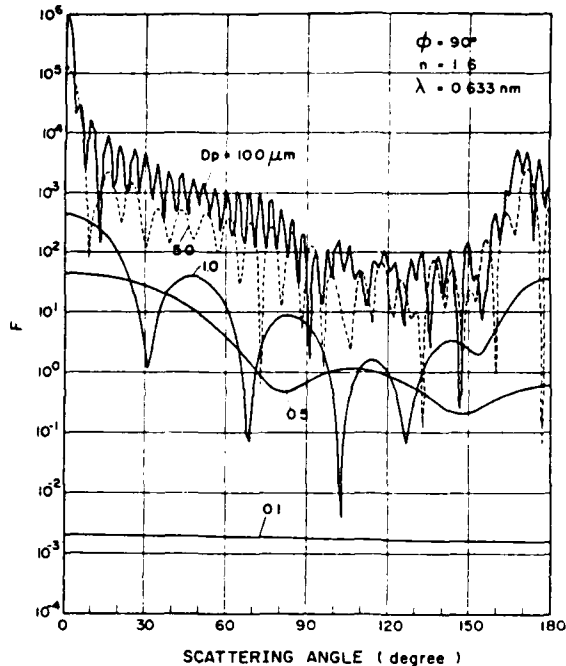


Fig. 3 Lorenz-Mie theory calculations of differential scattering cross-section  $F$  as a function of scattering angle  $\theta$  for various particle diameters after Handa et al. [5].

the reconstructed size distribution is determined by the number of optical property measurements (e.g. the number of scattering angles), but practical considerations often limit here. It is often advantageous to estimate average parameters of the aerosol such as a mean diameter rather than perform the complete inversion. Similarly the form of the size distribution can be assumed and the measurements used to estimate the best fit parameters for the assumed size distribution.

Several ensemble-averaged optical properties of aerosols can be used in size analysis. These include spectral extinction, the angular dependence of scattered light, and finally for very small particles the spectral properties of the scattered light as Doppler-shifted by the Brownian motions of the particles. The following paragraphs discuss in further detail these ensemble methods.

#### Extinction Methods

The amount of light removed from a beam passing through an aerosol directly indicates the extinction cross sections of the particles along the beam path. If the refractive index and the volume concentration of the particles are known, then the volume-to-surface area mean diameter  $D_{32}$  (or Sauter Mean Diameter, SMD) can be determined from a single transmission measurement [14]. Further, the authors [14] studied the ratio of the transmittance at two probe wavelengths and found that it exhibited monotonic behavior when plotted as a function of  $D_{32}$  for nonabsorbing particles in the range  $\lambda_1/3 < D_{32} < \lambda_1$ . Ariessohn et al. [15] also studied this two-wavelength approach and found that the specific form of the particle size distribution, if it was not very narrow, had little influence on the measurement. The authors [15]

considered measurements on coal ash particles which are weakly absorbing and found a compressed but useful sizing range of roughly  $\lambda_1/10 < D_{32} < 1.3\lambda_1$  for  $\lambda_1 = 0.325 \mu\text{m}$  and  $\lambda_2 = 3.39 \mu\text{m}$ . Lester and Wittig [16] and Bro [17] utilized a similar method in shock tube studies of soot formation. Powell et al. [18] used spectral transmission data coupled with scattering measurements to study smoke particle sizes. Although in the works referenced above only mean diameters are determined, there have also been a number of studies on the use of spectral transmission measurements to determine the size distribution as well [19]. For optimum sensitivity the wavelengths used must roughly bracket the particle sizes of interest, so these techniques are in general useful for intermediate particle sizes near practical wavelengths.

#### Multiangle Scattering Measurements

It is clear from Figs. 2, 3 and 4 that the angular scattering characteristics of an ensemble of particles will contain information on the particle size distribution. For small particles, say several  $\mu\text{m}$  and below, it is necessary to measure scattering characteristics over a large range of scattering angles. This can be accomplished for  $\theta$  from  $2^\circ$  to  $178^\circ$  using a polar nephelometer as discussed by Hansen and Evans [20]. Hansen then used this technique [21] to estimate size distributions and refractive indices of an atmospheric aerosol. In some situations it is impractical to traverse a detector around the aerosol to measure angular scattering characteristics, and a few detectors at selected scattering angles are used.

Multiangle scattering techniques are utilized in some situations where SPC and imaging methods are not applicable. Measurements in solid propellant rocket exhausts where the particle velocities are very high and the run times very short have been made by Weaver [22] using multiangle scattering and extinction. Measurements of soot particle sizes in flames require ensemble methods because of the small sizes ( $< 100\text{nm}$ ). Recent studies on soot by Santoro and Semerjian [23] and Chang and Penner [24] have been completed although the presence of nonspherical agglomerates complicate interpretation of the data. The authors [22,23,24] used an optical system similar to that

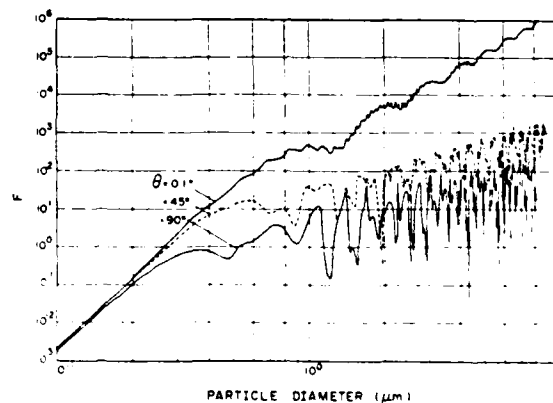


Fig. 4 Lorenz-Mie theory calculations of differential scattering cross-section  $F$  as a function of particle diameter for various  $\theta$ , after Handa et al. [5].

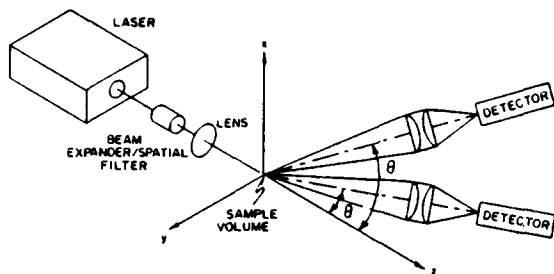


Fig. 5 Generalized Schematic of a Laser-based Single Particle Counter

in Fig. 5 but with some detectors oriented in the backscatter direction because of the small particle sizes. Measurement of the polarization state of the scattered radiation is also useful in particle size analysis by ensemble multiangle scattering.

One problem for all multiwavelength or multiangle diagnostics for particle sizes of several micrometers and below is that the scattering characteristics can be strongly influenced by the refractive index which is in general not known. By increasing the number of measurements and assuming that the size distribution is monodisperse or of some particular form it is possible in theory to determine the refractive index along with the size distribution [21,23,25].

As particle size increases it can be seen from Fig. 3 that the energy is scattered predominantly into the near-forward directions. Further, for particles greater than several  $\mu\text{m}$  the dominant contributor to the forward lobe is diffractive scatter as opposed to refraction or reflection. Analysis of the forward diffraction lobe has become a common diagnostic for particles and droplets larger than several micrometers in diameter.

The generalized schematic of a laser diffraction particle sizing apparatus is shown in Fig. 6. The beam from a laser, typically a several mW He-Ne model, is spatially filtered, expanded, and collimated to several mm diameter at the  $1/e^2$  intensity points. This collimated probe beam is directed through the aerosol of interest and the transmitted (unscattered) portion is focused on-axis to a spot at the back focal plane of the receiving lens. Light scattered by particles in the probe beam which passes through the aperture of the receiving lens is directed to off-axis points on the observation or detection plane. A monodisperse ensemble of spherical particles large compared to the wavelength would produce the characteristic Airy diffraction pattern shown in Fig. 6 as described by Fraunhofer diffraction theory:

$$I(\theta) = I_{\text{inc}} \frac{a^4 \lambda^3}{16\pi^2} \left\{ \frac{2J_1(a\theta)}{a\theta} \right\}^2 \quad (5)$$

where  $J_1$  is the first order Bessel function of first kind. The obliquity correction  $(1 + \cos^2\theta)/2$  has been neglected in Eq. (5) and the small angle approximation of  $\sin\theta \approx \theta$  has been made.

In practical systems a distribution or particle sizes or a polydispersion is generally encountered. The composite scattered intensity profile is a linear combination of the characteristic profile of each droplet size with a weighting coefficient equal to the number of

particles of that size in the sample volume. The diffraction signature of a polydisperse spray is given by:

$$I(\theta) = I_{\text{inc}} \int_0^{\infty} \frac{a^4 \lambda^3}{16\pi^2} \left\{ \frac{2J_1(a\theta)}{a\theta} \right\}^2 n(a) da \quad (6)$$

where  $n(a)da$  is the number of particles in the laser beam with sizes between  $a$  and  $a + da$  and truncation of light diffracted at large angles by the receiving lens has been neglected [26]. A primary effect of broadened size distributions is elimination of the contrast in the diffraction pattern as shown in the diffraction signatures calculated for several Rosin-Rammler particle size distributions in Fig. 7. The two parameters in a Rosin-Rammler distribution are the mean diameter  $x$  and the exponent  $N$ . The width of the distribution increases with decreasing  $N$ , and as  $N$  approaches infinity the distribution becomes monodisperse.

The basic task in laser diffraction particle sizing is to detect and analyze the diffraction signature  $I(\theta)$ , and then mathematically invert Eq. (6) to determine parameters of the particle size distribution. Chin et al. in 1955 [27] proposed several detection techniques, one of which was to traverse a pinhole/photodetector assembly across the diffraction pattern. Due to the mechanical traverse this detection approach requires a significant amount of time to cover the entire diffraction pattern. Further, the large dynamic range of the diffraction signature given by Eqs. 5 and 6 is another difficulty for such systems.

The advantages of real time analysis of the entire diffraction signature as opposed to traversing a detector across either the diffraction pattern itself or a photographic image thereof are obvious. Developments in monolithic solid state multi-element detector arrays in the 1970's improved the situation by allowing the entire diffraction signature to be analyzed instantaneously. A monolithic detector designed for forward scattering measurements is shown in Fig. 8. Note the increasing thickness of the annular detector elements which, when coupled with increasing length (circumference), result in a significant increase in detector area as radius increases. This effect compresses the dynamic range of the scattering measurements. A detector similar to that in Fig. 8 designed by Recognition Systems, Inc. [28] for parts recognition applications is utilized by Malvern Instruments Ltd. [29] in a commercial laser diffraction

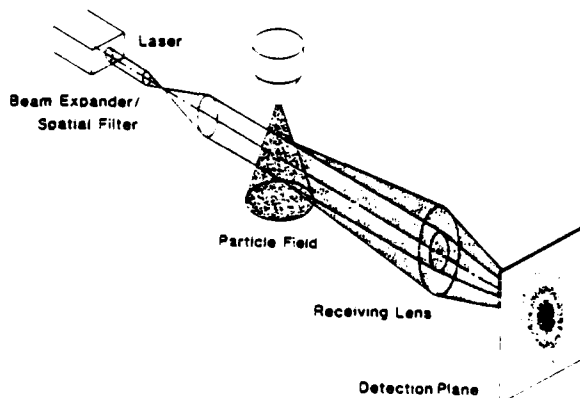


Fig. 6 Schematic of Laser Diffraction Particle Sizing Instrument

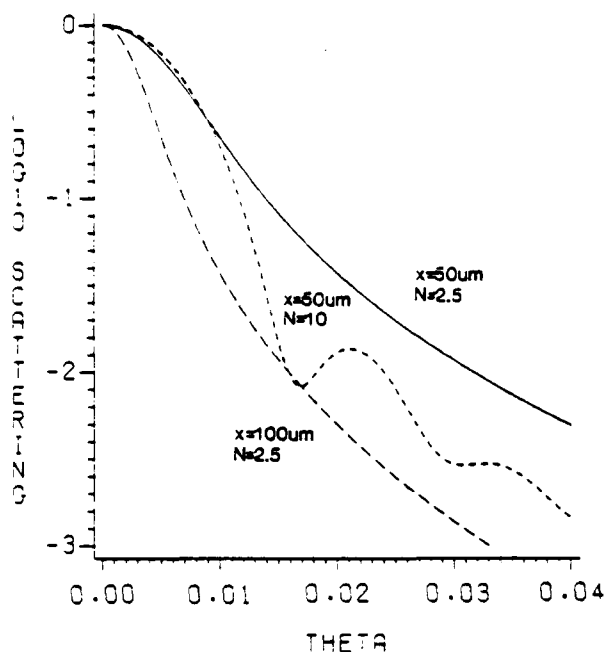


Fig. 7 Forward scattering signatures calculated using Fraunhofer diffraction theory for Rosin-Rammler particle size distributions.  $\lambda = 0.6328\mu\text{m}$ .

particle sizing instrument based on the work of Swithenbank et al. [30].

A number of data processing methods have been used to extract particle size information from measured diffraction patterns. Chin et al. [27] utilized the integral transform derivation of Titchmarsh [31] to analytically invert Eq. (6) to obtain  $n(a)$ . Dobbins et al. [32] somewhat paradoxically observed that the diffraction signatures were relatively independent of the form of the droplet size distribution and depended primarily on  $D_{32}$ . The authors [32] utilized a single parameter of the diffraction pattern, the angle at which the scattered light is down to 10% of the on axis value, to determine  $D_{32}$ . Others [33,34] have since modified slightly this approach and it is still in use today.

Swithenbank et al. [30] analyzed the diffraction pattern with the annular ring detector discussed above and subsequently did a numerical inversion (as opposed to integral transform) of a discretized form of Eq. (6) to obtain the volume distribution in 7 discrete size bins. The inversion problem is ill-conditioned and as second approach the authors [30] assumed that the size distribution was of Rosin-Rammler form with two independent parameters. Recent data processing developments do not require an assumption of the form of the size distribution [29,35].

#### Diffusion Broadening Spectroscopy

One problem with spectral extinction and multiangle scattering measurements of small particles is the dependence on refractive index which is generally unknown and might even vary between particles. One diagnostic which for certain applications does not require knowledge of

the refractive index is diffusion broadening spectroscopy. Light scattered by molecules or particles is Doppler shifted due to Brownian motion. The magnitude of the frequency shift depends on the velocity of the particle and the angle at which the scattered radiation is collected. Light scattered from a large number of particles undergoing Brownian motion in a medium with a mass mean velocity of zero contains a distribution of frequencies centered around the incident laser frequency. If the light scattered by these particles is collected and mixed on a single detector (homodyne detection) then the frequency differences between waves scattered from the various particles will be present in the detector output with a resulting spectrum centered around zero frequency. The theoretical analysis for predicting the power spectrum and autocorrelation function of the homodyne scattered light signal for particles suspended in a stagnant or laminar flow is well known [36]. The predictions depend on the scattering angle, the particle diameter, and the diffusion coefficient which in turn depends on temperature and viscosity. By measuring the half-width of the power spectra [37] after Penner et al. or the correlation time [38] from photon correlation after King et al. the diffusion coefficient of the particles can be determined. Introduction of some assumptions concerning the diffusion coefficient then allows the particle size of a monodisperse aerosol to be determined.

The optical system required for diffusion broadening spectroscopy is rather simple as shown in Fig. 5. The laser focus diameter is selected to minimize broadening effects due to finite particle residence time [38]. The output from the detector would then go to a spectrum analyzer or a digital photon correlator.

Diffusion broadening spectroscopy has been used successfully in flames [36,37,38] and other particle systems. It is only useful for particle diameters less than about 100nm because the frequency shifts become very small as the Brownian diffusion velocities decrease for larger particles. Further, this technique is only independent of refractive index for monodisperse aerosols, and successful application in polydisperse systems seems unlikely.

#### IV. Laser/Optical Single Particle Counters (SPC)

A generalized schematic of an optical SPC is presented in Fig. 5. The output beam from a laser or other source of radiation is directed (and

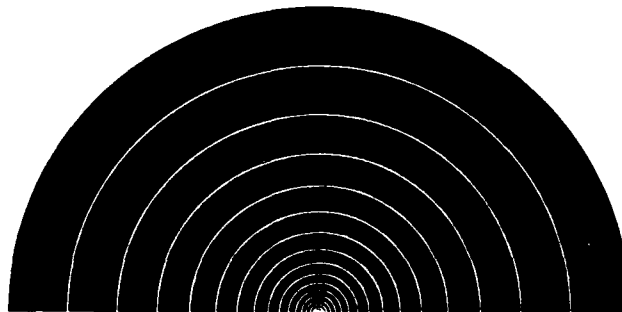


Fig. 8 Reproduction of the photosensitive elements of a monolithic P on N photodiode array detector after Hirleman [26].

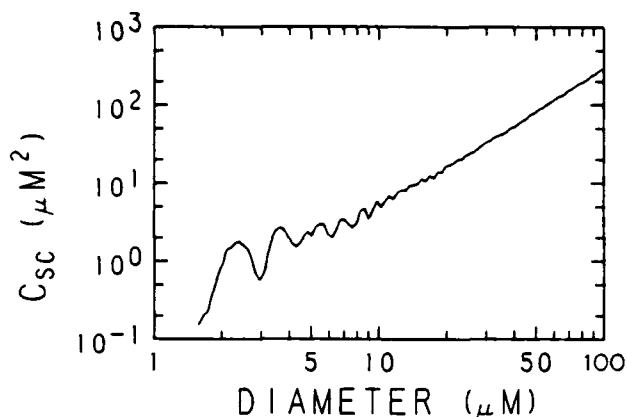


Fig. 9 Partial light scattering cross sections for spherical particles with refractive index  $n=1.47$  for  $f/1.96$  receiving optics oriented for  $10$  degrees off axis collection in the plane normal to the direction of polarization of the incident beam. The Lorenz-Mie theory calculations used  $\lambda = 0.6328 \mu\text{m}$ .

typically focused) into the optical sample volume. This sample or probe volume can be thought of as that region of space where a single particle can generate a sufficient detector signal to be discriminated or 'seen' over the background noise. As individual particles pass through the sample volume they interact with the incident radiation beam (i.e., scatter, absorb, and/or fluoresce light) and are observed by detection optics oriented at some angle(s)  $\theta$  with respect to the beam propagation direction. The single particle signal obtained at the photodetector(s) are processed to provide information on the size and possibly the velocity of each particle. The various SPC approaches to particle sizing are discussed below.

#### Light scattering cross section measuring techniques

The most common approach to particle sizing involves the principle that the amount of the light scattered by a particle is a nominally monotonic increasing function of particle size. It follows that measurement of a scattering or extinction cross section can be used to infer particle size. The SPC scattering signal response  $S$  to a particle in an incident radiation field (uniform over the particle) of intensity  $I_{\text{inc}}$  is given by:

$$S = k I_{\text{inc}} C_{\text{sc}} \quad (7)$$

where  $k$  is the system gain in transducing radiant energy to voltage using a photodetector and  $C_{\text{sc}}$  is the partial light scattering cross section as determined from Eq. (4). The partial cross sections, as opposed to total cross sections, depend on the specific finite aperture detector configuration in use. A response function  $S(d)$  relating measured signal levels to the diameters of spherical particles of known refractive index passing through a SPC sample volume of known incident intensity  $I_{\text{inc}}$  can be determined from theoretical calculations of  $C_{\text{sc}}(d)$ . Here the factor  $k$  must be determined by calibration.

A plot of partial light scattering cross section for spherical particles illuminated by a

coherent uniphase wave calculated using a Lorenz-Mie theory computer code [3] is given in Fig. 9. The calculations are for an off-axis  $f/1.96$  collection lens centered at  $\theta = 10^\circ$  from the incident radiation propagation direction (forward scattering). The oscillatory nature of the plot is a result of resonance interactions in the scattering process and results in ambiguities in particle size determination from SPC scattering measurements. Another problem inherent in using the laser as a SPC radiation source is the nonuniform intensity profile across the beam [12,39]. Unfortunately, another ambiguity in signal levels arises for *in-situ* SPC since the particles are free to traverse the sample volume at any position. Thus, particles will experience different peak incident intensities  $I_{\text{inc}}$  depending on the trajectory and even a monodisperse (uniform size) aerosol will generate a broad distribution of signal amplitudes  $S$ .

A number of methods have been devised to eliminate the unknown incident intensity effect in cross section measuring techniques. The basic approaches include: (1) analysis of only those particles which pass through a selected portion of the beam of known and constant intensity, (2) analysis of all particles and later correction for the known distribution of particle trajectories and corresponding incident intensities, (3) use of the ratio of scattering signals at two or more angles to cancel the incident intensity effect.

For *in-situ* measurements various optical methods of discriminating those particles which pass through a control portion of the beam have been used, including coincidence detectors at  $90^\circ$  by Ungut et al. [40] and in the forward direction by Knollenberg [41]. It has also been suggested that a pointer laser beam tightly focussed within a larger probe beam be used to discriminate those particles which pass through the center of the probe beam [42]. This latter approach does not eliminate the ambiguity, but rather shifts the problem to the pointer beam where the effect is less significant. It is also possible to change the intensity profile across the laser beam from Gaussian to something approximating a tophat using intensity filters. However any beam degradation due to windows or refractive index fluctuations would spread the profile and reintroduce the intensity ambiguity.

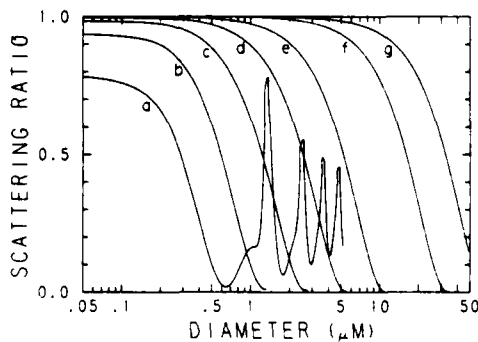


Fig. 10 Response functions for ratio-type SPC. The data apply to spherical particles with  $n=1.56-0.47i$  (soot) and  $\lambda = 0.6328 \mu\text{m}$ . The scattering angle pairs are a)  $48^\circ/24^\circ$ , b)  $24^\circ/12^\circ$ , c)  $12^\circ/6^\circ$ , d)  $6^\circ/3^\circ$ , e)  $3^\circ/1.5^\circ$ , f)  $1^\circ/0.5^\circ$ , g)  $0.5^\circ/0.25^\circ$ . All but the  $48^\circ/24^\circ$  curve were truncated after the first minimum.

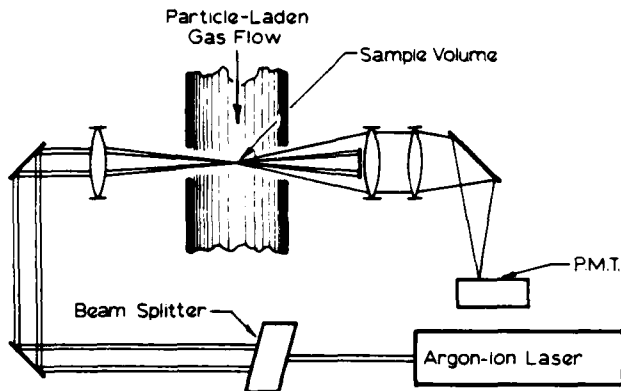


Fig. 11 Schematic of optical system for particle sizing interferometer after Houser [50].

It appears that no definitive studies on the use of top-hat profiles have been reported.

Another somewhat similar technique proposed by Hirleman [43] involves the use of signals generated by particles traversing two adjacent laser beams. The dual peak signature is used to determine two velocity components and the trajectory of each particle. Given known laser beam properties the incident intensity history for a particle is then completely determined which permits a real-time correction for the intensity ambiguity. After  $\tau_{inc}$  in Eq. (7) is determined a calibrated response function prediction such as Fig. 9 would be used to relate signal amplitudes to particle size. This technique [43] has been proposed for light scattering, extinction, and fluorescence cross section measurements although experiments to date have used only light scattering.

A second general approach to the ambiguous incident intensity problem is to correct after the fact. One implementation of this approach proposed by Holve and Self [44] is to first consider the distribution of scattering signal pulse heights generated by particles of one size passing with equal probability through all portions of the laser beam focus region. The optical system required again is like Fig. 5 using a single near-forward off-axis detector. The signal height distribution from a polydispersion is then a linear combination of the monodisperse particle response distributions. A numerical scheme was developed [44] to invert the resulting system of equations and solve for the linear coefficients which are proportional to concentrations in the discretized particle size intervals. This approach [44] has been successfully used for sizing burning droplets and particulates emitted from a coal combustor.

#### Scattering Intensity Ratio Techniques

The final method to eliminate the incident intensity ambiguity in SPC is to utilize the ratio of scattered light signals from two or more scattering angles to determine particle size. This approach is often used in ensemble multiangle scattering measurements where the relative scattering profile rather than the absolute scattering at some angle is used. Rodkinson [45] suggested and Gravatt [46] implemented an SPC based on the ratio technique which used scattering ratios from near-forward scattering angles where the sensitivity to particle shape and refractive index is minimized. The optical configuration of ratio

counters can be similar to that in Fig. 5, although annular detection schemes are often used [12,47]. A set of response functions for a ratio SPC is plotted in Fig. 10. One problem evident from Fig. 10 is the multivalued response function plotted for the largest angle pair. Outside particles, or those larger than the first minimum in the ratio response functions in Fig. 10, will be incorrectly sized by ratio instruments which utilize only a single pair of scattering angles. The multiple ratio concept (MRSPC) developed by Hirleman and coworkers [12,47] was designed to eliminate this ambiguity problem.

Ratio counters still have an optical sample volume which depends on particle size and corrections for this effect must be considered [12]. Also, since forward scattering is generally used, ratio counters are relatively insensitive to particle shape and refractive index [12].

A possible advance for ratio schemes may be to integrate photodiode array detectors to allow more scattering data to be collected without simply adding photomultiplier tubes. Bartholdi et al. [48] used a linear photodiode array in an SPC application and we are studying the use of intensified versions of the detector in Fig. 8.

Ratio SPC are applicable in the nominal size range of 0.3 - 10.0  $\mu\text{m}$  for practical laser sources. They have been successfully applied in engine exhausts [47], flame studies [49], fluidized bed off-gas [50], and in several other applications.

#### Particle Sizing Interferometry

Another approach which can provide particle size information independent of incident intensity is particle sizing interferometry (PSI). A schematic is shown in Fig. 11. As a single particle passes through the intersection region of two nonparallel laser beams, Doppler-shifted scattered light waves from each beam emanate from the particle. Heterodyning the two contributions of scattered light at a detector will produce the Doppler-difference frequency which is directly related to the particle velocity and the angle between the laser beam propagation vectors. This principle underlies the laser Doppler velocimeter (LDV). A particle crossing the LDV beam intersection region will produce an approximately Gaussian signal (pedestal) with the modulated Doppler-difference component written on the pedestal [51] as shown in Fig. 12. The ratio of the modulated signal amplitude to the pedestal amplitude, which is termed the visibility, provides a measure of particle size as shown by Farmer [51] and others [52,53] who used a scalar description of the process. For large apertures which collect all of the forward scattered (diffracted) light the visibility  $V$  as a function of particle diameter  $d$  and fringe spacing  $\delta$  was shown by Robinson and Chu [53] to be:

$$V = \frac{2J_1(\pi d/\delta)}{\pi d/\delta} \quad (8)$$

where  $J_1$  is a first order Bessel function of first kind. A plot of  $V$  is given in Fig. 13.

Calculations considering the complete problem of scattering by a sphere simultaneously in two coherent, collimated laser beams [54] predicted a strong dependence of the visibility on particle refractive index, the detector aperture, and detector position relative to the beams. A number of experimental studies have confirmed the importance of careful receiving optics design

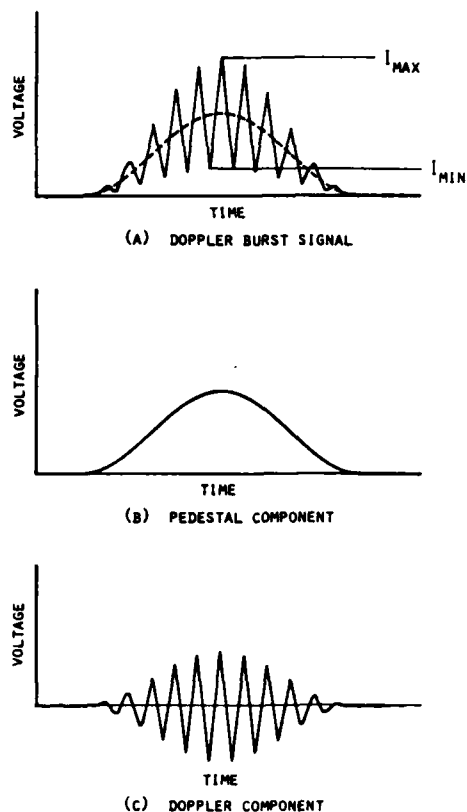


Fig. 12 Signals from particle sizing interferometer after Bachalo [57].

[54,55] although conflicting observations have also been made [56].

Another related approach is the off-axis PSI proposed by Bachalo [57] which utilizes the interference of refracted or reflected light scattering contributions rather than the diffractive scatter of a conventional PSI [51]. This method is applicable to particles significantly larger than the wavelength and is based on the difference in optical path length traveled by refracted rays from the two crossed beams which pass through the particle and arrive coincidentally at the detector. The visibility response function for a typical off-axis PSI collection angle [57] of  $20^\circ$  is also shown in Fig. 13, and the expanded  $d/\lambda$  sizing range for this concept is apparent.

Although the visibility is a relative measurement, absolute light scattering cross sections still control the PSI. Only those particles which scatter enough light to be detected above the background noise level can be sized. Whether or not a particle produces a scattering signal large enough to be discriminated against the background depends on the size and incident intensity. Thus a PSI will 'size' the particles using a relative measurement but the frequency at which particles are 'seen' or counted is biased toward large particles.

Another problem with PSI type instruments is the limited applicable particle size range. It has been suggested to utilize the amplitude of the Doppler bursts from PSI instruments to size particles in what basically is a scattering cross-section measurement approach. The incident

intensity ambiguity is then reintroduced and a correction must be made. Those particles traversing the center of the intersection region can be discriminated using coincidence detection with small aperture detectors or using an additional, tightly focused pointer beam. Unfortunately the latter approach merely shifts the trajectory ambiguity problem from the PSI beams to the Gaussian pointer beam.

#### V. Photographic and Holographic Methods

Several different imaging methods have been used for particle and droplet sizing. These rely on a short light pulse to 'freeze' the particle images so that direct measurements of size may be made. In the case of double flash photography two closely spaced light pulses are used to obtain double images of each droplet so that velocity can also be determined. Single and double pulse holography have been used as well, with the advantage that a volume of the aerosol can be captured rather than the limited depth of field afforded by photographic methods. The problem with both photographic and holographic methods is the tedious and expensive post processing needed to extract the data. Also, quantitative measurements of particle size distributions with imaging techniques are realistic only for particle sizes greater than  $5\mu\text{m}$  at best.

The data processing problem for particle photography has been automated by Simmons and Lopera [58] and Fleeter et al. [59]. In the Parker system [58], a strobe light is used to temporarily 'burn' an image onto the a vidicon tube. The image is scanned to obtain drop size information and then erased, and the cycle repeated roughly 10 times per second. The data is processed using appropriate computer programs. Mean diameters, size

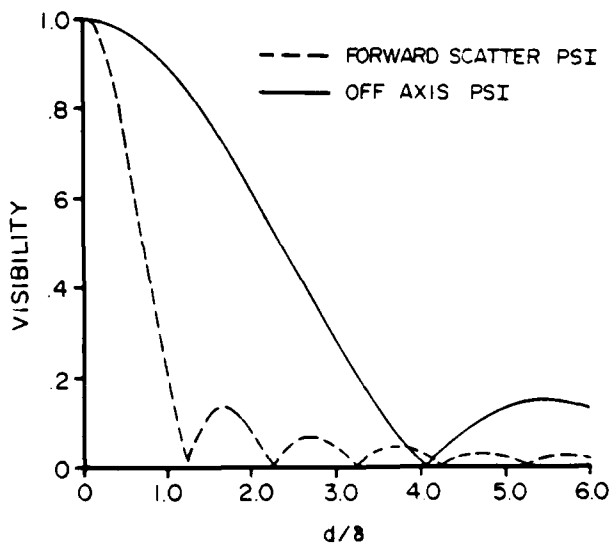


Fig. 13 Calculations for the fringe visibility  $V$  as a function of particle diameter to fringe spacing ratio  $d/\lambda$  for particle sizing interferometers (PSI). The data apply to a PSI collecting all of the forward scattered light and to an off-axis PSI with an  $f/2$  collection lens oriented at  $\theta = 20$  degrees.

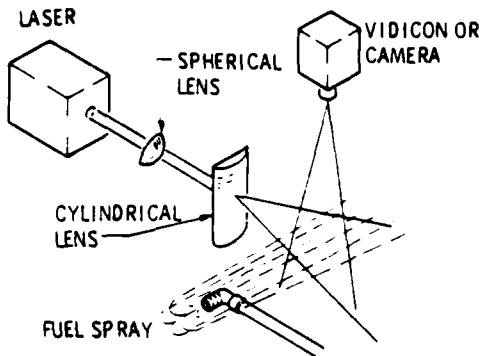


Fig. 14 Schematic of imaging particle sizing system after Fleeter et al. [59].

distributions, and concentration information can be obtained at each point in the spray [58]. Fleeter et al. [59] utilize a pulsed ruby laser as shown in Fig. 15 to illuminate the particles which are subsequently imaged onto a 512x512 diode array solid state camera. The image is then digitized [59] and transferred to a computer memory for processing. Knollenberg [41] analyzes individual particles by projecting images onto a linear photodiode array.

One correction factor required in the data analysis of incoherent imaging techniques is the effective depth of field vs. droplet size. (Large particles are visible over a larger axial distance from the exact object plane than small particles.) This correction is analogous to sample volume corrections required with SPC and is mandatory before useful data can be obtained.

Photographic image analysis is a very convenient method of particle and droplet sizing under cold flow conditions. One limitation is the typical resolution limit of about five micrometers. In hot flows one would expect substantially poorer results due to image distortion by refractive index fluctuations in the flow. Performance also suffers in applications where windows must be located between the spray and the camera, particularly when the optical aperture is limited. In a recent study of optical methods for Diesel engine research, for example, the threshold of size detection was 35 $\mu$ m for high speed photography and 8 $\mu$ m for holography [60].

Pulsed holography eliminates the sample volume correction required for photographic methods since the the holograms, which contain three dimensional information, can be observed in two-dimensions while the third is scanned. A schematic diagram of a holographic system is shown in Fig. 15. Holographic methods for particle and droplet size analysis have apparently been used to observe particles down to about 5 $\mu$ m [62,63]. Note however that the resolution of a holographic system is typically several micrometers so that the accuracy in sizing such small particles is very poor. Another problem encountered in particle holography is performance degradation when the laser beam transmission drops below about 10% [64].

#### VI. Conclusions

Laser-based techniques for nonintrusive diagnostics of particle size and concentration distributions have been reviewed. The most common diagnostics are imaging and light scattering techniques, and each instrument has its own unique

set of limitations and range of applicability. It is imperative that the subtle factors which control the accuracy and reliability of data obtained with laser/optical instruments be understood by the user.

#### Acknowledgements

The author's research in optical particle diagnostics has been generously supported over the past five years by the National Science Foundation, Particulate and Multiphase Processes Group, Dr. Morris Ojalvo, Program Director, and by the Office of Naval Research, Propulsion Group, Dr. Albert D. Wood, Project Director.

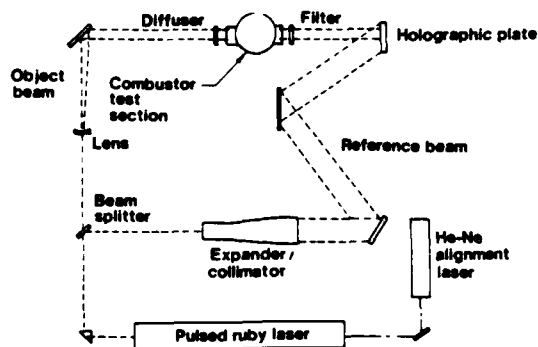


Fig. 15 Schematic of holographic particle sizing system after Chigier [61].

#### References

1. Born, M. and Wolf, E. Principles of Optics, Sixth edition, Pergamon Press, New York, 1980.
2. Hecht, E. and Zajac, A. Optics, Addison-Wesley New York, 1974.
3. van de Hulst, H. C., Light Scattering by Small Particles, John Wiley and Sons, New York, 1957.
4. Kerker, M., The Scattering of Light and Other Electromagnetic Radiation, Academic Press, 1969.
5. Handa, T., Suda, K., Nagashima, T., Kaneko, K., Yamamura, T., Takahashi, Y. and Suzuki, H., 'Size Determination of Submicron Particulates by Optical Counter', Fire Research, V. 1, pp. 255-263 (1978).
6. Asano, S., 'Light Scattering Properties of Spheroidal Particles', Applied Optics, V. 18, pp. 712-723 (1979).
7. Latimer, P. and Wamble, F., 'Light Scattering by Aggregates of Large Colloidal Particles', Applied Optics V. 21, pp. 2447-2455 (1982).
8. Borghese, F., Denti, P., Toscano, G. and Sinden, O. I., 'Electromagnetic Scattering by a Cluster of Spheres', Applied Optics V. 18, pp. 116-120 (1979).
9. Albini, F. A. and Nagelberg, E. R., Journal of Applied Physics, V. 33, pp. 1706-1713 (1962).
10. Schurman, D. W., Wang, R. T., Gustafson, B. A. S., and Schaefer, R. W., 'Systematic Studies of Light Scattering. 1. Particle Shape', Applied Optics V. 20, pp. 4039-4050 (1981).

11. Zerull, R. H. and Giese, R. H., in Planets, Stars and Nebulae Studied with Photopolarimetry, T. Gehrels, ed. (University of Arizona Press, Tucson, 1974) p. 901.
12. Hirleman, E. D. and Moon, H. K., 'Response Characteristics of the Multiple Ratio Single Particle Counter', J. Coll. Int. Sci. V. 87, pp. 124-139 (1982).
13. Chylek, P. and Ramaswamy, V., 'Lower and Upper Bounds on Extinction Cross Sections of Arbitrarily Shaped Strongly Absorbing or Strongly Reflecting Nonspherical Particles', Applied Optics V. 21, pp. 4339-4344 (1982).
14. Dobbins, R. A. and Jizmagian, G. S. J. Opt. Soc. Am. V. 56, p. 1351 (1966).
15. Ariessohn, P. C., Self, S. A., and Eustis, R. H., 'Two-wavelength Laser Transmissometer for Measurements of Mean Size and Concentration of Coal Ash Droplets in Combustion Flows', Applied Optics, V. 19, pp. 3775-3781 (1981).
16. Lester, T. W., and Wittig, S. L. K., in Proceedings of the Tenth International Shock Tube Symposium (G. Kamimoto, ed.) Kyoto, Japan, 1975.
17. Bro, K., 'The Optical Dispersion Quotient Method for Sizing of Soot in Shock-induced Combustion', Ph.D. Thesis, Purdue University, Lafayette, Ind., 1978.
18. Powell, E. A., Cassonova, R. A., Bankston, C. P. and Zinn, B. T. in Experimental Diagnostics in Gas Phase Combustion (B. T. Zinn, ed.) pp. 449-463, American Institute of Aeronautics and Astronautics, 1977.
19. King, M. D., Byrne, D. M., Herman, B. M., and Reagan, J. A. J. Atmos. Sci., V. 35, p. 2153 (1978).
20. Hansen, M. A., and Evans, W. H., 'Polar Nephelometer for Atmospheric Particulate Studies', Applied Optics, V. 19, pp. 3389-3395 (1980).
21. Hansen, M. Z., 'Atmospheric Particulate Analysis using Angular Light Scattering', Applied Optics, V. 19, pp. 3441-3448 (1980).
22. Weaver, D. P., 'Nonintrusive Particle Diagnostics in a Solid Rocket Motor Exhaust', AIAA Paper 83-1515, AIAA 18th Thermophysics Conference, June 1-3, 1983, Montreal, Canada.
23. Santoro, R. J. and Semerjian, H. G. 'Interpretation of Optical Measurements of Soot in Flames', AIAA Paper 83-1516, AIAA 18th Thermophysics Conference, June 1-3, 1983, Montreal, Canada.
24. Chang, P. H. P. and Penner, S. S., 'Particle Size Measurements in Flames using Light Scattering: Comparison with Diffusion Broadening Spectroscopy', J. Quant. Spectrosc. Radiat. Transfer, V. 25, pp. 97-110, (1981).
25. Powell, E. A. and Zinn, B. T. 'In-situ Measurements of Complex Refractive Index of Combustion Generated Particulates', AIAA Paper 83-1518, AIAA 18th Thermophysics Conference, June 1-3, 1983, Montreal, Canada.
26. Hirleman, E. D. 'On-line Calibration Technique for Laser Diffraction Droplet Sizing Instruments', ASME Paper 83-GT-232, 20th International Gas Turbine Conference, March 27-31, 1983, Phoenix, AZ.
27. Chin, J. H., Sliepcevich, C. M., and Tribus, M., 'Determination of Particle Size Distributions in Polydisperse Systems by Means of Measurements of Angular Variation of Intensity of Forward Scattered Light at Very Small Angles', J. Phys. Chem. Ithaca, V. 5, p. 841, (1955).
28. Recognition Systems Inc., Van Nuys, CA.
29. Malvern Instruments Ltd., Malvern, Worcestershire, England.
30. Swithenbank, J., Beer, J., Taylor, D. S., Abbot, D. and McCreath, C. G., 'A Laser Diagnostic Technique for the Measurement of Droplet and Particle Size Distribution', in Experimental Diagnostics in Gas-Phase Combustion Systems, (B. T. Zinn, ed.) pp. 421-447, Progress in Astronautics and Aeronautics, Vol. 53, 1977.
31. Titchmarsh, E. C., 'Extensions of Fourier's Integral Formula to Formulae involving Bessel Functions', Proc. London Math. Soc. V. 23, p. xxii (1924).
32. Dobbins, R. A., Crocco, L. and Glassmann, I., 'Measurement of Mean Particle Sizes of Sprays from Diffractively Scattered Light', AIAA Journal, V. 1, pp. 1882-1806, (1963).
33. Roberts, J. H. and Webb, M. J., 'Measurement of Droplet Size for Wide Range Particle Distributions', AIAA Journal, V. 2, pp. 583-585, (1964).
34. Dieck, R. H. and Roberts, R. L., 'The Determination of the Sauter Mean Droplet Diameter in Fuel Spray Nozzles', Applied Optics, V. 9, pp. 2007-2014, (1970).
35. Alger, T. W. 'Polydisperse-particle Size Distribution Function Determined from Intensity Profile of Angularly Scattered Light', Applied Optics V. 18, p. 3494, (1979).
36. Benedek, G. B. Polarization, Matter, and Radiation. Presses Universitaires de France, Paris, 1969.
37. Penner, S. S., Bernard, J. M., and Jerskey, T. 'Laser Scattering from Moving Polydisperse Particles in a Flame II: Preliminary Experiments', Acta Astronautica, V. 3, p. 93 (1976).
38. King, G. B., Sorenson, C. M., Lester, T. W., and Merklin, J. F. 'Photon Correlation Spectroscopy used as a Particle Size Diagnostic in Sooting Flames', Applied Optics, V. 21, pp. 976-978 (1982).
39. Hirleman, E. D., 'Laser-based Single Particle Counters for in-situ Particulate Diagnostics', Optical Engineering, V. 19, pp. 854-860 (1980).
40. Ungut, A., Yule, A. J., Taylor, D. S., and Chigier, N. A., 'Simultaneous Velocity and Particle Size Measurements in Two Phase Flows by Laser Anemometry', AIAA Paper 78-74, AIAA 16th Aerospace Sciences Meeting, Huntsville, Alabama, January 10-18, 1978.
41. Knollenberg, R. G., 'The Use of Low Power Lasers in Particle Size Spectroscopy', in Practical Applications of Low Power Lasers, pp. 137-152, SPIE V. 92, 1977.
42. Hess, C. Spectron Development Laboratories, Private Communication, May, 1983.
43. Hirleman, E. D., 'Laser Technique for Simultaneous Particle Size and Velocity Measurements', Optics Letters, V. 3, pp. 19-21, (1978).
44. Holve, D. and Self, S. A., 'Optical Particle Sizing for in situ Measurements, Parts I and II', Applied Optics, V. 18, pp. 1632-1652 (1979).
45. Hodkinson, J. R., 'Particle Sizing by Means for the Forward Scattering Lobe', Applied Optics, V. 5, p. 839, (1966).

46. Gravatt, C. C., 'Real Time Measurement of the Size Distribution of Particulate Matter by a Light Scattering Method,' APCA Journal, V. 23, p. 1035, (1973).
47. Hirleman, E. D., 'Optical Technique for Particulate Characterization in Combustion Environments: The Multiple Ratio Single Particle Counter,' Ph.D. Thesis, Purdue University, W. Lafayette, IN, 1977.
48. Bartholdi, M., Salzman, G. C., Hiebert, R. D., and Seger, G., 'Single Particle Light Scattering Measurements with a Photodiode Array,' Optics Letters, V. 1, pp. 223-225, (1977).
49. Samuelson, G. S., Hack, R. L., Poon, C. C., and Bachalo, W. D. 'Study of Soot Formation in Premixed and Nonpremixed Flows with Complex Aerodynamics', Paper WSSCI-80-10, presented at the Western States Section Combustion Institute Meeting, April 22, 1980, Irvine, CA.
50. Houser, M. J. 'Particle Field Diagnostics: Applications of Intensity Ratioing, Interferometry, and Holography', Optical Eng., V. 19, pp. 873-877 (1980).
51. Farmer, W. M., 'Measurement of Particle Size, Number Density, and Velocity Using a Laser Interferometer,' Applied Optics, V. 11, p. 2603, (1972).
52. Fristrom, R. M., Jones, A. R., Schwarz, M. S. R., and Weinberg, F. S., 'Particle Sizing by Interference Fringes and Signal Coherence in Doppler Velocimetry,' Faraday Symposia of the Chemical Society, V. 1, P. 183, (1973).
53. Robinson, D. M. and Chu, W. P. 'Diffraction Analysis of Doppler Signal Characteristics for a Cross-beam Laser Doppler Anemometer,' Applied Optics, V. 14, p. 2177, (1975).
54. Chu, W. P. and Robinson, D. M., 'Scattering from a Moving Spherical Particle by Two Crossed Coherent Plane Waves,' Applied Optics, V. 16, p. 619, (1977).
55. Yule, A. J. Chigier, N. A., Atakan, S. and Ungut, A., 'Particle Size and Velocity Measurement by Laser Anemometry,' AIAA Paper 77-214, 1977.
56. Farmer, W. M., 'Measurement of Particle Size and Concentrations Using LDV Techniques', in Proceedings of The Dynamic Flow Conference, 1978.
57. Bachalo, W. D., 'Method for Measuring the Size and Velocity of Spheres by Dual-Beam Light-Scatter Interferometry,' Applied Optics, V. 19, pp. 363-370 (1980).
58. Simmons, H. C. 'The Correlation of Drop-size Distributions in Fuel Nozzle Sprays', J. of Engineering for Power, V. 99, pp. 309-314 (1977).
59. Fleeter, R., Toaz, R., and Sarohia, V., 'Application of Digital Image Analysis Techniques to Antimisting Fuel Spray Characterization,' ASME Paper 82-WA/HT-23, American Society of Mechanical Engineers, New York, 1982.
60. Lennert, A. E., Sowls, R. E., Belz, R. A., Goethert, W. H., and Bentley, H. T., 'Electro-optical Techniques for Diesel Engine Research', in Experimental Diagnostics in Gas Phase Combustion (B. T. Zinn, ed.) pp. 629-656, American Institute of Aeronautics and Astronautics, 1977.
61. Chigier, N. 'Spray Combustion Processes: A Review', ASME Paper 82-WA/HT-86, American Society of Mechanical Engineers, New York, 1982.
62. Trolinger, J. D. 'Particle Field Diagnostics by Holography', AIAA Paper 80-0018, American Institute of Aeronautics and Astronautics, New York, 1980.
63. Thompson, B. J. J. Physics E, V. 7, pp. 781-788 (1974).
64. Jones, A. R. J. Physics D, V. 10, pp. L163-L165 (1977).



**AIAA 80-0350R**

**Non-Doppler Laser Velocimetry: Single Beam  
Transit-Time L1V**

**E. D. Hirleman**

Reprinted from

**AIAA Journal**

Volume 20, Number 1, January 1982, Page 86

Copyright American Institute of Aeronautics and Astronautics, Inc., 1980. All rights reserved.

# Non-Doppler Laser Velocimetry: Single Beam Transit-Time LIV

E. Dan Hirtleman\*  
Arizona State University, Tempe, Ariz.

## Abstract

RECENTLY the theoretical development of a laser-based particle sizing velocimeter (LSV) was presented.<sup>1</sup> The LSV is a non-Doppler laser velocimeter which determines two velocity components and size from scattering signatures of single particles passing through two adjacent, nominally parallel beams. Inherent to the LSV is use of the single beam transit-time laser velocimeter (LIV) concept. A recent paper,<sup>2</sup> a summary of which is presented herein, discussed some of the practical aspects of using the LIV including data acquisition/signal processing and presented some experimental data.

## Contents

### LIV Signal Processing

It has been shown<sup>1,3</sup> that the scattering signature from a particle traversing a single TEM<sub>00</sub> mode laser beam can be used to determine the particle speed in the plane normal to the laser beam. This is true for particles significantly (4-10×) smaller than the beam diameter at the exp(-2) intensity points. The time dependence of a scattered light signal  $S$  generated by a particle traveling at speed  $V_{\perp}$  in the plane normal to the beam is given by

$$S(t) = S_0 \exp(-2(V_{\perp}(t-t_0)/w)^2) \quad (1)$$

where  $w$  is the Gaussian beam radius at the exp(-2) intensity points and time  $t_0$  represents the center of the Gaussian peak corresponding to a maximum signal amplitude  $S_0$ . Here  $w$  is known independently and  $V_{\perp}$  is to be determined from  $S(t)$ .

Analog signal processing methods have been proposed<sup>1,2</sup> and utilized<sup>1,4</sup> but our efforts have been directed toward high-speed analog to digital (A/D) conversion of the signal followed by microprocessor-based digital signal processing (DSP). In the discrete time domain Eq. (1) becomes

$$S_i(t_i) = S_0 \exp(-2(t_i - t_0)^2 / (w/V_{\perp})^2) \quad (2)$$

and the LIV problem becomes one of the estimation of signal parameters  $t_0$ ,  $S_0$ , and the pulse width  $w/V_{\perp}$  from the discrete samples  $S_i$  at times  $t_i$ . There are several digital signal processing methods applicable to this problem including the discrete Fourier transform (DFT), least-squares curve fitting methods, and other simpler but less accurate estimation/reconstruction algorithms. High-frequency noise on the signal precludes simple digital peak sensing/constant-fraction discrimination algorithms, and this noise can be rejected by least-squares curve fitting or by digital filtering of the DFT spectrum. The following logarithmic least-squares algorithm seems to optimize the tradeoff between processing speed and accuracy.

Presented as Paper 80-0350 at the AIAA 18th Aerospace Sciences Meeting, Pasadena, Calif., submitted Feb. 6, 1980; synoptic received May 22, 1981. Copyright © American Institute of Aeronautics and Astronautics, Inc., 1980. All rights reserved. Full paper available from AIAA Library, 555 W. 57th Street, New York, N.Y. 10019. Price: Microfiche, \$3.00; hard copy, \$7.00. Remittance must accompany order.

\*Professor, Mechanical and Energy Systems Engineering Department.

Taking the natural log of Eq. (2) for linearization purposes

$$\ln S_i = \ln S_0 - 2(t_i - t_0)^2 / (w/V_{\perp})^2 \quad (3)$$

and expanding results in the form

$$\ln S_i = a + bt_i + ct_i^2 \quad (4)$$

where

$$a = \ln S_0 - 2(t_0 V_{\perp} / w)^2 \quad (5)$$

$$b = +4t_0 / (V_{\perp} / w)^2 \quad (6)$$

$$c = -2(V_{\perp} / w)^2 \quad (7)$$

Minimizing the sum-square error results in the system of normal equations

$$\begin{bmatrix} \sum \ln S_i \\ \sum t_i \ln S_i \\ \sum t_i^2 \ln S_i \end{bmatrix} = \begin{bmatrix} n & \sum t_i & \sum t_i^2 \\ \sum t_i & \sum t_i^2 & \sum t_i^3 \\ \sum t_i^2 & \sum t_i^3 & \sum t_i^4 \end{bmatrix} \begin{bmatrix} a \\ b \\ c \end{bmatrix} \quad (8)$$

where  $n$  is the number of samples. Equation (8) can be solved for  $a$ ,  $b$ , and  $c$  using Kramer's rule and in turn for  $V_{\perp}$ ,  $t_0$ , and  $S_0$  using Eqs. (5-7). This algorithm has been implemented using a Nicolet digital oscilloscope with sample rates to 2 MHz (12 bits) and to 20 MHz (8 bits) in conjunction with a TI 9900 16-bit microcomputer system. By implementing the  $\ln$  operations in a ROM look-up table and calculating and storing the elements and determinant of the  $3 \times 3$  matrix prior to the experiment, the curve fit and subsequent estimation of  $V_{\perp}$  can be completed using  $2n + 10$  multiply/divides plus a square root. For reasonable values of the number of samples  $n$  per Gaussian peak an LIV throughput rate of 10 kHz is attainable easily with present microelectronic technology. For a noncustom system using for example a stand-alone transient digitizer interfaced to a standard microcomputer (without parallel or multiprocessing) a throughput of more than 1 kHz is possible.

### LIV Sample Volume Characterization

A primary concern for the LIV is the need for accurate characterization of the exp(-2) beam radius  $w$  at the optical sample volume. We use a calibrated microscope assembly coupled with a 1000 element linear photodiode array (25  $\mu$ m centers) mounted at the image plane to perform beam diagnostics. To analyze the beam profile, the peak output values from each diode are digitized and fit to a Gaussian profile using the logarithmic least-squares technique. The curve fitting is performed by the TI 9900 microprocessor system which controls the diode scan, the A/D conversion, transferring the data into microcomputer memory, and, finally, performs the curve fit calculations. Beam diameters are analyzed for several positions along the laser beam ( $z$  axis) and a least-squares curve fit of the axial data to the predicted Lorentzian form<sup>5</sup> for  $w(z)$  near a diffraction-limited TEM<sub>00</sub> laser beam waist is used to estimate  $w$  at the waist. The uncertainty in a single measurement of  $w$  at one axial location can be 10-20% in worst cases depending on the beam quality.

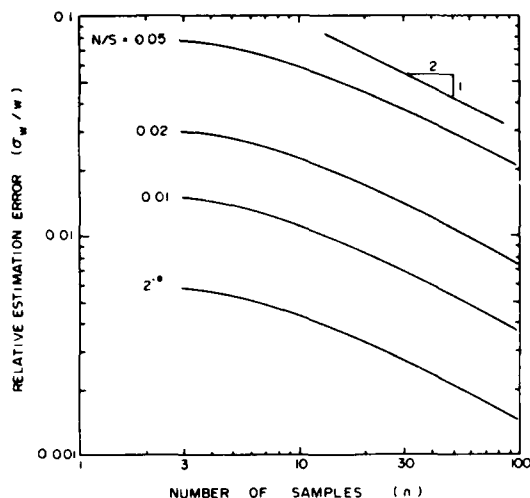


Fig. 1 Relative error for estimating the Gaussian signal width parameter  $w$  from  $n$  discrete digital samples (within  $1/e^2$  points) with normally distributed random noise contributions. The predictions are for the indicated values of rms noise to signal (amplitude) ratio  $N/S$  with least-square fits of Gaussian curves to the data, and assume a 12-bit A/D converter.

diode-to-diode response variations, and aberrations in the objective system for small beam waists ( $\leq 20 \mu\text{m}$ ). By measuring the axial  $w(z)$  profile this uncertainty can be decreased significantly since the measurement accuracy is better in larger portions of the beam. For  $1/e^2$  beam diameters of roughly  $50 \mu\text{m}$  or greater the technique is accurate to about 1%.

#### LIV Accuracy

The tradeoff necessary to have the optical system simplicity of the LIV is potentially decreased accuracy in the velocity measurement. Uncertainties can be introduced through the beam radius  $w$  which must be known a priori or through digital signal processing errors. For nonhostile, optically thin flows the uncertainty in knowing  $w$  at the sample volume can be made very small. In more difficult measurement environments, for example internal flows in turbulent combustion systems, the value for  $w$  clearly will be less certain. In those cases it will probably be necessary to form an "image" of the waist on the output side of a two-ended optical access system to infer properties of the waist in the sample volume using Gaussian beam optics.<sup>5</sup> These uncertainties from  $w$  are important but must be considered on a case-by-case basis. The following discussion considers the only DSP errors from the Gaussian curve fit algorithm discussed previously.

The parameters controlling the accuracy of the digital Gaussian curve fit algorithm and, hence, of the LIV velocity measurement include: the number of A/D samples during a Gaussian peak  $n$ ; the ratio of rms noise (high frequency) to the peak amplitude; and the ratio of A/D resolution or digitizing error to the peak amplitude. It is well known from DSP theory<sup>6</sup> that the latter digitizing error is equivalent to an

rms basis to  $F/(2^b/12)$  where  $F$  is the full-scale signal value and  $b$  the number of bits of A/D resolution. This number is typically 0.11% or less and is, in general, negligible compared to other rms noise contributions.

A computer simulation of LIV signal processing has been used to evaluate the accuracy. Figure 1 indicates predictions of the normalized or relative uncertainty  $\sigma_w/w$  for reconstructing a Gaussian peak from discrete digital samples as a function of the number of samples  $n$  and the rms noise/signal ratio. The values for  $\sigma_w$  were estimated by: 1) assuming a set of Gaussian peak parameters; 2) taking  $n$  A/D samples of the assumed signal and perturbing each sample by adding a random noise contribution using a normal distribution random number generator; and, finally, 3) applying the curve fit algorithm to the signal + noise samples. The width parameter of the reconstructed Gaussian less the initially assumed value is then the error in  $w$  (and velocity) determination. This process was repeated 1000 times using different random noise perturbations for statistics of the error, and the standard deviation of these errors is reported as  $\sigma_w$  in Fig. 1. The mean values of the errors were effectively zero and the data are valid for a 12 bit A/D converter with a full-scale peak signal level.

Figure 1 confirms what one would expect, that the uncertainty in determining  $w$  decreases with the number of samples  $n$  and increases with the noise level. Three is the minimum number of samples required for the three parameter curve fit. Increasing the number of samples for a given particle velocity involves higher speed A/D conversion and the tradeoffs of cost, fewer bits of A/D resolution, and increased data analysis time. In the limit of large  $n$  the slope for any noise level in Fig. 1 approaches  $-0.5$  which agrees with classical statistical sampling theory. The acceptable LIV uncertainty would depend on the turbulence intensity levels of interest since data processing errors ultimately appear as velocity broadening. Accuracy comparable to that of LDV seems attainable with the LIV concept.

#### Acknowledgment

This research was supported, in part, by the Office of Naval Research.

#### References

- Hirleman, E. D., "Laser Technique for Simultaneous Particle-Size and Velocity Measurements," *Optics Letters*, Vol. 3, 1978, p. 19.
- Hirleman, E. D., "Recent Developments in Non-Doppler Laser Velocimetry," AIAA Paper 80-0350, Jan. 1980.
- Rudd, M. J., "Non-Doppler Methods of Laser Velocimetry," *Proceedings of Second International Workshop on Laser Velocimetry*, Vol. II, edited by W. H. Stevenson and D. Thompson, Purdue University Press, 1974, p. 300.
- Holve, D. J., "A Transit-Timing Technique for Velocity (Slowness) Measurements," Paper 80-49, 1980 Fall Meeting of the Combustion Institute, Western States Section, Oct. 1980, University of Southern California, Los Angeles, Calif.; submitted to *Combustion and Flame*.
- Hirleman, E. D. and Stevenson, W. H., "Intensity Distribution Properties of a Gaussian Laser Beam Focus," *Applied Optics*, Vol. 17, 1978, p. 3496.
- Gold, B. and Radar, C. M., *Digital Processing of Signals*, McGraw-Hill, New York, 1969.

E. Dan Hirleman<sup>1</sup>

## Particle Sizing by Optical, Nonimaging Techniques

---

**REFERENCE:** Hirleman, E. D., "Particle Sizing by Optical, Nonimaging Techniques," *Liquid Particle Size Measurement Techniques*, ASTM STP 848, J. M. Tishkoff, R. D. Ingebo, and J. B. Kennedy, Eds., American Society for Testing and Materials, 1984, pp. 35-60.

**ABSTRACT:** Optical, nonimaging techniques for sizing liquid particles of diameters greater than 1  $\mu\text{m}$  are reviewed. Nonimaging optical diagnostics separate into two classes, ensemble or multi-particle analyzers and single particle counters (SPC). A discussion and analysis of the theoretical basis, performance characteristics, and calibration considerations for the various methods in each class is presented. Laser diffraction ensemble techniques, crossed-beam dual-scatter interferometric SPC, and finally single beam SPC based on the measurement of partial light-scattering cross sections of the particles are considered in detail.

**KEY WORDS:** liquid particles, particle sizing, nonimaging techniques, light scattering, optical techniques

The myriad of methods for sizing liquid particles (droplets) presents a significant problem for both the potential user and one trying to review the technology as well. The scope of this paper includes optical, nonimaging diagnostics for liquid particles with diameters greater than 1  $\mu\text{m}$ . These particle dimensions also correspond to the nominal sizing range of photographic and holographic imaging techniques. The reader is referred to previous reviews [1-3] for a discussion of optical diagnostic techniques outside the scope of this paper.

The techniques for sizing particles and droplets can be divided into two generic approaches: optical in situ (or in vivo to use medical terminology) methods; and batch sampling, with subsequent in vitro or external analysis. In the latter a hopefully representative sample of the aerosol is extracted from the original environment and transported to a remote artificial site for either on-line or off-line size analysis. Quite often a laser/optical particle sizing instrument is used for the remote size analysis. With batch sampling the possibility of size segregation or

<sup>1</sup>Associate professor, Mechanical and Aerospace Engineering, Arizona State University, Tempe, AZ 85287.

biasing in the sampling process and condensation, deposition or coagulation in the sampling lines are always of utmost concern. In contrast, in situ methods attempt to perform the sizing in place without removing an aerosol sample.

The significant advantages accruing from the nonintrusive nature of in situ methods must be discounted to varying degrees as the measurements are generally less direct and more equivocal. For example, a solid particle sample might be extracted, analyzed by optical microscopy, and then stored with the possibility for analyzing it again at a later time. In contrast an in situ laser light-scattering single particle counter (SPC) collects scattered light from individual particles which traverse an illuminated optical sample volume in microseconds. If the scattered light deriving from the particle is significantly larger than the background noise level during the transit time across the sample volume the sizing instrument will recognize it as a particle and attempt a size classification based on the amplitude or the time dependence of the scattered light signal. Unfortunately several potential sources of error are present since pulses at the output of a photodetector can derive from a number of phenomena other than scattering from particles or droplets in the sample volume. Despite some potential and demonstrated problems optical in situ methods are desperately needed in those applications where batch sampling techniques are impossible due either to lack of probe access, for example between blades in a steam turbine, or due to survivability problems as in gas turbine combustors.

Laser/optical methods for particle sizing can be subdivided into three main classes:

1. Ensemble or multi-particle techniques.
2. Single particle counters (SPC).
3. Imaging techniques, photographic or holographic.

The former two do not involve the formation of optical images of the particles or droplets and will be discussed here. For a discussion of imaging methods the reader is referred to the paper by Thompson [1] in this volume.

Ensemble techniques analyze the aggregate effect that a distribution of particles or droplets has on incident laser radiation. In contrast to SPC a large number of droplets are in the optical sample volume at any particular time. Since a multitude of droplet sizes contribute to the interaction of radiation with the aerosol, several properties of the radiation exchange process must be studied to determine a droplet size distribution. For example, the attenuation of radiation by the aerosol as a function of wavelength (dispersion quotient) might be measured [2]. For useful precision with these dispersion quotient methods probe wavelengths which bracket the size distribution of interest are generally required. In the case of sprays where droplet sizes may be several hundred microns it becomes very impractical to utilize such methods. Generally for sprays the light scattering pattern as a function of scattering angle  $\theta$  (measured from the forward or light beam propagation direction) is utilized for size distribution measurements. The maximum information content of the scattering from an ensemble

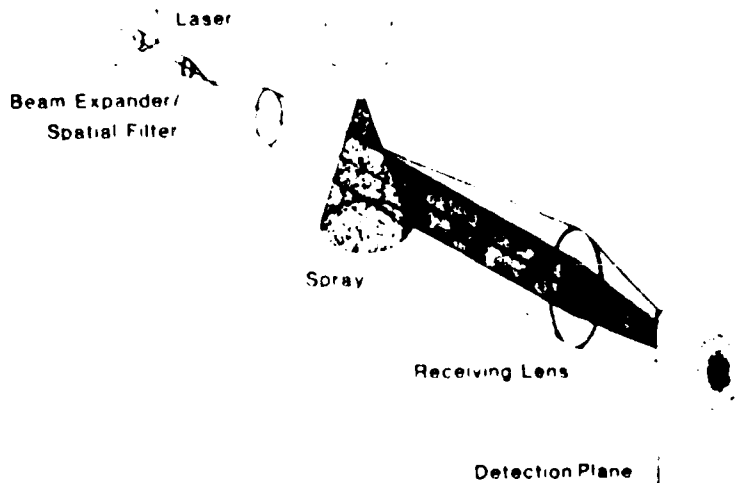


FIG. 1. — Schematic of laser diffraction particle sizing instrument.

of particles larger than several microns is in the near-forward scattering angles, and since the dominant contribution to forward scattering is diffraction, laser diffraction techniques have become the most common diagnostic for multi-particle size analysis in this size range. The optical configuration (less detector) for a laser diffraction droplet sizing instrument is shown in Fig. 1. This technique will be described in detail later; at this time note that the optical sample volume comprises the entire collimated beam between the exit lens of the spatial filter and the receiving lens, and the technique is an ensemble, line-of-sight diagnostic.

Single particle counters serve a complementary purpose to ensemble methods. A generalized schematic of an SPC is given in Fig. 2. In SPC the characteristic dimension of the optical sample volume is made small compared to the mean particle spacing by using focused probe beams and by optically limiting the axial extent of the sample volume with the detector field(s) of view. Thus only one particle at a time is present in the optical sample volume, and these are sized individually. A statistically significant number of particles is then analyzed as the aerosol flows through the probe volume. Either a single beam or two intersecting probe laser beams can be used, and one advantage of SPC over ensemble methods derives from the fact that particle velocity can be measured simultaneously with size. Particle size analysis using SPC for sizes  $>1 \mu\text{m}$  has generally been performed using one of two light scattering properties. First, a partial light scattering cross section can be measured and related to particle size, and, secondly, the phenomenon of interference between the two scattered waves produced by a particle traversing the intersection region of two crossed laser beams can be used. Regardless of the specific analysis technique an SPC must accomplish two things in order to measure a meaningful size distribution. First and rather obviously, those particles "seen" by the instrument must be sized correctly, and, second, all particle sizes must either be sampled in an unbiased (with respect to size) manner or a correction for size-selective sampling bias must be made. In the following

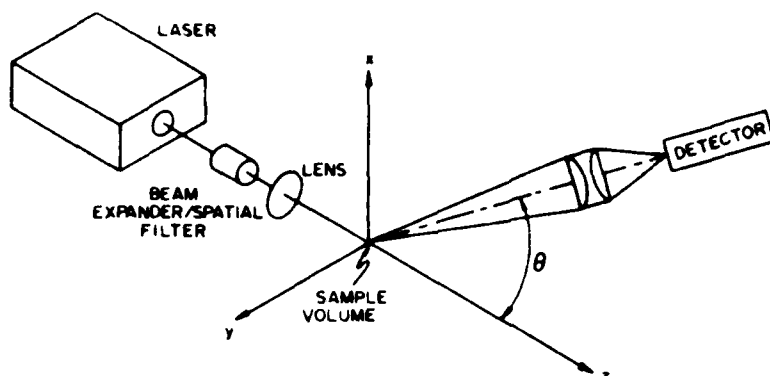


FIG. 2—Generalized schematic of a laser-based single particle counter.

paragraphs a discussion of the specific SPC methods used in particle sizing applications will be presented. A recent and somewhat more comprehensive review directed solely toward SPC has been published elsewhere [3].

The balance of this paper addresses the theoretical basis of the laser diffraction and SPC techniques most commonly used for sizing liquid particles  $>1 \mu\text{m}$ . In addition, calibration methods and the absolute accuracy of the various techniques are discussed.

### Laser Diffraction Particle Sizing Techniques

The generalized schematic of a laser diffraction droplet sizing apparatus is shown in Fig. 1. The beam from a laser, typically a several mW He-Ne model, is spatially filtered, expanded, and collimated to several millimetre diameter at the  $1/e^2$  intensity points. This collimated probe beam is directed through the aerosol of interest, and the transmitted (unscattered) portion is focused to a spot at the back focal plane of the receiving lens. Light scattered by particles in the probe beam which passes through the aperture of the receiving lens is directed to off-axis points on the observation or detection plane. A monodisperse ensemble of spherical particles with diameter  $d$  significantly greater than the wavelength  $\lambda$  would produce the characteristic Airy diffraction pattern shown in Fig. 1 as described by Fraunhofer diffraction theory

$$I(\theta) = I_{inc} \frac{\alpha^4 \lambda^2}{16\pi^2} \left( \frac{2J_1(\alpha\theta)}{\alpha\theta} \right)^2 \quad (1)$$

where

$I_{inc}$  = intensity incident on the particles (assumed constant),

$\alpha = \pi D/\lambda$  the size parameter,

$J_1$  = first order Bessel function of first kind, and

$\theta$  = scattering angle measured from the incident beam propagation direction.

A small angle approximation has been invoked in Eq 1 by dropping sin functions and the obliquity correction. The receiving lens in Fig. 1 converts angular scattering information into a spatial distribution at the detection plane as

dictated by  $\theta = r/f$  where  $r$  is radial distance measured from the center of the diffraction pattern and  $f$  is the receiving lens focal length. The diffraction signature is independent of droplet position for all scattered light which actually passes through the receiving lens (that is, neglecting vignetting). However, the fraction of diffracted light truncated by the receiving aperture is a function of particle position, and the diffracted light actually detected is biased toward larger particles as distance from the receiving lens increases.

In practical systems a distribution of droplet sizes or a polydispersion is generally encountered. The composite scattered intensity profile is a linear combination of the characteristic profile of each droplet size with a weighting coefficient equal to the number of particles of that size in the sample volume. The diffraction signature of a polydisperse spray is given by

$$I(\theta) = \int_0^{\infty} n(\alpha) I_{inc} \frac{\alpha^4 \lambda^2}{16 \pi^2} \left( \frac{2J_1(\alpha\theta)}{\alpha\theta} \right)^2 d\alpha \quad (2)$$

where  $n(\alpha) d\alpha$  is the number of droplets with sizes between  $\alpha$  and  $\alpha + d\alpha$  and the small angle approximation has been made. A primary effect of broadened size distribution is elimination of the contrast in the diffraction pattern.

A common two-parameter size distribution form which often adequately describes liquid sprays is the Rosin-Rammler distribution given by

$$F = e^{-(D/\bar{x})^N} \quad (3)$$

where

$F$  = cumulative volume fraction greater than the particle diameter  $D$ ,

$\bar{x}$  = mean diameter such that 36.8% of volume is in sizes greater than  $\bar{x}$ , and

$N$  = width parameter.

As  $N$  increases the distribution becomes more monodisperse, and typical fuel nozzles produce sprays with  $N$  in the range 2 to 3. The scattering signatures  $I(\theta)$  for Rosin-Rammler distributions with some representative parameter values are plotted in Fig. 3.

The basic task in laser diffraction droplet sizing is to detect and analyze the diffraction signature  $I(\theta)$ , and then mathematically invert Eq 2 to determine parameters of the particle size distribution. Chin et al in 1955 [4] proposed several detection techniques, one of which was to traverse a pinhole photo-detector assembly across the diffraction pattern. Due to the mechanical traverse this detection approach requires a significant amount of time to cover the entire diffraction pattern. Further, the large dynamic range of the diffraction signature seen in Fig. 3 is another difficulty for such systems. Thus application to transient sprays is not very practical although Peters and Mellor [5] have reported data using a multiplexing technique that assumes the transient spray injection characteristics do not change appreciably between injections.

The advantages of real time analysis of the entire diffraction signature as opposed to traversing a detector across either the diffraction pattern itself or a

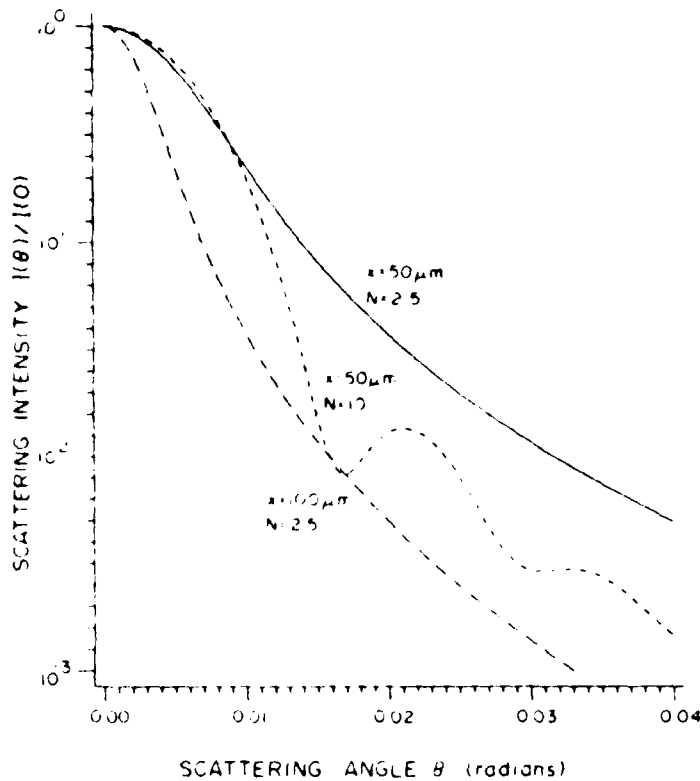


FIG. 3—Forward scattering intensity signatures calculated using Fraunhofer diffraction theory with  $\lambda = 0.6328 \mu\text{m}$  for three Rosin-Rammler particle size distributions  $\bar{x}$  is the Rosin-Rammler mean diameter such that 36.8% of the volume is in sizes greater than  $\bar{x}$ .  $N$  is a width parameter.

photographic image thereof are obvious. McSweeney and Rivers [6] developed an optical fiber faceplate assembly which collected the diffracted light in a number of annular concentric rings and transferred the energy from each ring to a separate photodetector using fiber optics. Cornillault [7] designed a rotating circular mask to be placed at the detection plane which had a series of apertures situated at various distances from the center of rotation. The optical system of Wertheimer et al [8] involved an additional field lens behind a detection plane mask which directed the diffracted light onto a single stationary photodetector. A second mask was also used [8] to effectively time multiplex the diffraction contributions at the various angles onto the photodetector. A commercial instrument based on this concept is available [9].

Developments in monolithic solid state multi-element detector arrays in the 1970s improved the situation by allowing the entire diffraction signature to be analyzed instantaneously. The detector designed by Recognition Systems, Inc. [10] for parts recognition applications was utilized by Malvern Instruments Ltd. [11] in a commercial diffraction particle sizing instrument based on the work of Swithenbank et al [12]. The original circular detector [10] was comprised of 31 semicircular annular ring detector elements on one half, 32 wedge elements on the other half, and a small circular detector in the center. The dimensions of the detector elements of this detector are given in Table 1. Note the in-

TABLE 1—Dimensions of the annular ring detector elements on the Recognition Systems Inc., Model WRD 6400 photodiode array [10]. These dimensions are virtually identical (within 0.001 mm) to those for the Malvern Instruments Ltd. detector as reported [54]. The only discrepancy is the inner radius of Ring No. 1 which has been reported [54] as 0.124 mm. However, the corresponding elements of the scattering matrix used in the Malvern 2200 instrument [11] are consistent with the value of 0.149 mm shown here. Note however that the area correction factors (ratio of photosensitive area to geometric area) due to the conductor leads are different for each element of the two detectors.

Detector Ring No.	Inner Radius, mm	Outer Radius, mm
1	.149	.218
2	.254	.318
3	.353	.417
4	.452	.518
5	.554	.625
6	.660	.737
7	.772	.856
8	.892	.986
9	1.021	1.128
10	1.163	1.285
11	1.321	1.461
12	1.496	1.656
13	1.692	1.880
14	1.915	2.131
15	2.167	2.416
16	2.451	2.738
17	2.774	3.101
18	3.137	3.513
19	3.549	3.978
20	4.013	4.501
21	4.536	5.085
22	5.121	5.738
23	5.773	6.469
24	6.505	7.282
25	7.318	8.184
26	8.219	9.185
27	9.220	10.287
28	10.323	11.501
29	11.537	12.837
30	12.873	14.300
31	14.336	15.900

creasing thickness of the annular detector elements which, when coupled with increasing circumferential length, result in a significant increase in detector area as radius increases. This effect compresses the dynamic range of the scattering measurements as indicated in Fig. 4.

A number of data processing methods have been used to extract particle size information from measured diffraction patterns. Chin et al [4] utilized the integral transform derivation of Titchmarsh [13] to analytically invert Eq 2 to obtain

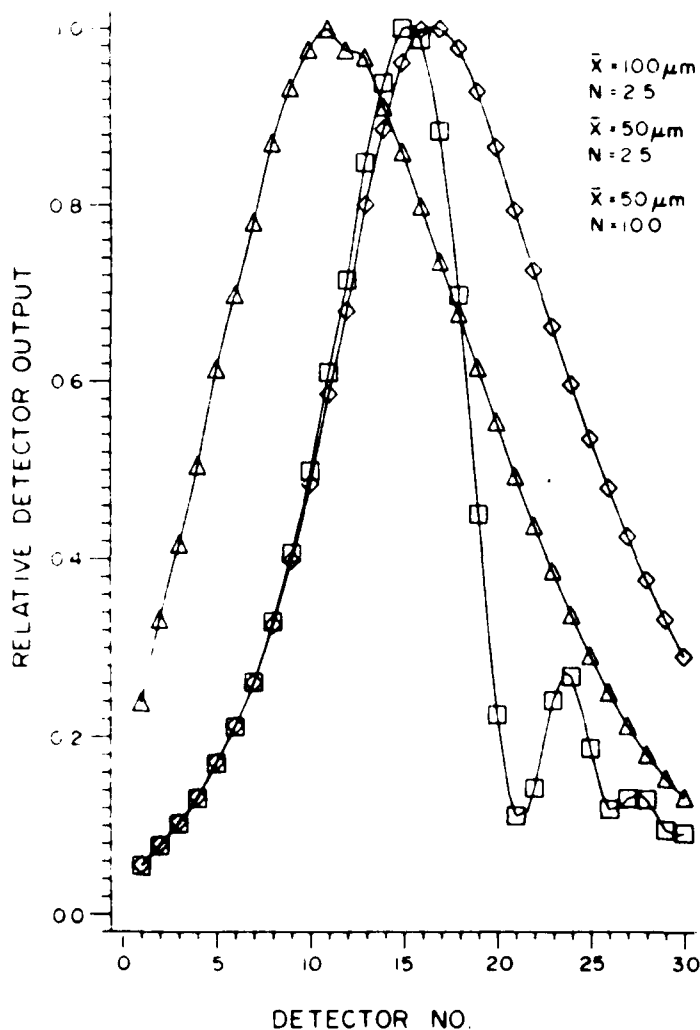


FIG 4—Forward scattering signature as indicated by relative outputs of the annular ring detector geometry of Table I. The data were calculated using Fraunhofer diffraction theory with  $\lambda = 0.6328 \mu\text{m}$  for Rosin-Rammler particle size distributions with the indicated parameters.

$n(\alpha)$ . Dobbins et al [14] somewhat paradoxically observed that the diffraction signatures were relatively independent of the form of the droplet size distribution and depended primarily on the volume to surface area mean diameter  $D_{32}$  (Sauter mean) defined as

$$D_{32} = \frac{\int_0^x n(D)D^3 dD}{\int_0^x n(D)D^2 dD} \quad (4)$$

The authors [14] utilized a single parameter of the diffraction pattern, the angle at which the scattered light is down to 10% of the on axis value, to determine  $D_{32}$ .

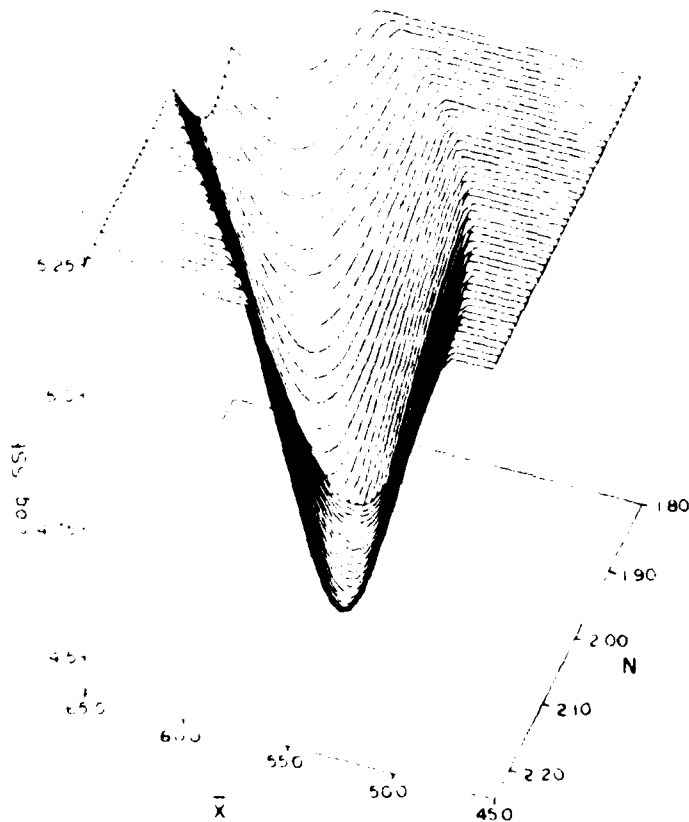


FIG. 5—Typical plot of sum square error (SSE) between measured diffraction signature and that calculated assuming Rosin-Rammler distributions with parameter values shown for Malvern 2200. The SSE is calculated after normalizing the relative detector outputs to a maximum of 2047.

Others [15,16] have since modified slightly this approach and it is still in use today.

Swithenbank et al [12] analyzed the diffracted pattern with the annular ring detector just discussed and subsequently did a numerical inversion (as opposed to integral transform) of a discretized form of Eq 2 to obtain the volume distribution in 7 discrete size bins. There were some problems with that approach, and the authors [12] also assumed that the size distribution was of the Rosin-Rammler form of Eq 3 and estimated the two parameters. The early commercial instruments of Malvern Instruments Ltd. [11] adopted the same data processing algorithm where the  $\bar{x}$  and  $N$  parameter values which produced the best least squares fit between the measured and calculated diffraction pattern were determined. An example of the error surface for a calibration run from the present study on a Malvern 2200 instrument is given in Fig. 5. For each value of  $\bar{x}$  and  $N$  the annular detector scattering signature predicted from the Rosin-Rammler distribution was compared with the measured scattering signals at each of 15 detector pairs and the sum square error calculated. This was repeated for the range of parameter values indicated in Fig. 5, and the values  $\bar{x} = 56$  and  $N = 2.04$  were

TABLE 2—Size class limits for Malvern 2200  
laser diffraction particle sizing instrument  
with 300 mm focal length receiving lens

Size Class No.	Lower Size Limit, $\mu\text{m}$	Upper Size Limit, $\mu\text{m}$
1	5.8	7.2
2	7.2	9.1
3	9.1	11.4
4	11.4	14.5
5	14.5	18.5
6	18.5	23.7
7	23.7	30.3
8	30.3	39.0
9	39.0	50.2
10	50.2	64.6
11	64.6	84.3
12	84.3	112.8
13	112.8	160.4
14	160.4	261.6
15	261.6	564.0

found to minimize the error. Note that the scattering data are normalized to a maximum value of 2047 [11] and minimum log error in Fig. 5 was 4.38. Recent developments in "model independent" software [11] do not require an assumption of the form of the size distribution but provide a 15 parameter least squares fit to the scattering data using the 15 discrete size bins of Table 1.

One unfortunate property of the Malvern instruments is the poor resolution for the large particle sizes as shown in Table 2. The size limits in Table 2 are determined [11,12] by the detector geometry of Table 1 and the property that a given particle size  $\alpha$  has a maximum in the function  $I(\theta)\theta$  (the so-called "energy distribution" [12]) at  $\alpha\theta = 1.357$ . To improve the resolution in Table 2 for large particles would require a redesign of the detector.

A series of papers [17-19] have focused on the integral transform suggested by Chin et al [4]. One problem with inverting Eq 2 is the fact that the diffracted intensity  $I(\theta)$  can be measured only for a finite range of scattering angles, and the inversion integral is truncated. The authors [17-19] have addressed some of the theoretical and experimental problems in this general inversion approach.

In practical applications of laser diffraction particle sizing, two phenomena often lead to erroneous results. First, if either the particle number density or the optical path length become too large multiple scattering becomes important and Fraunhofer diffraction theory no longer applies. The importance of multiple scattering effects is indicated by the obscuration or attenuation of the incident laser beam. The second problem arises in systems with refractive index gradients due to evaporation or thermal gradients present, for example, in combusting sprays. In this situation significant steering of the probe laser beam can occur causing the diffraction pattern to shift off-center at the detection plane and

thereby invalidating the scattering data for the smallest angles. In order to extract meaningful data under either of these conditions it is necessary to first detect the problem and then hopefully correct the data accordingly. The calibration reticles discussed below offer the potential for on-line detection and correction for these effects.

### Laser/Optical Single Particle Counters (SPC)

A generalized schematic of an optical SPC is presented in Fig. 2. The output beam from a laser or other source of radiation is directed (and typically focused) into the optical sample volume. This sample or probe volume can be thought of as that region of space where a single particle can generate a sufficient detector signal to be discriminated or "seen" over the background noise. As individual particles pass through the sample volume they interact with the incident radiation beam (that is, scatter, absorb, or fluoresce light or all three) and are observed by detection optics oriented at some angle(s)  $\theta$  with respect to the beam propagation direction. The single particle signal obtained at the photodetector(s) are processed to provide information on the size of each particle.

### Light-Scattering Cross-Section Measuring Techniques

The most common approach to particle sizing in the range of interest here involves the principle that the magnitude is a nominally monotonic increasing function of particle size; hence, measurement of a scattering cross section can be used to infer particle size. The SPC signal response  $S$  to a particle in an incident radiation field (uniform over the particle) of intensity  $I_m$  is given by

$$S = kI_m C_i \quad (5)$$

where

$k$  = system gain in transducing radiant energy to voltage using a photodetector, and

$C_i$  = appropriate partial light-scattering cross section for the radiation process under study.

The partial cross sections, as opposed to total light-scattering cross sections, depend on the specific finite aperture detector configuration in use. For light scattering and extinction by spherical particles the cross sections are functions of the particle diameter  $D$ , the complex refractive index  $n$ , and the radiation wavelength  $\lambda$  as predicted by the Lorenz-Mie theory [2]. Thus, a response function  $S(D)$  relating measured signal levels to the diameters of spherical particles of known refractive index passing through a SPC sample volume of known incident intensity  $I_m$  and given  $k$  can be determined from theoretical calculations of  $C_i(D)$ .

A plot of partial light-scattering cross section for spherical particles illuminated by a coherent uniphase wave calculated using a Lorenz-Mie theory computer code [2] is given in Fig. 6. The calculations are for an off-axis  $f/1.96$  collection

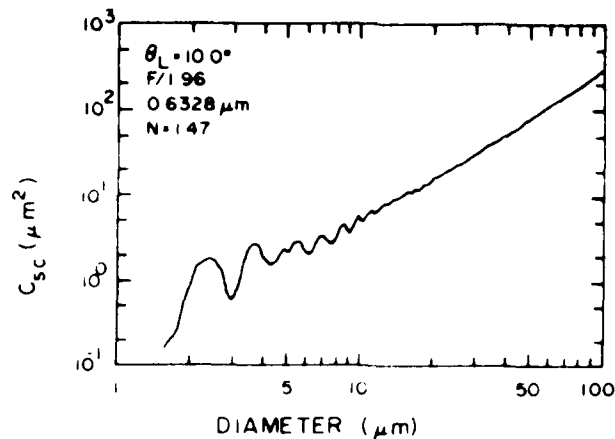


FIG. 6. Partial light scattering cross sections for spherical particles with refractive index  $n = 1.47$  for an  $f/1.96$  receiving lens oriented for  $10^\circ$  deg off axis collection in the plane normal to the direction of polarization of the incident beam. The Mie theory calculations used  $\lambda = 0.6328 \mu\text{m}$ .

lens centered at  $\theta = 10^\circ$  from the incident radiation propagation direction (forward scattering). The oscillatory nature of the plot is a result of resonance interactions in the scattering process and results in ambiguities in particle size determination. Another problem inherent in using the laser as a SPC radiation source is the nonuniform intensity profile across the beam [3]. Unfortunately, an ambiguity in signal levels arises for in situ SPC since the particles are free to traverse the sample volume at any position. Thus, particles will experience different peak incident intensities  $I_{inc}$  depending on the trajectory and even a monodisperse (uniform size) aerosol will generate a broad distribution of signal amplitudes  $S$ .

A number of methods have been devised to eliminate the unknown incident intensity effect in cross section measuring techniques. The basic approaches include: (1) analysis of only those particles which pass through a selected portion of the beam of known and constant intensity, (2) analysis of all particles and later correction of the distribution of particle trajectories and corresponding incident intensities, (3) use of the ratio of scattering signals at two or more angles to cancel the incident intensity effect. The ratio technique, which has been reviewed elsewhere [3,28,29], is difficult to apply for particles larger than several micrometers and will not be discussed here. The early laser light-scattering SPC of Heyder et al [20] aerodynamically focused the aerosol sample through a small region at the center of the laser beam of known and constant intensity. For in situ measurements various optical methods of discriminating those particles which pass through a control portion of the beam have been used, including coincidence detectors at  $90^\circ$  by Hirleman [21] and Chigier et al [22] and in the forward direction by Knollenberg [23].

A second general approach to the ambiguous incident intensity problem is to correct after the fact. One implementation of this approach demonstrated by Holve and Self [24] is to first consider the peak signal height distribution generated by particles of one size passing with equal probability through all portions

of the laser beam focus region. The signal height distribution from a polydispersion is then a linear combination of the monodisperse particle response distributions. A numerical scheme was developed [24] to invert the resulting system of equations and solve for the linear coefficients which are proportional to concentrations in the discretized particle size intervals.

Another somewhat similar approach proposed by Hirleman [25] involves the use of signals generated by particles traversing two adjacent laser beams. The dual peak signature is used to determine two velocity components and the trajectory of each particle. Given known laser beam properties the incident intensity history for a particle is then completely determined which permits a real-time correction for the intensity ambiguity. After  $I_{inc}$  in Eq 5 is determined a calibrated response function prediction such as Fig. 2 would be used to relate signal amplitude to particle size. This technique [25] has been proposed for light-scattering, extinction, and fluorescence cross-section measurements although experiments to date have used only light scattering.

#### *Particle Sizing Interferometry*

Another approach which can provide particle size information independent of incident intensity is particle sizing interferometry (PSI). As a single particle passes through the intersection region of two nonparallel laser beams, Doppler-shifted scattered light waves from each beam emanate from the particle. Heterodyning the two contributions of scattered light at a detector will produce the Doppler-difference frequency which is directly related to the particle velocity and the angle between the laser beam propagation vectors. This principle underlies the laser Doppler velocimeter (LDV). A particle crossing the LDV beam intersection region will produce an approximately Gaussian signal (pedestal) with the modulated Doppler-difference component written on the pedestal [30]. The ratio of the modulated signal amplitude to the pedestal amplitude (that is, the visibility or contrast) provides a measure of particle size as shown in Farmer [30] and others [31,32] who used a scalar description of the process. For large apertures which collect all of the forward scattered (diffracted) light the visibility  $V$  as a function of particle diameter  $D$  and fringe spacing  $\delta$  was shown by Robinson and Chu [32] to be

$$V = \frac{2J_1(\pi D/\delta)}{\pi D/\delta} \quad (6)$$

A plot of  $V$  is given in Fig. 7.

Calculations considering the complete problem of scattering by a sphere simultaneously in two coherent, collimated laser beams [33] predicted a strong dependence of the visibility on particle refractive index, the detector aperture, and detector position relative to the beams. A number of experimental studies have confirmed the importance of careful receiving optics design [33,34] although conflicting observations have also been made [35].

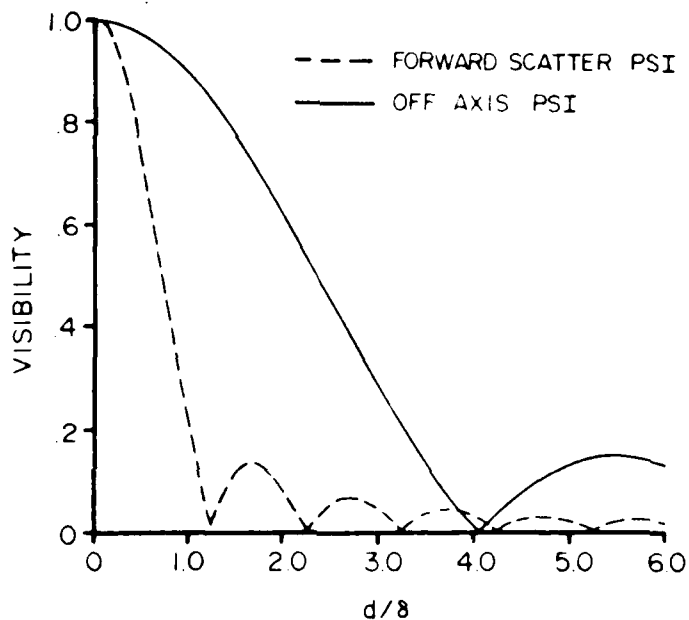


FIG. 7 — Calculations for the fringe visibility  $V$  as a function of particle diameter to fringe spacing ratio  $d/\delta$  for particle sizing interferometers (PSI). The data apply to a PSI collecting all of the forward scattered light and to an off-axis PSI with an  $1/2$  collection lens oriented at  $\theta = 20$  deg.

Another related approach is the off-axis PSI proposed by Bachalo [36] which utilizes the interference of refracted or reflected light-scattering contributions rather than the diffractive scatter of a conventional PSI [30]. This method is applicable to particles significantly larger than the wavelength and is based on the difference in optical path length traveled by refracted rays from the two crossed beams which pass through the particle and arrive coincidentally at the detector. The visibility response function for a commercial [37] off-axis PSI with a collection angle [36] of  $20^\circ$  is also shown in Fig. 7, and the expanded  $D/\delta$  sizing range for this concept is apparent.

One problem with PSI type instruments is the limited applicable particle size range. It has been suggested to utilize the amplitude of the Doppler bursts from PSI instruments to size particles in what basically is a scattering cross section measurement approach. The incident intensity ambiguity is then reintroduced and a correction must be made. Those particles traversing the center of the intersection region can be discriminated using coincidence detection with small aperture detectors or using an additional, tightly focused pointer beam. Unfortunately the latter approach merely shifts the trajectory ambiguity problem from the PSI beams to the Gaussian pointer beam.

### Calibration

Optical nonimaging techniques for measuring droplet sizes are inherently indirect and without exception require calibration in some form. As the terms

calibrate or calibration can be somewhat ambiguous we quote the three applicable definitions from the ASTM Standards Compilation [40]:

1. *Calibrate* — General — to determine the indication or output of a measuring device with respect to that of a standard.

2. *Calibration* — Determination of the values of the significant parameters by comparison with values indicated by a reference instrument or by a set of reference standards.

3. *Calibration* — The process of comparing a standard or instrument with one of greater accuracy (smaller uncertainty) for the purpose of obtaining quantitative estimates of the actual value of the standard being calibrated, the deviation of the actual value from a nominal value, or the difference between the value indicated by an instrument and the actual value. These differences are usually tabulated in a "Table of Corrections" which apply to that particular standard or instrument.

Now to define the term introduced previously we refer to the same source [40]:

1. *Calibration Standard* — Any of the standards of various types having accepted parameters. The calibration standard may be used to adjust the sensitivity setting of test instruments at some predetermined level and for periodic checks of the sensitivity.

Now there are a number of unknowns and uncertainties in optical, nonimaging particle sizing instruments including relative detector sensitivities in multiple detector instruments, absolute detector sensitivities in single detector SPC, and the background noise level which determines the lower threshold or sizing limit of the instrument, to name but a few. Since these are generally very difficult if not impossible to quantify independently, calibration with particles of known size is the necessary approach.

Single particle counters must perform two operations correctly, (1) sizing of particles in the sample volume, and (2) counting of particles in an unbiased manner to provide valid concentration data. Thus, primary calibration of a single particle counter requires both size and concentration calibration standards, the latter of which appears to be often overlooked. Ensemble analyzers have somewhat different requirements as concentration calibration is less critical. Finally, imaging techniques are relatively easy to calibrate for size determination, but it is considerably more difficult to account for sample volume effects due to depth-of-field variations with particle size.

The fundamental problem in calibration is the generation of monodisperse, spherical particles or droplets of known and preferably controllable size and concentration. As an alternative, one might utilize a polydisperse particle system of known concentration and size distribution as a primary calibration standard for droplet sizing instruments. Unfortunately, in the words of an ASTM Standard Test Method for particle sizing and from the experience of this author and countless other researchers, there is no totally acceptable particle size and

concentration standard available. There are however some possibilities which include:

1. *Polystyrene Latex Spheres*—These polystyrene spheres are generally very monodisperse for sizes below about  $5\ \mu\text{m}$  (0.1% relative standard deviation typical) but have significantly broader distributions for larger sizes. Polystyrene spheres are subject to size changes with age and steps must be taken to prevent agglomeration. Polystyrene spheres larger than about  $5\ \mu\text{m}$  cannot be reliably atomized and must be used in suspension which requires a mechanical pumping or stirring system [42]. Polystyrene spheres are commercially available [43].

2. *Glass Microspheres*—Distributions of glass microspheres are commonly used as sedimentation standards and in other industrial applications. A sample of these spheres could be size analyzed using a calibrated imaging system, and then in turn used to calibrate SPC or ensemble analyzing optical instruments. These microspheres have been utilized for calibration while attached to glass slides [8] and in liquid suspension as well [42]. The difficulties of differential settling, deposition, and differential separation in flow systems and associated problems in reproducibility make glass microspheres in suspension a very poor candidate as a primary calibration standard. Glass microspheres deposited on a glass slide would appear better suited, but the difficulties of manufacturing calibration slides with thousands of glass spheres of identical sizes and positions are formidable.

3. *Photomask Calibration Reticles*—An interesting property of light scattering is that near-forward scattering or diffraction signatures from spherical particles, opaque disks, and circular apertures of the same diameter are equivalent. Thus it has been suggested that carefully designed arrays of circular apertures photoetched into a chrome on glass substrate be used to calibrate optical non-imaging instruments which utilize diffractively scattered light or optical imaging. These calibration reticles, which [44,45] have been used successfully in both types of instruments, provide a stable, practical, and highly reproducible calibration standard. Unfortunately the reticles cannot be used to calibrate systems which utilize reflective or refractive (off-axis) scattering. The applicability of reticles for calibrating instruments for particle sizes below several microns is questionable.

4. *Droplet Generators*—Mechanical approaches for generating a stream or a cloud of nearly monodisperse droplets involve the systematic breakup of cylindrical or planar liquid jets. The natural frequencies or instabilities of the cylindrical jets are synchronously excited using a piezoelectric crystal to break the liquid stream into a series of droplets of constant diameter (to within typically 1%). This concept has been exploited using a jet forced through an orifice in a vibrating thin plate [46,47] and a syringe jet [48]. The vibrating orifice technique [46,47] is theoretically capable of producing droplets ranging from  $10\ \mu\text{m}$  to about  $150\ \mu\text{m}$ , and syringe jets have reported [48] to be capable of generating droplets in the  $15$  to  $500\ \mu\text{m}$  diameter size range. Spinning disk droplet generators have been also utilized but generally are limited to relatively small droplets. Un-

fortunately there have apparently been no developments which allow generation of specified distributions of droplet sizes as would be useful for the calibration of ensemble scattering instruments. The possibility of utilizing a vibrating plate with an array of orifice sizes to generate controlled droplet size distributions has been discussed, although this author is not aware of published results on this approach.

Droplet generators based on the breakup of cylindrical liquid jets can theoretically be used to calibrate both single particle and ensemble analyzers. For SPC the optical sample volume has been placed very near the jet breakup point to provide a spatially constrained stream of droplets with constant size and velocity. In this way it is possible to map out the SPC response as a function of droplet trajectory and size. Although this mapping exercise would satisfy both the size and concentration calibration requirements, most instrument manufacturers using this technique have only reported results obtained by directing the droplet stream through the center of the sample volume which constitutes only a size calibration. The potential for droplet deposition and coagulation introduce some uncertainties into the concentration calibration.

Another powerful calibration application would be to disperse monodisperse droplets of low vapor pressure by diluting the stream with known and controlled amounts of air to generate practical 2-D flows with monodisperse droplets of known concentration. This flow stream could then be used to calibrate either SPC or ensemble instruments. Unfortunately the very low droplet concentrations produced by these generators make calibration of laser diffraction instruments rather impractical. Some problems with jet breakup droplet generators concern questions about long term droplet size stability, the susceptibility to orifice clogging, and difficulty in day-to-day reproducibility of stable operation conditions.

5. *Polydisperse Sprays*—A final approach to droplet size calibration is to standardize on a particular spray nozzle or other spray source. Presumably manufacturing tolerances could be maintained so that the spray characteristics could be at least as good as the instrumentation. This concept has been tested with mixed success by the ASTM Subcommittee E29.04 on Droplet Sizing. Problems concerned with the liquid supply system reproducibility and test position definition must be addressed in the future.

### *SPC Calibration*

As an example of SPC calibration some work performed by this author and co-workers on the Multiple Ratio Single Particle Counter (MRSPC) will be discussed. Calibration studies by numerous other researchers could have been discussed as well (see for example [24] and [27]) but are not in the interest of brevity.

The details of the MRSPC have been exhaustively covered elsewhere [3,28], for our purposes here it is an instrument in the general form of Fig. 2 but with multiple detectors. A focused laser beam of typically 50 to 200  $\mu\text{m}$  diameter is

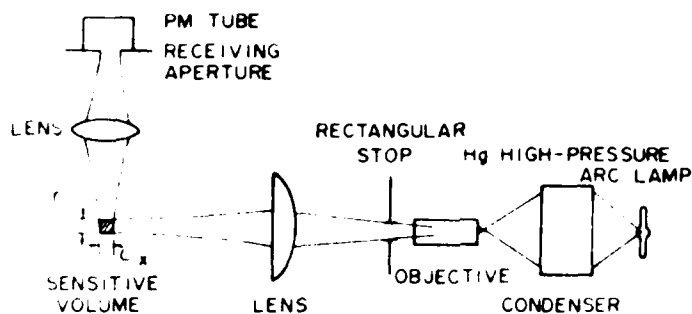


FIG. 8 Schematic of 90 degrees white (incoherent) light particle counter.

used to illuminate individual particles. The ratios of scattered light signals at three or more detectors oriented in the near-forward direction are used to determine particle sizes in the nominal range 0.1 to 10  $\mu\text{m}$ . Since incident laser beam has a Gaussian radial intensity profile which drops off well inside the detector fields of view, the optical sample volume is a function of particle size. A large droplet passing through the shoulder of the Gaussian beam may still scatter enough light to be detected above the noise, but a significantly smaller particle must pass through the very center of the Gaussian intensity peak to be detected over the same noise level. For this reason SPC typically have a bias toward large particle sizes, that is, since the optical probe volume is larger for large particles they are preferentially sampled. This size-selective sampling bias can be predicted analytically, but it was necessary to perform some concentration calibrations to validate the model.

The MRSPC calibration was performed using polystyrene microspheres which were atomized from a dilute ethanol suspension and then dried before passing through the sample volume. Size calibration was done using the polystyrene particle sizes provided by the manufacturer, but concentration calibration was a problem as a significant but unknown fraction of the particles in the solution never reached the sample volume due to deposition or other losses. For that reason it was necessary to design an independent sizing instrument to characterize the size-selective sampling bias. This was done by overlapping the sample volumes from the 90° scattering white-light particle counter shown in Fig. 8 and the MRSPC. The intensity profile at the optical sample volume of the 90° white-light particle counter is shown in Fig. 9. The approximately "tophat" profile eliminates the incident intensity ambiguity for all but the edges of the sample volume which comprised a relatively small portion of the cross section. Thus the 90° SPC provided an on-line measurement of absolute concentration of the particles used to calibrate the MRSPC. Data for the sensitive area (projection of the sample volume) of the MRSPC are given in Fig. 10, where experiment and theory agree reasonably well. Unfortunately the sensitivity of the 90° counter was not sufficient to permit concentration calibration for particles sizes smaller than 1.011  $\mu\text{m}$ . This experiment provided both the size and concentration calibrations necessary to validate all single particle counting and instruments.

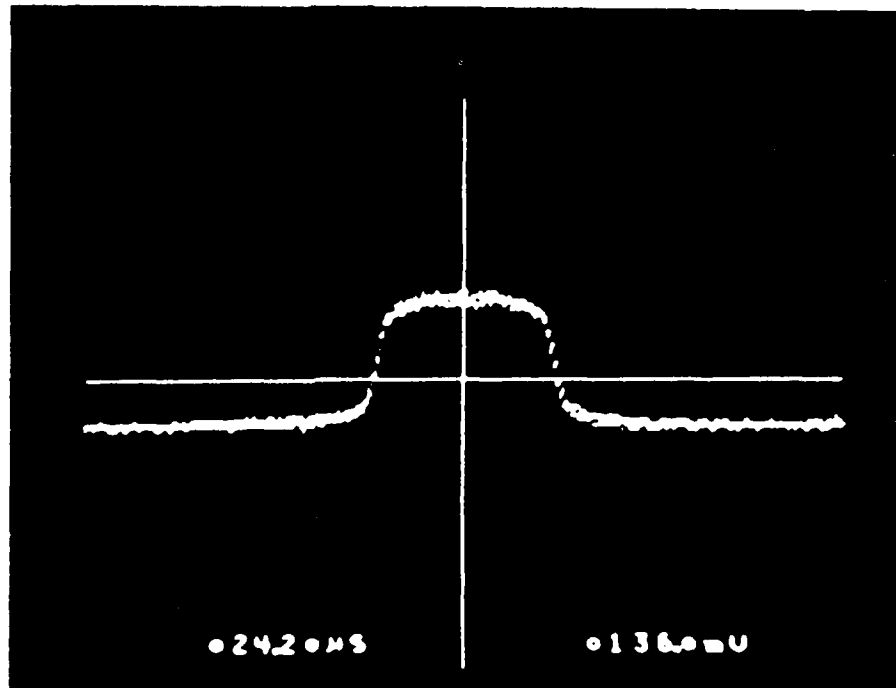


FIG. 9 — Scan of the output from 1024 element linear photodiode array facing the incident laser at the sample volume of the SPC of Fig. 8. The diodes are on 25.4  $\mu\text{m}$  centers and the indicated width shown is about 1.27 mm (after Ref. 49).

#### Calibration of Laser Diffraction Instruments

We consider here laser diffraction instruments which utilize multiple detector elements to measure the diffraction pattern including commercial instruments by CILAS [50], Malvern Instruments Ltd. [15], and Leeds and Northrup [9]. It has been incorrectly stated by some manufacturers that laser diffraction instruments need no calibration. This statement is true only for instruments which traverse a single detector across the diffraction pattern, but even then it is rather ill-advised to trust data from an instrument whose performance has never been verified. With respect to the commercial instruments which have detector arrays the statement concerning unnecessary calibration is incorrect. Clearly any variation in the detector responsivities or pre-amplifier gains will change the measured scattering signature, and there is no rational justification for assuming *a priori* that these quantities are constant. Even manufacturers of solid-state photodiode arrays specify  $\pm 10\%$  variation in responsivity between detector elements on a monolithic array [10,51]. Further, the potential problems of detector contamination, optical element contamination, thermal degradation, and amplifier drift should not be ignored. A laser diffraction instrument user should request calibration data from the manufacturer and periodically verify the instrument performance using one of the secondary calibration techniques just discussed.

Most users have tried one or more of these calibration methods to verify the performance of laser diffraction particle sizing instruments. Published data com-

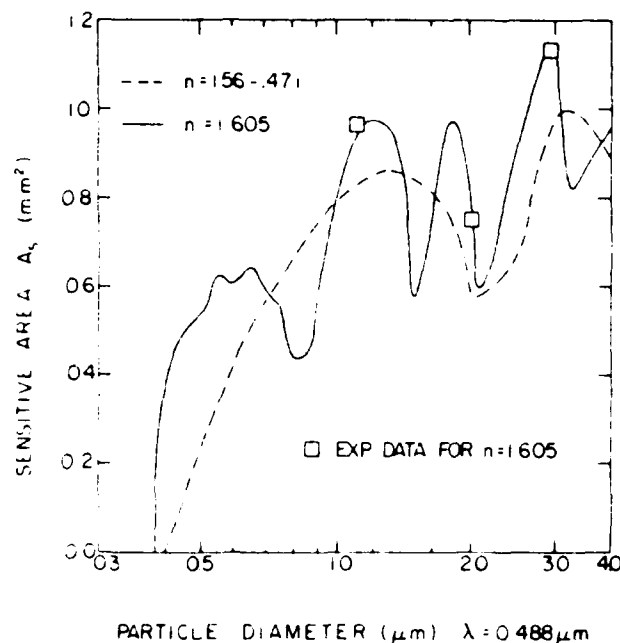


FIG. 10—Plot of sensitive area  $A_s$  versus particle size for the 12/6 deg ratio pair of the MRSPC [53]. Plotted with the theoretical predictions are experimental data for polystyrene latex spheres ( $n = 1.605$ ) taken at  $\lambda = 0.4416 \mu\text{m}$ . One undetermined calibration factor for the experimental data (the same factor for all 3 data points) was fixed by optimizing the fit between theory and experiment (after Ref. 49).

paring the performance of several instruments on the same particle field are scarce, but some data for comparison between instruments have been obtained [45] using photomask calibration reticles on Malvern 2200 instruments [11] as shown in Fig. 11. The commercially available reticles [52] were fabricated by photoetching arrays of randomly positioned opaque circles of chrome thin film on a glass substrate. This reticle configuration is designated clear field (CF), and the photographic negative thereof with circular apertures in an opaque background is designated dark field (DF). The calibration sample area of the reticles was 8 mm diameter and provided a discrete approximation (using 23 different circle sizes) to a Rosin-Rammler droplet sizes distribution with nominal mean diameter of  $50 \mu\text{m}$  and nominal Rosin-Rammler exponent of 2.0. The standard Rosin-Rammler software supplied by the manufacturer was used in the size distribution inversion. Results from a series of runs on three different commercial instruments are plotted in Fig. 12. The data points in Fig. 12 are independent as both background and scattering signature measurements were taken each time. The elliptical patterns of the data points for each reticle on a particular instrument are consistent with normally distributed fluctuations (noise) in scattering measurements with standard deviations in the range of 1 to 2% of the peak signal level. The curves in Fig. 12 correspond to equal error contours at 1, 2, and 3% of peak signal level RMS from Fig. 5, which was calculated using the scattering signature averaged over all runs for the clear reticle on Instrument A. The

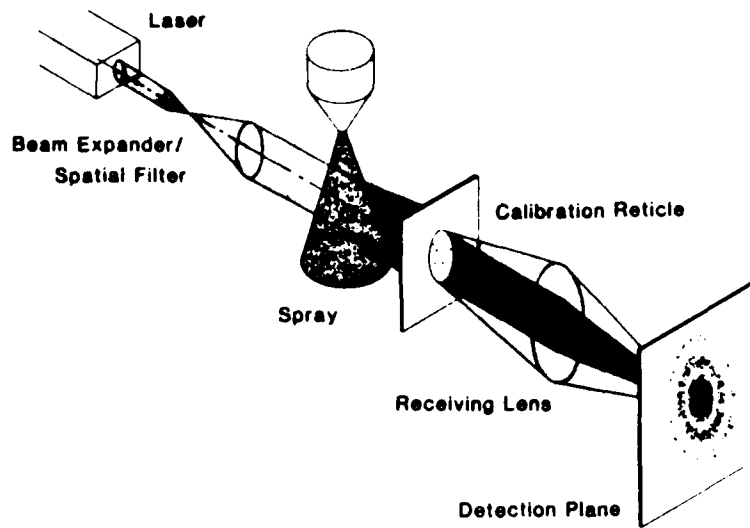


FIG. 11 — Schematic of laser diffraction particle sizing instrument with clear field calibration reticle.

instrument-to-instrument variations are statistically significant when compared the run-to-run variations discussed previously. Differences between instrument responses appears to be on the order of 20% as expected from sensitivity variations between monolithic detector elements. In order to obtain absolute accuracy better than 20% with the Malvern 2200 or similar laser diffraction instruments the sensitivity of each element in the photodiode detector array must be calibrated using reticles or uniform illumination.

**Optical Sampling: Spatial (Concentration) Versus Temporal (Flux)**

Optical sizing instruments operate in one of two basic sampling modes. In the first mode an optical instrument samples all droplets in a volume of space, and therefore might be considered a concentration-sensitive diagnostic. Laser diffraction droplet sizing instruments in which the detector resolving time is much less than a typical droplet residence time in the laser beam operate in this concentration diagnostic mode. Size distribution parameters determined with these techniques would be volume-weighted, for example, a  $D_{32}$  consistent with Eq 4 could be obtained. There is, however, another weighting technique of interest in sprays, that of flux weighting.

Define here a particle-flux-weighted mean diameter  $D_{32, f}$

$$D_{32, f} = \frac{\int_0^{\infty} n(D)U(D)D^3 dD}{\int_0^{\infty} n(D)U(D)D^2 dD} \tag{7}$$

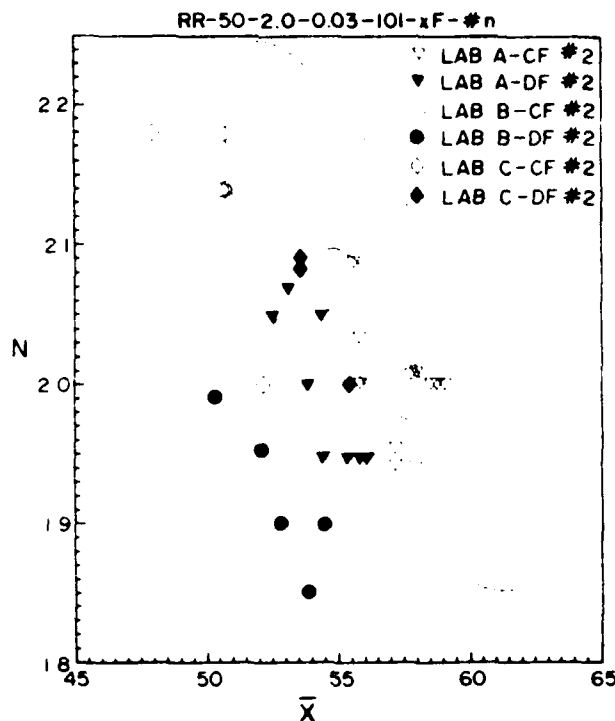


FIG. 12— Experimental data from three different labs with Malvern 2200 instruments analyzing the same two calibration reticles RR-50-2.0-0.03-101-CF- #2 (clear field) and RR-50-2.0-0.03-101-DF- #2 (dark field). Each data point represents a separate background and signal run. Also shown are equal error contours from Fig. 5 corresponding to 1, 2, and 3% of peak signal RMS error for the averaged scattering signature for the clear field reticle at Lab A.

where the additional subscript  $f$  indicates a quantity determined by a flux-sensitive diagnostic, and  $U$  is the velocity of particles of diameter  $D$ . Note that this  $D_{32}$ ,  $f$  may be the most relevant one in some situations, say for example in the idealized case of thin, one-dimensional spray flame front. In that case the important quantity controlling the combustion would be the flux or  $n(D)U(D)$  product rather than just the concentration or number density.

The second mode of instrument operation is one which actually measures this flux of particles across a surface during some finite measurement time. Optical single particle counters which utilize input beam focusing, and the detector field of view to optically define a relatively small optical probe volume are an example of a flux-sensitive diagnostic. The sensitive surface or sensitive area would be the projected area of the optical sample volume (projected into the direction of the droplet velocity vectors).

Results obtained with concentration-sensitive and flux-sensitive diagnostics are related through the velocity, which may be a function of droplet size. The rate  $J(D)$  at which particles with diameters between  $D$  and  $D + \Delta D$  are sampled by an SPC is given by

$$J(D) = n(D)U(D)A_s(D) \Delta D \quad (8)$$

where  $A_s$  is the optically sensitive area. The sensitive area  $A_s$  is a function of droplet diameter as controlled by the light-scattering properties and the threshold or droplet signal validation electronics.

It is seen from Eq 8 that for velocities independent of droplet size both concentration and flux-sensitive devices measure equivalent quantities. However, for typical sprays where velocity is a function of droplet size the differences in the two diagnostics can become quite significant. Data from flux-sensitive diagnostics such as single particle counters which do not simultaneously measure droplet velocity as well as size cannot be used to determine particle concentration or number density. Such instruments would directly measure  $J$  and have a known sensitive area correction factor  $A_s$  so that

$$\frac{J(D)}{A_s(D)} = n(D)U(D) \Delta D \quad (9)$$

where the left-hand side would be measured/known in order to determine the right hand side of Eq 9. Then since  $n$  and  $U$  cannot be separated mean quantities would be calculated using  $J(D)/A_s(D)$  or equivalently  $n(D)U(D)$  as in Eq 8.

The similarity between these effects and velocity bias in laser velocimetry (LV) should be noted. Considering Eq 6, the rate of particle events or observations by SPC and counter-based LV systems is biased toward high velocities, or in other words particles with high velocities are sampled proportionally more often than particles travelling at low velocities. Several methods have been used in LV to correct for velocity bias and obtain an unbiased velocity estimator. One method is to sample LV signals at equal time intervals rather than sample every particle event and thereby perform time-averaged rather than particle averaged statistics. Similar methods might be adopted for droplet sizing instruments which measure velocity in addition to size, but again it depends on where spatial-averaged or flux-averaged information is more relevant.

Note also that as the velocity field changes so does the concentration in a spray with differential velocities and a constant initial droplet size distribution. Therefore, assuming that a concentration measure is of interest, measurements of droplet size distributions on a laboratory spray into a stagnant gas will in general not be indicative of concentration-size distributions present under other conditions where the dependence of droplet velocity on size has changed due for example to a change in the velocity of the gas surrounding the spray as discussed by Wittig et al [53].

## Conclusions

Optical nonimaging methods for droplet sizing have been reviewed. Single droplet analyzing instruments as well as ensemble analyzing techniques using multi-angle scattering or diffraction were discussed. Calibration of single particle counters must include both size and concentration measurement standards. Laser

diffraction instruments, despite suggestions to the contrary, require calibration as demonstrated by a series of experiments using calibration reticles. Finally, detailed characteristics of each droplet sizing instrument concept must be considered before attempting to reconcile data obtained with different instruments. This is particularly true when comparing spatial or concentration-sensitive techniques such as laser diffraction with data from temporal or droplet flux-sensitive instruments such as single particle counters.

#### Acknowledgments

The author's research in optical particle diagnostics has been supported by the National Science Foundation, Particulate and Multiphase Processes Program, Dr. Morris Ojalvo, Director, and by the Office of Naval Research, Dr. Albert D. Wood, Project Director.

Further, the author is grateful to Brookhaven Instruments, Garrett Turbine Engine Co., Parker-Hannifin Co., and Carnegie-Mellon University for assistance in providing data reported herein.

#### References

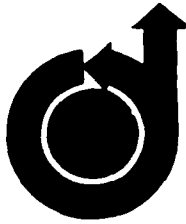
- [1] Thompson, B. J., this publication, pp. 111-122.
- [2] Kerker, M., *The Scattering of Light and Other Electromagnetic Radiation*, Academic Press, NY, 1969.
- [3] Hurlleman, E. D., *Optical Engineering*, Vol. 19, No. 6, pp. 854-860, 1980.
- [4] Chin, J. H., Shlepceovich, C. M., and Tribus, M., *Journal of Physical Chemistry Ithaca*, Vol. 59, 1955, p. 841.
- [5] Peters, J. and Mellor, A. M., *Journal of Energy*, Vol. 5, No. 1, 1981, pp. 57-59.
- [6] McSweeney, A. and Rivers, W., *Applied Optics*, Vol. 11, 1972, p. 2101.
- [7] Cornillault, J., *Applied Optics*, Vol. 11, No. 2, 1972, pp. 265-268.
- [8] Wertheimer, A. L., Frock, H. N., and Muly, E. C. in *Effective Utilization of Optics in Quality Assurance*, Vol. 129, Society of Photo-Optical Instrumentation Engineers, Bellingham, WA, 1977, pp. 49-58.
- [9] Leeds and Northrup Co., St. Petersburg, FL.
- [10] Recognition Systems Inc., Van Nuys, CA.
- [11] Malvern Instruments Ltd., Malvern, England.
- [12] Swithenbank, J., Beer, J., Taylor, D. S., Abbot, D., and McCreath, C. G. in *Experimental Diagnostics in Gas Phase Combustion Systems*, B. T. Zinn, Ed., Progress in Astronautics and Aeronautics, Vol. 53, 1977, pp. 421-447.
- [13] Litchmarsh, E. C., *Proceedings London Mathematic Society*, Series 2, Vol. 23, p. xxii, 1925.
- [14] Dobbins, R. A., Crocco, L., and Glassmann, I., *American Institute of Aeronautics and Astronautics Journal*, Vol. 1, 1963, pp. 1882-1906.
- [15] Roberts, J. H. and Webb, M. J., *Journal*, American Institute of Aeronautics and Astronautics, Vol. 2, No. 3, 1964, pp. 583-585.
- [16] Dieck, R. H. and Roberts, R. L., *Applied Optics*, Vol. 9, No. 9, 1970, pp. 2007-2014.
- [17] Shifrin, K. S., *Izvestiya*, USSR Academy of Sciences, Atmospheric and Oceanic Physics, Vol. 2, 1966, pp. 928-932 (English translation).
- [18] Shifrin, K. S. and Kolmakov, I. B., *Izvestiya*, USSR Academy of Sciences, Atmospheric and Oceanic Physics, Vol. 3, 1967, pp. 749-753 (English translation).
- [19] Perelman, A. Y. A. and Shifrin, K. S., *Izvestiya*, USSR Academy of Sciences, Atmospheric and Oceanic Physics, Vol. 15, 1979, pp. 66-73 (English translation).
- [20] Heyder, J., Roth, C., and Stahlhofen, W., *Journal of Aerosol Science*, Vol. 2, 1971, p. 341.

- [21] Hirleman, E. D., "An Optical Method for Exhaust Gas Particulate Sizing," Laboratory for Energiteknik Report RE-74-14, Technical University of Denmark, 2800 Lyngby, Denmark, Aug. 1974.
- [22] Ungut, A., Yule, A. J., Taylor, D. S., and Chigier, N. A., "Simultaneous Velocity and Particle Size Measurements in Two Phase Flows by Laser Anemometry," AIAA Paper #78-74, presented at the AIAA 16th Aerospace Sciences meeting, Huntsville, AL, 10-18 Jan. 1978.
- [23] Knollenberg, R. G., Vol. 92 in *Practical Applications of Low Power Lasers*, Society of Photo-Optical Instrumentation Engineers, 1977, p. 137.
- [24] Holve, D. and Selt, S. A., *Applied Optics*, Vol. 18, 1979, p. 1632.
- [25] Hirleman, E. D., *Optics Letters*, Vol. 3, 1978, pp. 19-21.
- [26] Hodgkinson, J. R., *Applied Optics*, Vol. 5, 1966, p. 839.
- [27] Gravatt, C. C., *Journal of the Air Pollution Control Association*, Vol. 23, 1973, p. 1035.
- [28] Hirleman, E. D., "Optical Technique for Particulate Characterization in Combustion Environments. The Multiple Ratio Single Particle Counter," Ph.D. dissertation, Purdue University, Aug. 1977.
- [29] Bartholdi, M., Salzman, G. C., Hiebert, R. D., and Seger, G., *Optics Letters*, Vol. 1, 1977, p. 223.
- [30] Farmer, W. M., *Applied Optics*, Vol. 11, 1972, p. 2603.
- [31] Erstrom, R. M., Jones, A. R., Schwarz, M. S. R., and Weinberg, F. S., *Faraday Symposia of the Chemical Society*, Vol. 1, 1973, p. 183.
- [32] Robinson, D. M. and Chu, W. P., *Applied Optics*, Vol. 14, 1975, p. 2177.
- [33] Chu, W. P. and Robinson, D. M., *Applied Optics*, Vol. 16, 1977, p. 619.
- [34] Yule, A. J., Chigier, N. A., Atakan, S., and Ungut, A., "Particle Size and Velocity Measurement by Laser Anemometry," Paper No. 77-214, American Institute of Aeronautics and Astronautics, 1977.
- [35] Farmer, W. M., "Measurement of Particle Size and Concentrations Using LDV Techniques," in *Proceedings of The Dynamic Flow Conference*, 1978.
- [36] Bachalo, W. D., *Applied Optics*, Vol. 19, 1980, p. 363.
- [37] Spectron Development Labs, Costa Mesa, CA.
- [38] Kratochvil, J. P., Lee, M. P., and Kerker, M. P., *Applied Optics*, Vol. 17, p. 1978, 1978.
- [39] Alger, T. W., *Applied Optics*, Vol. 18, 1979, p. 3494.
- [40] *Compilation of ASTM Standard Definitions*, ASTM Committee on Terminology, American Society for Testing Materials, Philadelphia, PA, Fourth Edition, 1979, pp. 88-89.
- [41] Dos Santos, R. and Stevenson, W., *Applied Physics Letters*, Vol. 30, 1977, p. 236.
- [42] Negus, C. and Azzopardi, B. J., "Malvern Particle Size Distribution Analyzer: Its Accuracy and Limitations," Report AERE-R 9075, U. K. Atomic Energy Authority, Harwell, Dec. 1978.
- [43] Duke Standards, Palo Alto, CA.
- [44] Hirleman, E. D., "Aperture Arrays for the Calibration of Droplet Sizing Instruments," in *CLEOS Conference Digest*, IEEE OSA CLEOS, 1982.
- [45] Hirleman, E. D., "On-line Calibration Technique for Laser Diffraction Droplet Sizing Instruments," ASME Paper 83-GT-232, International Gas Turbine Conference, Phoenix, AZ, March 1983.
- [46] Berglund, R. N. and Liu, B. Y. H., *Environmental Science Technology*, Vol. 7, 1973, pp. 147-153.
- [47] Vibrating Orifice Droplet Generator, available commercially from TSI Inc., St. Paul, MN.
- [48] Mason, B. J., Jayaratne, O. W., and Woods, J. D., *Journal of Scientific Instruments*, Vol. 40, 1963, pp. 247-249.
- [49] Hirleman, E. D., and Moon, H. K., *Journal of Colloid and Interface Science*, Vol. 87, No. 1, 1982, pp. 124-139.
- [50] Compagnie Industrielle des Lasers (CILAS), Paris, France and Marco Scientific, Sunnyvale, CA.
- [51] Reticon, Inc., Sunnyvale, CA.
- [52] Wittig, S. L. K., Aigner, M., Sakbani, K., and Sattelmayer, T., "Optical Measurements of Droplet Size Distributions: Special Considerations in the Parameter Definition for Fuel Atomizers," Paper 13 in *Proceedings of AGARD Conference on Combustion Problems in Turbine Engines*, Oct. 1983, Chesme, Turkey.

60 LIQUID PARTICLE SIZE MEASUREMENT TECHNIQUES

[53] Laser Electro-optics, Ltd., Tempe, AZ.

[54] Felton, P. G., "Measurement of Particle droplet size Distributions by a Laser Diffraction Technique," presented at the 2nd European Symposium on Particle Characterization, Nurnberg, West Germany, 24-26 Sept. 1979, available from Department of Chemical Engineering, University of Sheffield, England.



**AIAA-80-0350**

**Recent Developments in Non-Doppler Laser Velocimetry**

**E. D. Hirleman, Arizona State University, Tempe, Ariz.**

**AIAA 18th  
AEROSPACE SCIENCES MEETING**

January 14-16, 1980/Pasadena, California

RECENT DEVELOPMENTS  
IN NON-DOPPLER LASER VELOCIMETRY

E. Dan Hirleman\*  
Mechanical Engineering Department  
Arizona State University  
Tempe, Arizona 85281

Abstract

Alternative concepts in laser velocimetry which in some applications demonstrate significant advantages over conventional laser Doppler velocimeters (LDV) are discussed. The non-Doppler techniques discussed here are particle-counting velocimeters which measure the time for individual particles to traverse a known distance to determine velocity. The methods considered include the two-spot or time-of-flight velocimeter L2V, the single beam transit-timing laser velocimeter L1V, and a recently proposed hybrid of these, the LSV, which measures two velocity components using the L2V optical system. The principles and relative advantages of these non-Doppler LV techniques will be discussed in addition to some of the first experimental results obtained with L1V and LSV systems.

I. Introduction

Laser velocimeter methods for nonintrusive flowfield measurements are routinely utilized in many research establishments. The velocity diagnostic technique most widely applied is the laser Doppler velocimeter (LDV or LDA); indeed, nearly every research lab has a laser Doppler system. Extensive literature is available on LDV principles and applications with comprehensive reviews by Stevenson<sup>1</sup> and Durst et. al.<sup>2</sup>. The application of laser Doppler velocimeters in combustion environments is discussed by Self and Whitelaw<sup>3</sup>.

This paper discusses some alternative non-Doppler laser velocimeters which in some situations have significant advantages over the more common LDV. The advantages can include simplified optical or electronic system configurations, higher sensitivity, and better rejection of background scattering from surfaces adjacent to the sample volume. The non-Doppler laser velocimeters considered here are: the two-spot or time-of-flight laser velocimeter L2V; the single beam transit-time laser velocimeter L1V; and finally the two-component, two-spot laser velocimeter LSV, recently proposed by Hirleman.<sup>4</sup>

Of these methods, only the L2V has been used by enough research groups in diverse applications to permit a reasonable evaluation of its effectiveness. A brief review of the principles of L2V, some of the past experimental results, and a comparative analysis with LDV will be presented here. In contrast, the L1V and LSV concepts which may improve on the L2V are relatively untested

with very limited experimental results published on the L1V<sup>5</sup> and none available for the LSV. We are actively investigating these new techniques, and the principles of operation and an analysis of recent experimental results are presented.

II. Non-Doppler Laser Velocimetry

The non-Doppler LV techniques considered here involve measurement of the time for a particle to traverse known distances, either the distance between two laser beams or the distance across a single beam. A real fringe differential Doppler LDV counter system can be interpreted as measuring the time for a particle to traverse fringes of known spacing, but this LDV configuration depends on radiation scattered from coherent, intersecting beams. In contrast, the non-Doppler methods do not require either beam intersection or coherence.

The principles for the LV techniques of interest can be illustrated using the optical systems of Figure 1. It is desired to form two laser beam waists or foci separated by a known distance in the optical sample volume. This can be accomplished using birefringent optics which angularly separate the polarizations of a circularly polarized laser beam (e.g. Rochon or Wollaston prisms), followed by a lens placed one focal length behind the beam separator as shown in Fig. 1a. A lens placed in front of a calcite beam displacer will accomplish the same results as in Fig. 1b. The beam expander is used to control the beam waist sizes in the measurement volume and a  $\lambda/4$  waveplate is required for linearly polarized lasers.

The laser focus characteristics of the sample volume are shown in more detail in Fig. 2, with some illustrative particle trajectories. Assuming a trajectory in the x-y or focal plane ( $z=0$ ) which projects to Fig. 2b, and for light scattering and detection processes which are effectively instantaneous, detector output as in Fig. 2c would be obtained. The maxima in the output signals occur when the particle is at the points of closest proximity to the laser beam axes. The time-of-flight  $t_f$  between the peaks of these signals is given (for  $z=0$  trajectory) by:

$$t_f = 2x_b \cos \alpha / V_L \quad (1)$$

where  $V_L$  is the particle speed in the x-y plane. Now the x-component of  $V_L$  is given by:

\*Assistant Professor, Mechanical Engineering  
Member AIAA

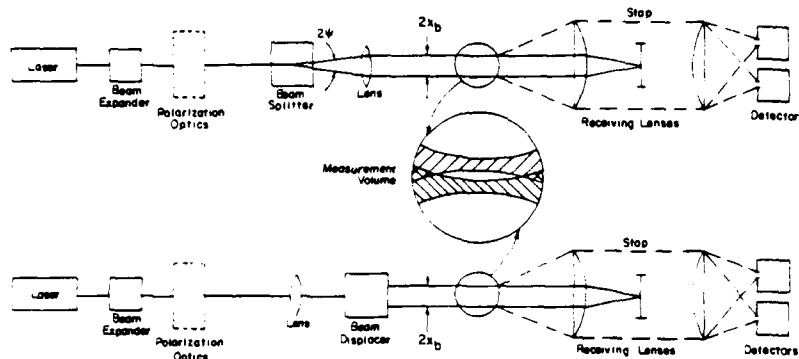


Fig. 1. Schematics of a L2V optical systems in forward scattering receiving configurations. Beam separation with a) Rochon or Wollaston prisms and b) calcite beam displacer.

$$V_x = V_{\perp} \cos \alpha \quad (2)$$

Rearranging Eqs (1) and (2) gives:

$$\frac{2x_b}{t_f} = \frac{V_x}{\cos^2 \alpha} \quad (3)$$

which indicates that for small  $\alpha$  ( $\cos^2 \alpha \approx 1$ ), measurement of the time-of-flight  $t_f$  between the peaks directly indicates the particle velocity component in the plane containing laser beam axes. This simple time-of-flight concept was apparently first proposed for laser velocimetry by Thompson<sup>6</sup> in 1968, several years after the earliest LDV papers<sup>1, 2</sup>. Tanner<sup>7</sup> suggested the present day version of the L2V which utilizes a large beam spacing/beam diameter ratio  $2x_b/2w$  to ensure that only particles following trajectories of small  $\alpha$  scatter enough light from both laser beams to be detected as a dual peak event. Acceptance of signal pairs from particles with large  $\alpha$  results in a broadening of L2V velocity data. Ratios  $x_b/w$  of typically 20 or greater ( $2x_b = 0.5 \text{ mm}$ ) have been used in L2V applications in rotating turbomachinery by Shodl<sup>8, 9</sup> and Smart<sup>10</sup>, in free jets by Lading<sup>11</sup>, and in the atmosphere at up to 70m range by Lading et al<sup>11, 12</sup> and Bartlett and She<sup>13</sup>.

The major advantages of L2V over LDV are higher sensitivity and better signal/noise ratios which derive from the possibility of using smaller beam focus diameters in the L2V sample volume. The laser beam diameters in the LDV fringe volume are constrained by frequency requirements for the processing electronics. Typical LDV counting processors need on the order of 10 fringe crossings minimum per Doppler burst (e.g. within the  $1/e^2$  points) for an accurate velocity determination. Thus, the minimum required fringe spacing decreases linearly as the beam diameter is decreased and hence the processor frequency requirements become more stringent. To illustrate, a particle moving at 100m/sec through a 10 $\mu\text{m}$  beam with 10 stationary fringes (1 $\mu\text{m}$  spacing) will generate a 100MHz Doppler burst which is difficult to process

accurately. In practice LDV probe volume beam diameters are about 100 $\mu\text{m}$  or greater at  $1/e^2$  points. Conversely, the L2V has no such constraint since the temporal characteristics of laser light scattered during the transit of a particle through a beam is of little interest; thus the L2V focus spots in the sample volume are typically made as small as possible, subject to the diffraction limit. L2V beam diameters as small as 10 $\mu\text{m}$  are not unreasonable and this results in a laser power density of 100x greater than for the above LDV example. Then for a given laser and equivalent receiving optics, the peak scattered flux from a specific particle will 100x be greater in the L2V system than in LDV, resulting in a similar improvement in L2V signal/noise ratio. This higher L2V sensitivity can be exploited in various ways in terms of smaller and less expensive lasers, smaller seed particles, measurements closer to adjacent surfaces, or measurements at higher velocities.<sup>14, 15, 16</sup> Additional advantages of L2V relative to LDV include less complex data processing requirements and potential insensitivity to beam steering since the L2V beams are practically coincident until just at the focal plane (see Fig.1) and turbulent disturbances in the path should affect both beams simultaneously. Conversely, the 2 beams in LDV take completely different paths to the fringe volume and separate disturbances on the beams which may cause fringe shifting or prevent beam intersection are more likely.

The advantages of L2V over LDV for some specific applications have been well established.<sup>15, 17</sup> However, there are some significant problems with the conventional L2V. First, the L2V has a highly directional sample space due to the large beam spacing/beam diameter ratio required by accuracy considerations discussed earlier, i.e. only particles with very small traverse angles  $\alpha$  in Fig. 2b will generate two peaks. It is, therefore, necessary to rotate the spots to get information for more than one flow direction,<sup>9</sup> and simultaneous measurement of 2 velocity components is not possible with the L2V systems.

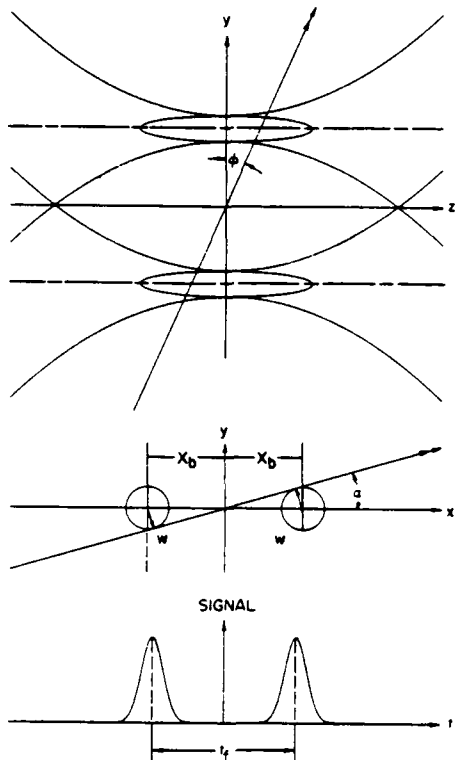


Fig. 2. L2V sample volume. a) laser focus properties indicating  $1/e^2$  intensity contours along laser beam axes. Sample particle traverse indicated with double arrows. b) cross-section of sample volume in a) along z or optical axis. c) detector output from particle traverse indicated in b) with  $\phi = 0$ .

Also, the quality of optical components becomes more critical for L2V applications where use of diffraction limited spots are desired. Finally, there is the question of possible degradation of L2V performance in highly turbulent environments.<sup>18</sup> These relative advantages are discussed in more detail elsewhere<sup>16</sup>, but additional experiments directly comparing L2V and LDV systems are necessary to further delineate the overlap in ranges of applicability for these laser velocimeter techniques.

### III. Single Beam Transit-Time Velocimeter (LIV)

A non-Doppler velocimeter concept used even less than L2V is the single beam transit-time velocimeter proposed by Rudd<sup>5</sup> and discussed by Hirleman<sup>7</sup>. A typical optical system for LIV would be similar to that in Fig. 1 with forward, back-scatter or off-axis scattering geometry possible. However, beamsplitting optics would be unnecessary since this method uses a single TEM<sub>00</sub> laser beam. Referring to Fig. 3, the intensity distribution in any plane perpendicular to the beam propagation vector is given by:

$$I(r) = I_0 \exp(-2r^2/w^2), \quad (4)$$

where  $I(r)$  is the intensity at a radial distance  $r$  from the beam or optical axis,  $I_0$  is the peak intensity at the beam center ( $r=0$ ),  $w$  is the beam radius at the  $1/e^2$  intensity points, and these quantities can vary along the optical axis. For Cartesian coordinates  $x^2+y^2=r^2$ , and a particle traveling in a plane normal to the beam and parallel to the  $y$  axis at some  $x$  traverse position  $x_t$  as in Fig. 3 will experience an incident intensity history:

$$I(x_t, y) = I_0 \exp(-2x_t^2/w^2) \exp(-2y^2/w^2). \quad (5)$$

Note that any linear particle trajectory will fit Eq. (5) since the orientation of the  $x$ - $y$  coordinate system is arbitrary. For a constant velocity  $V_{\perp}$  in the perpendicular ( $x$ - $y$ ) plane, the temporal incident intensity (and therefore scattered-light detector response, assuming the light scattering and detection processes to be effectively instantaneous and particle diameter much smaller than the beam diameter) will then be

$$I(x_t, t) = I_0 \exp(-2x_t^2/w^2) \exp(-2V_{\perp}^2 t^2/w^2). \quad (6)$$

Since the first exponential is time independent, scattered-light signals from particles moving linearly at constant speed will always be geometrically similar Gaussians (same  $1/e^2$  width), as indicated in Fig. 4. Then measurement of the transit-time  $t_t$  between the  $1/e^2$  points of a scattering signal uniquely determines the magnitude of the particle velocity component in the plane normal to the beam axis by<sup>5</sup>:

$$V_{\perp} = w/t_t \quad (7)$$

regardless of the traverse position  $x_t$ . Although this property of Gaussian beams has been known for some time, the electronics required for accurate measurements of the transit-time have been a problem.<sup>5</sup> However the rapid advances in high speed electronics are finally making such a measurement

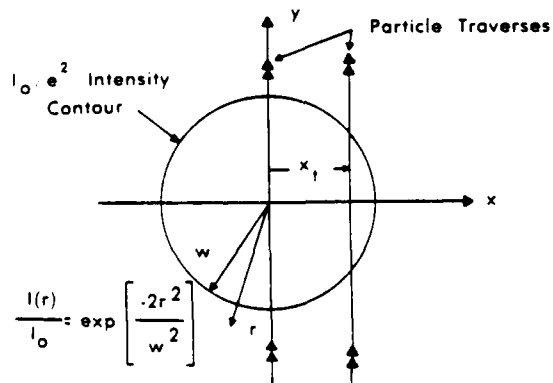


Fig. 3. Laser beam properties and linear particle traverses in a plane normal to the laser beam axis.

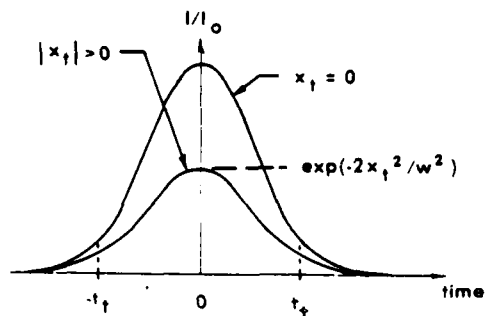


Fig. 4. Time dependence of laser intensity incident on particle traverses of Fig. 3.

practical and our lab is currently making a comprehensive study of the LIV concept.

For the measurements it is assumed that the beam diameter  $w$  is known *a priori* and is effectively constant in the particle-sampling region. This condition can be satisfied either by utilizing a collimated beam (constant  $w$ ) or by optically defining the axial extent with the detector field of view as certain axial length of the laser-focus region that has approximately constant  $w$ . Laser-focus intensity contours are elongated along the optical axis for typical systems with relatively high ( $>4$ )  $f$  number optics<sup>19</sup>, and therefore the second technique for defining  $w$  is practical.

The LIV data processing system must determine the width parameter  $w$  of the Gaussian detector output pulses for each particle. Possible analog techniques include the differentiation method suggested by Rudd<sup>9</sup> and a delay line/peak sensor/discriminator/timer concept we have utilized.<sup>16</sup> For moderate speed applications we have found a digital approach to be advantageous. This microprocessor-based system uses high speed A/D conversion and a procedure to fit the data to a Gaussian peak as discussed later.

The major advantage of the LIV is the relatively simple optical system necessary to measure one velocity component. Also, the LIV is not dependent on spatial coherence of the laser beam (as is LDV) which could be important for measurements in highly turbulent environments. On the other hand, the LIV requires more sophisticated electronics than L2V or LDV, requires detailed knowledge of the beam properties at sample volume, and gives erroneous velocity measurements for particle diameters significant ( $d/w \geq 0.1$ ) compared to the beam diameter. However, the digital curvefitting approach discussed later has the potential for identifying and rejecting signatures from large particles.

#### IV. L2V Revisited: The LSV

Returning to consider the L2V in light of the previous LIV development, it is clear that the output from an L2V detector such as Fig. 2c contains more information than just one velocity component. Since the width of the Gaussian peak from

either beam in Fig. 2c determines a velocity, the measured time-of-flight  $t_f$  between beams then can be used to determine the traverse angle  $\alpha$  through Eq. (1). The values for  $V_{\perp}$  and  $\alpha$  can be easily transformed into two velocity components using:

$$V_x = \pm V_{\perp} \cos \alpha \quad V_y = \pm V_{\perp} \sin \alpha \quad (8)$$

where the sign uncertainty in  $V_x$  can be eliminated by determining which beam the particle passed through first. The ambiguity in the sign of  $\alpha$  in  $V_y$  can only be eliminated by rotating the beam orientation until the flowfield character precludes many particles with trajectories at both  $\pm\alpha$ . Thus combining the principles of LIV and L2V permits the measurement of 2 velocity components with an L2V. This hybrid system is termed the LSV here since the concept is also the basis for a particle-sizing scheme proposed by Hirleman<sup>4</sup>.

The next LSV consideration is the beam spacing/diameter ratio which was large in the L2V due to errors or broadening introduced by nonzero  $\alpha$  trajectories. However, in LSV the particle traverse angle  $\alpha$  is measured and the problem disappears. In fact the optimum beam spacing/diameter ratio for LSV is on the order of one, i.e. with the two beams partially overlapped. The beams would be of different wavelengths or polarizations to prevent interference and for the overlap case two detectors would be required, with each detector sensitive primarily to light scattered from only one of the beams. The LSV has optics as in Fig. 1, and a sample volume similar to Fig. 2 but with the beams of Fig. 2b and the Gaussian pulses of Fig. 2c overlapped. Data acquisition can again be either analog or digital.

The LSV concept eliminates several important L2V disadvantages while maintaining some L2V advantages and potentially providing the measurement of two velocity components simultaneously with the optical system complexity of a single component LDV. For example, LSV sample times would be comparable to LDV and much less than for L2V since the percentage of invalid particles crossing only one of the beams would decrease drastically. Some tradeoffs would be required as the closer beam spacing would increase the frequency response requirements of the conventional L2V. However, the sensitivity advantage over LDV would still remain since the LIV measures transit-time across one beam whereas LDV again needs roughly 10 fringes across the beam. Again however, the data acquisition system is relatively complex and accurate characterization of the beam properties at the sample volume is essential.

#### V. Experiments

To investigate the LIV and LSV concepts an experimental program is underway. Our analysis can be divided into three areas: laser beam property measurements; data acquisition and processing considerations; and flow measurements on an axisymmetric laminar jet.

##### Laser Beam Characterization at Sample Volume

As discussed earlier, accurate characterization of the beam properties in the LIV or LSV sample volume is essential. For beam diagnostics we use a calibrated microscope assembly coupled with a 1000

element linear photodiode array (25 $\mu$ m centers) mounted at the image plane to perform beam diagnostics. This microscope assembly is shown in Fig. 5. The position of the objective relative to the photodiode array was calibrated by imaging an illuminated aperture of known radius. For small beam waists as used here the objective system obeys standard geometrical optics relating the magnified Gaussian beam diameter at the image plane to that at the object plane (not true in general for Gaussian beams<sup>19</sup>). A sample output from scanning the diode array of Fig. 5 with a Gaussian laser beam incident at the object plane is shown in Fig. 6. Each peak represents the radiation intensity integrated over a 25 $\mu$ m square diode and over some sample time; the radial laser beam intensity profile covering about 70 diodes is indicated.

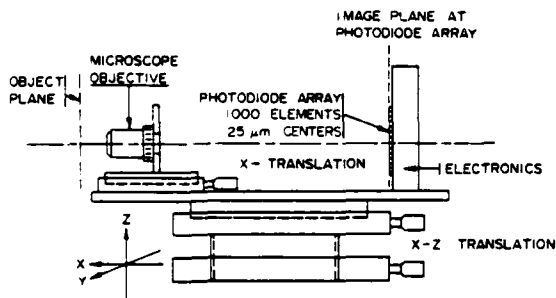


Fig. 5. Schematic of Microscope Objective Photodiode Array Assembly used for laser beam diagnostics.

To analyze the beam profile, the peak output values from each diode are digitized and fit to a Gaussian profile using a logarithmic least squares technique (See next section). The curvefitting is performed by a TI 990 microprocessor system which controls the diode scan, the A/D conversion, transferring the data into microcomputer memory, and finally performs the curvefit calculations. A number of traces such as Fig. 6 are analyzed for each position along the laser beam axis. A plot of the measured  $1/e^2$  beam radius at several axial positions along a laser focus are shown in Fig. 7. The data of Fig. 7 are for a He-Cd laser beam at 441.6nm which was spatially filtered and expanded 6x, focused using a 96mm lens, and analyzed with a 40x microscope objective using the apparatus of Fig. 5. Also plotted in Fig. 7 are the beam radius profile predicted assuming diffraction-limited-optics<sup>19</sup> and a least squares curvefit of the axial data to the predicted Lorentzian form for  $w(z)$  near a diffraction-limited TEM<sub>00</sub> laser beam waist.

To use the LIV or LSV concepts it is necessary to know the Gaussian beam waist radius  $w$  at the sample volume. The uncertainty in a single measurement of  $w$  using the apparatus of Fig. 5 can be 10-20% in worst cases depending on the beam quality, diode-to-diode response variations, and aberrations in the objective system for small beam waists ( $\leq 20\mu$ m) as in Fig. 7. By measuring an axial  $w(z)$  profile this uncertainty can be decreased significantly since the measurement accuracy is better in larger portions of the beam. For  $1/e^2$  beam diameters of roughly 50 $\mu$ m or greater the measurements are probably good to better than 1%.

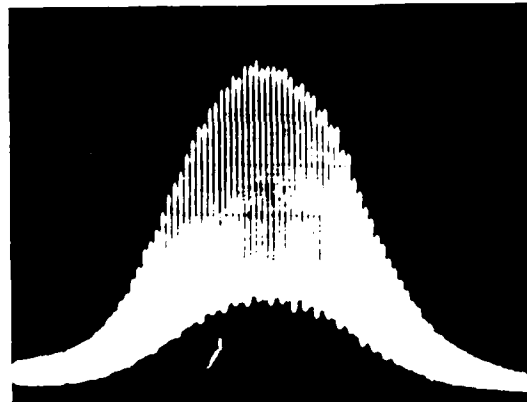


Fig. 6. Scan of photodiode array outputs.

#### Data Acquisition System

The data processing technique we are presently using for the various non-Doppler LV is primarily digital as shown in Fig. 8. High speed A/D conversion (2-20MHz) of the photomultiplier output(s) is performed by a Nicolet Digital Oscilloscope. The digitized data such as that shown in Fig. 9 is clocked out of the Nicolet through a parallel interface into the memory (RAM) of a TI 990 16-bit microcomputer. A multiple variable linear regression routine is used by the microprocessor to determine a logarithmic least squares fit of Gaussian peaks to the data. The three parameters in the Gaussian curvefit algorithm based on linearizing Eq. (4) are (see Fig. 4): the mean (time) value or time of maximum signal amplitude; the peak height; and finally the variance or transit-time  $t_t$  and which directly indicates the velocity from Eq. (7). The time-of-flight  $t_f$  is the time between successive peak centers. An example curvefit to digital LSV data performed by the microprocessor is shown in Fig. 10.

A major concern with the LIV concept is accuracy. The parameters controlling the accuracy

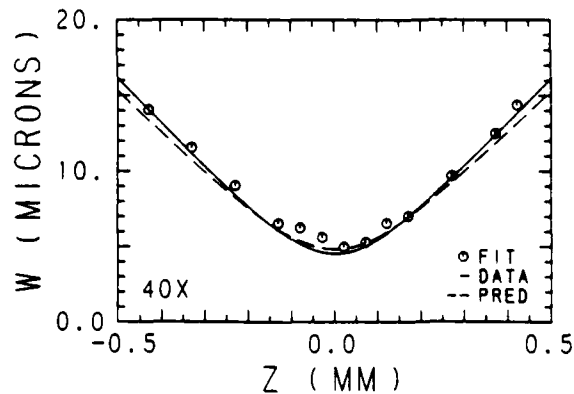


Fig. 7. Laser beam radius at  $1/e^2$  points.

of the curvefit and of the LIV velocity determination include: the number of A/D samples during a Gaussian peak  $n$ ; the ratio of RMS noise to the peak amplitude; and the ratio the A/D resolution or digitizing error to the peak amplitude. A computer simulation of the LIV digital data processing system has been utilized to investigate these effects. Table I indicates the normalized uncertainty  $\sigma_w/w$  in reconstructing a Gaussian peak from discrete digital samples predicted by the simulation as a function of the number of samples  $n$  and the RMS noise/signal ratio. The values for  $\sigma_w$  were estimated by: assuming a set of Gaussian peak parameters; taking  $n$  A/D samples of the assumed signal and perturbing each sample by adding a random noise contribution using a normal distribution random number generator; and finally applying the curvefit algorithm to the signal + noise samples. The width parameter of the reconstructed Gaussian less the initially assumed value is then the error in  $w$  (and velocity) determination. This process was repeated 1000 times using different random noise perturbations for statistics of the error, and the standard deviation of these errors is reported as  $\sigma_w$  in Table I. The mean values of the errors were effectively zero and the data of Table I are valid for a 12 bit A/D converter with a full scale peak signal level.

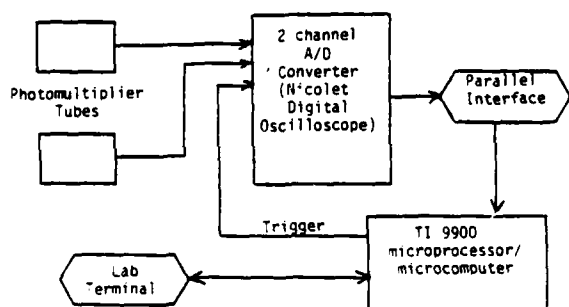


Fig. 8. Schematic of Digital Data Acquisition System for LIV, L2V and LSV.

Table I confirms what one would expect, that the uncertainty in determining  $w$  decreases with the number of samples  $n$  and increases with the noise level. Three is the minimum number of samples required for the three parameter curvefit. Increasing the number of samples for a given particle velocity involves higher speed A/D conversion and the tradeoffs of cost, fewer bits of A/D resolution, and increased data analysis time. The acceptable LIV uncertainty would depend on the turbulence intensity levels of interest since data processing errors ultimately appear as velocity broadening. Accuracy comparable to that of LDV seems attainable with the LIV concept.

#### Flow Experiments

We have made and are continuing experiments to verify the LIV and LSV simulations and hardware. A laminar, axisymmetric free jet ( $Re = 1200$ ) of air seeded with  $1.099\mu\text{m}$  polystyrene spheres was

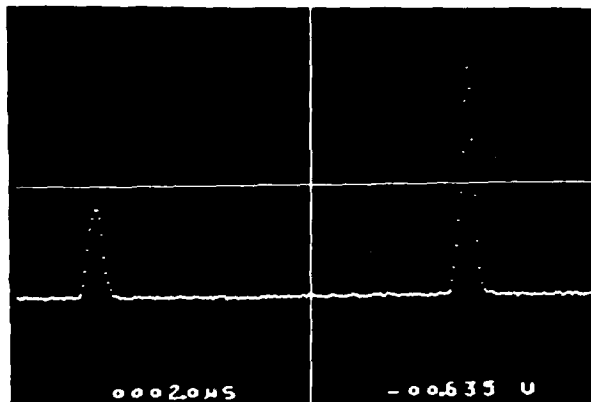


Fig. 9. Digitized Photomultiplier output from L2V displayed on Nicolet Digital Oscilloscope.

utilized. Optical and electron microscopy studies were undertaken to verify the monodispersity of the aerosol generated by atomizing polystyrene/isopropyl alcohol solutions. A 12.5mm I.D. glass pipe 100 diameters long with a constriction at the entrance was used to provide fully developed laminar flow. Our measurements were made 1/2 diameter downstream of the pipe exit in stagnant air.

Figure 11 is a plot of the mean axial velocity profile measured across the jet. The data were corrected for biasing<sup>20</sup> and were taken with an optical system similar to Fig. 1b using a 15mW He-Cd laser but with receiving optics at 90° to the laser beam. A 0.1 mm slit in front of the photomultiplier tube was imaged 1:1 at the beam waist to define a sample volume of constant beam diameter  $w$ .

The baseline data were taken with the conventional L2V concept using a 0.5mm beam spacing and the beam foci mapped out in Fig. 7. This beam spacing/diameter ratio of greater than 50:1 coupled with a high threshold setting for peak acceptance ensured minimal velocity broadening due to nonzero  $x$  traverses (Fig. 2b). This fact was supported by turbulence intensity measurements which averaged less than 0.7% for positions within one-half radius of the centerline ( $R/RO < 0.5$ ). This figure

Table I: Standard Deviation of Gaussian Reconstruction Errors  $\sigma_w/w$

Number of Samples $n$	Noise/Signal Ratio			
	0.	0.01	0.02	0.04
3	.001	.016	.030	.062
6	.001	.013	.026	.053
12	.001	.010	.020	.043
24	.001	.008	.015	.032

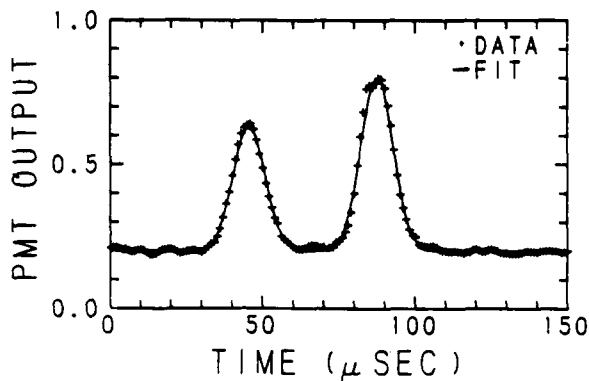


Fig. 10. Gaussian curvefits to digital LSV data.

compares with the 1% centerline turbulence intensity measured by Owens and Rogers<sup>21</sup> for internal fully-developed laminar flow at  $Re=1800$ .

Flow measurements with the LIV were made on the same laminar jet and the results are also presented in Fig. 11. The LIV optical system was identical to that used in the L2V measurements except for the focal length of the collimating lens in the spatial filter which was decreased by half. This modification doubled the beam waist radius at the sample volume to  $9.8\mu m$  which made axial adjustments of the receiving optics less critical and gave longer transit times through the beam so that the effects of the number of samples  $n$  could be investigated experimentally. The mean velocity profiles measured with both the LIV and L2V are in good agreement with the predicted parabolic profile. We observed discrepancies between measurements and predictions near the jet boundary due to shear effects. Biasing effects were negligible since the dimensions of the optical sample volume here were about 0.1% of the pipe diameter. These experiments are conclusive in proving the LIV concept with digital data processing to be a viable alternative for laser velocimeter applications.

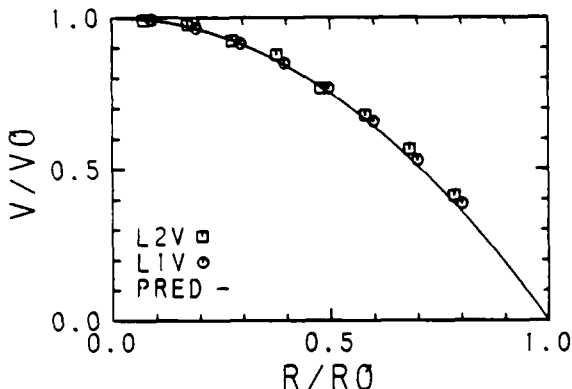


Fig. 11. Measured mean axial velocity normalized to centerline velocity  $V_0$  as a function of radial position for a laminar jet,  $Re=1300$  where  $R_0$  is the inner radius of the pipe.

A comparison of measured RMS velocity components (or apparent turbulence intensity) on the laminar jet centerline is given in Table II. The contribution of nonzero  $\alpha$  traverses to L2V broadening for  $x_p/w > 50$  was more than an order of magnitude lower than the measured L2V RMS component, and the observed distribution of velocities was due to flow system fluctuations and inaccuracies introduced in the electronics. The measured RMS velocity for the LIV was considerably higher than for the L2V due to the additional errors introduced in the Gaussian curvefit data processing. The LIV data were taken at 3 digitizing rates to give nominally 5, 10, and 20 samples per particle signature as indicated in Table II. The actual number of A/D samples above the noise threshold depends on the peak height which varied somewhat for each sampling rate, but the average values for  $n$  are indicated. It appears that the data of Table II would fit into the predictions of Table I between N/S ratios of 0.02 and 0.04 with reasonable agreement. However, the actual N/S ratio was close to 0.01 which should give lower RMS values, and we are presently unable to fully

Table II: Measured RMS velocity normalized to centerline velocity in laminar jet.

LV system	L2V	LIV	LIV	LIV
$n$	5	5	10	20
$\frac{V_{RMS}}{V_0}$	0.006	0.044	0.030	0.022

explain this discrepancy. It was also found that by rejecting those Gaussian peaks with low curvefit correlation coefficients the apparent turbulence intensity was lowered; however, for the data of Table II this rejection method was not used. Also the logarithmic least squares technique weights those samples near the baseline quite heavily which can adversely affect the curvefit process if a high threshold level is not selected. Unfortunately an ordinary least squares fit would require a non-linear curvefitting algorithm. We are continuing experiments to gain further insight into the accuracy and limitations of the LIV concept.

We have also made preliminary investigations of LSV performance on the laminar jet. The two beams were oriented at some predetermined angle ( $25^\circ$  typical) relative to the known preferred flow direction. The standard deviations of LSV measurements to date are considerably higher than for the LIV or L2V since errors in the LIV measurement propagate through the LSV calculations. However, the measured mean flow angles agree reasonably with the known flow angle. Improvements in the accuracy of LIV measurements will be important in the practical success of the LSV concept.

#### Conclusions

Several recent developments in non-Doppler laser velocimeters show the potential for substantive advantages over conventional LDV. The LIV uses a single laser beam for a velocity measurement and has the obvious advantage of a simple optical system. The LSV is a hybrid two-spot velocimeter L2V which

uses the principle of the LIV to measure two velocity components with essentially the hardware of a single channel LDV.

We have designed and tested LIV and LSV systems on a laminar jet and found the results to be quite encouraging. A microprocessor-based, digital data acquisition and processing design proved quite advantageous, and future developments in electronics will continue to make this approach more viable. Further experiments and detailed comparisons of LDV and non-Doppler LV systems in identical flow systems is warranted.

#### Acknowledgements

This research was accomplished with partial support from the National Science Foundation through Research Initiation Grant ENG78-06210 and Equipment Grant ENG78-11462, and from Project SQUID, Office of Naval Research.

#### References

1. Stevenson, W.H. "Principles of Laser Velocimetry", p. 307 in Experimental Diagnostics in Gas Phase Combustion, B.T. Zinn ed., Vol. 53 Progress in Astronautics and Aeronautics, AIAA, 1977.
2. Durst, F., Melling A., and Whitelaw, J. Principles and Practice of Laser Doppler Anemometry, Academic Press, New York, 1976.
3. Self, S.A., and Whitelaw, J.H. "Laser Anemometry for Combustion Research", Combustion Science and Technology 13:171 (1976).
4. Hirleman, E.D. "Laser Technique for Simultaneous Particle-size and velocity measurements", Optics Letters 3:19 (1978)
5. Rudd, M.J. "Non-Doppler Methods of Laser Velocimetry", in Proceedings of Second International Workshop on Laser Velocimetry, Vol. II, p. 300, Eds. W.H. Stevenson and D. Thompson, Purdue University Press, 1974.
6. Thompson, D.H. "A Tracer-particle Fluid Velocity Meter Incorporating a Laser", Journal of Physics E: Scientific Instruments 1:929 (1968).
7. Tanner, L.H. "A Particle Timing Laser Velocity Meter", Optics and Laser Technology, p. 108, June 1973.
8. Shodl, R. "A Laser Dual-beam Method for Flow Measurements in Turbomachines" ASME Paper 74-GT-157 (1974).
9. Shodl, R. "The Laser-Dual-Focus Flow Velocimeter", AGARD Conference Proceedings No. 193, Paper 21 (1976).
10. Smart, A.E. "Applications of Digital Correlation to the Measurement of Velocity by Light Scattering", presented at CLEOS 1978, Sponsored by IEEE/OSA, 9 February 1978, San Diego, CA.
11. Lading, L. "The Time-of-Flight Laser Anemometer", AGARD Conference Proceeding No. 193, Paper 23 (1976).
12. Lading, L., Jensen, A.S., Fog, C., and Anderson, H. "Time-of-Flight Laser Anemometer for Velocity Measurements in the Atmosphere", Applied Optics 17:1486 (1978).
13. Bartlett, K.G. and She, C.V. "Single Particle Correlated Time-of-Flight Velocimeter for Remote Wind-speed Measurement", Optics Letters 1:175 (1977).
14. Lading, L. "The Time-of-Flight Laser Anemometer versus the Laser Doppler Anemometer", p. 26 in Laser Velocimetry and Particle Sizing, D. Thompson and W. Stevenson Eds., Hemisphere Publishing Co., NY 1979.
15. Smart, A.E. "Laser Anemometry Close to Walls", presented at 1978 Dynamic Flow Conference, Baltimore, MD, September 18, 1978.
16. Hirleman, E.D. "Recent Developments in Non-Doppler Laser Velocimetry", an expanded version of this paper, Western States Section, Combustion Institute Paper 79-50, Berkely, CA, Oct. 15-16, 1979.
17. Lading, L. "Comparing a Laser Doppler Anemometer with a Laser Correlation Anemometer" in The Engineering Uses of Coherent Optics, p. 493, Ed. E.R. Robertson, Cambridge University Press, 1976.
18. Panel Discussion session moderated by H.D. Thompson, p. 539 in Laser Velocimetry and Particle Sizing, H.D. Thompson and W.H. Stevenson, Eds., Hemisphere Publishing Co., 1979.
19. Hirleman, E.D. and Stevenson, W.H. "Intensity Distribution Properties of a Gaussian Laser Beam Focus", Applied Optics 17:3496 (1978).
20. McLaughlin, D.K. and Tiederman, W.G. "Biasing Correction for Individual Realization of Laser Anemometer Measurements in Turbulent Flow" Phys. Fluids 16:2082 (1973)
21. Owen, J.M. and Rogers, R.H. "Velocity Biasing in Laser Doppler Anemometers", p. 89 in The Accuracy of Flow Measurements by Laser Doppler Anemometry, Proceedings of the LDA Symposium, Technical University of Denmark, Copenhagen, 1975.

*A reprint from*

# Optical Engineering

19(6), 854-860 (1980)

ISSN 0036-1860

THE JOURNAL OF THE SOCIETY OF PHOTO-OPTICAL INSTRUMENTATION ENGINEERS

## LASER-BASED SINGLE PARTICLE COUNTERS FOR IN SITU PARTICULATE DIAGNOSTICS

**E. Dan Hirleman**

Arizona State University  
Mechanical and Energy Systems Engineering  
Tempe, Arizona 85281

# Laser-based single particle counters for *in situ* particulate diagnostics

E. Dan Hirlleman

Arizona State University  
Mechanical and Energy  
Systems Engineering  
Tempe, Arizona 85281

**Abstract.** Optical techniques for particulate analysis have inherent and significant advantages over those conventional methods which involve batch sampling and subsequent analysis. Optical particle diagnostic techniques can be divided into three broad categories: ensemble methods which analyze the integrated optical properties of an assembly of particles; single particle counters (SPC) which analyze individual particles; and, finally, imaging techniques based on photography or holography. This paper is primarily concerned with laser-based single particle counters applicable to *in situ* sizing of particles and droplets in the diameter range 0.1  $\mu\text{m}$  to 1 mm. Theoretical principles of the various single particle counter designs are discussed with emphasis on comparing performance characteristics and relative advantages. The effects of size-dependent sample space, nonspherical particles, unknown particle composition, and applicable size ranges are considered.

**Keywords:** laser; particulates; diagnostics; optical particle-sizing; aerosol; combustion.

*Optical Engineering* 19(6), 854-860 (November/December 1980).

## 1. INTRODUCTION

The inherent advantages of optical techniques for particulate analysis have been responsible for considerable research and development over the past years. Optical methods, as compared to conventional batch sampling techniques with external particle analysis, are closer to real time, eliminate handling of the sample, and generally do not interfere with the aerosol processes of interest. *In-situ* optical techniques are not without disadvantages as they require optical access, require relatively sophisticated instrumentation, and are presently unable to provide detailed information on the chemical composition of the particles. The optical diagnostics also, because of their remote nature, suffer from an additional uncertainty not present when a particulate sample, however biased, is physically in hand. Furthermore, optical methods are still for the most part in the development or demonstration phases rather than being widely accepted methods for particulate monitoring in ambient or stack gases.

Optical techniques for particle measurements can be divided into three broad areas. Ensemble analyzing methods are so described because the light scattering or extinction integrated over the contributions from a large number of particles is used to determine parameters of the particle size distribution. In contrast, single particle counters (SPC) analyze individual particles traversing a relatively small optical sample volume, and a sequence of particles are sampled in order to build up a discrete size distribution. Photographic and holographic methods analyze simultaneously recorded images of a number of individual particles to similarly build a discrete particle size histogram. Single particle counters are the optimum choice for sizing micron and submicron particles in applications demanding high specificity and the potential for simultaneous velocity measurements, with requirements for temporal resolution of a few seconds and spatial resolution on the order of 1 mm<sup>3</sup>. The existing commercial technology of imaging techniques is generally limited to particles larger than a few micrometers with time response longer than a few seconds. There

is, however, considerable research in progress on nearly real-time analysis of particle field holograms.<sup>1</sup> Ensemble methods are also difficult to apply to submicron particles, may give erroneous data for bimodal particle size distributions, and are generally line-of-sight methods with relatively poor spatial resolution.

This paper is directed to those applications where *in situ*, SPC measurements are advantageous. An overview of SPC techniques is presented, and the relative advantages and regimes of applicability of the various SPC concepts are discussed.

## 2. LASER/OPTICAL SINGLE PARTICLE COUNTERS (SPC)

A generalized schematic of an optical SPC is presented in Fig. 1. The output beam from a laser or other source of radiation is directed (and typically focused) into the optical sample volume. This sample or probe volume can be thought of as that region of space where a single particle can generate a sufficient detector signal to be discriminated or "seen" over the background noise. As individual particles pass through the sample volume they interact with the incident radiation beam (i.e., scatter, absorb, and/or fluoresce light) and are observed by detection optics oriented at some angle(s)  $\theta$  with respect to the beam propagation direction. The single particle signatures obtained at the photodetector are processed to provide information on the size of each particle.

One family of particle counters, designated here as sampling SPC as opposed to *in situ* SPC, has been commercially available for many years. These sampling SPCs direct a batch sample of the aerosol of interest through a well-defined optical sample volume internal to the instrument. The reader is referred to the accompanying paper by Lieberman<sup>1</sup> for more discussion of sampling SPCs.

### 2a. Radiation cross section measuring techniques

The most common approach to particle sizing involves the principle that the magnitude of radiation-particle interaction is a nominally monotonic increasing function of particle size; hence, measurement of a radiation cross section can be used to infer particle size. The SPC signal response  $S$  to a particle in an incident radiation field

Original manuscript OP-101 received June 13, 1980; accepted for publication June 20, 1980.

1980 Society of Photo-Optical Instrumentation Engineers.

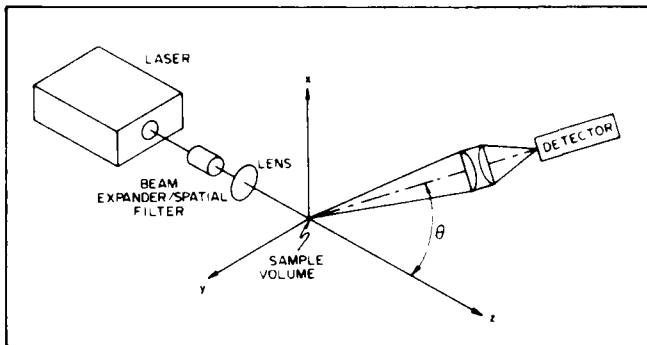


Fig. 1. Optical techniques for particle or droplet size measurements.

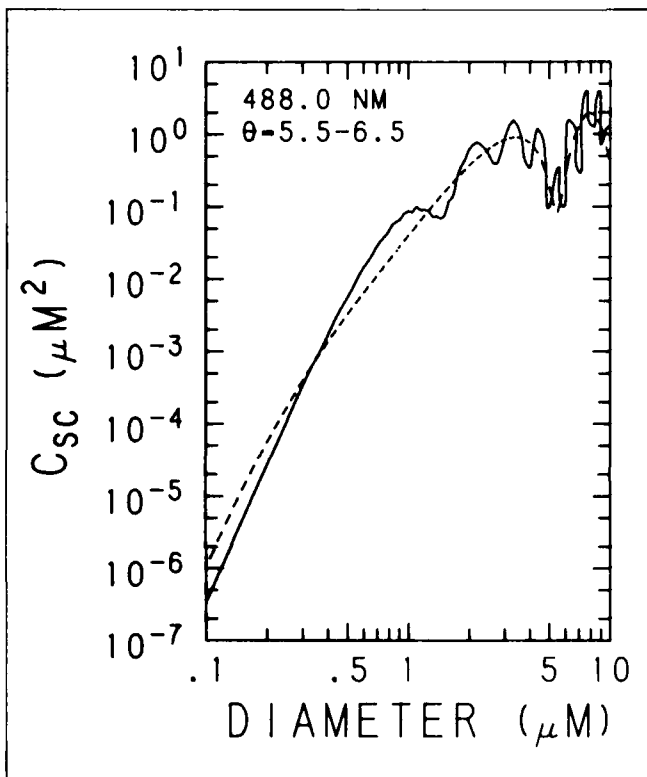


Fig. 2. Response function for a SPC collecting all forward scattered light between  $\theta = 5.5^\circ$  and  $6.5^\circ$ . The data were calculated from Lorenz-Mie theory for scattering by spherical particles. The solid line corresponds to the refractive index of a liquid hydrocarbon ( $n = 1.40$ ) and the dashed line is for soot ( $n = 1.56-0.47i$ ).

(uniform over the particle) of intensity  $I_0$  is given by:

$$S = k I_0 C_i \quad (1)$$

where  $k$  is the system gain in converting radiant energy to voltage using a photodetector;  $C_i$  is the appropriate partial cross section for the radiation process under study. The partial cross sections, as opposed to total cross sections, depend on the specific finite aperture detector configuration in use. The cross sections of interest here are designated by the subscripts:  $sc$  for light scattering,  $ex$  for extinction, and  $f$  for fluorescence cross sections. For light scattering and extinction by spherical particles the cross sections are functions of the particle diameter  $d$ , the complex refractive index  $n$ , and the radiation wavelength  $\lambda$  as predicted by the Lorenz-Mie theory. Thus, a response function  $S(d)$  relating measured signal levels to

the diameters of spherical particles of known refractive index passing through a SPC sample volume of known incident intensity  $I_0$  and given  $k$  can be determined from theoretical calculations of  $C_i(d)$ .

A plot of partial light scattering cross section for spherical particles illuminated by a coherent uniphase wave calculated using a Lorenz-Mie theory computer code<sup>2</sup> is given in Fig. 2. The calculations are for an off-axis  $f/2$  collection lens centered at  $\theta = 20^\circ$  from the incident radiation propagation direction (forward scattering). The oscillatory nature of the plots is a result of resonance interactions in the scattering process and creates the common uniqueness problem of multivalued SPC response functions. The use of broadband radiation in a scattering SPC can damp out these oscillations as shown in the paper by Lieberman.<sup>3</sup> Knollenberg<sup>4</sup> has shown that use of a multimode laser (nonuniform phase) can also significantly decrease these oscillations. Extinction coefficient plots are qualitatively similar to that of Fig. 2 as indicated in the papers by Knollenberg<sup>4</sup> and Faxvog.<sup>5</sup>

On-line applications for *in situ* particle analyzers require working spaces up to tens of cm, which places practical limits on the detector collection aperture. In order to generate sufficient signal levels from individual submicron particles in these applications it is invariably necessary to use a laser for sufficiently high incident intensity. Unfortunately, lasers introduce some problems not present with incoherent, broadband (white light) radiation sources.

Another problem inherent in using the laser as a SPC radiation source is the nonuniform intensity profile across the beam.<sup>6</sup> Unfortunately, an ambiguity in signal levels arises for *in situ* SPC since the particles are free to traverse the sample volume at any position. Thus, particles will experience different peak incident intensities  $I_0$  and even a monodisperse (uniform size) aerosol will generate a broad distribution of signal amplitudes  $S$ .

A number of methods have been devised to eliminate the unknown incident intensity effect in cross-section measuring techniques. Two basic approaches include: (1) analysis of only those particles which pass through a selected portion of the beam of known and constant intensity and (2) analysis of all particles and later correction of the distribution of particle trajectories and corresponding incident intensities. The early laser light scattering SPC of Heyder et al.<sup>7</sup> aerodynamically focused the aerosol sample through a small region at the center of the laser beam of known and constant intensity. For *in situ* measurements various optical methods of discriminating those particles which pass through a control portion of the beam have been used, including coincidence detectors at  $90^\circ$  by Hirleman<sup>8</sup> and Chigier et al.<sup>9</sup> and in the forward direction by Knollenberg.<sup>10</sup> This approach becomes very difficult for small laser focus diameters and another approach utilized by Knollenberg<sup>4</sup> and laser by Faxvog<sup>11</sup> involved the use of single particle extinction and the  $\text{TEM}_{01}$  or "donut" mode laser beam. With this concept those particles passing through the "donut hole" which generate double pulse signatures all experience the same maximum incident intensity. The instrument of Faxvog<sup>11</sup> then discriminates and analyzes only particles signatures with this double pulse and thus fixes  $I_0$  in Eq. (1). This concept of determining  $I_0$  could also be used with light scattering or fluorescence in addition to extinction although apparently neither has been tried to date.

A second general approach to the ambiguous incident intensity problem is to correct after the fact. One implementation of this approach demonstrated by Holve and Self<sup>12</sup> is to first consider the peak signal height distribution generated by particles of one size passing with equal probability through all portions of the laser beam focus region. The signal height distribution from a polydispersion is then a linear combination of the monodisperse particle response distributions. A numerical scheme was developed<sup>12</sup> to invert the resulting system of equations and solve for the linear coefficients which are proportional to concentrations in the discretized particle size intervals. The method of Holve and Self<sup>12</sup> has been tested only for light scattering measurements although the concept is readily extendable to either extinction or

fluorescence systems.

Another somewhat similar approach recently proposed by Hirleman<sup>13</sup> involves the use of signals generated by particles traversing two adjacent laser beams. The dual peak signature is used to determine two velocity components and the trajectory of each particle. Given known laser beam properties the incident intensity history for a particle is then completely determined which permits a real-time correction for the intensity ambiguity. After  $I_0$  in Eq. (1) is determined a calibrated response function prediction such as Fig. 2 would be used to relate signal amplitudes to particle size. This technique<sup>13</sup> has been proposed for light scattering, extinction, and fluorescence cross section measurements although experiments to date have used only light scattering.<sup>14</sup>

**2b. Scattering ratio techniques**

A second method of eliminating the incident intensity ambiguity which is applicable to light scattering techniques is to analyze the angular scattering pattern and effectively normalize out the incident intensity factor. This approach is commonly used in light scattering ensemble analyzing techniques (nephelometry) since the scattering pattern on the average is constant in time and a single detector can be rotated around the sample to different scattering angles relative to the incident laser beam. Phillips and Wyatt<sup>15</sup> have discussed a similar instrument for single particles suspended in a laser beam although *in situ* analysis with this concept<sup>15</sup> is impossible. To observe the normalized scattering pattern in real time requires an array of detectors placed at strategic scattering angles. Hodgkinson<sup>16</sup> suggested and Gravatt<sup>17</sup> tested the use of ratios of signals at two scattering angles for single particle sizing. A response curve for the ratio technique as calculated by Lorenz-Mie theory indicates multivalued response problems as shown in Fig. 3 and the addition of more angles providing additional signal ratios eliminates the ambiguity as discussed by Hirleman.<sup>2</sup> The multiple ratio single particle counter (MRSPC)<sup>2</sup> concept has been used with four angles although it becomes less practical as the number of angles increases. Bartholdi et al.<sup>16</sup> have used a photodiode array to get a finely resolved measurement of the angular scattering pattern from individual particles. This diode approach for SPC has considerable promise and will probably be used in the future.

**2c. Interferometric or crossed-beam techniques**

A third approach which can provide particle size information independent of incident intensity is particle sizing interferometry (PSI). As a single particle passes through the intersection region of two nonparallel laser beams, Doppler-shifted scattered light waves from each beam emanate from the particle. Heterodyning the two contributions of scattered light at a detector will produce the Doppler-difference frequency which is directly related to the particle velocity and the angle between the laser beam propagation vectors. This principle underlies the laser Doppler velocimeter (LDV). A particle crossing the LDV beam intersection region will produce an approximately Gaussian signal (pedestal) with the modulated Doppler-difference component written on the pedestal.<sup>17</sup> The ratio of the modulated signal amplitude to the pedestal amplitude (i.e., the visibility or contrast) provides a measure of particle size as shown by Farmer<sup>18</sup> and others<sup>18,19</sup> who used a scalar description of the process. For large apertures which collect all of the forward scattered (diffracted) light the visibility  $V$  as a function of particle diameter  $d$  and fringe spacing  $\delta$  was shown by Robinson and Chu<sup>20</sup> to be:

$$V = \frac{2J_1(\pi d/\delta)}{\pi d/\delta} \tag{2}$$

where  $J_1$  is a first order Bessel function of first kind. A plot of  $V$  is given in Fig. 4.

Calculations considering the complete problem of scattering by a sphere simultaneously in two coherent, collimated laser beams<sup>21</sup> predicted a strong dependence of the visibility on particle refractive

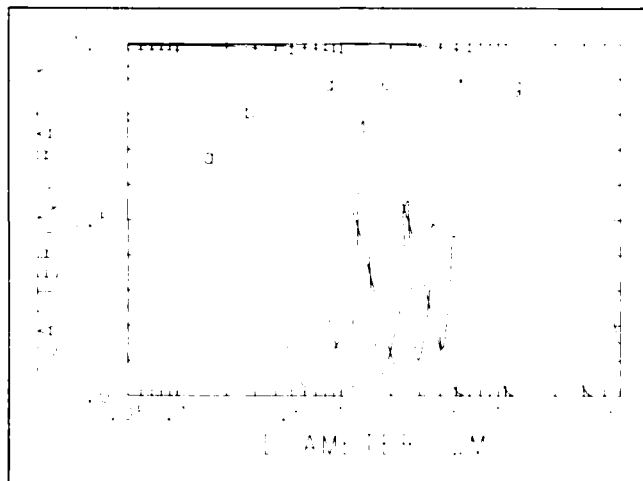


Fig. 3. Response function for a ratio-type light scattering SPC. The data were calculated for spherical particles with  $n = 1.56-0.47$  (soot) and  $\lambda = 0.488 \mu\text{m}$ . The scattering angle pairs are a)  $48^\circ/24^\circ$ , b)  $24^\circ/12^\circ$ , c)  $12^\circ/6^\circ$ , d)  $6^\circ/3^\circ$ , e)  $3^\circ/1.5^\circ$ , f)  $1^\circ/0.5^\circ$ , and g)  $0.5^\circ/0.25^\circ$ . The latter curves were truncated at the first minimum although all of the response curves have oscillations after the first minimum similar to the data for  $48^\circ/24^\circ$ .

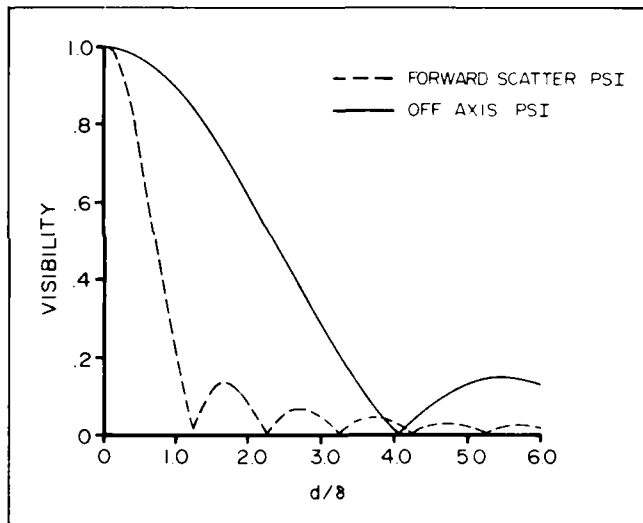


Fig. 4. Calculations for the fringe visibility  $V$  as a function of particle diameters to fringe spacing ratio  $d/\delta$  for particle-sizing interferometers (PSI). The data apply to a PSI collecting all of the forward-scattered light<sup>20</sup> and to an off-axis refractive scatter PSI<sup>21</sup> with an  $f/2$  collection lens oriented at  $\theta = 20^\circ$ .

index, the detector aperture, and detector position relative to the beams. A number of experimental studies have confirmed the importance of careful receiving optics design,<sup>20,21</sup> although conflicting observations have also been made.<sup>22</sup>

Another related approach is the off-axis PSI proposed by Bachalo<sup>23</sup> which utilizes the interference of refracted or reflected light scattering contributions rather than the diffractive scatter of a conventional PSI.<sup>17</sup> This method is applicable to particles significantly larger than the wavelength and is based on the difference in optical path length traveled by refracted rays from the two crossed beams which pass through the particle and arrive coincidentally at the detector. The visibility response function for a typical off-axis PSI collection angle<sup>23</sup> of  $20^\circ$  is also shown in Fig. 4. The expanded  $d/\delta$  sizing range for this concept<sup>23</sup> is apparent.

The use of the Doppler-difference laser velocimeter for sizing fluorescent particles using the modulation (visibility) of fluorescent radiation signals has been proposed by dos Santos and Stevenson.<sup>24</sup>

TABLE I. Diameter of a spherical soot particle ( $n = 1.56 - .47i$ ) with partial light scattering cross section equivalent to that of indicated background contaminants in a scattering volume of  $\pi \times 10^{-7} \text{ cm}^3$ . Data for  $\lambda = 0.488 \text{ }\mu\text{m}$ .

	Air Molecules (1 atm, 300 K)	$10^7 \text{ cm}^{-3}$ 40 nm Soot Particles	$10^9 \text{ cm}^{-3}$ 40 nm Soot Particles
f/4 lens at $90^\circ$	.028 $\mu\text{m}$	.048 $\mu\text{m}$	.106 $\mu\text{m}$
f/4 lens at $10^\circ$	.028 $\mu\text{m}$	.048 $\mu\text{m}$	.102 $\mu\text{m}$
Annular Receiver $5.5^\circ - 6.5^\circ$	.028 $\mu\text{m}$	.048 $\mu\text{m}$	.103 $\mu\text{m}$

The nature of the nonresonant fluorescence process makes the fluorescent radiation nominally incoherent and isotropic. The fluorescence visibility is claimed to be independent of detector configuration<sup>24</sup> although recent calculations by Kratochvil et al.<sup>25</sup> indicate some nontrivial effects. Detailed experiments on fluorescence visibility for different detector orientations have not been performed, although calibration experiments were successful.<sup>24</sup>

### 3. DISCUSSION

The theoretical principles of the various *in situ* single particle counters were developed in the previous section. In this portion of the paper some practical aspects of SPC applications are addressed. Important SPC performance characteristics including: applicable particle size range; particle shape and refractive index effects; size-selective sampling bias or sample space; and resolution are discussed.

#### 3a. Size range

The three important characteristics for evaluating the performance of a SPC in terms of the applicable particle sizing range are: the lower or threshold size limit; the upper size limit; and the dynamic range of a particular SPC configuration. A controlling parameter in all optical particle diagnostics is the ratio of some particle length scale to wavelength, typically the particle circumference to wavelength ratio  $\alpha = \pi d/\lambda$ . SPC instruments are considered here in detail followed by a discussion of possible future advances.

The lower particle sizing limit of a SPC can be controlled by either signal/noise considerations or insensitivity of the response function at small particle sizes.

Consider a volume of  $\pi \times 10^{-7} \text{ cm}^3$  determined by a laser focus waist diameter of  $20 \text{ }\mu\text{m}$  at the  $1/e^2$  intensity points and truncated to an axial length of 1 mm by the detection optics field-of-view. This volume is representative of the sample volume for a forward scatter SPC with a working space of tens of cm. The data of Table I indicate the soot particle sizes with equivalent light scattering cross sections for several examples of background scattering which might be encountered in practice. Thus a single soot particle of diameter  $0.106 \text{ }\mu\text{m}$  when illuminated with  $0.488 \text{ }\mu\text{m}$  radiation would scatter the same amount of energy into f/4 receiving optics at  $90^\circ$  as  $10^9 \text{ cm}^{-3}$  40 nm soot particles in a  $\pi \times 10^{-7} \text{ cm}^3$  sample volume.

Particle diameters as indicated in Table I would be indicative of threshold size limits for scattering cross section SPC and would be lower bounds for ratio-type and interferometric devices. The latter devices may be further constrained by a decreasing sensitivity of the response function to particle size for small particles. For example, the  $12^\circ/6^\circ$  ratio response of Fig. 3 flattens out for sizes below  $0.3 \text{ }\mu\text{m}$ . For larger scattering angle pairs the sensitivity to small particles increases; and taking a generous largest scattering angle of  $30^\circ$  for a  $30^\circ/15^\circ$  ratio (f/1.4 receiving optics) results in reasonable sensitivity for soot particles down to about  $0.1 \text{ }\mu\text{m}$ . This lower limit was ar-

TABLE II. Size range characteristics for single particle counters using visible radiation. Dynamic range is defined here as the ratio of upper to lower size limits for a single system configuration; i.e., interchangeable optics and cascading systems were not considered. Values taken from the literature are referenced.

	Lower Limit	Upper Limit	Dynamic Range
Ratio Counter (MRSPC)	0.1 $\mu\text{m}$	10 $\mu\text{m}$	20:1 <sup>2</sup>
PSI	1 $\mu\text{m}$	200 $\mu\text{m}$	10:1 <sup>36</sup>
Refractive/Reflective Scattering PSI	3 $\mu\text{m}$ <sup>23</sup>	5 mm <sup>27</sup>	10:1 <sup>34</sup>
Scattering Cross-Section SPC	0.1 $\mu\text{m}$	100 $\mu\text{m}$	16:1 <sup>12</sup>
Extinction Cross-Section SPC	0.04 $\mu\text{m}$ <sup>11</sup>	10 $\mu\text{m}$	25:1

bitrarily defined as that size where the derivative of the ratio response function with respect to particle diameter (i.e., sensitivity) drops to 50% of the maximum value. This estimated threshold size of  $0.1 \text{ }\mu\text{m}$  for the response sensitivity-limited case (rather than the signal/noise-limited case) is reflected in Table II. In practice the typical lower limits have been about  $0.3 \text{ }\mu\text{m}$ <sup>2,26</sup> for maximum  $12^\circ/6^\circ$  ratios. However, Bachalo and Hess<sup>27</sup> discuss ratio measurements at  $60^\circ/30^\circ$  down to  $0.1 \text{ }\mu\text{m}$ .

The practical lower size limit of PSI particle counters is a subject of conflicting opinions in the literature. Bachalo and Hess<sup>27</sup> suggest  $3 \text{ }\mu\text{m}$  as a lower practical limit. Farmer<sup>22</sup> reports independently verified backscatter PSI measurements of water droplets of  $2 \text{ }\mu\text{m}$  to  $30 \text{ }\mu\text{m}$  diameter in addition to noncalibrated measurements<sup>22</sup> of  $0.1 \text{ }\mu\text{m}$  to  $7.0 \text{ }\mu\text{m}$  particles. However, data for the submicron range<sup>22</sup> were taken with only four particle size intervals.

The extinction SPC of Faxvog<sup>11</sup> was designed with the objective of measuring very small particle sizes. This configuration is advantageous because small particles ( $\alpha \leq 1$ ) have extinction cross sections which are generally larger than the light scattering cross sections. Faxvog<sup>11</sup> reports lower size limits of  $0.04 \text{ }\mu\text{m}$  for absorbing particles (e.g., soot) and about  $0.1 \text{ }\mu\text{m}$  for nonabsorbing particles as determined by signal/noise considerations.

The fluorescence methods in general have significantly lower background noise because fluorescence is predominantly at wavelengths longer than the laser line and scattered radiation at the laser wavelength can be blocked out. However, the fluorescence cross sections and hence fluorescence signals will generally be smaller than elastic light scattering signals. This technique has no response function limitation, and any estimate of the signal/noise constrained lower limit would require information on the amount of fluorescent species in a given particle and the noise contributions other than laser light scattering. Unfortunately, no experimental studies on fluorescence cross section have been made, the value of  $0.5 \text{ }\mu\text{m}$  in Table II was estimated.

The fluorescence visibility concept<sup>24</sup> has a response function identical to that for forward scatter PSI as in Fig. 4. Therefore, the response sensitivity limitations of the PSI will also apply to the fluorescence visibility approach. The signal/noise limit will be similar to that imposed on fluorescence cross section, and thus, the visibility response function considerations will limit this method as indicated in Table II.

#### Dynamic range

The data in Table II are for a single SPC configuration; i.e., neither alterations in the optical system nor cascading of systems was considered. The multiple ratio concept as discussed by Hirleman<sup>2</sup> uses only one laser beam and multiple, simultaneous detectors and as such was considered in Table II as a single configuration. Dynamic range of the PSI and ratio techniques are inherently response-function-limited as a result of size insensitivity for small particles

and multivalued oscillating response function behavior after the first minimum. The light scattering methods in particular are affected by the large range in cross section; e.g., for particles from  $0.1 \mu\text{m}$  to  $10 \mu\text{m}$  diameter  $C_{sc}$  varies over about 8 orders of magnitude for the system of Fig. 2. This puts very difficult requirements on the electronics and thereby limits the ranges as indicated. The fluorescence visibility method would have the same dynamic range limitations as light scattering PSI, but fluorescence cross section methods fare better in some cases since the fluorescence signals would go as  $d^3$  (volume) as compared to scattering which varies as  $d^6$  in the Rayleigh regime ( $\pi d/\lambda \ll 1$ ) with a transition to a  $d^2$  dependence in the diffraction regime ( $\pi d/\lambda \gg 1$ ).

#### Future advances

The upper size limits of SPC are adequate for most applications which might be encountered. The dynamic ranges are reasonable, and improvements will most likely come at the expense of increased complexity, probably by cascading instruments. There is, however, a clear need to lower the sizing range of SPC as far as possible into the range  $.01 \mu\text{m}$  to  $0.1 \mu\text{m}$  where a number of important phenomena take place. The nucleation and growth of combustion particulates such as soot and flyash occur in this range along with some important atmospheric aerosol processes.

One approach is to lower the laser probe wavelength to analyze smaller particles. Unfortunately, wavelengths below about 200 nm are highly absorbed by the atmosphere and 10 cm or longer pathlengths would be a problem. Also, continuous wave (CW) laser power in the ultraviolet is not presently available at reasonable power due to the inefficiency of frequency doubling crystals at low power densities. The use of pulsed lasers or excimer lasers may provide some advances in small particle sizing, although only about a factor of two. Other problems are the increased background scattering from molecules in the scattering volume ( $\propto 1/\lambda^4$ ) and the high number densities of these small particles which may be as great as  $10^{10} \text{ cm}^{-3}$ . A sample volume of  $10^{-10} \text{ cm}^3$  (approximately a  $5 \mu\text{m}$  cube) might be possible using microscope objectives, but the working space would be severely limited. Improvements in lower size thresholds of greater than about a factor of two for *in situ* SPC measurements seem rather unlikely.

#### 3b. Sample space considerations

The optical sample volume or probe volume of a SPC is defined as the locus of points in space where a particle can generate a signal of sufficient magnitude (i.e., a valid signal) to be resolved over the background noise. The sample volume therefore, depends upon both the laser beam intensity distribution and the fields of view of the SPC detector(s). Typically the axial extent of the sample volume (in the laser beam direction) is controlled by the detection optics, and the radial extent by the laser focus intensity distribution. This radial extent is often defined solely in terms of incident laser intensity levels, e.g., the  $1/e^2$  points for single beam SPC or the  $1/e^2$  modulation contour for LDV/PSI type instruments. However, this approach leads to serious errors when attempts are made to interpret valid signal data rates in terms of particle size distributions. This is due to a strong data rate bias toward particles with large radiation cross sections. This is, for a given background noise level and associated signal processing threshold a large particle can generate a valid signal at points farther off-axis (lower incident laser intensity) than can a smaller particle. The sample volume for particles smaller than the lower threshold limit is zero as they cannot generate signals of sufficient amplitude even at the geometric laser focus center of highest intensity.

An expression for the sample rate  $\dot{N}$  (valid particle signals/sec) for particles with diameter  $d$  is given by:

$$\dot{N}(d) = V_{\perp}(d) \cdot A_s(d) \cdot N(d) \quad (3)$$

where:  $V_{\perp}$  is the particle velocity component normal to the laser beam; and  $N$  is the number density (particles/ $\text{cm}^3$ ). Eq. (3) is usu-

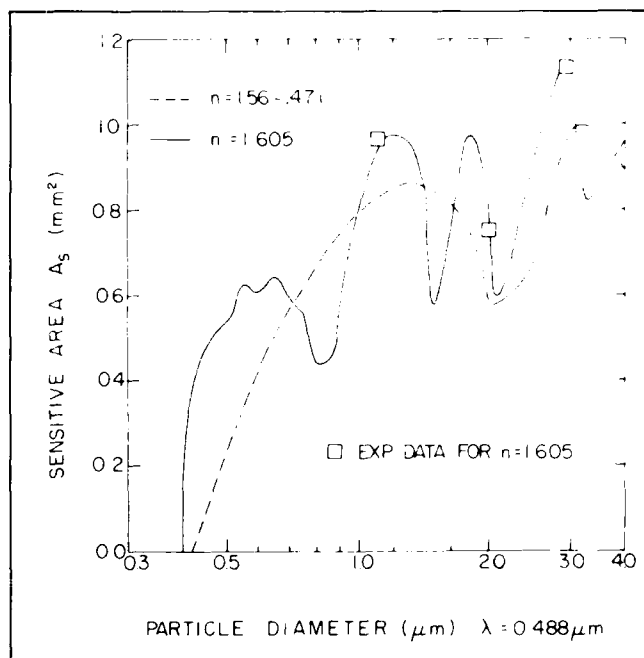


Fig. 5. Plot of sensitive area  $A_s$  vs particle size for  $12/6^\circ$  ratio pair. Plotted with the theoretical predictions are experimental data for polystyrene calibration spheres ( $n = 1.605$ ) taken at  $\lambda = 0.4416 \mu\text{m}$ . One undetermined calibration factor for the experimental data (the same factor for all 3 data points) was fixed by optimizing the fit between theory and experiment.

ally discretized into diameter intervals of finite width.

To utilize Eq. (3) for size distribution measurements it remains to relate a measured histogram of signal levels to particle sizes, i.e., for each discrete signal level interval or "bin" there is a corresponding range of particle diameters which generate signals of these levels. This is done using response function calculations as plotted in Figs. 3 and 4. Then the number density  $N$  can be determined by correcting the raw data rate  $\dot{N}$  for the size and velocity biases using the weighting factor  $1/V_{\perp} A_s$ . Note that  $A_s$  and the response function relating signal levels to particle sizes are actually functions of the shapes and refractive indices of the particles as well. Eq. (3) also indicates the necessity for simultaneous size and velocity measurements if significant variations of velocity with particle size are present. Computer predictions of  $A_s(d)$  for a ratio counter are presented in Fig. 5 for a  $12/6^\circ$  ratio and two refractive indices.<sup>2</sup> The data of Fig. 5 accounted for the laser beam intensity distribution, the light scattering properties of spheres, the fields of view of the detectors and threshold-type signal processing. The dependence of  $A_s$  on refractive index is clear, with the oscillating behavior for nonabsorbing particles similar to light scattering response functions. In practice,  $A_s(d)$  for the absorbing particles is used to correct for size-selective sampling bias when particles of unknown refractive index are being analyzed. A similar dependence of PSI sample space on refractive index is expected although detailed calculations have apparently not been reported to date.

Also indicated on Fig. 5 are some recent experimental data for  $A_s$ .<sup>2</sup> The value of  $A_s$  was determined experimentally using Eq. (3) by independently measuring  $N(d)$  with a  $90^\circ$  white light scattering SPC which has a well defined  $A_s$  that is (except for edge effects) independent of particle size. The few data points show reasonable agreement with predictions; we are continuing these experiments. It seems that similar but more detailed sample space measurements for both PSI and cross section measuring SPC are warranted.

The technique of Holve and Self<sup>2</sup> is unique with respect to sample space considerations; correction for size-selective sample space bias is inherent in the data inversion method. The values of  $A_s$  are effectively calibrated concurrently with the particle size calibration.

This method has only been calibrated for large droplets of known refractive index, and for the analysis of particles with unknown properties the  $A_{\lambda}$  correction will be uncertain with this method as well as with the SPC techniques discussed previously.

### 3c. Nonspherical particle effects

The response of a single particle counter is generally related to particle size using a combination of calibration experiments and theoretical predictions. Since the prediction of light scattering by irregular particles is in general impossible, most SPC response curves are based on spherical particles. Unfortunately, many of the currently relevant applications for *in situ* particulate analysis (e.g., combustion exhaust) involve aerosols containing highly nonspherical particles. Thus, questions concerning SPC response to nonspherical particles are clearly of importance.

When analyzing a nonspherical particle a scattering SPC would measure a light-scattering equivalent particle diameter, or that diameter corresponding to a spherical particle of the calibration index of refraction which would produce a signal identical to the one observed from the nonspherical particle. Unfortunately, a radiative-interaction-equivalent diameter is not always of direct interest, except possibly for visibility and radiation studies. Relating this diameter to the measure of interest, e.g., aerodynamic equivalent or mass-equivalent diameter, is then imperative, but in general uncertain. This is true because SPC response to nonspherical particles can be highly dependent on the instrument configuration and the unknown particle surface characteristics.

Very few detailed studies of nonspherical particle effects on the *in situ* SPC discussed here have been made. One exception is the ratio counter for which some predicted responses to nonspherical particles are presented in Table III. The calculations were made using a diffraction theory approximation<sup>2</sup> and relate response predictions to cross-sectional area equivalent diameters for the particles shown. Here area-equivalent diameter is defined as  $d_{ae} = \sqrt{2(A/\pi)}$  where  $A$  is the projected cross-sectional area of the particle. The MRSPC does a reasonable job of measuring a projected particle size with typical errors on the order of 20% for small aspect ratios. Note also, however, that the response is independent of the third dimension (into the paper) of the particles in Table III, and determination of the mass of highly unsymmetric particles with a ratio counter is uncertain.

A few *in situ* single particle counting experiments with nonspherical particles have been made. Moon and Hirleman<sup>28,29</sup> are using the vibrating orifice generator method to generate particles as done by Pinnick et al.<sup>30</sup> to characterize the ratio counter response. Holve and Self<sup>31</sup> analyzed coal particles and found reasonable agreement with independent Coulter counter data.

In most studies of nonspherical particle effects it appears that optical SPC measure a diameter which is reasonably close to some geometric particle length scale such as cross-sectional area. This is encouraging, but it seems that additional careful experiments should be done to further justify this conclusion.

### 3d. Refractive index effects

The classical problem of sizing particles of unknown refractive index has been important since the first generation of optical particle counters. It has been known for some time that the forward scattering characteristics of particles and droplets are relatively independent of the refractive index since diffractive scatter rather than refractive or reflective scatter dominates. For this reason, most of the *in situ* SPC discussed here are operated in a forward scattering mode.

Figure 2 gives an indication of the variation of light scattering cross-sections with refractive index. SPC response curves for particles with some absorption (imaginary component  $\approx 0.01$ ) in the refractive index generally collapse onto a common curve to within a few percent.<sup>32</sup> To minimize errors the response function for an absorbing particle is usually assumed, with the scattering characteristics of nonabsorbing particles typically oscillating about

TABLE III. Predictions for 12°/6° ratio-type single particle counter response to nonspherical particles. The projected particle cross-sections indicated were scaled to various area-equivalent diameters  $d_{ae}$ , and the particle diameter predicted as the ratio counter response is tabulated. Thus, according to the predictions, a doublet particle with  $d_{ae} = 0.93 \mu\text{m}$  (made up of 2 primary particles of diameters  $0.66 \mu\text{m}$ ) would be sized at  $1.00 \mu\text{m}$  diameter by a 12°/6° ratio counter. Predicted responses are based on a diffraction theory approximation<sup>2</sup>, and are independent of particle orientation in the plane of the paper.

	$d_{ae}$			
	0.47 $\mu\text{m}$	0.93 $\mu\text{m}$	1.40 $\mu\text{m}$	1.86 $\mu\text{m}$
	0.54 $\mu\text{m}$	1.00 $\mu\text{m}$	1.42 $\mu\text{m}$	1.71 $\mu\text{m}$
	0.69	1.19	1.34	1.43
	0.47	0.87	1.30	1.75
	0.54	1.01	1.49	1.84
	0.60	1.07	1.49	1.79

this curve. Detailed calculations of response functions for a large number of collection optics geometries published by Oeseburg<sup>32</sup> also show the general behavior indicated in Fig. 4 including the multivalued response regions. *In situ* measurements in applications where there is no *a priori* knowledge of the aerosol refractive index will typically incur maximum sizing uncertainties of 50 to 100% for light-scattering cross-section SPC.<sup>32</sup> Refractive index effects for ratio-type SPC have been studied extensively<sup>23,33,34</sup> and it was found that maximum sizing errors in a similar application will be 20 to 30%. The PSI has a comparable dependence on refractive index if the complete wave solution is considered. If a forward scatter PSI geometry is utilized, uncertainties on the order of 20 to 30% are attributable to unknown refractive index.<sup>31</sup> However, for a backscatter geometry the errors can become much larger<sup>33,34</sup> (more than 100%) which is understandable since back-scattered light (reflection and refraction) is highly dependent on the optical properties of the particle. A refractive scatter PSI is somewhat sensitive to refractive index, and a measurement uncertainty of  $\pm 6\%$  is reported<sup>34</sup> for a range of nonabsorbing liquids typical of sprays. However, if the droplets have some absorption the errors in a refractive scatter PSI can become extremely large; in that case a reflective scatter geometry would be required.<sup>34</sup>

Extinction SPC are highly sensitive to refractive index,<sup>35</sup> with errors of 500% possible for unknown particle compositions. If it is known that the aerosol is either absorbing or not, these errors can be reduced considerably, down to the range of 50 to 100%. The dependence of extinction counter response on the complex refractive index is much stronger than for ratio or cross-section light scattering SPC.

In summary, the effects of unknown refractive index on SPC response are relatively easy to predict theoretically (for spherical particles) and are reasonably well understood. Some experimental studies have confirmed the predictions.<sup>36</sup> Potential errors range

from 10% up to 100% or more depending on the approach. The forward scatter arrangement of most SPC capable of *in situ* analysis minimizes this problem.

#### 4. CONCLUSIONS

Laser-based single particle counters show excellent potential for applications requiring *in situ*, nearly real time sizing of particles in hostile environments. A number of instrument concepts have been proposed and they are generally in the advanced development or early application stages. Several successful field tests have been made and it is clear that *in situ* particle analyzers will have a very important impact on process steam monitoring in the future. There are, however, several characteristics of single particle counter *in situ* performance which need further clarification and research. Future work on laser instruments for *in situ* particle sizing should follow two parallel paths. First, testing of the instruments in the hostile environments encountered in the field should be pursued. Second, further laboratory research should be directed toward characterizing and modeling the instruments' *in situ* performance in these real environments where nonspherical, polydisperse particles of unknown refractive index will be encountered.

#### 5. ACKNOWLEDGMENTS

The author wishes to acknowledge long term support of the National Science Foundation during his work on the topic of this paper. NSF support included a Graduate Fellowship for Ph.D. Studies, a Research Initiation Grant NSF# 78-06210, and specialized Research Equipment Grant NSF# 78-11462. This support was through the Solid and Particulate Processes Program, Dr. Morris Ojalvo, Director. The author is also grateful to Project SQUID of the Office of Naval Research for additional support.

#### REFERENCES

- Trolinger, J. D. and Field, D., Particle Field Diagnostics by Holography, AIAA Paper No. 80-0018 presented at the 18th AIAA Aerospace Sciences meeting, Pasadena, California, January 14, 1980.
- Hirleman, E. D., Optical Technique for Particulate Characterization in Combustion Environments: The Multiple Ratio Single Particle Counter, Ph.D. dissertation, Purdue University, August 1977.
- Lieberman, A., Laboratory comparison of forward and wide scattering angle optical particle counters, Opt. Eng. 19(6), this issue (1980).
- Knollenberg, R. G., Particle Size Measurements from Aircraft Using Electro-optical Techniques, p. 218 in *Proceedings of the 1971 Electro-Optical Systems Design Conference*, Anaheim, Ca, May 18-20, 1971.
- Faxvog, F. R., Detection of Airborne Particles using Optical Extinction Measurements, Appl. Opt. 13, 1913 (1974).
- Hirleman, E. D. and Stevenson, W. H., Intensity Distribution Properties of a Gaussian Laser Beam Focus, Appl. Opt. 17, 3496 (1978).
- J. Heyder, C. Roth, and W. Stahlhofen, A Laser Spectrometer for Size Analysis of Small Airborne Particles, J. Aerosol. Sci. 2, 341 (1971).
- Hirleman, E. D., An Optical Method for Exhaust Gas Particulate Sizing, Laboratory for Energiteknik Report RE-74-14, Technical University of Denmark, 2800 Lyngby, Denmark, August 1974.
- Ungut, A., Yule, A. J., Taylor, D. S., and Chigier, N. A., Simultaneous Velocity and Particle Size Measurements in Two Phase Flows by Laser Anemometry, AIAA Paper #78-74, presented at the AIAA 16th Aerospace Sciences meeting, Huntsville, Alabama, January 10-18, 1978.
- Knollenberg, R. G., The Use of Low Power Lasers in Particle Size Spectrometry, Proc. SPIE Vol. 92, 137 (1977).
- Faxvog, F. R., New Laser Particle Sizing Instrument, SAE Paper #770140 (1977).
- Holve, D. and Self, S. A., Optical Particle Sizing for *in situ* measurements, Parts I and II, Appl. Opt. 18, 1632 (1979).
- Hirleman, E. D., Laser Technique for Simultaneous Particle Size and Velocity Measurements, Opt. Lett. 3, 19 (1978).
- Hirleman, E. D., Recent Developments in Non-Doppler Laser Velocimetry, AIAA Paper 80-0350, presented at 18th AIAA Aerospace Sciences Meeting, Pasadena, California, January 14-16, 1980.
- Phillips, D. T. and Wyatt, P. J., Single-Particle light-scattering measurement: Photochemical aerosols and atmospheric particulates, Appl. Opt. 11, 2082 (1972).
- Bartholdi, M., Salzman, G. C., Hiebert, R. D., and Seger, G., Single-Particle Light-scattering Measurements with a Photodiode Array, Opt. Lett. 1, 223 (1977).
- Farmer, W. M., Measurement of Particle Size, Number Density, and Velocity Using a Laser Interferometer, Appl. Opt. 11, 2603 (1972).
- Fristrom, R. M., Jones, A. R., Schwar, M. S. R., and Weinberg, F. S., Particle Sizing by interference fringes and signal coherence in Doppler Velocimetry, Faraday Symposia of the Chemical Society 1, 183 (1973).
- Robinson, D. M. and Chu, W. P., Diffraction Analysis of Doppler Signal Characteristics for a Cross-beam Laser Doppler Anemometer, Appl. Opt. 14, 2177 (1975).
- Chu, W. P. and Robinson, D. M., Scattering from a Moving Spherical Particle by Two Crossed Coherent Plane Waves, Appl. Opt. 16, 619 (1977).
- Yule, A. J., Chigier, N. A., Atakan, S. and Ungut, A., Particle Size and Velocity Measurement by Laser Anemometry, AIAA Paper No. 77-214, 1977.
- Farmer, W. M., Measurement of Particle Size and Concentrations Using LDV Techniques, in Proceedings of The Dynamic Flow Conference 1978.
- Bachalo, W. D., Method for Measuring the Size and Velocity of Spheres by Dual-Beam Light-Scatter Interferometry, Appl. Opt. 19, 363 (1980).
- Dos Santos, R. and Stevenson, W., Aerosol Sizing by Means of Laser-induced Fluorescence, App. Phys. Lett. 30, 236 (1977).
- Kratohvil, J. P., Lee, M. P., and Kerker, M. P., Angular distribution of Fluorescence from Small Particles, Appl. Opt. 17, 1978 (1978).
- Wittig, S. L. K. and Sakbani, K., Simultaneous Particle Size and Velocity Measurements in Postflame Gases, p. 404 in *Laser Velocimetry and Particle Sizing*, H. D. Thompson and W. H. Stevenson, Eds., Hemisphere Pub. Corp. NY, 1979.
- Bachalo, W. D. and Hess, C. F., Optical Diagnostic Techniques for Particulate and Turbulence Measurements in Combustion Research, presented at the 1980 Spring meeting of the Western States Section, Combustion Institute, April 21-22, 1980, Irvine, CA.
- Moon, H. K., Response Characteristics of the Multiple Ratio Single Particle Counter, M. S. Thesis, Arizona State University, Mechanical Engineering Dept. June, 1980.
- Moon, H. K. and Hirleman, E. D., Response Characteristics of the Multiple Ratio Single Particle Counter, in Digest of Technical Papers, CLEOS 1980, Optical Society of America, New York, 1980.
- Pinnick, R. G., Carroll, D. E., and Hofmann, D. J., Polarized Light Scattered from Monodisperse Randomly-oriented Nonspherical Aerosol Particles: Measurements, Appl. Opt. 15, 384 (1976).
- Hirleman E. D., and S. L. K. Wittig, Laser Applications in Particulate Analysis: The Multiple Ratio Single Particle Counter, Laser 77 Optoelektronik Conference Proceedings, p. 740, W. Waidelich, Ed., IPC Science and Technology Press, 1977.
- Oeseburg, F., The Influence of the Aperture of the Optical System of Aerosol Particle Counters on the Response Curve, J. of Aerosol Science 3, 307 (1972).
- Boron, S. and Waldie, B., Particle Sizing by forward Lobe Scattered Intensity Ratio Technique: Errors introduced by Applying Diffraction Theory in the Mie Regime, Appl. Opt. 17, 1644 (1978).
- Hong, N. S. and Jones, A. R., A Light Scattering Technique for Particle Sizing Based on Fringe Anemometry, J. of Physics D Applied Physics 9, 1839 (1976).
- Bachalo, W., Hess, C. F., and Hartwell, C. A., An Instrument for Spray Droplet Size and Velocity Measurements, ASME paper #79-WA GT-13, American Society of Mechanical Engineers, New York, 1979.
- Hodkinson, J. R., Particle Sizing by Means for the Forward Scattering Lobe, Appl. Opt. 5, 839 (1966).
- Gravatt, C. C., Real Time Measurement of the Size Distribution of Particulate Matter by a Light Scattering Method, APCA Journal 23, 1035 (1973).

**END**

**FILMED**

**3-85**

**DTIC**